



HAL
open science

Serviceability and safety in the design of rigid inclusions and combined pile-raft foundations

Cécilia Bohn

► **To cite this version:**

Cécilia Bohn. Serviceability and safety in the design of rigid inclusions and combined pile-raft foundations. Civil Engineering. Université Paris-Est; Technische Universität (Darmstadt, Allemagne), 2015. English. NNT : 2015PESC1096 . tel-01259962

HAL Id: tel-01259962

<https://pastel.hal.science/tel-01259962>

Submitted on 21 Jan 2016

HAL is a multi-disciplinary open access archive for the deposit and dissemination of scientific research documents, whether they are published or not. The documents may come from teaching and research institutions in France or abroad, or from public or private research centers.

L'archive ouverte pluridisciplinaire **HAL**, est destinée au dépôt et à la diffusion de documents scientifiques de niveau recherche, publiés ou non, émanant des établissements d'enseignement et de recherche français ou étrangers, des laboratoires publics ou privés.

Serviceability and safety in the design of rigid inclusions and combined pile-raft foundations

Cécilia Bohn

PhD thesis in double degree programme, defended on the 30th September 2015 at the Technical University Darmstadt

Examination committee:

Prof. Matthias Becker (Technical University Darmstadt)	President
Prof. Eduardus Koenders (Technical University Darmstadt)	Referee
Prof. Hussein Mroueh (Lille University)	Referee
Prof. Norbert Vogt (Technical University Munich)	Referee
Prof. Roger Frank (ENPC, University Paris-Est)	PhD supervisor
Prof. Rolf Katzenbach (Technical University Darmstadt)	PhD co-supervisor
Prof. Stefan Schäfer (Technical University Darmstadt)	Additional examiner

Acknowledgements

First of all and above all, I would like to express my deepest gratitude to my PhD supervisor Prof. Roger Frank for giving the best supervision I could imagine for my thesis. It was an extraordinary combination of great scientific support, constant availability (despite ISSMGE presidency), and permanent confidence in me and in the directions I chose to give to my thesis. His warm understanding helped me a lot in the many difficult times I encountered organizing all double degree appointments. Roger, I will miss our discussion times in Paris! I would like to thank as well the members of the Navier-Geotechnics laboratory (Cermes) for immediately giving me the feeling that I am part of the team, even if I spent only few months there.

I wish to thank Prof. Rolf Katzenbach for accepting to co-supervise my thesis in this double degree programme. Thanks to the team of the Institute and Laboratory of Geotechnics of the Technical University Darmstadt for hosting me and for the experience I could gain in teaching activities there during the first year of my thesis.

I appreciated particularly the detailed reviewing of the referees, Prof. Eduardus Koenders, Prof. Hussein Mroueh and Prof. Norbert Vogt, who showed a great interest in my work. The very kind participation of Prof. Matthias Becker as president of the examination committee and of Prof. Stefan Schäfer completed perfectly the French-German examination committee. Special thanks go to Cécile Blanchemanche and Claudia Castrillon from both partner institutions for their efforts helping me organizing the double degree programme.

I would like to thank of course my supervisors of the company Keller Holding GmbH for developing this subject together with me and for supporting technically and financially this research from the beginning. I am very grateful to my colleagues of the EMEA Corporate Services team and of the Keller branch offices all over the world for the very motivating and pleasant work, helping me giving the right orientation of my research to make it as useful as possible for the engineering practice.

I would like to thank warmly Prof. Ulrich Trunk and Timo Ackermann for their particular dedication to our common work. Special thanks go to Alexandre Lopes dos Santos and Arefeh Rostami for their strong initiative carrying out useful analyses for my thesis during their internships within Keller. Many thanks go to Dorian Nogneng, Matthieu Appenzeller and Thomas Reichl as well for their valuable advice and support in programming. Thanks a lot to Sébastien Burlon, Sabrina Perlo, Michel Gambin and Olivier Combarieu for the pleasant exchanges and for the indispensable background they provided to me in foundation engineering and in the pressuremeter theory.

Contents

List of appendices	IV
List of figures	V
List of tables	XVII
List of symbols and abbreviations	XX
1 Introduction	1
2 State of the art and literature analysis	4
2.1 Design of shallow foundations according to Eurocode 7	4
2.1.1 Current practice in Germany	4
2.1.1.1 Bearing capacity	4
2.1.1.2 Settlement	6
2.1.2 Current practice in France	6
2.1.2.1 Bearing capacity	7
2.1.2.2 Settlement	10
2.2 Design of pile foundations according to Eurocode 7	11
2.2.1 Current practice in Germany	11
2.2.2 Current practice in France	15
2.2.2.1 Bearing capacity	15
2.2.2.2 Settlement	20
2.3 Pile groups	22
2.3.1 Principle and behaviour	22
2.3.2 Pile group system calculation	23
2.3.2.1 Empirical methods	23
2.3.2.2 Elastic continuum methods	24
2.3.2.3 Hybrid methods with load transfer curves	31
2.3.2.4 Continuum methods	33
2.4 Combined pile-raft foundations (CPRF)	34
2.4.1 Principle and behaviour	34
2.4.2 CPRF system calculation	38
2.4.2.1 Elastic continuum methods	38
2.4.2.2 Analytical hybrid methods with load transfer curves	43
2.4.2.3 Continuum methods	45
2.5 Rigid inclusions (RI)	49
2.5.1 Principle and behaviour	49
2.5.2 RI system calculation	53
2.5.2.1 Simplified and equivalence methods	53
2.5.2.2 Load transfer method (LTM) with load transfer curves	55
2.5.2.3 Continuum methods	61
2.6 Stone columns	62
2.6.1 Principle and behaviour	62

2.6.2	Deformation parameters and settlement	64
2.7	Comparison of safety concepts for usual and combined foundation systems	67
2.7.1.1	Safety concept for RI after ASIRI (IREX 2012)	68
2.7.1.2	External bearing capacity (GEO)	70
2.7.1.3	Internal structural capacity (STR)	72
3	Investigation of the settlement of shallow foundations	74
3.1	Application of moduli correlations for linear elastic calculation	74
3.2	Single footing non-linear settlement behaviour	77
4	Investigation of the settlement of pile foundations	83
4.1	Pile load test database	83
4.2	Single pile axial behaviour with the FEM and moduli correlations	85
4.2.1	Need of relevant correlations for single pile loading	85
4.2.2	Example of moduli back-calculation for an instrumented single pile	88
4.3	Development of axial load transfer curves for LTM applications	97
4.3.1	Existing load transfer curves	97
4.3.2	Development of load transfer curves based on instrumented load tests	101
4.3.2.1	Analysis of existing curves	101
4.3.2.2	Proposal of new explicit curves	106
4.3.3	Validation based on non-instrumented load tests	111
5	Application of Load Transfer Method (LTM) to combined foundation systems	118
5.1	Load transfer method development for combined systems	118
5.1.1	General aspects	118
5.1.2	Large slabs or embankments: unit cell calculation	119
5.1.3	Single footings: oedometer and pressuremeter method	121
5.2	Comparison and transition between CPRF and RI systems based on reference cases with measurements	124
5.2.1	Infinite grid system	124
5.2.1.1	Reference RI infinite grid case with measurements	124
5.2.1.2	Variation of load	129
5.2.1.3	Variation of LTP thickness	132
5.2.1.4	Comparison between rigid and flexible slab cases	134
5.2.2	Single footing system	137
5.2.2.1	Reference CPRF case with measurements	137
5.2.2.2	Variation of load	139
5.2.2.3	Variation of LTP thickness	142
5.2.3	High-rise building example	144
5.2.3.1	Reference case with measurements	144
5.2.3.2	Variation of load	151
5.2.3.3	Variation of LTP thickness	154
5.3	Comparison of LTM with FEM for theoretical single footing combined system	156

5.3.1	General modelling aspects	156
5.3.2	Calibration on case without columns	162
5.3.3	Comparison in CPRF case	165
5.3.4	Comparison in RI case	171
6	Sensitivity investigation	182
6.1	Influence of column material in a unit cell system	182
6.1.1	General modelling aspects	182
6.1.2	Concrete column and stone column reference cases	185
6.1.3	Variation of column modulus and material type	188
6.2	Influence of geometrical imperfections on a single column	190
6.2.1	General modelling aspects	190
6.2.2	Diameter reduction over whole column length	194
6.2.3	Necking and bulging	197
6.2.4	Inclination	202
6.2.5	Curvature	208
6.2.6	Load eccentricity	214
6.3	Comparison and recommendations	217
6.3.1	Column material imperfections	217
6.3.2	Column geometrical imperfections	218
7	Summary and outlook	221
8	Zusammenfassung und Ausblick	226
9	Résumé et perspectives	231
	References	236

List of appendices

Appendix A. Soil deformation parameters and settlement of usual foundations

- A.1 General aspects
- A.2 Oedometer test
- A.3 Plate load test
- A.4 Pressuremeter test (PMT)

Appendix B. Soil resistance parameters and bearing capacity of usual foundations

- B.1 Laboratory tests
- B.2 Cone penetration test (CPT)
- B.3 Pressuremeter test (PMT)

Appendix C. Correlations between soil parameters

- C.1 CPT and PMT and other tests parameters
- C.2 CPT parameters and soil moduli
- C.3 Different soil moduli

Appendix D. Main properties of pile load tests in database

- D.1 Instrumented non-displacement pile load tests
- D.2 Instrumented displacement pile load tests
- D.3 Non-instrumented non-displacement pile load tests (or considered as such)
- D.4 Non-instrumented displacement pile load tests (or considered as such)

List of figures

Fig. 1.1	Rigid inclusion (RI) system in comparison with usual foundation systems from ASIRI (IREX 2012)	1
Fig. 2.1	Diagrams for factor k_p for bearing capacity of shallow foundations after NF P94-261 (2013)	9
Fig. 2.2	Load-settlement curve for bored piles after EA-Pfähle (DGGT 2012)	13
Fig. 2.3	Definition of f_{sol} for ultimate skin friction translated from NF P94-262 (2012)	20
Fig. 2.4	Load transfer method for axially loaded piles	21
Fig. 2.5	Load transfer curves after Frank and Zhao (1982) for skin friction (left) and base resistance (right) after NF P94-262 (2012)	21
Fig. 2.6	Massive fictive pile for calculation of bearing capacity of pile groups (Frank 1999)	23
Fig. 2.7	Pile group settlement for floating piles after Terzaghi method (Frank 1999)	24
Fig. 2.8	Shear stress distribution around the pile for single pile settlement after Frank (1975) and Randolph (Mossallamy 1997)	25
Fig. 2.9	Superposition of settlement profiles for a pile group (Fleming et al. 2008)	26
Fig. 2.10	Linear elastic calculation for settlement of a single pile after Poulos (1994), cited by Smoltczyk (2001): settlement factor I_p vs. relative length	28
Fig. 2.11	Group interaction factors vs. relative spacing between two piles after Poulos and Davis (1980), cited by Frank (1999)	29
Fig. 2.12	Group interaction factors between two piles (Viggiani et al. 2011)	30
Fig. 2.13	Charts for calculation of exponent e for pile group settlement (Fleming et al. 1985)	31
Fig. 2.14	Skin friction displacement factor γ for group effect with load transfer curves	32
Fig. 2.15	Inclination reduction of skin friction load transfer curve for group effect (Randolph 1994)	32
Fig. 2.16	Diagram for S_1 and S_2 vs. load level for cohesive soils (I) (EA-Pfähle, DGGT 2012)	34
Fig. 2.17	Schematic design concept of shallow foundations (a), CPRFs (b) and deep foundations (c) (Borel 2001)	35
Fig. 2.18	Interactions in CPRF system (Katzenbach and Choudhury 2013)	36
Fig. 2.19	Theoretically mobilised pile skin friction with and without loading of the soil adapted from (Borel 2001)	37

Fig. 2.20	Pile load-settlement behaviour: single pile, pile in a group, pile in a CPRF adapted from El-Mossallamy (1997)	37
Fig. 2.21	Interaction between pile and raft foundation elements (Borel 2001)	39
Fig. 2.22	Settlement of pile-raft system vs. raft/pile diameter ratio compared to single rigid pile in an elastic continuum after Poulos and Davis (1980), cited by Borel (2001)	41
Fig. 2.23	Settlement of CPRF and pile group vs. relative pile spacing compared to single rigid pile in an elastic continuum from Butterfield and Banerjee (1971), cited by Borel (2001)	42
Fig. 2.24	Combined boundary element and finite element method for CPRF (El-Mossallamy 1996)	43
Fig. 2.25	Principle of a hybrid method for CPRF from Clancy and Randolph (1993), cited by Borel (2001)	44
Fig. 2.26	Soil and pile settlement profiles with the LTM after Combarieu (1988a)	45
Fig. 2.27	3D-modelling of CPRF-subsystem using symmetrical properties (Hanisch et al. 2002)	46
Fig. 2.28	Full 3D-modelling of CPRF-system (Skyper-Tower in Frankfurt am Main) (Richter and Lutz 2010)	46
Fig. 2.29	Increasing modulus with depth for FEM-modelling (Richter and Lutz 2010)	47
Fig. 2.30	Predesign-diagrams for a CPRF in theoretically infinitely deep Frankfurt clay (Reul 2000): settlement vs. number of piles and pile length	48
Fig. 2.31	Predesign-diagram for a CPRF in the Frankfurt clay with finite depth (Reul 2000): settlement relatively to the case with infinite clay depth vs. relative clay depth	49
Fig. 2.32	Rigid inclusion (RI) application cases adapted from ASIRI (IREX 2012)	50
Fig. 2.33	Settlement, load-transfer behaviour and planes with equal settlements in RI grid	51
Fig. 2.34	Influence of LTP thickness and slab rigidity on efficiency and settlement behaviour adapted from (Höppner 2011)	52
Fig. 2.35	Equivalent raft settlement calculation for groups of rigid columns (CSV-guideline, DGGT 2002)	54
Fig. 2.36	RI system as interpolation between unimproved footing and CPRF from ASIRI (IREX 2012)	55
Fig. 2.37	Equivalent modulus E_{oe} for equivalent raft calculation (Combarieu 1990)	55
Fig. 2.38	Unit cell RI system for calculation with mobilisation functions adapted from ASIRI (IREX 2012)	56
Fig. 2.39	Development of shear along the fictive columns to model the arching effect from ASIRI (IREX 2012)	58

Fig. 2.40	Load in the soil at the top of the columns after Combarieu from ASIRI (IREX 2012)	58
Fig. 2.41	Prandtl's failure mechanism for the compatibility check in the LTP after ASIRI (IREX 2012)	59
Fig. 2.42	Diagram with domain of allowable stresses in LTP, adapted from ASIRI (IREX 2012)	59
Fig. 2.43	Soil settlement profile under footing for calculation with load transfer curves from ASIRI (IREX 2012)	60
Fig. 2.44	Steps for hybrid monolith method for RIs under footing (IREX 2012)	61
Fig. 2.45	Deformation of stone columns under service loads (Kirsch 2004)	63
Fig. 2.46	Failure mechanisms for stone columns from Datye (1982), cited by Soyez (1985)	64
Fig. 2.47	Elastic calculation method for compressible piles from Mattes and Poulos (1969), cited by Soyez (1985): settlement factor I_p vs. column/soil stiffness ratio	65
Fig. 2.48	Settlement relatively to unimproved settlement vs. stone columns spacing after Greenwood (1970)	65
Fig. 2.49	Comparison of settlement calculation methods for stone columns (Greenwood and Kirsch 1983): settlement reduction ratio vs. area ratio	67
Fig. 2.50	Check of geotechnical capacity of single columns in function of column diameter according to standards and recommendations	71
Fig. 3.1	Example site with in situ soil tests for settlement calculation of shallow foundations	74
Fig. 3.2	Example site: soil configuration and shallow foundation cases	75
Fig. 3.3	Proposal of Combarieu (1988a) for footing load-settlement curve (spherical and deviatoric components)	78
Fig. 3.4	Proposal of Briaud (2007) for footing load-settlement curve	78
Fig. 3.5	Measured and modelled footing load-settlement curves	81
Fig. 3.6	Proposed hyperbolic mobilisation curve for single footing resistance	82
Fig. 4.1	Example of pile instrumentation with the "removable extensometer" system	84
Fig. 4.2	Main results of an instrumented load test with "removable extensometer". Left: load-settlement curve for head and tip; Middle: shaft load distribution between blockers and extrapolation for tip load; Right: skin friction load transfer curve	84
Fig. 4.3	Stress path of soil around axially loaded single pile in comparison with usual tests and shallow foundations	86
Fig. 4.4	Comparison of modulus ranges from usual correlations for different foundation types for clay and sand	87
Fig. 4.5	Definition of E_{50} from deviatoric stress vs. axial strain diagram (Plaxis 2014)	89

Fig. 4.6	2D-FEM-model of single pile Ifsttar 35 B (layers with main parameters, pile, interfaces and mesh)	91
Fig. 4.7	Comparison of measured mobilisation curve of skin friction in the third layer with the back-calculated FEM model and with the Frank and Zhao (1982) prediction (instrumented load test Ifsttar 35B)	92
Fig. 4.8	Measured and modelled load-settlement curve after back-calculation at pile head and at pile tip (instrumented load test Ifsttar 35B)	93
Fig. 4.9	Measured and modelled load in pile with depth (instrumented load test Ifsttar 35B)	94
Fig. 4.10	Comparison of back-calculated moduli in each layer of the FEM model with usual correlations (instrumented load test Ifsttar 35B)	95
Fig. 4.11	Stress paths of stress point at the interface half way down the second layer and of stress point directly under the pile tip in the FEM model (instrumented load test Ifsttar 35B)	96
Fig. 4.12	Example of level of agreement of predicted load transfer curves	102
Fig. 4.13	Percentage of measured skin friction curves with peaks for different soil and pile types	103
Fig. 4.14	Variability in measured and modelled peak behaviours	103
Fig. 4.15	Level of agreement of the existing load transfer curves	104
Fig. 4.16	Level of agreement of the existing load transfer curves for the initial stiffness	104
Fig. 4.17	Example of calibration of cubic root curves at shaft and at tip	106
Fig. 4.18	Cubic root curves – Calibration of limit settlements $s_{s,lim}$ and $s_{b,lim}$	107
Fig. 4.19	Limit settlements $s_{s,lim}$ and $s_{b,lim}$ in function of CPT cone resistance for cubic root curves ($q_c = 0$ MPa means no CPT data)	107
Fig. 4.20	Example of calibration of hyperbolic curve at shaft and at tip	109
Fig. 4.21	Hyperbolic curves – Calibration of parameters M_s and M_b	110
Fig. 4.22	Shaft parameter M_s and tip parameter M_b in function of cone resistance for hyperbolic curves ($q_c = 0$ MPa means no CPT data)	110
Fig. 4.23	Level of agreement of the proposed load transfer curves compared with Frank and Zhao curves (global agreement and initial stiffness)	111
Fig. 4.24	LTM single column system with required input parameters	112
Fig. 4.25	Example of a single pile analysis with test Ifsttar 1-A1 under a given load with the LTM: output under 1000 kN	113
Fig. 4.26	Example of a single pile analysis with test Ifsttar 1-A1 with the LTM: load-settlement curve and load distribution along the shaft for different loads	114
Fig. 4.27	Examples of comparison between measured and predicted load-settlement curves at pile head	115
Fig. 4.28	Ratio between predicted and measured settlement for both proposed load transfer curves	116

Fig. 5.1	Unit cell for large slabs or embankments with required input parameters	119
Fig. 5.2	System for calculation of slab bending moments m after plate theory	121
Fig. 5.3	Soil settlement profile under a single footing according to the pressuremeter theory (Combarieu 1988a)	123
Fig. 5.4	LTM Single footing with oedometer method or pressuremeter method with required input parameters	123
Fig. 5.5	Cross section of monitored RI field test for ASIRI in Saint-Ouen-l'Aumône with main soil and foundation parameters (Briançon and Simon 2010)	125
Fig. 5.6	Results of LTM calculation of infinite grid system of the ASIRI field test with a rigid slab with Frank and Zhao load transfer curves	126
Fig. 5.7	Results of LTM calculation of infinite grid system of the ASIRI field test with a rigid slab with proposed cubic root load transfer curves	127
Fig. 5.8	Results of LTM calculation of infinite grid system of the ASIRI field test with a rigid slab with proposed hyperbolic load transfer curves	127
Fig. 5.9	Results of LTM calculation of infinite grid system of the ASIRI field test with a flexible slab with Frank and Zhao load transfer curves	128
Fig. 5.10	Differential settlement measured in central unit cell of ASIRI field test (Briançon and Simon 2010)	129
Fig. 5.11	Surface load-settlement based on ASIRI reference case with Frank and Zhao load transfer curves (infinite grid, rigid loading)	130
Fig. 5.12	Column load share vs. area load based on ASIRI reference case with Frank and Zhao load transfer curves (infinite grid, rigid loading)	130
Fig. 5.13	Neutral plane variations vs. area load based on ASIRI reference case with Frank and Zhao load transfer curves (infinite grid, rigid loading)	131
Fig. 5.14	Load-settlement behaviour based on ASIRI reference case with Frank and Zhao load transfer curves (infinite grid, rigid loading) compared to single column case	132
Fig. 5.15	Settlement at the top vs. LTP thickness based on ASIRI reference case with Frank and Zhao load transfer curves (infinite grid, rigid loading)	133
Fig. 5.16	Column load share vs. LTP thickness based on ASIRI reference case with Frank and Zhao load transfer curves (infinite grid, rigid loading)	133
Fig. 5.17	Neutral plane variations vs. LTP thickness based on ASIRI reference case with Frank and Zhao load transfer curves (infinite grid, rigid loading)	134
Fig. 5.18	Settlement at the top vs. LTP thickness based on ASIRI reference case with Frank and Zhao load transfer curves (infinite grid, rigid and flexible loading)	135
Fig. 5.19	Column load share vs. LTP thickness based on ASIRI reference case with Frank and Zhao load transfer curves (infinite grid, rigid and flexible loading)	135

Fig. 5.20	Neutral plane variations vs. LTP thickness based on ASIRI reference case with Frank and Zhao load transfer curves (infinite grid, rigid and flexible loading)	136
Fig. 5.21	Bending moment at the edge and at the centre of the unit cell based on ASIRI reference case with Frank and Zhao load transfer curves (infinite grid, rigid loading)	137
Fig. 5.22	Test site picture and cross section of monitored CPRF field test in Merville (Borel 2001)	138
Fig. 5.23	Settlement with load in CPRF field test from Borel (2001): measurements and predictions with FONMIX and with proposed LTM calculation	140
Fig. 5.24	Pile load share with load in CPRF field test from Borel (2001): measurements and predictions with FONMIX and with proposed LTM calculation	140
Fig. 5.25	Results of LTM calculation of CPRF with rigid footing field test from Borel (2001) with Frank and Zhao load transfer curves for intermediate load level of 1091 kN	141
Fig. 5.26	Load-settlement behaviour based on Borel (2001) reference case: with Frank and Zhao load transfer curves compared to single column case	142
Fig. 5.27	Settlement at the top vs. LTP thickness based on Borel (2001) reference case with Frank and Zhao load transfer curves (rigid footing)	143
Fig. 5.28	Column load share vs. LTP thickness based on Borel (2001) reference case with Frank and Zhao load transfer curves (rigid footing)	143
Fig. 5.29	Neutral plane variations vs. LTP thickness based on Borel (2001) reference case with Frank and Zhao load transfer curves (rigid footing)	143
Fig. 5.30	Distribution of the soil modulus of oedometer type of the Frankfurt clay evaluated from pressuremeter tests along the depth z (Reul 2000)	145
Fig. 5.31	Simplified distribution of Young's modulus compared to pressuremeter reloading modulus (Reul 2000)	145
Fig. 5.32	Vertical cross section and plan view of monitored CPRF foundation of high-rise building Westend 1 in Frankfurt (Reul 2000)	146
Fig. 5.33	Pile load vs. settlement for different pile locations for CPRF Westend 1 (Reul 2000)	147
Fig. 5.34	Results of LTM calculation of CPRF Westend 1 as infinite grid system with a rigid slab with cubic root load transfer curves	149
Fig. 5.35	Results of LTM calculation of CPRF Westend 1 as infinite grid system with a rigid slab with hyperbolic load transfer curves	149
Fig. 5.36	Results of LTM calculation of CPRF Westend 1 as infinite grid system with a rigid slab with Frank and Zhao load transfer curves	150
Fig. 5.37	Measured settlement distribution along the depth of CPRF Westend 1 (Reul 2000)	151

Fig. 5.38	Settlement at the top vs. load based on Westend 1 reference case with cubic root and hyperbolic load transfer curves (infinite grid, rigid loading)	152
Fig. 5.39	Settlement share below pile tip vs. load based on Westend 1 reference case with cubic root and hyperbolic load transfer curves (infinite grid, rigid loading)	152
Fig. 5.40	Pile load share vs. load based on Westend 1 reference case with cubic root and hyperbolic load transfer curves (infinite grid, rigid loading)	153
Fig. 5.41	Load-settlement behaviour based on Westend 1 reference case: with cubic root load transfer curves (infinite grid, rigid loading) compared to single column case	154
Fig. 5.42	Settlement at the top vs. LTP thickness based on Westend 1 reference case with cubic root and hyperbolic load transfer curves (rigid loading)	155
Fig. 5.43	Column load share vs. LTP thickness based on Westend 1 reference case with cubic root and hyperbolic load transfer curves (rigid loading)	155
Fig. 5.44	Neutral plane variations vs. LTP thickness based on Westend 1 reference case with cubic root and hyperbolic load transfer curves (rigid loading)	155
Fig. 5.45	Bending moment at the edge and at the centre of the unit cell based on Westend 1 reference case with cubic root and hyperbolic load transfer curves (rigid loading)	156
Fig. 5.46	Plan view of footing with columns and position of sections A-A and B-B	157
Fig. 5.47	Mohr-Coulomb failure criterion for modelled concrete	158
Fig. 5.48	3D FEM model of footing without columns	159
Fig. 5.49	3D FEM model of footing with columns without LTP	160
Fig. 5.50	3D FEM model of footing with columns with LTP	161
Fig. 5.51	Footing load-settlement curves with 3D FEM and LTM	162
Fig. 5.52	Vertical stresses over bottom surface of the footing with 3D FEM for case without columns	163
Fig. 5.53	Profiles of vertical stress due to load with 3D FEM and LTM without columns	164
Fig. 5.54	Settlement profiles with 3D FEM and LTM without columns	164
Fig. 5.55	Vertical stresses over bottom surface of the footing with 3D FEM for CPRF case (right: only soil stresses; in Plaxis: compression negative)	165
Fig. 5.56	Vertical stresses in section A-A (see Fig. 5.46) with 3D FEM for CPRF case (in Plaxis: compression negative)	166
Fig. 5.57	Vertical stresses in section B-B (see Fig. 5.46) with 3D FEM for CPRF case (left: only column stresses; right: only soil stresses; in Plaxis: compression negative)	166
Fig. 5.58	Vertical displacement in section A-A (see Fig. 5.46) with 3D FEM for CPRF case	167

Fig. 5.59	Vertical displacement in section B-B (see Fig. 5.46) with 3D FEM for CPRF case	167
Fig. 5.60	Comparison of LTM and 3D FEM results for CPRF case: settlement and skin friction mobilisation (depth 0 m: column head position)	169
Fig. 5.61	Comparison of LTM and 3D FEM results for CPRF case: additional stress in the column and in the soil due to the load applied (depth 0 m: column head position)	170
Fig. 5.62	Footing load-settlement curve in CPRF with 3D FEM compared with load-settlement curves without columns	171
Fig. 5.63	Failure points in LTP (RI case) with 3D FEM (left: in section A-A; right: section B-B after Fig. 5.46)	172
Fig. 5.64	Vertical stresses over bottom surface of the footing with 3D FEM for RI case (in Plaxis: compression negative)	173
Fig. 5.65	Vertical stresses in section A-A (see Fig. 5.46) with 3D FEM for RI case (in Plaxis: compression negative)	173
Fig. 5.66	Vertical stresses in section B-B (see Fig. 5.46) with 3D FEM for RI case (left: only column stresses; right: only soil stresses; in Plaxis: compression negative)	174
Fig. 5.67	Detail of vertical stresses in LTP in section B-B (see Fig. 5.46) with 3D FEM for RI case (in Plaxis: compression negative)	174
Fig. 5.68	Skin friction mobilisation with 3D FEM for RI case	175
Fig. 5.69	Vertical displacement over bottom surface of the footing with 3D FEM for RI case	176
Fig. 5.70	Vertical displacement in section A-A (see Fig. 5.46) with 3D FEM for RI case	176
Fig. 5.71	Vertical displacement in section B-B (see Fig. 5.46) with 3D FEM for RI case	177
Fig. 5.72	Directions of principal stresses in section B-B (see Fig. 5.46) with 3D FEM for RI case	177
Fig. 5.73	Comparison of LTM and 3D FEM results on RI case: settlement and skin friction mobilisation (depth 0 m: column head position)	179
Fig. 5.74	Comparison of LTM and 3D FEM results in RI case: additional stress in the column and in the soil due to the load applied (depth 0 m: column head position)	181
Fig. 6.1	Axisymmetric FEM-model for column material variation (layers with main parameters and mesh)	183
Fig. 6.2	Young's modulus vs. compressive strength for usual concrete and lightweight concrete	184
Fig. 6.3	Comparison of vertical stresses between concrete column and stone column reference cases (in Plaxis: compression negative)	186

Fig. 6.4	Comparison of horizontal deformations between concrete column and stone column reference cases	187
Fig. 6.5	Comparison of failure points between concrete column and stone column reference cases	187
Fig. 6.6	Bending moments in the plate vs. distance to centre of the unit cell for the concrete column and for the stone column reference cases	188
Fig. 6.7	Settlement at the top vs. modulus ratio column to soil for bonded and coarse-grained column ($E_{\text{oed,soil}}^{\text{ref}} = 6.5 \text{ MPa}$)	189
Fig. 6.8	Settlement at the LTP base level vs. modulus ratio column to soil for bonded and coarse-grained column ($E_{\text{oed,soil}}^{\text{ref}} = 6.5 \text{ MPa}$)	189
Fig. 6.9	Column load share at the column head vs. modulus ratio column to soil for bonded and coarse-grained column ($E_{\text{oed,soil}}^{\text{ref}} = 6.5 \text{ MPa}$)	190
Fig. 6.10	Reference single column for analytical study	192
Fig. 6.11	Single column axisymmetric FEM reference model	193
Fig. 6.12	Diameter imperfection for analytical study	195
Fig. 6.13	Loss of resistance due to diameter variation over whole height from analytical study	195
Fig. 6.14	Load-settlement curves for different diameters from axisymmetric FEM analysis	196
Fig. 6.15	Loss of bearing capacity due to a diameter reduction of 10 cm from axisymmetric FEM analysis compared to analytical results	197
Fig. 6.16	Settlement increase under service load due to a diameter reduction of 10 cm from FEM analysis	197
Fig. 6.17	Necking and bulging imperfection for axisymmetric FEM analysis	198
Fig. 6.18	Vertical stress in necking zone from axisymmetric FEM analysis for $B = 30 \text{ cm}$	199
Fig. 6.19	Load-settlement curves with bulging and necking from axisymmetric FEM analysis for $B = 30 \text{ cm}$	200
Fig. 6.20	Directions of principal stresses in the soil with bulging and necking from axisymmetric FEM analysis for $B = 30 \text{ cm}$	201
Fig. 6.21	Increase of bearing capacity with bulging and necking from axisymmetric FEM analysis	201
Fig. 6.22	Inclination imperfection with parameters for analytical study	202
Fig. 6.23	Load section vs. normalized lever arm from analytical study	204
Fig. 6.24	Inclination imperfection for 3D FEM analysis	204
Fig. 6.25	Load-settlement curves with column inclination from 3D FEM analysis for $B = 30 \text{ cm}$	205
Fig. 6.26	Normal stress in the interface around the inclined columns under the maximum applied load from 3D FEM analysis for $B = 30 \text{ cm}$	206
Fig. 6.27	Skin friction in the interface around the inclined columns under the maximum applied load from 3D FEM analysis for $B = 30 \text{ cm}$	206

Fig. 6.28	Vertical stress (in Plaxis: compression negative) and bending moment in the inclined column from 3D FEM analysis for $B = 30$ cm	207
Fig. 6.29	Curvature imperfection with parameters for analytical study	209
Fig. 6.30	Buckling load and geotechnical bearing capacity in function of curvature imperfection for $B = 30$ cm	210
Fig. 6.31	Stresses in section in function of curvature imperfection for service load of 189 kN (half of bearing capacity) for $B = 30$ cm	211
Fig. 6.32	Curvature for 3D FEM analysis	211
Fig. 6.33	Load-settlement curves with column curvature from 3D FEM analysis for $B = 30$ cm	212
Fig. 6.34	Vertical stress in the curved column from 3D FEM analysis for $B = 30$ cm (in Plaxis: compression negative)	213
Fig. 6.35	Load eccentricity for analytical study	214
Fig. 6.36	Load eccentricity for 3D FEM analysis	215
Fig. 6.37	Load-settlement curves with load eccentricity from 3D FEM analysis for $B = 30$ cm	216
Fig. 6.38	Vertical stress at the top of the eccentric-loaded column from 3D FEM analysis for $B = 30$ cm (in Plaxis: compression negative)	216
Fig. A.1	Compression uni-axial test on elastic material (Combarieu 2006)	262
Fig. A.2	Compression tri-axial test on elastic material and on soil (Briaud 2000)	263
Fig. A.3	Different slopes in stress-strain curve, adapted from (Briaud 2000)	264
Fig. A.4	Modulus vs. amplitude of deformations (Ménard 1961)	265
Fig. A.5	Different initial slopes for different confinement level in tri-axial tests (Katzenbach, lecture notes 2015)	266
Fig. A.6	Shear modulus depending on shear strain and loading direction in hypoplastic model (Kudella and Reul 2002)	267
Fig. A.7	Oedometer test (Katzenbach, lecture notes 2015)	267
Fig. A.8	Deformation of soil element under large and limited loading area (Baguelin et al. 1978)	268
Fig. A.9	Stress-strain curve in oedometer test (non-linearity)	269
Fig. A.10	Influence of the nature of stress field on stress-strain relationship (Ménard 1961)	269
Fig. A.11	Void ratio vs. applied stress in logarithmic scale curve in oedometer test (adapted from Combarieu 2006)	270
Fig. A.12	Load distribution and segmentation for oedometric settlement method under shallow foundations (Philipponnat and Hubert 2000)	271
Fig. A.13	Corrective factor μ to take into account the tridimensional effects after Skempton and Bjerrum (1957), cited by Frank (1999)	272
Fig. A.14	Plate load test – Westergaard type (Cassan 1988)	274
Fig. A.15	Basic pressuremeter unit (Baguelin et al. 1978)	276

Fig. A.16	Pressuremeter testing on test field of Navier-Géotechnique (Cermes) in Lognes, France	276
Fig. A.17	Main components of a pressuremeter unit (Gambin 2005)	277
Fig. A.18	Shape of a pressuremeter curve (Cassan 1988)	277
Fig. A.19	Corrected pressuremeter curves with different phases (Ménard and Rousseau 1962)	279
Fig. A.20	Ratio between oedometer modulus and dynamic modulus (Smolczyk 2001)	279
Fig. A.21	Deformation of an initial square ring element for the cylindrical cavity expansion (Baguelin et al. 1978)	280
Fig. A.22	Distortion in simple-shear test (Combarieu 2006)	280
Fig. A.23	Evolution of shear modulus with distortion (Combarieu 2006)	281
Fig. A.24	Circular foundation with zone of spherical and deviatoric stresses (Ménard and Rousseau 1962)	286
Fig. A.25	Increase of the settlement in case of small embedment (Baguelin et al. 1978)	288
Fig. A.26	Subdivision in layers of thickness $B/2$ for equivalent modulus	289
Fig. A.27	Stress and strains along a vertical axis under a rigid circular foundation (elastic) (Baguelin et al. 1978)	290
Fig. A.28	Original transfer functions by Frank and Zhao for skin friction (top) and tip resistance (bottom) for fine-grained soils (Frank and Zhao 1982) and (Frank 1985)	291
Fig. B.1	Failure mechanism under a shallow foundation after Prandtl (Frank 1999)	293
Fig. B.2	Possible failure mechanism under a pile foundation for the methods based on soil shear parameters (Frank 1999)	294
Fig. B.3	Example of a tip of a CPT testing probe after EN ISO 22476-1 (2012)	295
Fig. B.4	1) Pressuremeter curve, 2) Creep pressuremeter curve (Gambin 2005)	297
Fig. B.5	Example of creep pressuremeter curve (Baguelin et al. 1978)	297
Fig. B.6	Constitutive models for soils -1) real elastic-plastic response, 2) elastic response without failure, 3) plastic rigid response, 4) simplified elastic-plastic model (Gambin 1979)	299
Fig. B.7	Different mobilisation levels of soil strength around foundation base (Ménard 1963a)	300
Fig. B.8	Distribution of stress isostatic lines around foundation base (Ménard 1963)	300
Fig. B.9	Bearing capacity versus depth of embedment (Ménard 1963a)	301
Fig. B.10	Plastic failure zones under shallow and deep foundation (Gambin 1979)	302
Fig. C.1	Measurements of E_M , p_1 and q_c for sand by Nazaret (Baguelin et al. 1978)	305

Fig. C.2	Ratio k_q between q_c and p_{LS} for sands of different densities ID^* (Cudmani and Osinov 2001)	306
Fig. C.3	p_{LC} ($= p_l$) and p_{LS} for different sands, different p_0 and different ID (Cudmani 2001)	307
Fig. C.4	Correlation between q_c (CPT), p_l (PMT) and N (SPT) (Bustamante and Ganeselli 2006)	308
Fig. C.5	Roberston's diagrams after NF P94-261 (2013)	312
Fig. C.6	Estimation of equivalent Young's modulus for sand based on degree of loading (Lunne et al. 1997)	313

List of tables

Table 2.1	Indicative values for bearing capacity of shallow foundations in coarse-grained soils in Germany translated from DIN 1054 (2010)	5
Table 2.2	Indicative values for bearing capacity of shallow foundations in clay in Germany translated from DIN 1054 (2010)	6
Table 2.3	Table for factor k_p for bearing capacity of shallow foundations translated from NF P94-261 (2013)	9
Table 2.4	Rheological factor α for different soil types and different ranges of E_M/p_1 translated from NF P94-261 (2013)	10
Table 2.5	Shape factors λ_c and λ_d for different soil types and different ranges of E_M/p_1 translated from NF P94-261 (2013)	11
Table 2.6	Tip resistance for bored piles in coarse-grained soils translated from EA-Pfähle (DGGT 2012)	14
Table 2.7	Tip resistance for bored piles in fine-grained soils translated from EA-Pfähle (DGGT 2012)	14
Table 2.8	Ultimate skin friction for bored piles in coarse-grained soils translated from EA-Pfähle (DGGT 2012)	14
Table 2.9	Ultimate skin friction for bored piles in fine-grained soils translated from EA-Pfähle (DGGT 2012)	15
Table 2.10	Ultimate skin friction for bored piles in rock translated from EA-Pfähle (DGGT 2012)	15
Table 2.11	Definition of classes of piles translated from NF P94-262 (2012)	17
Table 2.12	Table for k_{pmax} factor for pile base resistance translated from NF P94-262 (2012)	18
Table 2.13	Table of factor $\alpha_{pieu-sol}$ for ultimate skin friction translated from NF P94-262 (2012)	19
Table 2.14	Summary of prevalent settlement calculation methods for stone columns (Kirsch 2004)	66
Table 2.15	Chart of safety checks after ASIRI (IREX 2012)	69
Table 2.16	Partial resistance safety factors – ASIRI ULS-GEO	70
Table 2.17	Partial resistance safety factors – Eurocode 7 ULS-GEO	70
Table 2.18	Partial resistance safety factors – CPRF and CSV-guidelines ULS-GEO	71
Table 2.19	Partial resistance safety factors – ASIRI SLS-GEO	72
Table 2.20	Partial resistance safety factors – Eurocode 7 SLS-GEO	72
Table 2.21	Partial resistance safety factors – CPRF and CSV-guidelines SLS-GEO	72
Table 3.1	Example site: comparison of settlement calculation methods for shallow foundations and modulus calibration	76
Table 4.1	Instrumented pile load tests	85

Table 4.2	Pile load tests used for checking of developed load transfer curves (mainly non-instrumented)	85
Table 4.3	Comparison of calculation methods and oedometer modulus ranges from usual correlations for different foundation types in clay and sand	87
Table 4.4	Results of PMT and of CPT near the Ifsttar 35 B test pile	94
Table 4.5	Definition of the main simple load transfer curves (1/2)	99
Table 4.6	Definition of the main simple load transfer curves (continued, 2/2)	100
Table 4.7	Proposed cubic root load transfer curves	106
Table 4.8	Proposed hyperbolic load transfer curves	109
Table 4.9	Example of a single pile analysis with test Ifsttar 1-A1 under a given load with the LTM: input parameters	113
Table 5.1	LTM parameters for infinite grid system of the ASIRI field test	126
Table 5.2	Comparison of measurements with predictions for the ASIRI field test	129
Table 5.3	LTM parameters for CPRF with rigid footing field test in Merville after FONMIX calculation by Borel (2001)	139
Table 5.4	LTM parameters for CPRF Westend 1 as infinite rigid slab	148
Table 5.5	Comparison of measurements with predictions for the CPRF Westend 1	151
Table 5.6	LTM parameters for CPRF case	168
Table 5.7	LTM parameters for RI case	178
Table 6.1	Stress level at the corner of the necking for different planned diameters and necking position from axisymmetric FEM analysis	199
Table 6.2	Stresses at the edge of the column section for different diameters, settlement levels and inclination imperfections from 3D FEM analysis	208
Table 6.3	Stresses at the edge of the column section for different diameters, settlement levels and curvatures from 3D FEM analysis	213
Table 6.4	Stresses at the edge of the column section for different diameters, settlement levels and load eccentricities from 3D FEM analysis	217
Table 6.5	Influence of column material type and modulus according to the present study and to the published results	218
Table 6.6	Existing tolerances and recommendations for geometrical imperfections	220
Table A.1	Usual values of E_M for different types of soils (Techniques Louis Ménard 1975)	282
Table A.2	Rheological factor α for various soils (Baguelin et al. 1978)	284
Table B.1	Usual values of p_1 for different types of soils (Ménard 1975)	298
Table C.1	Ratio spans q_c/p_1 for clay, silt and sand (Techniques Louis Ménard 1975)	304
Table C.2	Correlations between PMT and CPT parameters (Cassan 1988)	305
Table C.3	q_c^*/p_1^* for different soil types according to Baguelin et al. (1978) in (Hamidi et al. 2011)	308

Table C.4	Correlations between PMT and CPT according to Briaud et al. (1985) in (Hamidi et al. 2011)	308
Table C.5	Correlations between usual in situ parameters (internal document Keller France)	309
Table C.6	Indicative ratio α to determine the oedometric modulus E_{oed} from the cone resistance q_c after EN 1997-2 (2007-2010) (based on Sanglerat 1972)	310
Table C.7	Indicative correlations values $\alpha_{\text{footing}} = E/E_M$ for a single footing loading case under serviceability loads from NF P94-261 (2013)	314
Table C.8	Comparison of moduli for equality of Ménard settlement method and elastic method (Combarieu 2006)	315

List of symbols and abbreviations

Abbreviations

CPRF	combined pile-raft foundation
CPT	cone penetration test
FEM	finite element method
LTP	load transfer platform
LTM	load transfer method
PMT	pressuremeter test
RI	rigid inclusion system
SLS	serviceability limit state in EN 1997-1 (2004-2009-2013)
ULS	ultimate limit state in EN 1997-1 (2004-2009-2013)

Symbols

Symbols defined differently or used only very locally (in particular from the literature) are defined in the text.

A	foundation surface
A_b	pile tip surface
B	foundation width (for piles: pile diameter)
B_0	reference foundation width in NF P94-261 (2013)
c	soil cohesion
c_u	undrained shear strength
C_C	compression index in oedometer test
C_S	swelling index in oedometer test
D	foundation embedment (for piles: pile length)
e	eccentricity (alternatively: void ratio)
E	Young's modulus
E^*	calculation modulus after DIN 4019 (2015) (alternatively: equivalent oedometric modulus in ASIRI, IREX 2012)
E_c	pressuremeter modulus of first layer under the foundation in pressuremeter theory
E_d	weighted pressuremeter modulus of layers under the foundation in pressuremeter theory
E_{oed}	constrained modulus (oedometer modulus)
E_M	pressuremeter modulus
E_{ur}	unloading/reloading modulus at strains of 10^{-3} to 10^{-2} in Hardening Soil Model (Plaxis 2013, Plaxis 2014)

E_v	plate load test modulus
E_{50}	secant modulus in tri-axial test in Hardening Soil Model (Plaxis 2013, Plaxis 2014)
f_c	concrete compressive strength in EN 1992-1-1 (2004-2010)
F_c	axial compression load on a pile in EN 1997-1 (2004-2009-2013)
G	shear modulus
h or H	layer thickness
k_c	cone penetration bearing factor in NF P94-261 (2013) and in NF P94-262 (2012)
k_p	pressuremeter bearing factor in NF P94-261 (2013) and in NF P94-262 (2012)
K_0	earth pressure at rest
L	foundation length
lm	linear meter (or running meter)
m	exponent for soil modulus definition in Hardening Soil Model (Plaxis 2013, Plaxis 2014)
M_s	stiffness parameter of skin friction hyperbolic load transfer curve
M_b	stiffness parameter of tip resistance hyperbolic load transfer curve
p'	mean effective stress
p_l	limit pressure in pressuremeter test
p_{ref}	reference stress for soil modulus definition in Hardening Soil Model (Plaxis 2013, Plaxis 2014)
q	deviatoric stress
q_b	mobilised tip resistance (alternatively: ultimate tip resistance in EN 1997-1 2004-2009-2013)
q_c	cone resistance from cone penetration test
q_{net}	net bearing pressure resistance in NF P94-261 (2013)
q_s	mobilised skin friction (alternatively: ultimate skin friction in EN 1997-1 2004-2009-2013)
$q_{b,ult}$	ultimate pile tip resistance
$q_{s,ult}$	ultimate pile skin friction
Q	footing load
Q_{ult}	footing ultimate load
R_0	soil weight over the foundation area between the original ground level and the foundation level in NF P94-261 (2013)
r	radius
R	bearing resistance in EN 1997-1 (2004-2009-2013)
R_c	compressive ultimate pile resistance in EN 1997-1 (2004-2009-2013)
R_v	net bearing resistance in NF P94-261 (2013)
s	settlement

S_b	pile tip settlement minus soil settlement in absence of the pile
$S_{b,lim}$	limit settlement for tip resistance cubic root curve
S_c	spherical component of the footing settlement in pressuremeter theory
S_d	deviatoric component of the footing settlement in pressuremeter theory
S_s	pile shaft settlement minus soil settlement in absence of the pile
S_{sg}	limit settlement in EA-Pfähle (DGGT 2012)
S_{soil}	soil settlement
$S_{s,lim}$	limit settlement for skin friction cubic root curve
V	vertical load on a foundation in EN 1997-1 (2004-2009-2013)
z	depth
α	structural or rheological factor in pressuremeter theory (alternatively: cone penetration test correlation factor in EN 1997-2 2007-2010)
$\alpha_{footing}$	correlation factor between pressuremeter modulus and Young's modulus for footing loading case
α_{pr}	pile-raft coefficient in CPRF-guideline (Katzenbach and Choudhury 2013)
ε	strain
φ	soil friction angle (alternatively: concrete creep factor in EN 1997-1 2004-2009-2013)
γ	unit weight (alternatively: distortion)
γ_b	partial factor for pile base (or tip) resistance in EN 1997-1 (2004-2009-2013)
γ_F	partial factor for an action in EN 1997-1 (2004-2009-2013)
γ_G	partial factor for a permanent action in EN 1997-1 (2004-2009-2013)
γ_Q	partial factor for a variable action in EN 1997-1 (2004-2009-2013)
$\gamma_{R;v}$	partial factor for bearing resistance in EN 1997-1 (2004-2009-2013)
$\gamma_{R;d;v}$	model factor for bearing resistance in NF P94-261 (2013)
$\gamma_{R;d1}$	first model factor for pile resistance in NF P94-262 (2012)
$\gamma_{R;d2}$	first model factor for pile resistance in NF P94-262 (2012)
γ_s	partial factor for pile shaft (or skin) friction resistance in EN 1997-1 (2004-2009-2013)
λ_{exp}	calibration parameter of exponential footing mobilisation curve
λ_{hyp}	calibration parameter of hyperbolic footing mobilisation curve
ν	Poisson's ratio
ψ	dilatancy

σ	stress
σ_R	bearing pressure resistance in DIN 1054 (2010)
τ	mobilised skin friction in NF P94-262 (2012)

1 Introduction

For given load levels, shallow foundations are acceptable foundations only for soils with sufficient stiffness and bearing capacity. If the load from the structures would lead to a ground failure or to excessive settlements, the use of deep foundations or soil reinforcements is required. Different systems can be used, like usual pile foundations, combined systems like combined pile-raft foundations (CPRF) and rigid inclusion systems (RI) as in Fig. 1.1, or other soil reinforcement systems like stone columns. Rigid inclusions represent the latest technique in which rigid columns, with relatively small diameter and often without steel reinforcement, are separated from the structure by the use of a load transfer platform (LTP) or load transfer layer (Fig. 1.1). In the recent years, calculation methods and safety concepts have been developed and actively used specifically in France for rigid inclusions, based mainly on the soil modulus measured with the pressuremeter test (PMT) which is the most widespread soil test in the country. For the calculation using the load transfer method (LTM), the pressuremeter test can easily provide the necessary load transfer curves. Furthermore, the load transfer method is particularly adequate to model the interactions in such systems and to allow a straightforward analysis. This explains why this method is well-established in France today for rigid inclusion analyses.

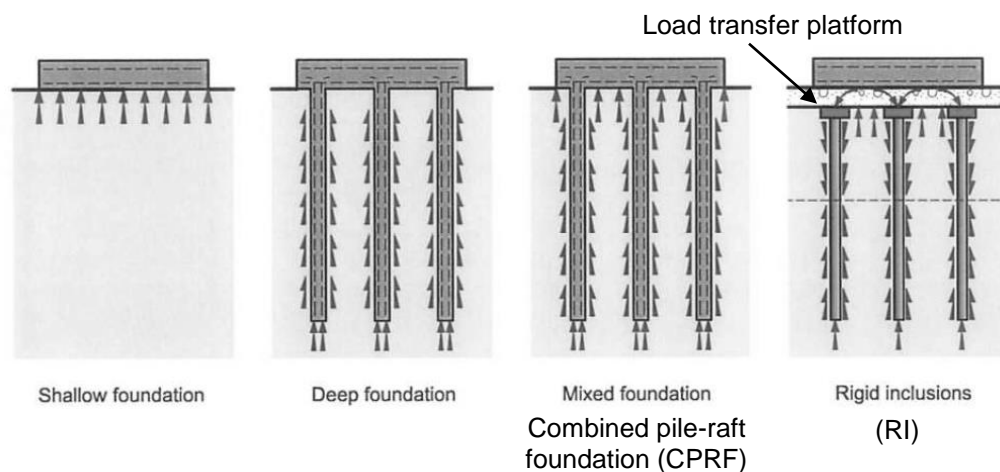


Fig. 1.1 Rigid inclusion (RI) system in comparison with usual foundation systems from ASIRI (IREX 2012)

The common pile foundation design relies on an estimation of the ultimate load and on an application of safety factors in order to guarantee allowable displacements. But if group effects occur, if the soil between the piles contributes to the load transfer mechanism or if a load transfer platform (LTP) separates the structure from the

foundation, allowable displacements cannot in general be ensured by a single safety check on the bearing capacity. A detailed study of the interactions in such combined systems is necessary. Furthermore, the development of numerical methods, like the finite element method (FEM) and the load transfer method (LTM) allows for reliable calculations of the displacements. A realistic determination of the whole non-linear load-displacement behaviour of a system gives indeed a full description of both its serviceability and safety. This trend is clearly suggested in the current European standard for foundation design, the Eurocode 7 (EN 1997-1 2004-2009-2013).

The design of combined foundation systems is not directly covered by the Eurocode 7 and is a matter of local practice and local recommendations developed in compatibility with the Eurocode 7. Currently, well-proven accurate calculation methods and recommendations for safety concepts for combined systems are established in practice only in limited world regions. For example, the CPRF-guideline (Hanisch et al. 2002, Katzenbach and Choudhury 2013) has obtained a wide application in Germany, and the ASIRI recommendations (IREX 2012) for rigid inclusions (RI) are widely used in France.

The goals of the present work are the following:

- unifying and developing displacement-based calculation methods for combined foundation systems under vertical loads, while still allowing for the local ground particularities and the local common usage;
- proposing load transfer curves for the use of the load transfer method (LTM) for combined foundation systems under vertical loads for the cases where no pressuremeter test results are available;
- highlighting the governing mechanisms and interactions in rigid inclusion systems (RI) under vertical loads, in particular by examining the transition to combined pile-raft foundation systems (CPRF);
- identifying the possible particularities of small-diameter rigid columns in terms of sensitivity to material and geometrical imperfections of execution, as a prerequisite for the serviceability and safety of such systems.

In section 2, a detailed state of the art about the design of conventional shallow and pile foundations and of combined systems is presented. The principles in terms of load bearing and settlement behaviour of combined systems are described together with the main calculation methods. The focus is put on the local French and German practices and on the use of in situ ground tests. In this regard, the French particularity of the use

of the pressuremeter test (PMT) and the methods based on the cone penetration test (CPT), widely used in Europe, are considered. The choice of the soil parameters based on ground test results, in particular the soil deformation parameters, is indeed the most decisive aspect in foundation design. The existing safety concepts for combined systems and conventional foundations are then compared.

As a first step in the investigation of the behaviour of combined systems, the settlement behaviour of shallow foundations and of deep foundations are studied separately, in sections 3 and 4 respectively. For shallow foundations, the usual existing correlations for soil moduli are compared and the non-linear settlement behaviour is investigated. The application of the axisymmetric finite element method (FEM) and of the load transfer method (LTM) for the modelling of the non-linear pile load-settlement behaviour is developed considering a database of pile load tests. The focus is set on the development of new load transfer curves for the load transfer method (LTM). The LTM is considered here as a straightforward method for foundation engineering practice for relatively simple foundation cases, and a very accurate one if the load transfer curves used are validated empirically.

Section 5 applies the results of the previous sections for the analysis of combined systems with the load transfer method (LTM). The load-settlement behaviours of combined pile-raft foundations (CPRF) and rigid inclusions (RI) are examined and compared based on reference cases with measurements. A theoretical example of a footing with columns is then studied in order to compare 3D finite element calculations with the load transfer method proposed.

In the section 6, use is made of the potentiality of the finite element method (FEM) in terms of geometry and of analysis of results, in order to investigate the sensitivity of unreinforced concrete columns with small diameter. Simple analytical calculations are made for comparison purposes. The effect of variations in the column material, in particular on the load distribution between the column and the soil, is studied in a unit cell case with a load transfer platform (LTP). The effect of diameter changes, of inclination, of curvature and of load eccentricity are analysed on a single column case. The results are extended to combined system cases. Recommendations are made in order to increase the safety by a more careful execution considering the decisive parameters.

Finally, the main results are drawn, as well as possible perspectives.

2 State of the art and literature analysis

2.1 Design of shallow foundations according to Eurocode 7

2.1.1 Current practice in Germany

The current standard in Germany for the design of shallow foundations is the Eurocode 7, made of the general European text EN 1997-1 (2004-2009-2013), as the German version DIN EN 1997-1 (2014), the national appendix for Germany DIN EN 1997-1/NA (2010) and the supplementary German application standard DIN 1054 (2010). There are several additional German standards such as DIN 4017 (2006) and DIN 4019 (2015) for shallow foundations.

2.1.1.1 Bearing capacity

The general inequality between the design vertical load V_d and the design value of the bearing capacity R_d according to DIN EN 1997-1 (2014) is given in (Eq. 2.1).

$$V_d \leq R_d \quad (\text{Eq. 2.1})$$

The design load calculation is shown in (Eq. 2.2) according to DIN EN 1997-1 (2014). The partial safety factor γ_F for unfavourable actions on foundations in the persistent load situation is equal to 1.35 (called γ_G) or 1.5 (called γ_Q) for permanent and variable loads respectively (DIN 1054 2010).

$$V_d = \gamma_F \cdot V_k \quad (\text{Eq. 2.2})$$

The design value of the resistance against base failure is calculated from the characteristic resistance denoted $R_{n,k}$ as in (Eq. 2.3) (DIN 1054 2010).

$$R_d = \frac{R_{n,k}}{\gamma_{R,v}} \quad (\text{Eq. 2.3})$$

The safety factor against base failure $\gamma_{R,v}$ on the resistance side in the permanent load situation (called “BS-P” in Germany) in ultimate limit state (ULS) is equal to 1.4, and no model factor is applied.

In DIN 1054 (2010), reference is made to the German standard DIN 4017 (2006) for the detailed calculation of the bearing capacity of shallow foundations with limited dimensions. The bearing capacity R_n is generally calculated based on the theory with laboratory parameters presented in Appendix B.1, using terms depending on the width of the foundation, on its embedment and on the cohesion of the soil (Eq. 2.4). N_b , N_d and N_c are factors representing the footing width, embedment and the soil cohesion. a' and b' are the footing width and length (corrected to consider possible load eccentricity) and d is the footing embedment. c is the soil cohesion, and γ_1 and γ_2 are the soil unit weight above and below the footing bottom level.

$$R_n = a' \cdot b' \cdot (\gamma_2 \cdot b' \cdot N_b + \gamma_1 \cdot d \cdot N_d + c \cdot N_c) \quad (\text{Eq. 2.4})$$

Another method with indicative design pressure values is allowed for simple usual cases (criteria among others: horizontal foundation base, static load, small load inclination etc.). A minimum density and a minimum cone resistance from a CPT q_c are required for coarse-grained soils for the application of this method (Table 2.1). This method is however in contradiction with statements of Briaud (2003a, 2007) who shows that the footing dimensions have no influence on the ultimate area load if the soil resistance remains approximately constant in the influence zone under the footing.

Table 2.1 Indicative values for bearing capacity of shallow foundations in coarse-grained soils in Germany translated from DIN 1054 (2010)

Smallest embedment depth of the foundation (m)	Design bearing pressure $\sigma_{R,d}$ b or b' (kN/m ²)					
	0.50 m	1.00 m	1.50 m	2.00 m	2.50 m	3.00 m
0.50	280	420	560	700	700	700
1.00	380	520	660	800	800	800
1.50	480	620	760	900	900	900
2.00	560	700	840	980	980	980
for structures with embedment depths $0.30 \text{ m} \leq d \leq 0.50 \text{ m}$ and with foundation widths $b \text{ or } b' \geq 0.30 \text{ m}$	210					

Analogously, indicative values are given for fine-grained soils, with different tables for pure silt, well-graded soils, silty clay and pure clay. As an example, values for clay are given in Table 2.2.

Table 2.2 Indicative values for bearing capacity of shallow foundations in clay in Germany translated from DIN 1054 (2010)

Smallest embedment depth of the foundation (m)	Design bearing pressure $\sigma_{R,d}$ b or b' (kN/m ²)		
	Average consistency		
	stiff	very stiff	hard
0.50	130	200	280
1.00	150	250	340
1.50	180	290	380
2.00	210	320	420
mean unconfined compression strength $q_{u,k}$ (kN/m ²)	120 to 300	300 to 700	> 700

2.1.1.2 Settlement

In DIN 1054 (2010), reference is made to the German standard DIN 4019 (2015) for the calculation of settlement of shallow foundations. The usual method standardized and used in Germany is the extended oedometric method; that means not only for widespread loads, but also for small shallow foundations. Here the oedometric modulus E_{oed} is in general used, called there E_S (“Steifemodul”) and considered as the reference deformation parameter for all soils types and loading cases in Germany. However, in DIN 4019 (2015), the modulus to be used is called more generally “calculation modulus” E^* based on experience, recalling the modulus dependency among others on the loading type and on the load level. Some correlations are sometimes used to determine $M = E_{oed}$ from CPTs, in particular for coarse-grained soils (see Appendix C.2).

2.1.2 Current practice in France

The current geotechnical standard in France is the Eurocode 7 EN 1997-1 (2004-2009-2013), as French version NF EN 1997-1 (2014), with the French national appendix NF EN 1997-1/NA (2006) and with the national application standard for shallow foundations NF P94-261 (2013). The design theories from the previous French standards with the preferred use of the pressuremeter method have been considered in these standards (Frank 2009, Frank 2010).

2.1.2.1 Bearing capacity

The general inequality between the design vertical load V_d and the design value of the bearing capacity $R_{v,d}$ after NF EN 1997-1 (2014) and NF P94-261 (2013) is given in (Eq. 2.5). R_0 is the soil weight over the foundation area between the original ground level and the foundation level.

$$V_d - R_0 \leq R_{v,d} \quad (\text{Eq. 2.5})$$

The design load calculation is shown in (Eq. 2.6) according to NF EN 1997-1 (2014). The partial safety factor γ_F for unfavourable actions on foundations in the persistent load situation is equal to 1.35 (called γ_G) or 1.5 (called γ_Q) for permanent and variable loads respectively (NF P94-261 2013).

$$V_d = \gamma_F \cdot V_k \quad (\text{Eq. 2.6})$$

The design value of the net resistance against base failure $R_{v,d}$ is calculated from the characteristic resistance denoted $R_{n,k}$ as in (Eq. 2.7) (NF P94-261 2013).

$$R_{v,d} = \frac{R_{v;k}}{\gamma_{R,v}} \quad (\text{Eq. 2.7})$$

The safety factor against base failure on the resistance side in the permanent load situation in ultimate limit state (ULS) $\gamma_{R,v}$ is equal to 1.4 (NF P94-261 2013), and a model factor depending on the method used is considered additionally.

Different methods are mentioned in the application text in France: the semi-empirical methods using results from pressuremeter or from CPTs (as normative annexes), and the analytical method based on the shear parameter of soils (as an informative annex) as described in Appendix B.1. But the most established and usual in France is the pressuremeter method based on the theory described in Appendix B.3. The method based on CPT results works with the same calculation principle (see Appendix B.2).

The net ultimate bearing capacity in terms of pressure is denoted q_{net} here. The characteristic bearing capacity is calculated with a model factor $\gamma_{R;d,v}$ equal to 1.2 for the pressuremeter method (Eq. 2.8), A' being the effective area of the spread foundation (NF P94-261 2013).

$$R_{v;k} = \frac{A' \cdot q_{net}}{\gamma_{R;d;v}} \quad (\text{Eq. 2.8})$$

The ultimate bearing pressure is calculated as in (Eq. 2.9). The factor i_δ is a reduction coefficient for load inclination, and the factor i_β is a reduction coefficient in the case of the proximity of a slope. In case of a vertical load without slope, all of the reduction factors are equal to 1.0. p_{le}^* is the equivalent limit pressure as the geometrical mean over a depth of 1.5 times the width of the foundation (Eq. 2.10). k_p (Eq. 2.11) is the factor of bearing capacity depending on the equivalent embedment D_e (mean value of the limit pressures above the foundation base divided by p_{le}^*) for $D_e/B \leq 2$, on the width B , of the length L of the foundation and of the type of soil (a, b and c in Table 2.3). For rectangular footings, k_p is calculated with interpolation between the values for the square and strip footing cases, considering that $B/L = 0$ for strip footings and $B/L = 1$ for square footings (Eq. 2.12). The calculated bearing pressure does not depend on the shallow foundation width and length in accordance with Briaud (2003a, 2007).

$$q_{net} = k_p \cdot p_{le}^* \cdot i_\delta \cdot i_\beta \quad (\text{Eq. 2.9})$$

$$p_{le}^* = \sqrt[n]{\prod_{i=1}^n p_{l;k;i}^*} \quad (\text{Eq. 2.10})$$

$$k_{p;\frac{B}{L}} = k_{p0} + \left(a + b \cdot \frac{D_e}{B} \right) \cdot \left(1 - e^{-c \cdot \frac{D_e}{B}} \right) \quad (\text{Eq. 2.11})$$

$$k_{p;\frac{B}{L}} = k_{p;\frac{B}{L}=0} \cdot \left(1 - \frac{B}{L} \right) + k_{p;\frac{B}{L}=1} \cdot \frac{B}{L} \quad (\text{Eq. 2.12})$$

Table 2.3 Table for factor k_p for bearing capacity of shallow foundations translated from NF P94-261 (2013)

Soil category – curve for variation of factor of bearing capacity		Expression of k_p			
		a	b	c	k_{p0}
Clay and silt	Strip footing – Q1	0.2	0.02	1.3	0.8
	Square footing – Q2	0.3	0.02	1.5	0.8
Sand and gravel	Strip footing – Q3	0.3	0.05	2	1
	Square footing – Q4	0.22	0.18	5	1
Chalk	Strip footing – Q5	0.28	0.22	2.8	0.8
	Square footing – Q6	0.35	0.31	3	0.8
Marl and altered rock	Strip footing – Q7	0.2	0.2	3	0.8
	Square footing – Q8	0.2	0.3	3	0.8

All those formulas are summarized and extended for all values of D_e/B in form of a diagram with different curves for different soil types and dimensions of the foundation (Fig. 2.1).

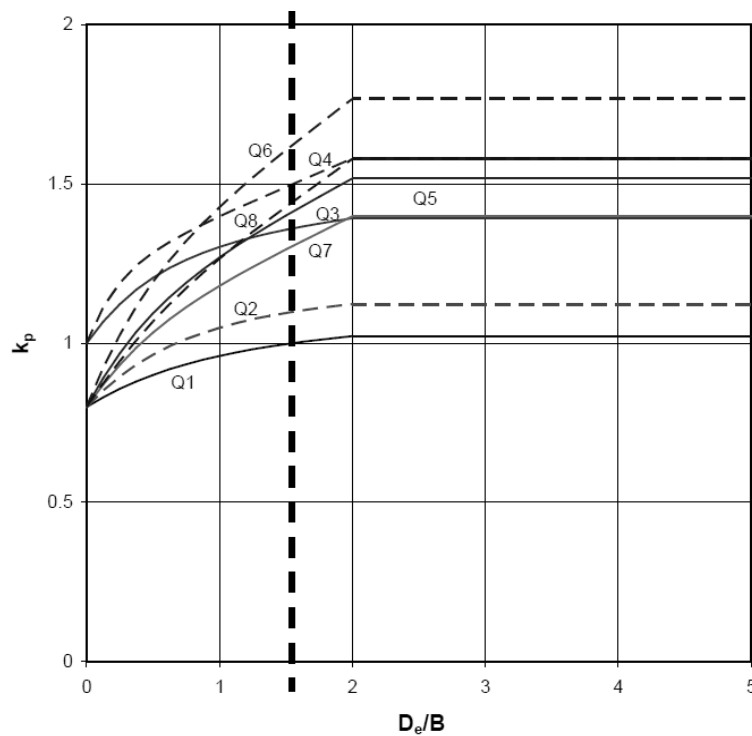


Fig. 2.1 Diagrams for factor k_p for bearing capacity of shallow foundations after NF P94-261 (2013)

2.1.2.2 Settlement

The method proposed is in particular relevant for single footings (relatively small shallow foundations). It does not concern very large raft foundations, for which the oedometric method is more appropriate and preferred in France (Combarieu 2006).

The expressions for the spherical (Eq. 2.13) and deviatoric (Eq. 2.14) parts correspond to those proposed by Ménard in the 1960's, q' being the area load from the structure and σ'_{v0} the initial effective stress at the level of the foundation base, and B_0 a reference width of 0.6 m.

$$s_c = \frac{\alpha}{9 \cdot E_c} \cdot (q' - \sigma'_{v0}) \cdot \lambda_c \cdot B \quad (\text{Eq. 2.13})$$

$$s_d = \frac{2}{9 \cdot E_d} \cdot (q' - \sigma'_{v0}) \cdot B_0 \cdot \left(\lambda_d \cdot \frac{B}{B_0} \right)^\alpha \quad (\text{Eq. 2.14})$$

E_c is equal to the pressuremeter modulus of the first layer under the foundation, and E_d takes into account the moduli in depth with the weighting according to Fig. A.26 and (Eq. A.35) in Appendix A.4.

The rheological or structural factor α is given for different soil types and for different ranges of the ratio E_M/p_1 (Table 2.4). The factors λ_c and λ_d depend strictly on the form and on the relative dimensions of the foundation (Table 2.5).

Table 2.4 Rheological factor α for different soil types and different ranges of E_M/p_1 translated from NF P94-261 (2013)

Type	Peat		Clay		Silt		Sand		Gravel	
	α	E_M/p_1	α	E_M/p_1	α	E_M/p_1	α	E_M/p_1	E_M/p_1	α
overconsolidated or very dense	–	> 16	1	> 14	2/3	> 12	1/2	> 10	1/3	
normally consolidated or normally dense	1	9 to 16	2/3	8 to 14	1/2	7 to 12	1/3	6 to 10	1/4	
overconsolidated, altered, disturbed or loose	1	7 to 9	1/2	5 to 8	1/2	5 to 7	1/3	–	–	

Table 2.5 Shape factors λ_c and λ_d for different soil types and different ranges of E_M/p_l translated from NF P94-261 (2013)

L/B	Circle	Square	2	3	5	≥ 20
λ_c	1.00	1.10	1.20	1.30	1.40	1.50
λ_d	1.00	1.12	1.20	1.78	2.14	2.65

No increase of the settlement is imposed in the standard in case of a small embedment, unlikely to the first recommendations of Ménard (see Fig. A.25 in Appendix A.4).

2.2 Design of pile foundations according to Eurocode 7

2.2.1 Current practice in Germany

Pile foundations are subjected to the German version of the Eurocode 7 (DIN EN 1997-1 2014 as German version of EN 1997-1 2004, DIN EN 1997-1/NA 2010, DIN 1054 2010). Apart from the use of numerical continuum methods, the pile bearing capacity and if necessary the pile settlement are determined in Germany after the empirical method from the EA-Pfähle (DGGT 2012) which are recommendations referred to by DIN 1054 (2010).

The general inequality between the design axial load $F_{c;d}$ and the design value of the bearing capacity $R_{c;d}$ after DIN EN 1997-1 (2014) is given in (Eq. 2.15).

$$F_{c;d} \leq R_{c;d} \quad (\text{Eq. 2.15})$$

The design load calculation is shown in (Eq. 2.16) according to DIN EN 1997-1 (2014). The partial safety factor γ_F for unfavourable actions on foundations in the persistent load situation is equal to 1.35 (called γ_G) or 1.5 (called γ_Q) for permanent and variable loads respectively (DIN 1054 2010).

$$F_{c;d} = \gamma_F \cdot F_{c;k} \quad (\text{Eq. 2.16})$$

For the simplified methods using correlations from CPT, the design value of the pile resistance is calculated as in (Eq. 2.17) (DIN EN 1997-1 2014). The safety factor for

resistance is denoted generally γ_R in the Eurocode 7. For pile resistance specifically, the safety factors are called γ_b and γ_s .

$$R_{c;d} = \frac{R_{b;k}}{\gamma_b} + \frac{R_{s;k}}{\gamma_s} \quad (\text{Eq. 2.17})$$

The characteristic total ultimate skin friction $R_{s;k}$ (perimeter P_s) and the total ultimate tip resistance $R_{b;k}$ (pile tip area A_b) are calculated as in (Eq. 2.18) and (Eq. 2.19).

$$R_{b;k} = A_b \cdot q_{b;k} \quad (q_{b;k}: \text{ultimate tip resistance pressure}) \quad (\text{Eq. 2.18})$$

$$R_{s;k} = \int_0^D P_s(z) \cdot q_{s;k}(z) \cdot dz \quad (q_{s;k}: \text{ultimate unit skin friction}) \quad (\text{Eq. 2.19})$$

The safety factors for pile resistance in the permanent load situation in ultimate limit state (ULS) in case of the use of these guide values are $\gamma_b = \gamma_s = 1.4$ for compression piles (and 1.5 for tension piles) in Germany, and no model factors are applied. As a comparison, the safety factors in the case with pile loading tests are $\gamma_b = \gamma_s = 1.1$ for compression piles (and 1.15 for tension piles).

The bearing capacity and the settlement of piles are presented together as a whole in EA-Pfähle (DGGT 2012). Ultimate values for the tip resistance and the skin friction and load-settlement curves are proposed as empirical results for the major pile types:

- prefabricated driven piles and site concrete driven piles;
- bored piles and partial displacement piles;
- screw piles (full displacement piles);
- injected mortar piles, vibro-injected piles and micropiles (here no load-settlement curve given).

The limit values are given as a function of the cone resistance from CPTs q_c in the case of coarse-grained soils, and as a function of the undrained shear strength c_u in the case of fine-grained soils. It can be assumed that the undrained shear strength c_u is determined either from laboratory tests or using correlations with the cone resistance q_c . The ultimate values are proposed for given values of q_c or c_u and a linear interpolation between these values is allowed.

As an example, the values for bored piles are presented here. The load-settlement curve is in general calculated for a pile as a whole. The total forces corresponding to the tip resistance and to the total skin friction for all layers are presented together over the pile depth (Fig. 2.2). A separated representation of the mobilisation of skin friction in terms of stresses for each layer is not a common practice in Germany. The shortening of the pile itself can thus not be taken into account with this method.

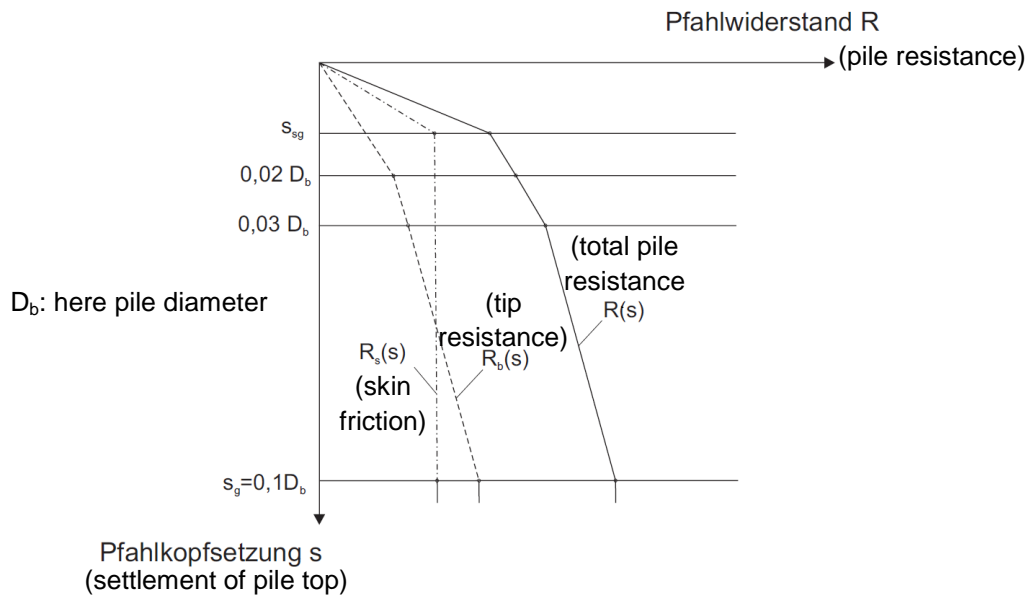


Fig. 2.2 Load-settlement curve for bored piles after EA-Pfähle (DGGT 2012)

The limit settlement s_{sg} , which defines the reaching of the ultimate resistance by skin friction R_s , is calculated using an empirical non-homogeneous equation (R_s in MN and 0.5 corresponding to cm), without the use of any measured soil parameter (Eq. 2.20). It cannot exceed 3 cm.

$$s_{sg} = 0.5 \cdot R_s(s_{sg}) + 0.5 \leq 3cm \quad (\text{Eq. 2.20})$$

The ultimate resistance values for bored piles depending on the type of soil are given in Table 2.6 to Table 2.9.

Table 2.6 Tip resistance for bored piles in coarse-grained soils translated from EA-Pfähle (DGGT 2012)

Relative settlement of the pile head (settlement/pile diameter) (m)	Pile base resistance $q_{b,k}$ (kN/m ²)		
	Mean CPT cone resistance q_c (MN/m ²)		
	7.5	15	25
0.02	550 to 800	1050 to 1400	1750 to 2300
0.03	700 to 1050	1350 to 1800	2250 to 2950
0.10 (s_g)	1600 to 2300	3000 to 4000	4000 to 5300

Table 2.7 Tip resistance for bored piles in fine-grained soils translated from EA-Pfähle (DGGT 2012)

Relative settlement of the pile head (settlement/pile diameter) (m)	Pile base resistance $q_{b,k}$ (kN/m ²)		
	Shear strength $c_{u,k}$ of the undrained soil (kN/m ²)		
	100	150	250
0.02	350 to 450	600 to 750	950 to 1200
0.03	450 to 550	700 to 900	1200 to 1450
0.10 (s_g)	800 to 1000	1200 to 1500	1600 to 2000

Table 2.8 Ultimate skin friction for bored piles in coarse-grained soils translated from EA-Pfähle (DGGT 2012)

Mean CPT cone resistance q_c (MN/m ²)	Ultimate limit state value $q_{s,k}$ of pile skin friction (kN/m ²)
7.5	55 to 80
15	105 to 140
≥ 25	130 to 170

Table 2.9 Ultimate skin friction for bored piles in fine-grained soils translated from EA-Pfähle (DGGT 2012)

Shear strength $c_{u,k}$ of the undrained soil (kN/m ²)	Ultimate limit state value $q_{s,k}$ of pile skin friction (kN/m ²)
60	30 to 40
150	50 to 65
≥ 250	65 to 85

Values are proposed for rock as well, depending on the uni-axial compression resistance (Table 2.10).

Table 2.10 Ultimate skin friction for bored piles in rock translated from EA-Pfähle (DGGT 2012)

Unconfined compressive strength $q_{u,k}$ (MN/m ²)	Ultimate limit state value $q_{b,k}$ of base resistance (kN/m ²)	Ultimate limit state value $q_{s,k}$ of skin friction (kN/m ²)
0.5	1500 to 2500	70 to 250
5.0	5000 to 10000	500 to 1000
20.0	10000 to 20000	500 to 2000

For displacement piles, the load-settlement curves are the same, with different skin friction and tip resistance values.

2.2.2 Current practice in France

The current geotechnical standard in France is the Eurocode 7 EN 1997-1 (2004-2009-2013), as French version NF EN 1997-1 (2014), with the French national appendix NF EN 1997-1/NA (2006) and with the national application standard for pile foundations NF P94-262 (2012). The design theories from the previous French standards with the use of the pressuremeter method have been considered in these standards (Frank 2009, Frank 2010).

2.2.2.1 Bearing capacity

The general equations of the Eurocode 7 (Eq. 2.15) to (Eq. 2.19) presented in section 2.2.1 for the design of piles under axial loads apply. The partial safety factor γ_F for

unfavourable actions on foundations in the persistent load situation is equal to 1.35 (called γ_G) or 1.5 (called γ_Q) for permanent and variable loads respectively (NF P94-262 2012).

Both PMT and CPT correlations for indicative values are allowed as normative annexes in the French standard (see Appendices B.2 and B.3). The safety factor for pile resistance in the permanent load situation in ultimate limit state (ULS) is 1.1 for compression piles (and 1.15 for tension piles). Two model factors $\gamma_{R;d1}$ and $\gamma_{R;d2}$ (Burlon et al. 2014, Frank and Kovarik 200) of 1.15 and 1.1 respectively for compression piles (and 1.4 and 1.1 respectively for tension piles), are applied in the case of the use of the pressuremeter method (case called “ground model” in French standard). The ultimate values for tip resistance $q_{b;k}$ and for skin friction $q_{s;k}$ are modified by the use of model factors as presented in (Eq. 2.25) and (Eq. 2.26) (NF P94-262 2012).

$$q_{b;k} = \frac{q_b}{\gamma_{R;d1} \cdot \gamma_{R;d2}} \quad (\text{Eq. 2.21})$$

$$q_{s;k} = \frac{q_s}{\gamma_{R;d1} \cdot \gamma_{R;d2}} \quad (\text{Eq. 2.22})$$

The general equation for the base resistance of piles is given in (Eq. 2.23) to (Eq. 2.26). B is the pile diameter, D its total embedment, h the pile height in the stiff subsoil, k_p the factor of bearing capacity and p_{le}^* the equivalent limit pressure. The CPT method proposed works after the same principle.

$$q_b = q_0 + k_p \cdot p_{le}^* \quad (\text{Eq. 2.23})$$

$$p_{le}^* = \frac{1}{b + 3a} \int_{D-b}^{D+3a} p_l^*(z) \cdot dz \quad (\text{Eq. 2.24})$$

$$a = \max\left(\frac{B}{2}; 0.5\right) \quad (\text{Eq. 2.25})$$

$$b = \min(a; h) \quad (\text{Eq. 2.26})$$

The k_p factor depends on the effective height D_{ef} of the pile in the soil (Eq. 2.38).

$$D_{ef} = \frac{1}{P_{le}^*} \cdot \int_{D-10B}^D p_l^*(z) \cdot dz \quad (\text{Eq. 2.27})$$

If D_{ef}/B exceeds 5, k_p is equal to k_{pmax} . The k_{pmax} values are given for different pile types or classes (Table 2.12) and for different soil types (Table 2.13).

If D_{ef}/B is smaller than 5: k_p is calculated as in (Eq. 2.28).

$$k_p = 1.0 + (k_{pmax} - 1.0) \cdot \frac{D_{ef}}{B} \cdot \frac{1}{5} \quad (\text{Eq. 2.28})$$

Table 2.11 Definition of classes of piles translated from NF P94-262 (2012)

Pile class	Pile category	Installation technique	Standard for installation
1: bored piles	1	bored pile with no support	NF EN 1536
	2	bored pile with slurry	
	3	bored pile with permanent casing	
	4	bored pile with recoverable casing	
	5	dry bored pile or slurry bored pile with grooved sockets	
2: continuous flight auger (CFA) piles	6	CFA pile	NF EN 1536
3: screw piles	7	screw cast in place pile without casing	NF EN 12699
	8	screw pile with casing	
4: closed-ended driven piles	9	pre-cast or pre-stressed concrete driven pile	NF EN 12699
	10	coated driven steel pile (coating: concrete, mortar, grout)	
	11	driven cast in place pile	
	12	driven steel pile, closed-ended	
5: open-ended driven piles	13	driven steel pile, open-ended	NF EN 12699
6: driven H piles	14	driven H pile	NF EN 12699
	15	driven grouted H pile	
7: driven sheet pile walls	16	driven sheet pile	NF EN 12699
1bis: micropiles	17	micropile I (gravity pressure)	NF EN 1536/14199/12699
	18	micropile II (low pressure)	
8: injected micropiles	19	micropile III (high pressure)	
	20	micropile IV (high pressure with multi-stage grouting)	

Table 2.12 Table for k_{pmax} factor for pile base resistance translated from NF P94-262 (2012)

Pile class	Ground type				
	Silt and clay, percentage $CaCO_3 < 30\%$	Sand and gravel	Chalk	Marl and calcareous marl	Weathered rock
1	1.15	1.1	1.45	1.45	1.45
2	1.3	1.65	1.6	1.6	2.0
3	1.55	3.2	2.35	2.1	2.1
4	1.35	3.1	2.3	2.3	2.3
5	1.0	1.9	1.4	1.4	1.2
6	1.2	3.1	1.7	2.2	1.5
7	1.0	1.0	1.0	1.0	1.2
8	1.15	1.1	1.45	1.45	1.45

The general equation for the ultimate skin friction of piles is (Eq. 2.29). $\alpha_{pieu,sol}$ (Table 2.13) depends on the soil type and on the pile type, and f_{sol} depends on the soil type (Fig. 2.3).

$$q_s(z) = \alpha_{pieu-sol} \cdot f_{sol} \cdot p^*_l(z) \quad (\text{Eq. 2.29})$$

Table 2.13 Table of factor $\alpha_{\text{pieu-sol}}$ for ultimate skin friction translated from NF P94-262 (2012)

Pile category	Ground type				
	Silt and clay, percentage $\text{CaCO}_3 < 30\%$	Sand and gravel	Chalk	Marl and calcareous marl	Weathered rock
1	1.1	1	1.8	1.5	1.6
2	1.25	1.4	1.8	1.5	1.6
3	0.7	0.6	0.5	0.9	–
4	1.25	1.4	1.7	1.4	–
5	1.3	–	–	–	–
6	1.5	1.8	2.1	1.6	1.6
7	1.9	2.1	1.7	1.7	–
8	0.6	0.6	1	0.7	–
9	1.1	1.4	1	0.9	–
10	2	2.1	1.9	1.6	–
11	1.2	1.4	2.1	1	–
12	0.8	1.2	0.4	0.9	–
13	1.2	0.7	0.5	1	1
14	1.1	1	0.4	1	0.9
15	2.7	2.9	2.4	2.4	2.4
16	0.9	0.8	0.4	1.2	1.2
17	–	–	–	–	–
18	–	–	–	–	–
19	2.7	2.9	2.4	2.4	2.4
20	3.4	3.8	3.1	3.1	3.1

Ground type	Silt and clay, percentage $\text{CaCO}_3 < 30\%$	Sand and gravel	Chalk	Marl and calcareous marl	Weathered rock
Choice of curve	Q1	Q2	Q3	Q4	Q5

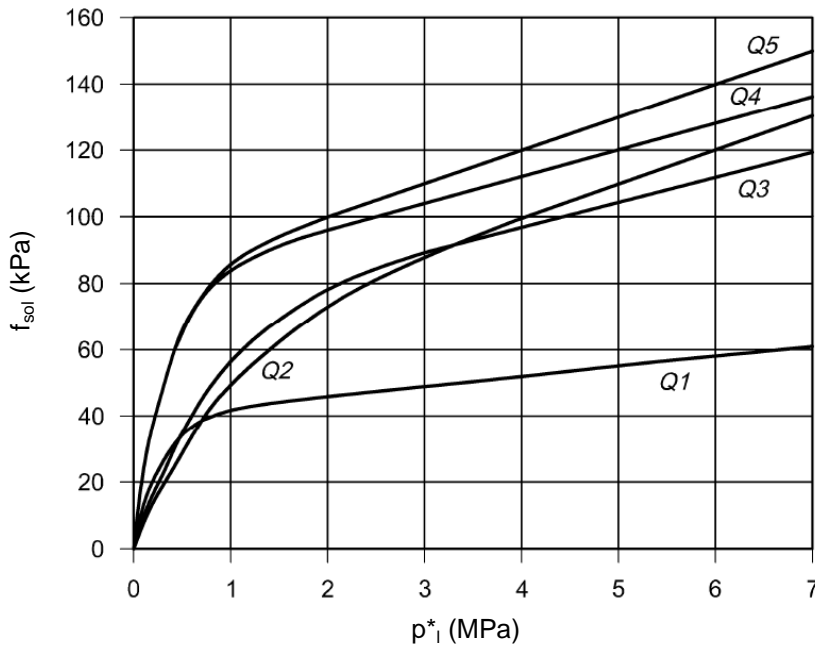


Fig. 2.3 Definition of f_{sol} for ultimate skin friction translated from NF P94-262 (2012)

2.2.2.2 Settlement

The prevalent pile settlement calculation method in France apart from numerical continuum methods is the load transfer method (LTM) with the use of load transfer curves (or mobilisation curves or “t-z” and “q-z” curves) for skin friction and base resistance (Fig. 2.4). The equilibrium of the load transfer curves over the pile height and base is calculated in order to determine the pile settlement under a given load. The problem is described by (Eq. 2.30) and (Eq. 2.31) in each pile subdivision at the depth z , leading to the differential equation (Eq. 2.32). The boundary conditions are the load applied at the pile head and the load transfer curve at the pile tip. The system solving can be made for example with matrix inversion or with the unidimensional finite difference method in an iterative manner. The pile load-settlement curve can be determined by repeating this procedure for different load values. A free soil settlement can be considered by subtracting the free soil settlement to the pile settlement (s_s and s_b :

pile settlement minus soil settlement in absence of the pile, at the shaft and at the tip respectively).

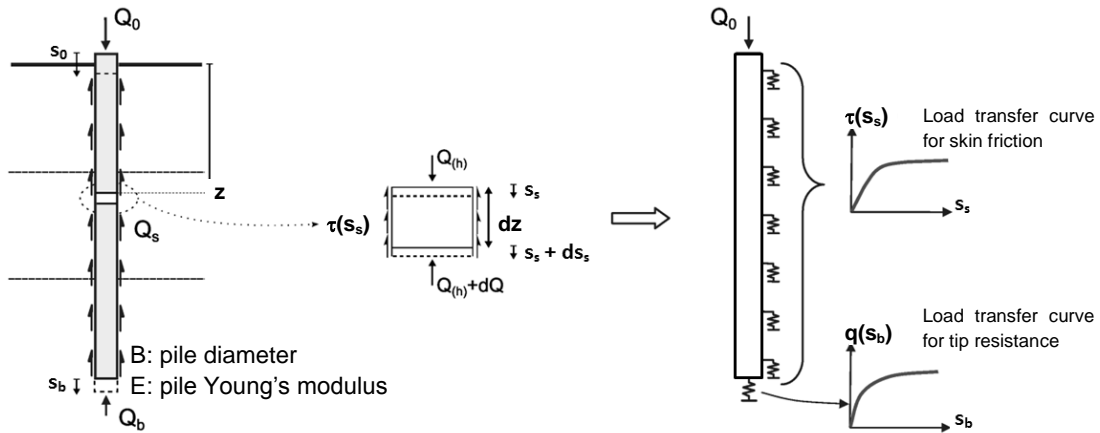


Fig. 2.4 Load transfer method for axially loaded piles

$$\frac{dQ(z)}{dz} = -\pi \cdot B \cdot \tau(s_s(z)) \quad (\text{Eq. 2.30})$$

$$\frac{ds_s(z)}{dz} = -\frac{Q(z)}{E \cdot \pi \cdot (B/2)^2} \quad (\text{Eq. 2.31})$$

$$E \cdot \pi \cdot (B/2)^2 \cdot \frac{d^2s_s(z)}{dz^2} - \pi \cdot B \cdot \tau(s_s) = 0 \quad (\text{Eq. 2.32})$$

The load transfer curves used in general in France are those in Fig. 2.5 developed by Frank and Zhao (1982).

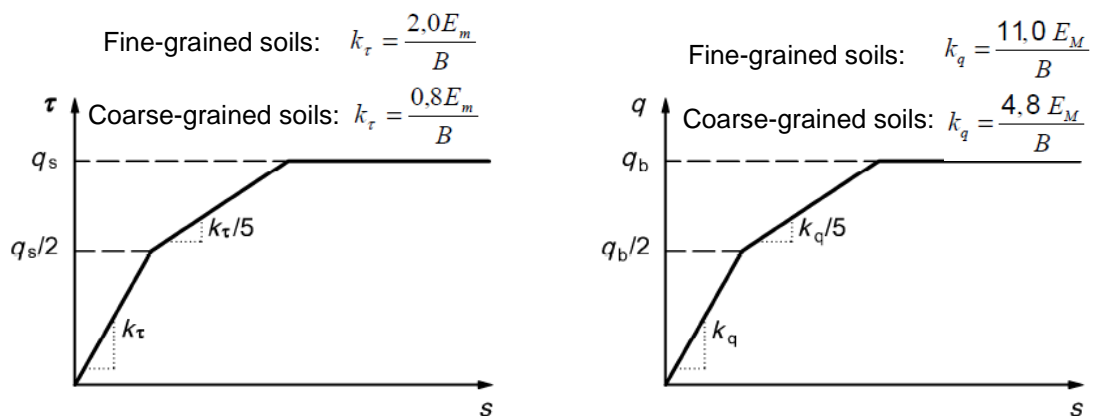


Fig. 2.5 Load transfer curves after Frank and Zhao (1982) for skin friction (left) and base resistance (right) after NF P94-262 (2012)

2.3 Pile groups

2.3.1 Principle and behaviour

The interaction between relatively close piles in a group is related on the one hand to the mechanical interaction of loads and displacements between them, and on the other hand to the soil disturbance generated by the pile installation in comparison to the single pile case. The group effect leads to a modification of the bearing capacity of the group under axial loads (mainly due to the pile installation effects) and to an increase of settlements in comparison to single piles.

The group effect depends on the geometry (pile spacing, pile diameter, pile length), on the load level, on the soil layer configuration, on the number of piles in the group and on the pile material type and execution method. The effect of the rigidity of the slab above the piles is in general eliminated in the different models by considering an infinitely rigid slab or by assuming a given load distribution between the piles. It is often stated that the group effect affects essentially the skin friction and has a minor effect on the load-deformation behaviour at the tip because of the very local impacted field around the tip compared to the shaft (Fleming et al. 1985, Frank 1999). It is commonly admitted that the group effect on settlements under axial loads is negligible for a pile spacing axis to axis larger than 6 to 8 times the pile diameter (Frank 1999, Franke 1979, Viggiani et al. 2012). This can be reduced to 3 times the diameter for end-bearing piles (Rudolph 2005).

In the case of cohesive soils, the bearing capacity of a pile in a group is smaller than the one of a single pile. For spacings smaller than 3 times the pile diameter, the bearing capacity of the group is usually empirically calculated considering the whole pile group as a large fictive pile (Frank 1999) (Fig. 2.6). For higher spacing values up to 8 times the diameter (spacing for which the group effect on bearing capacity becomes negligible), the empirical Converse-Labarre formula can be used, giving an efficiency coefficient defined as the bearing capacity of the pile in a group compared to the single pile depending on the number of piles, on their diameter and on their spacing (Frank 1999, Viggiani et al. 2012). In the case of cohesionless soils, the efficiency can be higher than 1, in particular for loose sands and displacement piles due to the densification and confinement between the piles (FOREVER, IREX 2004). An efficiency equal to 1 on the safe side is often considered in this case (Viggiani et al. 2012). Additional methods to estimate the bearing capacity of pile groups based on numerical parametric studies are given by Rudolph (2005).

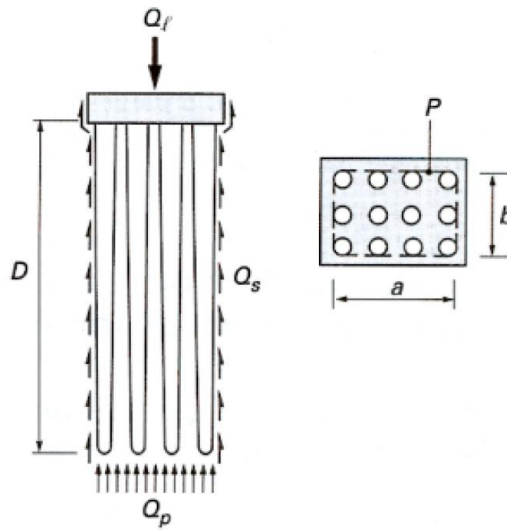


Fig. 2.6 Massive fictive pile for calculation of bearing capacity of pile groups (Frank 1999)

The safety concept for pile groups in the international standards is in general the same as for piles, taking into account the corrected bearing capacity due to the group effect.

Different empirical, analytical and numerical methods to estimate the settlement of a pile group are presented in the next section.

2.3.2 Pile group system calculation

2.3.2.1 Empirical methods

The most widespread empirical method to estimate the average settlement of a pile group as a whole is the equivalent footing method. The position of the fictive footing depends on the layers configuration (pile embedment or not) and varies depending on the authors (Viggiani et al. 2012). The French application standard of the Eurocode 7 NF P94-262 (2012) proposes the method after Terzaghi for piles in a homogeneous normally consolidated fine-grained soil consisting in calculating the settlement of a footing situated at $2/3$ of the total pile length, with a surface equal to the surface of the pile group. A diffusion ratio of 1:2 under this level has been proposed by Frank (1999) (Fig. 2.7). In the case of embedded piles with compressible layers under the pile tip, NF P94-262 recommends the same method with the fictive footing placed at the pile tip level.

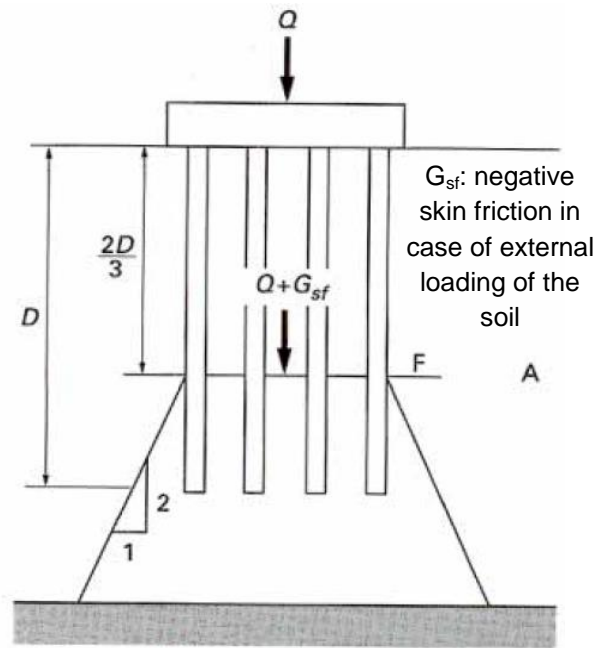


Fig. 2.7 Pile group settlement for floating piles after Terzaghi method (Frank 1999)

The footing settlement has to be calculated according to the usual linear methods and using the usually defined soil moduli for each method.

For relatively long piles in comparison to the width of the group, the equivalent pier method has been mentioned by Poulos and Davis (1980), cited by Viggiani et al. (2012), considering a pile with the same length as the piles in the group and with the same size in plane as the whole pile group. The modulus of the equivalent pier is the weighted average between the real pile modulus and the soil modulus, defined as a Young's modulus chosen with judgement according to the stress and strain level in the soil.

2.3.2.2 Elastic continuum methods

The interaction between two piles has been studied for different subsoil conditions, based on the elasticity theory using either the boundary element method (integral equations method, in general with elastic modelling of the soil), which reduces the volume of equations to be solved, or closed analytical solutions.

The interaction has been calculated analytically based on the elasticity theory by the following authors:

- Randolph and Wroth (1979), and Randolph (1994);
- Chow (1986), cited by Rudolph (2005), and Shen et al. (2000).

The most widespread analytical continuum method is the one proposed by Randolph and Wroth (1978). The settlement of the pile group is based on the method developed for single piles following the work of Frank (1975). The settlement of the single pile (assumed to be rigid) is calculated from the radial distribution of shear stresses around the pile as a function of $1/r$ (Fig. 2.8).

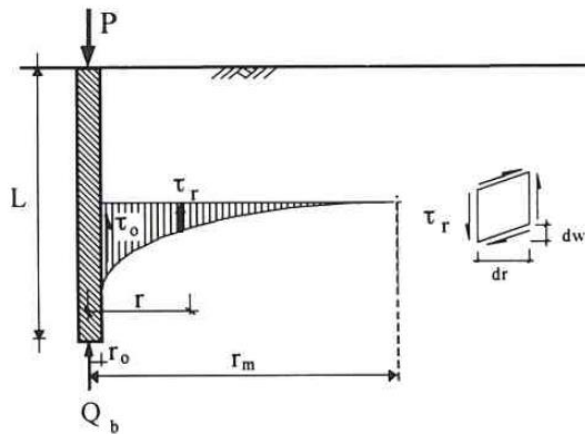


Fig. 2.8 Shear stress distribution around the pile for single pile settlement after Frank (1975) and Randolph (Mossallamy 1997)

The integration of the resulting deformation of the whole soil volume (infinite radius) would lead to an infinite pile settlement, which is clearly unrealistic. The stiffening effect of the soil layer below the pile tip on the soil layers over the pile depth has to be taken into account. For this purpose, different authors like Frank (1975) proposed methods to limit this integration value to a realistic one. Randolph and Wroth (1978) proposes empirically a so-called “magical” radius r_m in accordance with finite element computations they carried out (Eq. 2.33) (L : pile length; ν : Poisson’s ratio).

$$r_m = 2.5 \cdot L \cdot (1 - \nu) \quad (\text{Eq. 2.33})$$

With G defined as the elastic shear modulus of the soil, chosen in a relevant way according to the strain and stress level in the soil (Randolph 1994), the settlement due to the shear stress q_s at the pile shaft s_s for a single pile in a homogeneous soil is given by (Eq. 2.34).

$$s_s = \frac{q_s \cdot r_0}{G} \ln\left(\frac{r_m}{r_0}\right), \text{ or } s_s = \frac{q_0 \cdot r_0}{G} \cdot k \quad (\text{Frank 1975}) \quad (\text{Eq. 2.34})$$

Randolph calculates the pile base settlement s_b due to the load Q_b after the theory of Boussinesq (1885), cited by Vogt (2015), as shown in (Eq. 2.35).

$$s_b = \frac{Q_b \cdot (1-\nu)}{4 \cdot r_0 \cdot G} \quad (\text{Eq. 2.35})$$

The resulting settlement s for a rigid pile in a homogeneous elastic soil under the load P is given in (Eq. 2.36).

$$s = \frac{\frac{P}{(r_0 \cdot G)}}{\frac{4}{(1-\nu)} + \frac{2\pi \cdot L}{r_0 \cdot \ln\left(\frac{r_m}{r_0}\right)}} \quad (\text{Eq. 2.36})$$

The settlement of the pile group is calculated considering the superposition of the settlement fields around each pile (Fig. 2.9).

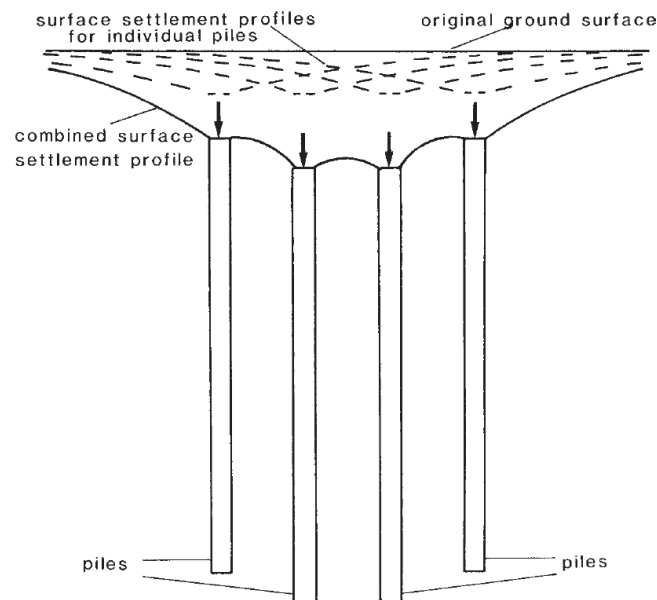


Fig. 2.9 Superposition of settlement profiles for a pile group (Fleming et al. 2008)

For two identical piles loaded with the same load P and with a spacing a_p , the total pile settlement in the group can be calculated based on the modified shaft and tip components s_{sg} (Eq. 2.37) and s_{bg} (Eq. 2.38) due to the deformation field of the neighbouring pile (Randolph and Wroth 1979).

$$s_{sg} = \frac{q_s \cdot r_0}{G} \cdot \ln\left(\frac{r_m}{r_0}\right) \cdot \left[1 + \frac{\ln\left(\frac{r_m}{s}\right)}{\ln\left(\frac{r_m}{r_0}\right)}\right] = s_s \cdot \left[1 + \frac{\ln\left(\frac{r_m}{s}\right)}{\ln\left(\frac{r_m}{r_0}\right)}\right] \quad (\text{Eq. 2.37})$$

$$s_{bg} = \frac{Q_b \cdot (1-\nu)}{4 \cdot r_0 \cdot G} \cdot \left(1 + \frac{2 \cdot r_0}{\pi \cdot a_p}\right) = s_b \cdot \left(1 + \frac{2 \cdot r_0}{\pi \cdot a_p}\right) \quad (\text{Eq. 2.38})$$

$\frac{\ln\left(\frac{r_m}{a_p}\right)}{\ln\left(\frac{r_m}{r_0}\right)}$ and $\frac{2 \cdot r_0}{\pi \cdot a_p}$ can be seen as interaction factors between both piles.

The resulting settlement s_g for a group of two piles in a homogeneous elastic soil under the load P is calculated as the combination of both settlement components (Eq. 2.39).

$$s_g = \frac{P/r_0 \cdot G}{\frac{4}{(1-\nu)} \cdot \frac{s}{r_0 \cdot \frac{2}{\pi} + s} + \frac{2\pi \cdot L}{r_0 \cdot \left[\ln\left(\frac{r_m}{r_0}\right) + \ln\left(\frac{r_m}{a_p}\right)\right]}} \quad (\text{Eq. 2.39})$$

For three or more piles placed in a configuration for which their relative position to each other is the same for all of them (around a pitch circle), the principle is the same with the corresponding additional interaction factors in the brackets of the previous formulas. The extended results including consideration of pile compressibility and modulus increase with depth are given by Randolph and Wroth (1979).

The boundary element elastic continuum method describes a settlement increase in comparison to the single pile settlement, calculated with usual methods with the corresponding soil moduli or from a pile load test. The use of the following elastic abacuses for the group is often associated with the use of corresponding linear elastic solutions for the single pile settlement calculation as well, for example after Poulos and Davis (1968), taking into account the pile compressibility (Lutz et al. 2006) (Fig. 2.10).

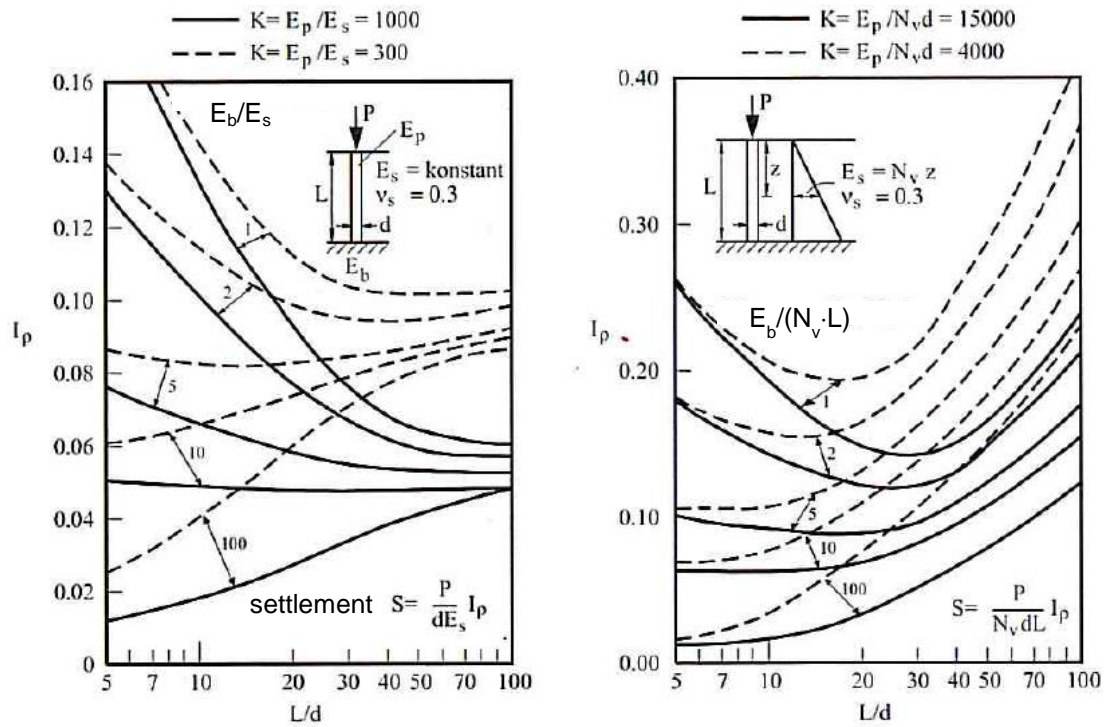


Fig. 2.10 Linear elastic calculation for settlement of a single pile after Poulos (1994), cited by Smoltczyk (2001): settlement factor I_p vs. relative length

The elastic interaction has been calculated using the boundary element method by the following authors:

- Poulos (1968), cited by Viggiani et al. (2012), using the superposition method;
- Banerjee and Butterfield (1981), cited by Fleming et al. (2008), modelling the system as a whole;
- Caputo and Viggiani (1984), cited by Viggiani et al. (2012).

One of the most widespread methods is the one using the boundary element method with superposition using the Mindlin equations by Poulos with an interaction coefficient α defined as the settlement increase due to another pile, relatively to the single pile settlement (Poulos 1981). This coefficient depends on the soil layer configuration (for example floating piles or end-bearing piles), on the spacing between the piles relatively to the pile diameter, on the pile slenderness, on the Poisson’s ratio, on the pile to soil stiffness ratio K , the soil modulus being defined here as an equivalent soil elastic Young’s modulus for the interaction calculation. Fig. 2.11 shows examples of α -values for floating piles (index F) and end-bearing piles (index E). A higher pile/soil stiffness

ratio leads to higher interaction effects in the case of floating piles (defined here as piles embedded into a unique homogeneous soil layer, independently from the soil stiffness), unlike for end-bearing piles. This may be used to consider the soil densification in the case of an execution with soil displacement as an increase in soil stiffness (in particular for close piles) and thus to a decrease of the stiffness ratio, which would lead to smaller interaction effects for floating piles or columns.

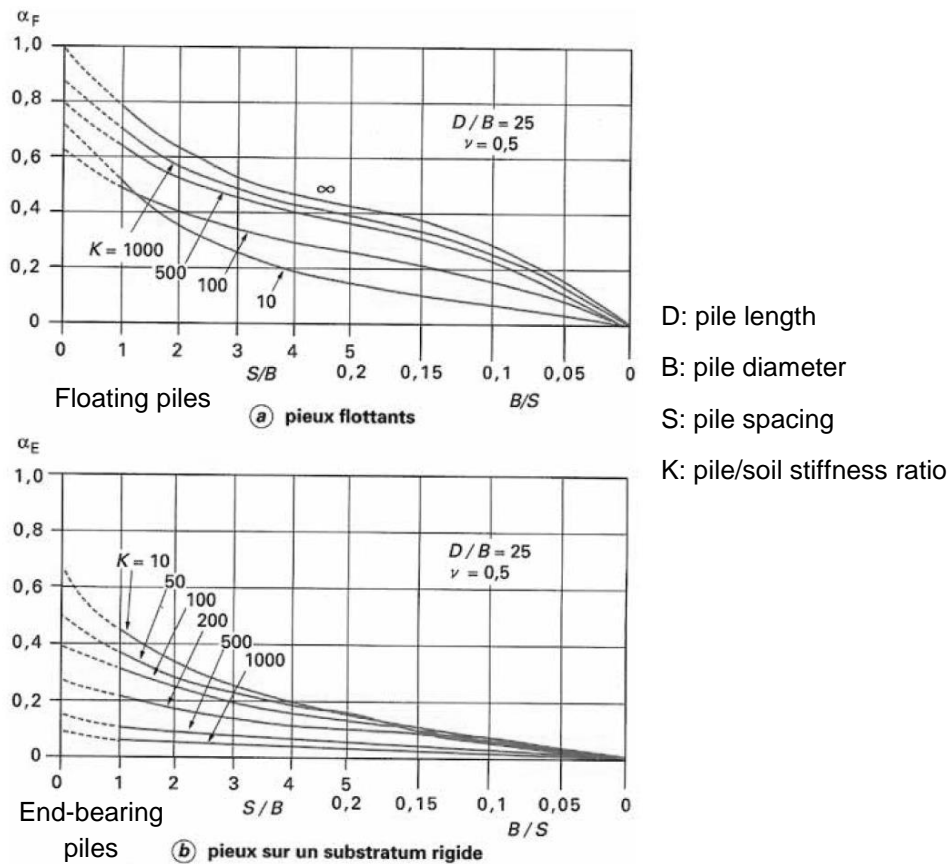


Fig. 2.11 Group interaction factors vs. relative spacing between two piles after Poulos and Davis (1980), cited by Frank (1999)

According to Fig. 2.11, the settlement increase due to pile interaction after the elastic method is higher in the case of floating piles than for end-bearing piles: the interaction coefficient for two piles becomes smaller than 10% for spacing values higher than approximately 20 times the diameter in the first case and approximately 5 times the diameter in the second case.

Fig. 2.12 shows the effect of a length variation for piles in the floating case. The longer and the more deformable the piles are, the more they interact with each other.

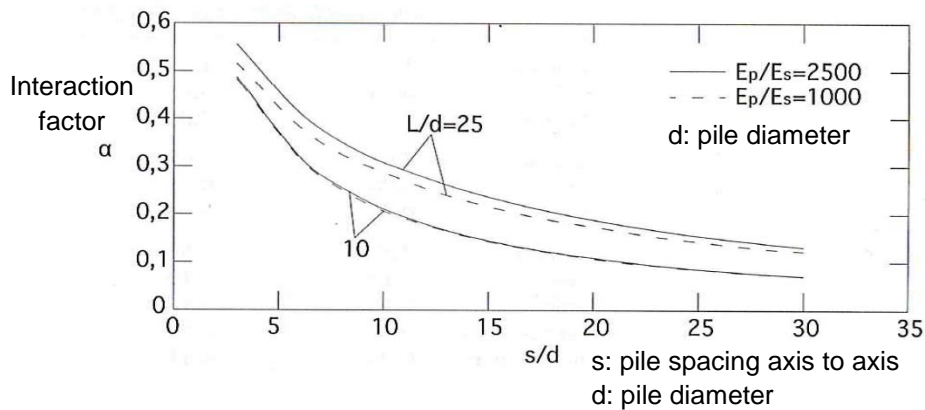


Fig. 2.12 Group interaction factors between two piles (Viggiani et al. 2011)

For usual piles groups with more than two piles, the superposition principle can be applied with this elastic method. With s_G the settlement of one pile in a group of n identical and uniformly loaded piles, s_S the settlement of the single pile under the same load than one pile in the group and α_{1i} the interaction factor between the considered pile 1 and the pile i is given in (Eq. 2.40).

$$s_G = s_S \cdot \left(1 + \sum_2^n \alpha_{1n} \right) \quad (\text{Eq. 2.40})$$

For example, with the conditions of Fig. 6 and $K = 1000$, in the case of a large square grid of floating piles identically loaded with a pile spacing of 5 times the pile diameter, the settlement would be increased by a factor of approximately 4 in comparison to the single piles.

Fleming et al. (1985) propose the calculation of the settlement of a pile group under a rigid pile cap (uniform settlements) using diagrams taking into account the pile length l , the pile stiffness (pile to soil stiffness ratio λ), the pile spacing (relative spacing s/d), the homogeneity of the soil (ratio of soil moduli at pile mid-depth and at pile tip ρ) and the Poisson's ratio of the soil ν ((Eq. 2.41) and Fig. 2.13). The curves have been developed considering four of the five parameters constant and considering average values of $l/d = 25$, $\lambda = 1000$, $s/d = 3$, $\rho = 0.75$ and $\nu = 0.3$. The corrections factors are thus only approximate for other values of the main parameters. The exponent e lies between 0.4 and 0.6 for most pile groups.

$$s_G = s_S \cdot n^e \quad (\text{Eq. 2.41})$$

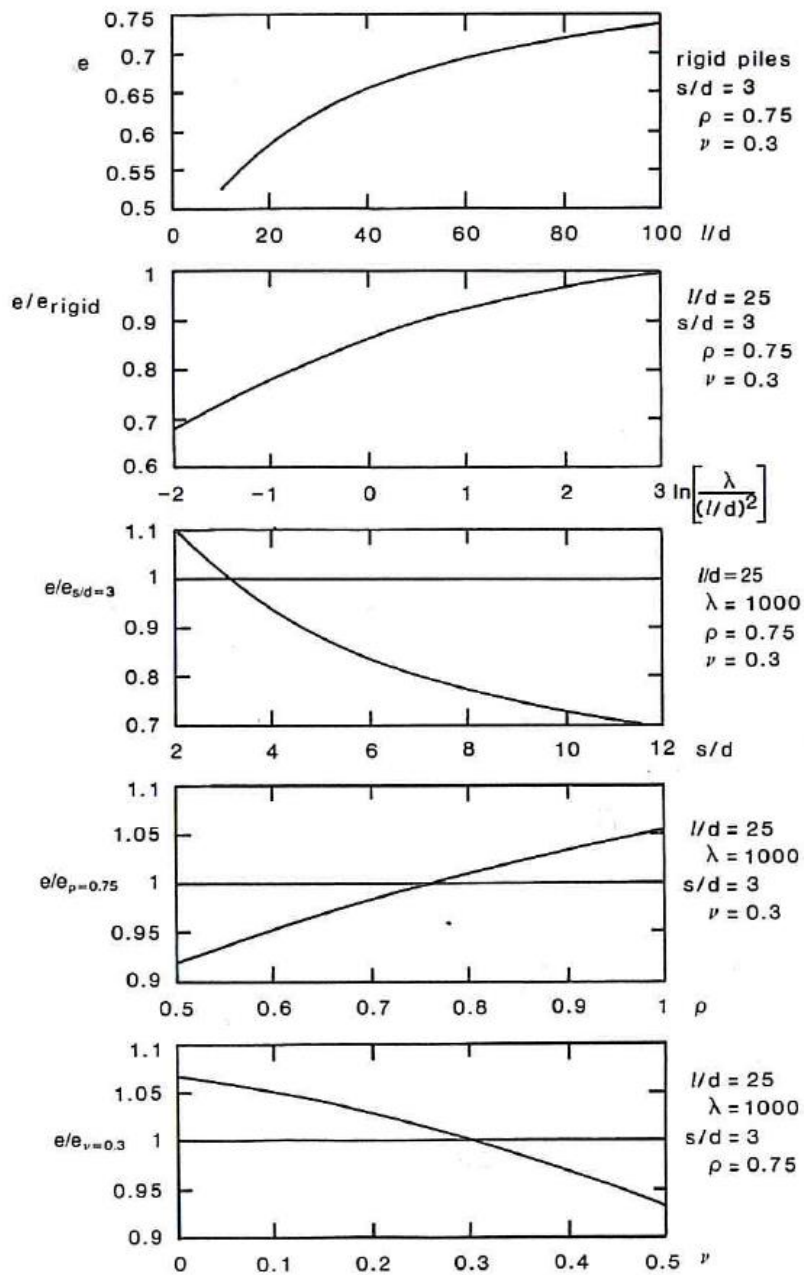


Fig. 2.13 Charts for calculation of exponent e for pile group settlement (Fleming et al. 1985)

2.3.2.3 Hybrid methods with load transfer curves

The hybrid elastic method corresponds to the case where the pile settlement is calculated using non-linear mobilisation curves or load transfer curves or springs for pile skin friction (“t-z” curves) and tip resistance (“q-z” curves) with corresponding soil deformation parameters for discrete pile elements (see section 2.2.2.2), with the group

effect directly integrated in the mobilisation curves considering the soil as an elastic continuum. One of the first investigations about this has been made by O'Neill and Ghazzaly (1977). The consideration of the group effect can be done empirically by weighting factors given by the user (Degny and Romagny, 1989), or using automatically the interaction equations of Mindlin giving the stresses and strains developed by a point force in the soil considered as an homogeneous elastic medium (Estephan et al. 2006, Perlo 2003). For axial loads, this leads to a decrease of the stiffness of the skin friction reaction corresponding to a decrease of the inclination of the mobilisation curve (method called displacement factor γ , Fig. 2.14 and Fig. 2.15). The ultimate skin friction can be adapted by the user if necessary taking into account pile installation effects in the group. The tip resistance reaction remains approximately unchanged.

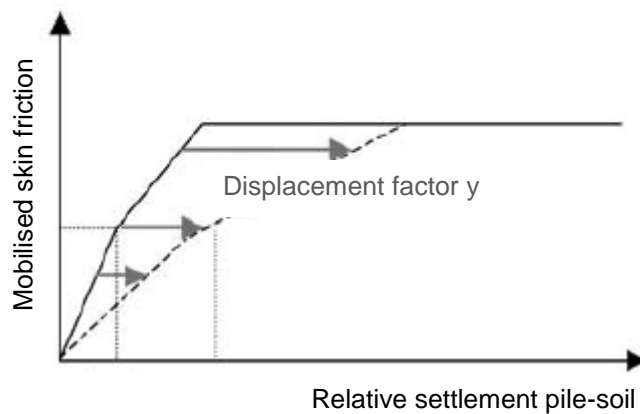


Fig. 2.14 Skin friction displacement factor γ for group effect with load transfer curves

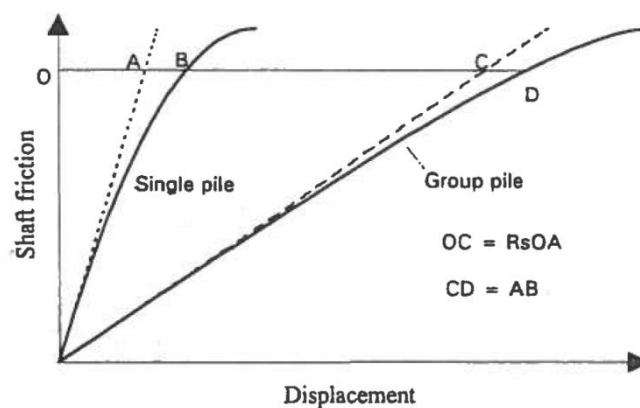


Fig. 2.15 Inclination reduction of skin friction load transfer curve for group effect (Randolph 1994)

2.3.2.4 Continuum methods

Finite-element calculations (FEM) can be carried out on an individual basis as well for relatively complex projects considering the specific soil and geometry conditions and using for example elastic-plastic constitutive laws. The parameters used for the soil model should be calibrated based on an available single pile load test in the given soil conditions, or at least calibrated in order to reflect the single pile bearing capacity according to empirical values given in national standards.

The calculation method with abacuses recommended by the German guideline EA-Pfähle (DGGT 2012) bears on a finite-element parametric study made by Rudolph (2005). Rudolph modelled the pile as an elastic material with a modulus of 30 MPa (Poisson's ratio of 0.2) for concrete and the soil with an elastic-plastic law considering the Mohr-Coulomb failure criterion. Different load levels, pile diameters, pile spacings, pile embedment lengths and soil types have been investigated. The soil types have been divided in 3 classes depending on the oedometer modulus. This modulus calculated from the Young's modulus considered in the numerical model using the elasticity theory with a Poisson's ratio of 0.3: cohesive soils with moduli of 5-15 MPa (I), cohesive soils with moduli of 15-30 MPa (II) and non-cohesive soils with moduli higher than 25 MPa (or corresponding Young's moduli with Poisson's ratio of 0.3). The pile is considered embedded in a unique homogeneous layer. The pile embedment length is defined as the length in the homogeneous soil layer with an oedometer modulus higher than 5 MPa, all softer layers above are not considered. Diameters of 0.3 m up to 1.5 m and pile spacings equal to 3, 6 and 9 times the diameter have been considered. The embedment lengths studied correspond to values higher than 2/3 of the spacing. Rudolph found that the diameter has no influence on the results for the considered conditions and for the considered diameter range studied. The pile spacing is expressed normalized with the embedment length instead of the spacing here.

The interaction is determined directly for a whole group of bored piles with a factor $S_1 \cdot S_2$ corresponding to the ratio of the average pile group settlement s_G to the single pile settlement s_S (Eq. 2.42). The settlement of the single pile is supposed to be known. A complementary factor S_3 can be defined for other pile types, but no precise recommendation about this is given in EA-Pfähle (DGGT 2012).

$$s_G = s_S \cdot S_1 \cdot S_2 \cdot S_3 \quad (\text{Eq. 2.42})$$

Examples of diagrams are presented in Fig. 2.16 for the first soil class. On the x-axis, the load applied is represented relatively to the ultimate load of all piles considered as single piles (defined as the load for a settlement of 10 % of the pile diameter). For spacings a/d smaller than 0.36, the ultimate load of the group is smaller than the sum of

the single pile bearing capacities, that is why the S_1 values cannot be represented up to the end of the diagram. For ultimate load levels and for spacings for which no group effect affects the bearing capacity (curves going up to 1 on the x-axis), no group effect is noticed on the settlement, unlike for the serviceability loads.

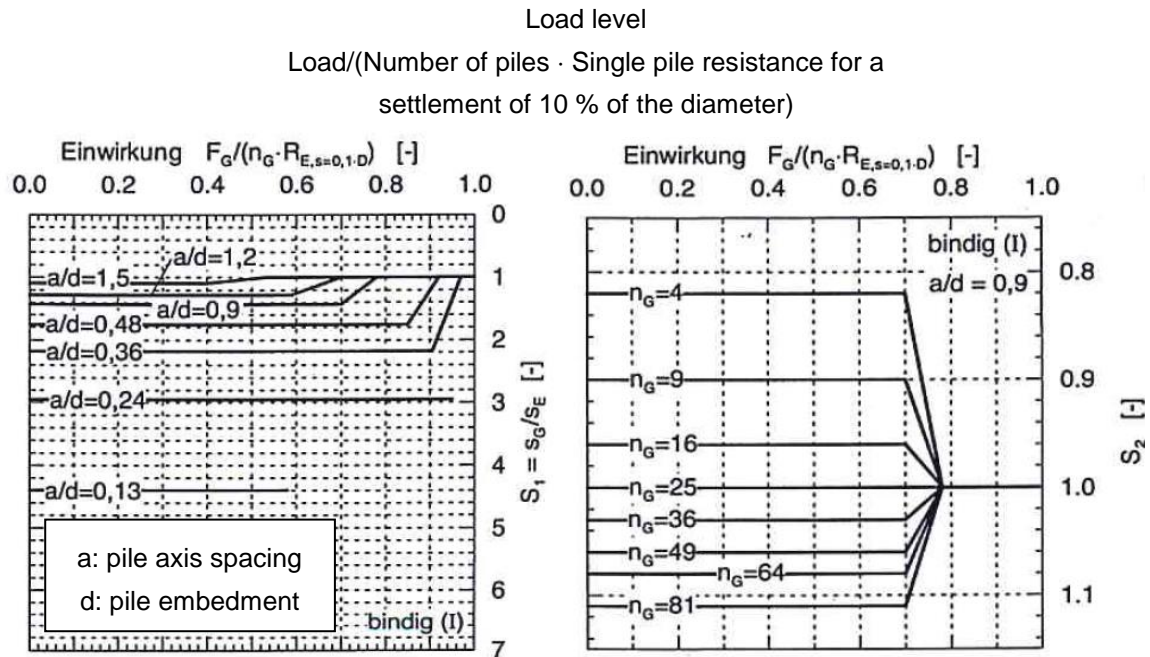


Fig. 2.16 Diagram for S_1 and S_2 vs. load level for cohesive soils (I) (EA-Pfähle, DGGT 2012)

2.4 Combined pile-raft foundations (CPRF)

2.4.1 Principle and behaviour

The term “combined pile-raft foundations” corresponds to a design concept of pile foundations considering the effect of the contact of the raft with the soil between the piles (Fig. 2.17 b). This contact exists actually in most of the piles foundations, but is not often taken into account, so that the classical pile foundation design is made as if the plate was placed above the ground level (Fig. 2.17 c). A pure pile foundation would correspond to the Fig. 2.17 c with the raft above the ground level. A CPRF design can be done only if the contact between the raft and the soil can be guaranteed over the lifetime of the structure. Very weak soil under the raft in combination with very stiff soils under the pile tip exclude thus the possibility of a CPRF consideration (Katzenbach and Choudhury 2013, and limit of stiffness ratio bottom to top equal to 10

after CPRF-guideline after Hanisch et al., 2002). The load share in the piles compared to the total load applied is called efficiency or pile-raft coefficient (equal to 1 for usual pile foundations, Fig. 2.17 c).

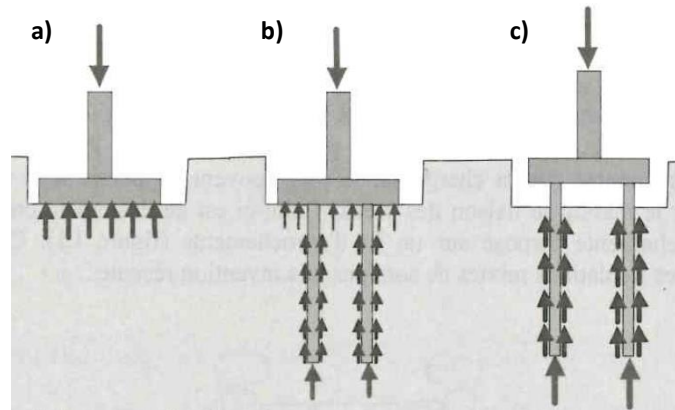


Fig. 2.17 Schematic design concept of shallow foundations (a), CPRFs (b) and deep foundations (c) (Borel 2001)

The first consideration of a pile foundation as a CPRF appeared in the 1970s. The development of calculation methods for CPRF happened mainly in the 1990s. Two different points of view raised the interest in such systems:

- for systems where piles are necessary for the bearing capacity, taking into account the soil bearing capacity leads to a reduction of the required number of piles (design philosophy as a pile foundation);
- for raft systems with excessive settlements without problems of bearing capacity, adding piles is a solution for settlement reduction, in this case the piles are often highly loaded and this concept is thus often internationally known as “creep piling” (design philosophy as a raft foundation);
- a third approach is related to the raft design itself, in which the piles are placed in the middle of the raft in order to decrease the stresses in the raft or to reduce the differential settlement.

In all cases, as opposed to the design of usual piles with only bearing capacity check (assumed automatically associated with small settlements), here a detailed settlement calculation is absolutely required to represent the compatibility of both subsystems (pile and raft) and due to the reduced number of piles compared to a traditional design. In the past, the problem of pile settlement has often been ignored, and this explains the remaining reluctance about CPRF design in some countries (Combarieu 1999).

The study of CPRF systems consists in taking into account the interactions between the different elements in the system (Fig. 2.18). The raft-soil-interaction and the pile-soil-interaction correspond to the behaviour of usual raft foundations and single piles. The pile-pile-interaction corresponds to the group effect described in 2.3. The new element to be considered here is the pile-raft-interaction, representing the effect of a loading of the soil on the load-settlement behaviour of the pile.

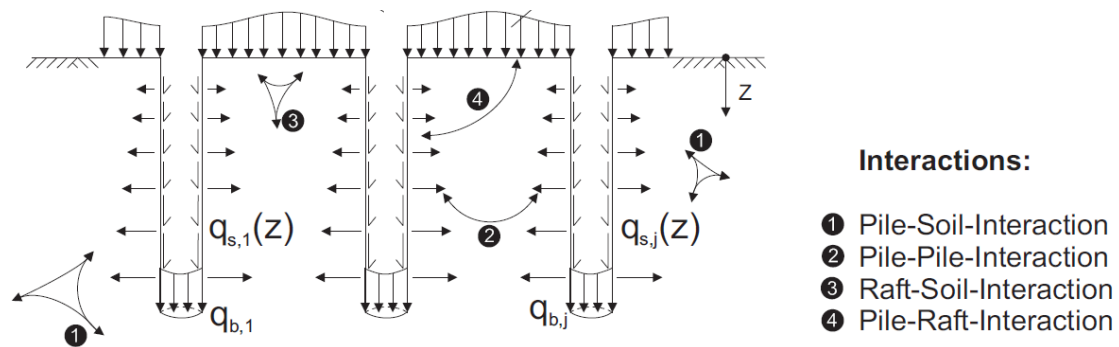


Fig. 2.18 Interactions in CPRF system (Katzenbach and Choudhury 2013)

The pile-raft interaction has an influence mainly on the maximal and mobilised skin friction of the pile, the behaviour of the pile tip remaining approximately unchanged for usual pile lengths. Combarieu (1988a) asserts that the raft has no influence on the pile tip for piles longer than the width of the raft, but the zone of influence of a footing is in general considered reaching a depth of 2.5 times the footing width. The development of the skin friction over the pile length is different from the one in the single pile case. As opposed to the classical pile design where the skin friction would be theoretically first mobilised at the top of the pile due to pile compressibility, the maximum skin friction appears first at the bottom of the pile, if the raft is in contact with the soil, because of the imposed equality of settlements of pile and soil at the top (Fig. 2.19).

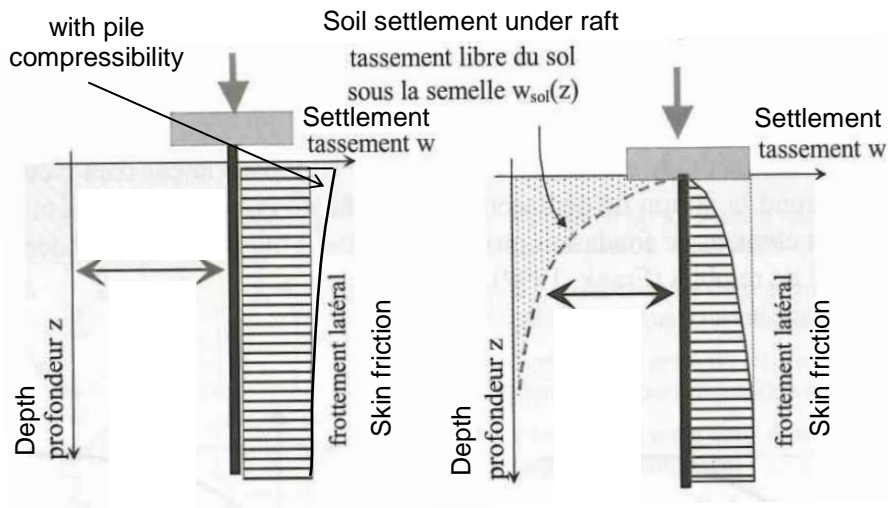


Fig. 2.19 Theoretically mobilised pile skin friction with and without loading of the soil adapted from (Borel 2001)

The response of a pile in a CPRF is less stiff than the one of a single pile due to the pile-pile-interaction (group effect, see 2.3) and due to the pile-raft-interaction with a smaller mobilised skin friction, in particular in the upper part of the system (El-Mossallamy and Franke 1997) (Fig. 2.20). On the contrary, the bearing capacity of the pile is increased in comparison to the single pile, due to the possible increase from the group effect if the group efficiency coefficient is higher than 1 (like in Fig. 2.20) and due to the soil confinement between the piles created by the loading of the soil. The position of the pile in the CPRF plays a role in its behaviour as well.

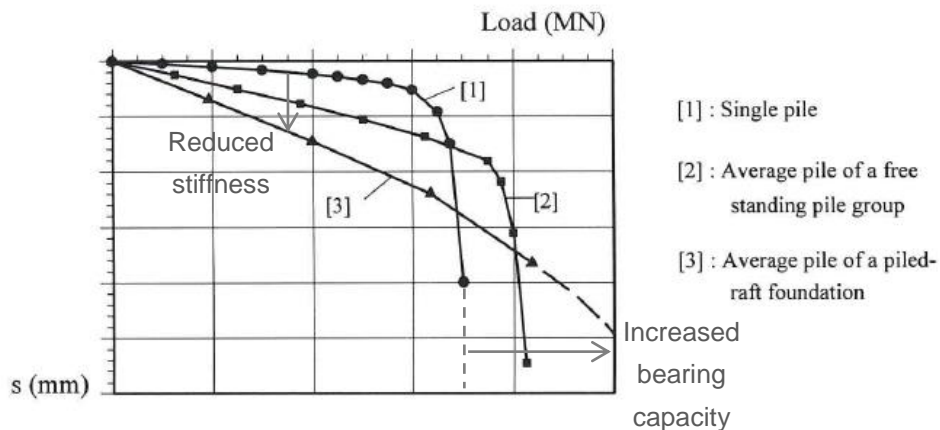


Fig. 2.20 Pile load-settlement behaviour: single pile, pile in a group, pile in a CPRF adapted from El-Mossallamy (1997)

The bearing capacity of the whole CPRF system is defined in general as the resistance mobilised for a visible sharp increase of settlements in the load-settlement relation of the system (CPRF-guideline, Hanisch et al. 2002). Since the full resistance of the different components separately is activated for different settlement values (some millimetres for skin friction, some per cents of the pile diameter for the tip resistance, some per cents of the raft width for the raft resistance), and since the bearing capacity of the piles and of the raft are influenced by the pile-raft interaction, the calculation of the bearing capacity of the whole system is non-trivial. Borel (2001) reports that the bearing capacity of the whole system is approximately equal to the sum of the bearing capacity of the pile group and of the raft separately.

Although the stiffness of the pile in a CPRF is smaller than the one of the pile in the group, the settlement of the whole CPRF is often slightly smaller than the one of the pile group alone due to the load share taken by the soil under the raft. The settlement reduction is in general in an order of 10 % despite a significant load share in the raft of 30 % for example (Fleming et al. 2008). However, only a detailed settlement study can assess if the participation of the raft leads to a settlement increase or to a settlement reduction.

The ultimate limit state of a CPRF involves a punching failure of the entire block of soil containing the piles (Randolph 1994), so that the safety concepts for CPRF should always consider the system as a whole. The safety concept of the German CPRF-guideline (Hanisch et al. 2002), presented in shorter version in the international CPRF-guideline (Katzenbach and Choudhury 2013), is compared to the safety concept for usual pile foundations in chapter 2.7.

In the next section, different settlement calculation methods for CPRFs are presented, mainly for rigid rafts with identical piles. Focus of this summary is the modelling of the additional interaction component in comparison to pile groups which is the pile-raft interaction. A comparison of the majority of them on the basis of an example has been done by Richter and Lutz (2010).

2.4.2 CPRF system calculation

2.4.2.1 Elastic continuum methods

This method is based on the analytical elastic continuum for piles groups of Randolph presented in 2.3, with the same notations here and the same idea of a relevant choice of the elastic modulus employed. In analogy to the interaction factors defined between

piles in the group, interaction factors can be defined between piles and raft elements (Fig. 2.21).

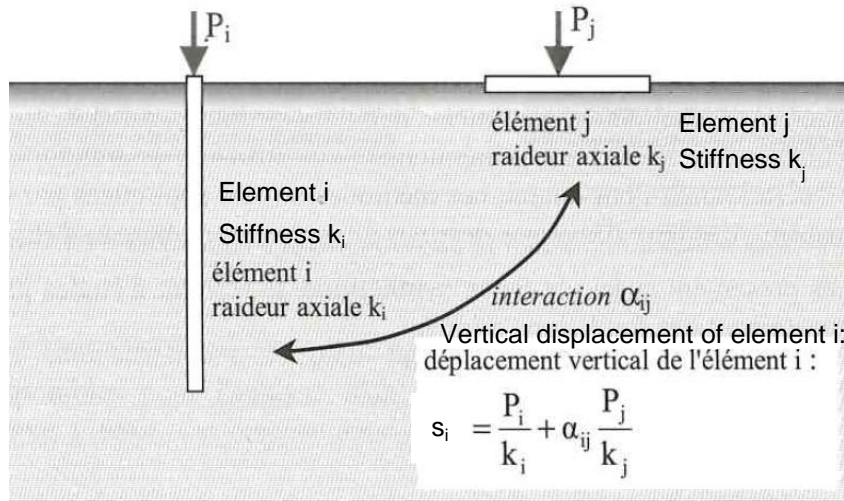


Fig. 2.21 Interaction between pile and raft foundation elements (Borel 2001)

The theory of elasticity allows a superposition of the different interaction mechanisms, taking into account the boundary conditions. The pile group is modelled as a component and the raft as another one. The raft stiffness under loading and the pile group stiffness are determined using the usual moduli for rafts and pile groups according to 2.1, 2.2 and 2.3. In (Eq. 2.43), s_r is the settlement of the raft, P_r and P_p the load in the raft and in the pile group, k_p and k_r the stiffness of the pile group and of the raft, α_{pr} the pile-raft interaction factor and α_{rp} the raft-pile interaction factor (Randolph 1983).

$$\begin{bmatrix} s_p \\ s_r \end{bmatrix} = \begin{bmatrix} 1/k_p & \alpha_{pr}/k_r \\ \alpha_{rp}/k_p & 1/k_r \end{bmatrix} \cdot \begin{bmatrix} P_p \\ P_r \end{bmatrix} \quad (\text{Eq. 2.43})$$

(Eq. 2.44) results from the reciprocal theorem in the theory of elasticity.

$$\alpha_{rp}/k_p = \alpha_{pr}/k_r \quad (\text{Eq. 2.44})$$

For a rigid slab, $s_p = s_r$. Hence the resulting stiffness of the CPRF k_{CPRF} relating the settlement of the system to a given load is the following (Eq. 2.45).

$$k_{CPRF} = \frac{k_p + (1 - 2 \cdot \alpha_{rp}) \cdot k_r}{1 - \alpha_{rp}^2 \cdot k_r / k_p} \quad (\text{Eq. 2.45})$$

The corresponding load share in the pile is equal to (Eq. 2.46):

$$\frac{P_p}{P_r + P_p} = \frac{k_p - k_r \cdot \alpha_{rp}}{k_p + k_r \cdot (1 - 2 \cdot \alpha_{rp})} \quad (\text{Eq. 2.46})$$

Considering the displacement field for a single pile with a circular cap of radius r_c , Randolph (1994) shows that α_{rp} can be approximated by (Eq. 2.47).

$$\alpha_{rp} = 1 - \frac{\ln\left(\frac{r_c}{r_0}\right)}{\ln\left(\frac{r_m}{r_0}\right)} \quad (\text{Eq. 2.47})$$

This relation may be used for larger groups, r_c being the radius of the associated raft area for each pile. However, more detailed analyses by Clancy and Randolph (1983), cited by Randolph (1994), show that for an increasing pile group size, α_{rp} tends to a constant value of approximately 0.8, independently of the piles geometry, spacing and pile-soil stiffness ratio. Thus for groups of more than 4 piles, the following approximation can be considered, showing that k_{CPRF} is very close to k_p (Eq. 2.48).

$$k_{CPRF} = \frac{1 - 0.6 \cdot k_r / k_p}{1 - 0.64 \cdot k_r / k_p} \quad (\text{Eq. 2.48})$$

Lutz (2002) and Lutz et al. (2006) based their calculation on the pile group theory of Randolph and Fleming presented above, but determined the pile-raft interaction differently using an assumption based on the concept of negative skin friction down to a neutral plane considering the single pile subsystem. On the contrary, in the CPRF system as a whole, no negative skin friction actually occurs in general because of the relative high rigidity of the slab imposing comparable settlement of the soil and of the pile under the slab. This effect is considered for the separated components raft and pile, the compatibility being guaranteed separately by the equality of settlements at the top in the final calculation like in the previous equations of Randolph. The level of the neutral plane, here denoted z_N (equality of settlement of pile and soil), is determined for a loading of the soil only, and the interaction factor here is calculated as the settlement of the raft under this plane divided by the total settlement of the raft (Eq. 2.49). Lutz

(2002) calculated this level based on the equilibrium of skin friction and tip resistance after Randolph in a homogeneous soil (Eq. 2.50).

$$\alpha_{rp} = \frac{s_r(z = z_N)}{s_r} \tag{Eq. 2.49}$$

$$z_N = 0.5 \cdot D + r_0 \cdot \frac{\ln\left(\frac{r_m}{r_0}\right)}{\pi \cdot (1 - \nu)} \tag{Eq. 2.50}$$

For the footing settlement calculation, Lutz et al. (2006) proposed the use of the modulus from the plate load test $E_v = \frac{E}{1 - \nu^2}$ (Eq. A.12) instead of the oedometric modulus, but did not describe how those moduli are determined based on soil tests.

Van Impe and De Clercq (1994) extended the Randolph theory for CPRF for layered soils, considering a modulus decrease with strain and with a new proposal for the influence radius r_m .

Poulos and Davis (1980), cited by Borel (2001), extended their boundary element method analysis with the influence of a rigid raft element above a single rigid pile. The settlement of the pile-raft system is 10 to 20 % smaller than the settlement of the single pile for usual pile-raft diameter ratios and pile lengths (Fig. 2.22).

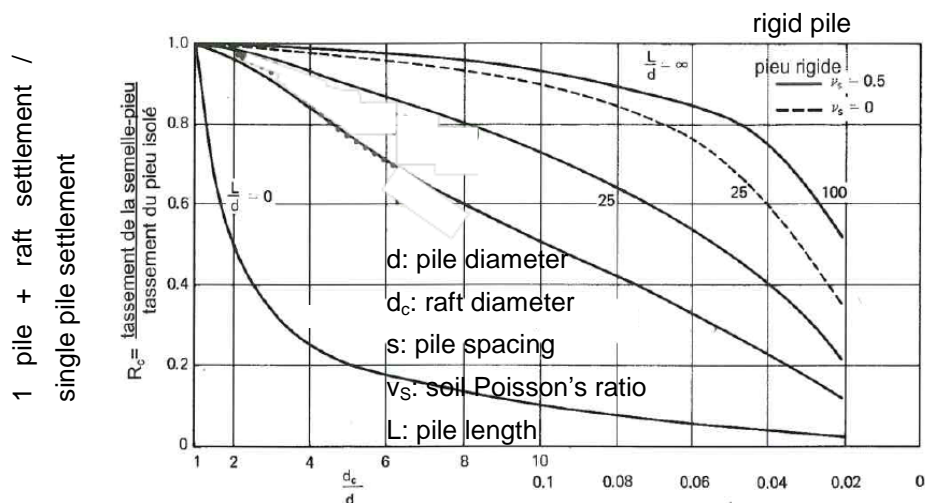


Fig. 2.22 Settlement of pile-raft system vs. raft/pile diameter ratio compared to single rigid pile in an elastic continuum after Poulos and Davis (1980), cited by Borel (2001)

Butterfield and Banerjee (1971), cited by Borel (2001), analysed the settlement of pile groups and CPRF with several piles in comparison to the settlement of the single pile. Fig. 2.24 shows the relative small influence of the contact raft-soil on the settlements.

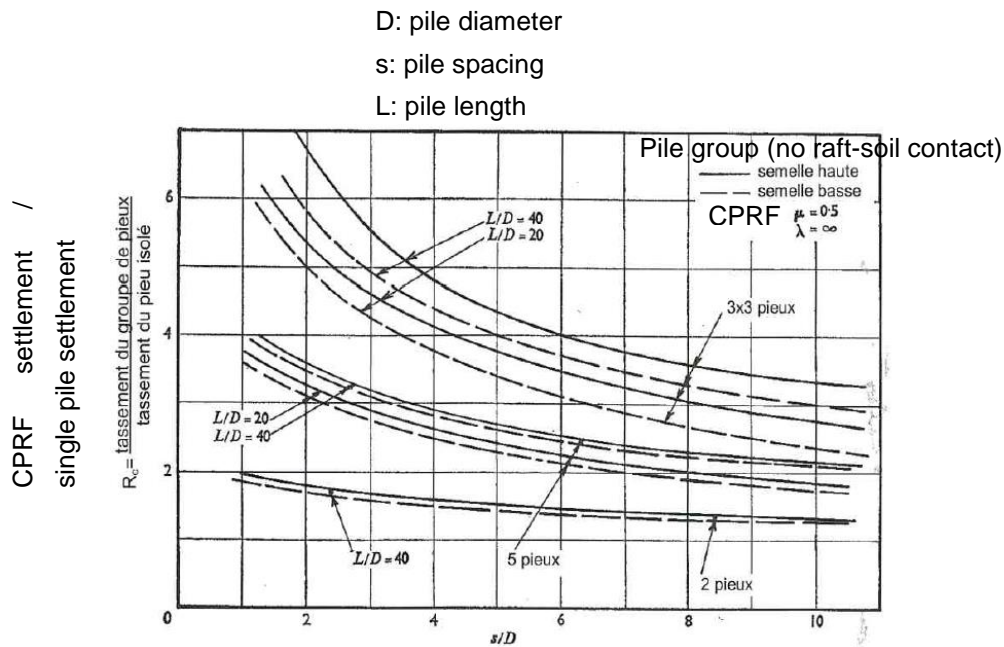


Fig. 2.23 Settlement of CPRF and pile group vs. relative pile spacing compared to single rigid pile in an elastic continuum from Butterfield and Banerjee (1971), cited by Borel (2001)

Combined elastic methods exist, calculating the soil deformations as an elastic continuum with the boundary element method, and for example calculating the plate separately using FEM (Fig. 2.24). This has been done by El-Mossallamy (1996) who took the non-linear effects into account considering an increasing soil modulus with depth, or the non-linear elastic model of Duncan-Chang (1970), as well as interfaces for possible slip between pile and soil (El-Mossallamy 1996, El-Mossallamy and Franke 1997, Lutz et al. 1994).

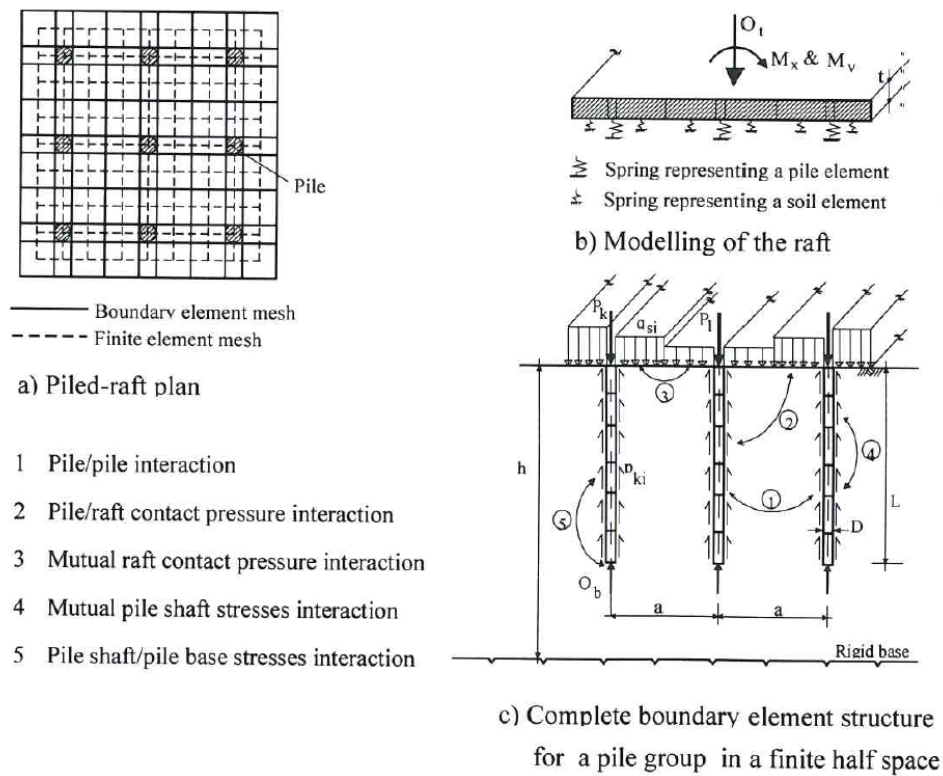


Fig. 2.24 Combined boundary element and finite element method for CPRF (El-Mossallamy 1996)

2.4.2.2 Analytical hybrid methods with load transfer curves

Analytical hybrid methods with load transfer functions are based on non-linear springs like in section 2.3.2.3 with additional springs for the raft elements. In the same way as for the group effect (interaction 5 in Fig. 2.25), the pile-raft interaction (interaction 6 in Fig. 2.25) can be taken into account using elastic integral equations after Mindlin for example.

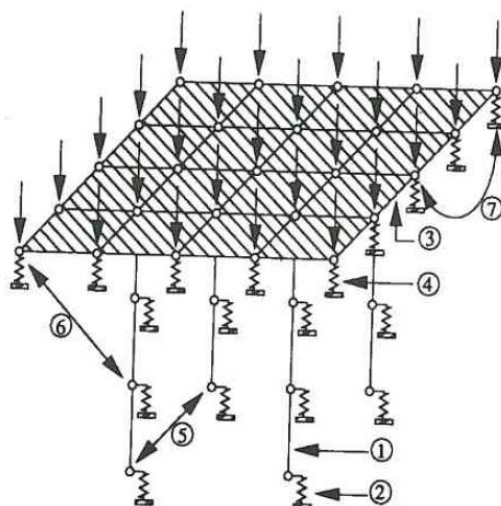


Fig. 2.25 Principle of a hybrid method for CPRF from Clancy and Randolph (1993), cited by Borel (2001)

Combarieu and Morbois (1982) and Combarieu (1988a) proposed an iterative LTM method to calculate the settlement of the system and the corresponding load distribution between the raft, the pile friction and the pile tip (Fig. 2.26). The soil settlement profile under the raft is calculated with usual methods with the corresponding soil moduli, using for example the linear pressuremeter method or a non-linear pressuremeter method taking into account the bearing capacity of the raft (Combarieu 1988a). According to the definition of the load-transfer curves (Frank and Zhao 1982), the soil settlement to be considered is the soil free settlement “in the absence of the pile”, that is why no influence of the piles on the soil settlement profile is considered here. The load transferred from the pile to the soil is determined with mobilisation functions depending on the pile-soil settlement at each depth (e.g. in Combarieu after the Frank and Zhao curves) based on the method developed originally for single piles (see Fig. 2.4 and (Eq. 2.30) to (Eq. 2.32) in section 2.2.2). The pile-pile interaction is not automatically taken into account; the stiffness of the mobilisation curves used should be adapted by the user or the influence of the other piles on the soil settlement should be considered. The pile compressibility can be taken into account (Fig. 2.26). The iterative procedure may be made for example by trying different settlement values at the top for the given load, and calculating backwards the load and the load transfer in the soil and in the pile down to the pile tip, until the resulting load at the tip is consistent with the mobilisation law imposed at the tip.

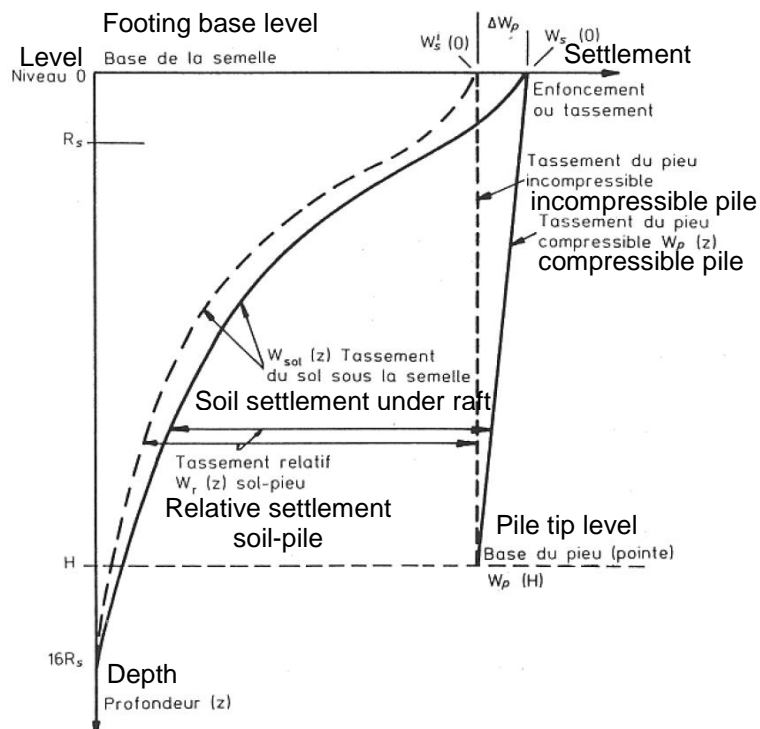


Fig. 2.26 Soil and pile settlement profiles with the LTM after Combarieu (1988a)

For very large CPRF areas, a LTM calculation considering a unit cell is possible. This calculation corresponds to the calculation for rigid inclusions presented in section 2.5.2.2, here without load transfer platform.

2.4.2.3 Continuum methods

For complex CPRF-geometries and for large-scale projects, the modelling of the system as a whole is necessary. The advantage of numerical calculations is in particular to cover directly all interaction effects in the CPRF, under the condition that appropriate soil models are used. The parameters used for the soil model should be calibrated if possible based on single pile load test results in the given soil conditions, or at least calibrated in order to reflect the single pile and raft bearing capacity according to empirical values given in national standards or recommendations.

The CPRF-guideline recommends the use of axisymmetric unit cells for large foundations (pile grid), of 3D modelling for subsystems using symmetrical properties (Fig. 2.27) or of full 3D models for systems with complex geometries (Fig. 2.28), and a

refined geometry in the contact zone between the structural elements (plate and piles) and the soil without necessity of interface elements.

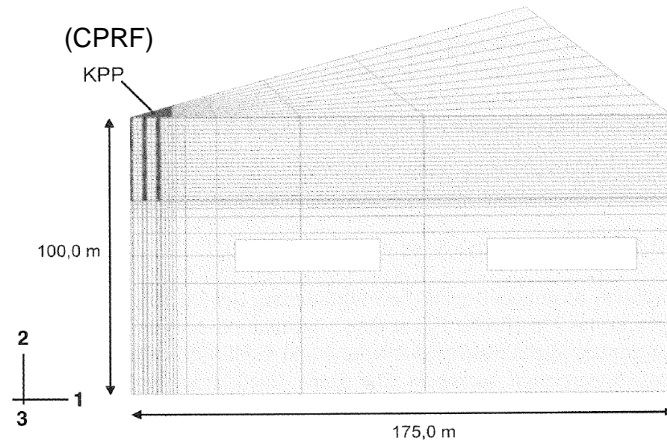


Fig. 2.27 3D-modelling of CPRF-subsystem using symmetrical properties (Hanisch et al. 2002)

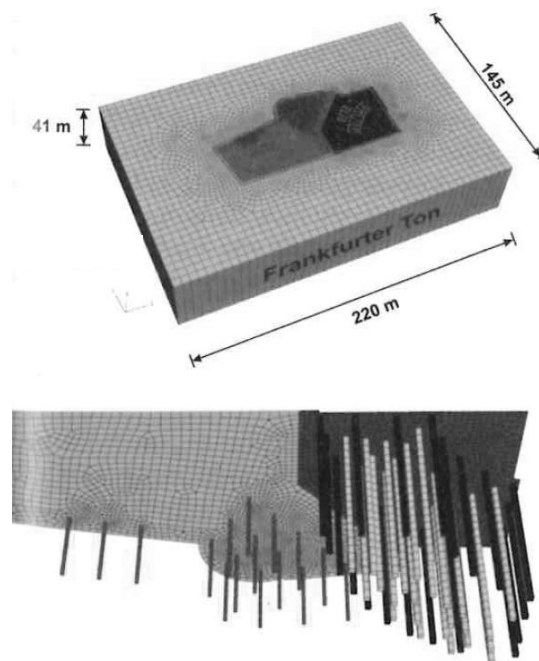


Fig. 2.28 Full 3D-modelling of CPRF-system (Skyper-Tower in Frankfurt am Main) (Richter and Lutz 2010)

Structural elements can be simply modelled by a linear elastic constitutive law if no problem of structural failure is expected, whereas for the soil an elastic-plastic law with a non-associated yield surface using for example a Cap model after Drucker and Prager

is advised (Hanisch et al. 2002). The application examples related to the CPRF-guideline development concern mainly numerous high-rise buildings in Frankfurt am Main, and the required parameter for the soil constitutive laws have been calibrated from previous sites. The increase of the soil modulus with depth due to the increase of the total stresses in the natural soil can be modelled numerically by an elastic modulus linearly increasing with depth, or using the Hardening Soil model. In the well-known Frankfurt clay, the relationship proposed for the oedometric modulus with depth z is $E_{\text{oed}} = 7 \cdot (1 + 3.5 \cdot z)$ after Breth and Amann, cited by Borel (2001) (Fig. 2.29).

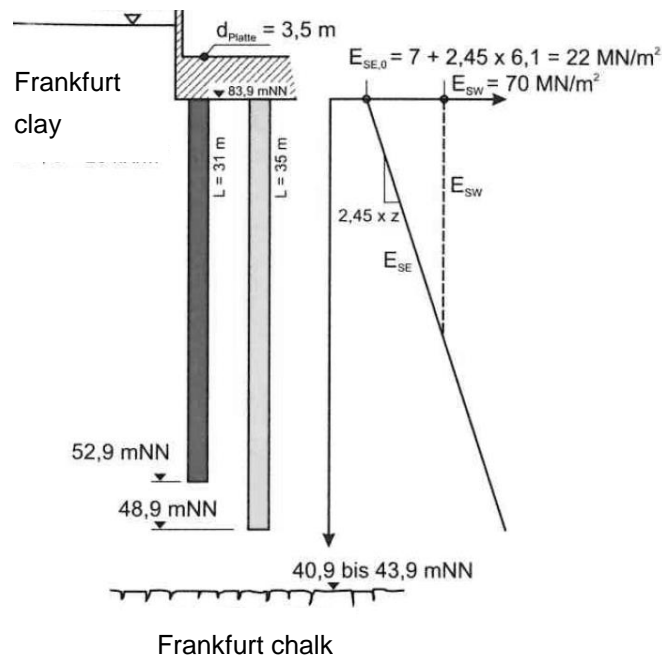


Fig. 2.29 Increasing modulus with depth for FEM-modelling (Richter and Lutz 2010)

Reul (2000, 2002) proposed predesign-diagrams for CPRF in the Frankfurt clay using the modelling conditions cited in the previous paragraph with increasing soil modulus with depth, for different values of the raft foundation size and stiffness, of the number of piles, of the pile length and of the pile diameter for different loading levels. Fig. 2.30 shows an example for a CPRF in theoretical infinitely deep Frankfurt clay, and Fig. 2.31 a correction diagram for a finite depth of the same soil.

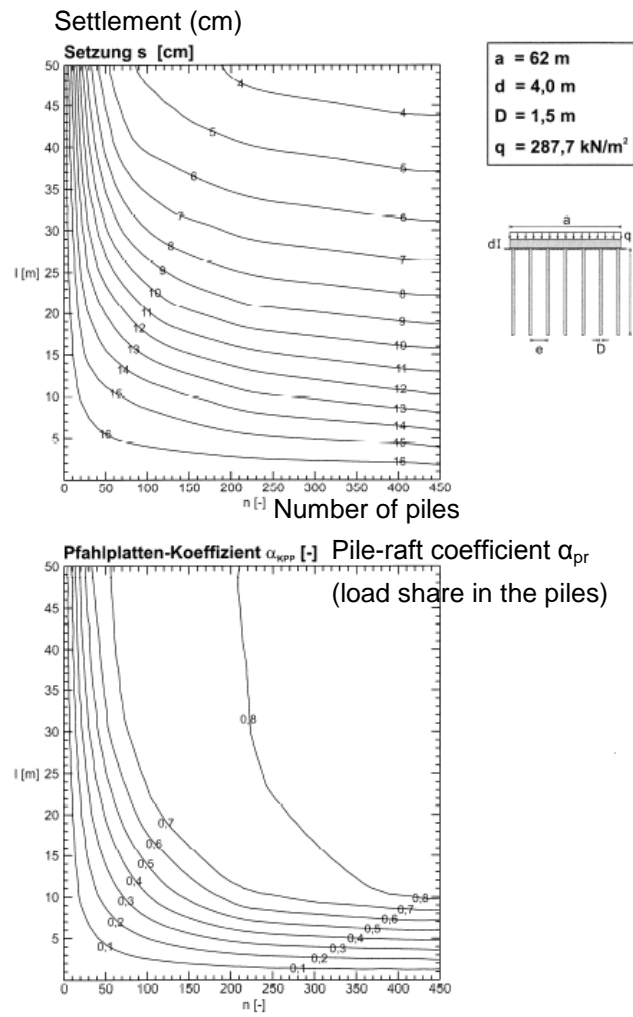


Fig. 2.30 Predesign-diagrams for a CPRF in theoretically infinitely deep Frankfurt clay (Reul 2000): settlement vs. number of piles and pile length

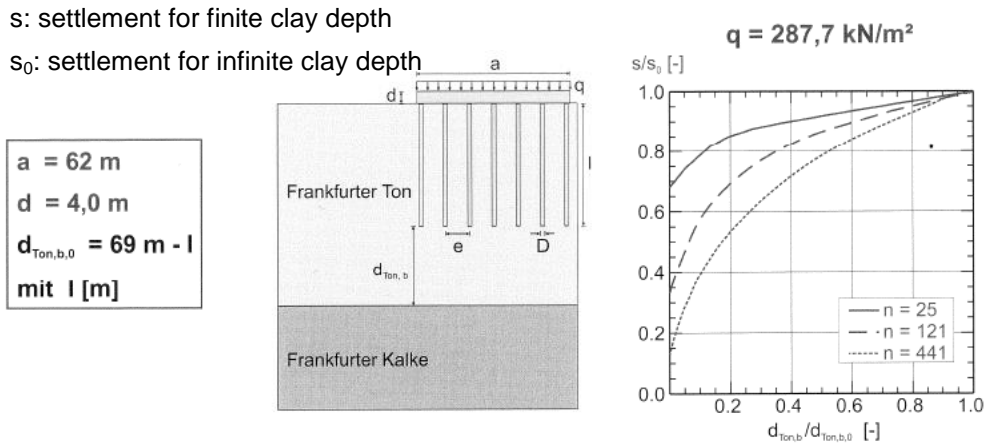


Fig. 2.31 Predesign-diagram for a CPRF in the Frankfurt clay with finite depth (Reul 2000): settlement relatively to the case with infinite clay depth vs. relative clay depth

2.5 Rigid inclusions (RI)

2.5.1 Principle and behaviour

The rigid inclusion design method has been developed particularly in France in the 1990s as an alternative to pile foundations and to vibro stone columns, in this country where the CPRF design was never widely used. Compared to pile and CPRF foundations, RI systems present a structural discontinuity between the superstructure and the columns (Fig. 2.32). The load is transferred from the structure to the columns through a load transfer platform (LTP), which can be made of granular material or of material treated with a binding agent. The advantage of this discontinuity is a stress reduction in the slab (reduced “hard point” effect) and in the column heads. In the case of vertical loads, the columns are in general not steel-reinforced. The column diameter is in general smaller than for usual piles, pile groups or CPRFs, in the range of 25 cm to 80 cm. The soil reinforcement technique with RIs is regulated by the French recommendations ASIRI (IREX 2012), which are the most advanced regulations on the subject existing today. In Germany, the CSV-guideline (DGGT 2012) apply to stabilizing rigid column systems with smaller diameters of 12 to 20 cm, but provides only very simplified assumptions which are currently being re-developed for an updated version.

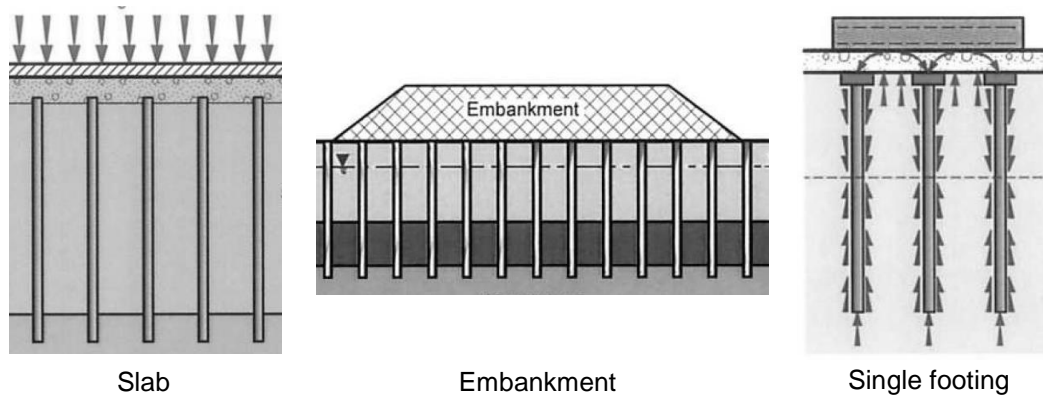


Fig. 2.32 Rigid inclusion (RI) application cases adapted from ASIRI (IREX 2012)

Columns in rigid inclusion systems are often executed with a soil displacement technique, for example with a displacement auger or with a vibrated tube (Keller Company 2013). In addition to the usual pile concrete material, a wider range of material exists for rigid inclusions. All execution techniques and column materials are allowed but in any case, rigid inclusions are made of a bonded material. They thus do not require any soil confinement for the stability of their constitutive material, as opposite to granular columns. For example lime-cement columns, mortar columns or deep soil mixing columns fall into this category of bonded columns. The concept of rigid inclusions (as well as piles in general), suppose a stiffness of the column significantly greater than that of the soil. This assumption is necessary for the use of the concepts of skin friction and tip resistance specific of piles or rigid columns. The horizontal deformations of the column remain negligible. Different authors showed that, for values of column to soil stiffness ratio higher than a given value, the behaviour of a bonded column in the soil is not influenced by the stiffness column/soil ratio anymore. This corresponds to the typical pile behaviour, where in particular the horizontal deformations do not play any role in the global behaviour. Han and Gabr (2002) and Gangakhedkar (2004) studied non-floating bonded columns in axisymmetric conditions (infinite grid pattern) under an embankment, with or without with geosynthetics reinforcement above the top of the columns, for different column moduli. Han & Gabr used the software FLAC and a hyperbolic elastic constitutive law for the soil. Gangakhedkar modelled the soil with a Soft Soil model in Plaxis. In both references, the column was modelled as a linear elastic material. The maximum and differential settlements remain approximately constant for column moduli higher than 1000 MPa, This corresponds to a relative stiffness of 200 to 1000 according to Gangakhedkar (2004) and Han and Gabr (2002) respectively. The German guideline EBGEO (DGGT 2010) recommends a check of the stresses in the geotextile layers above the columns for a ratio between the subgrade reaction of the bonded column and of the soil (different

from material stiffness, see Appendix A.1) larger than 75, reflecting a distinction in the behaviour above and below this ratio.

In comparison to CPRFs, the following additional interaction effects have to be considered:

- Load transfer behaviour in the LTP and resulting load distribution between soil and columns (arching effect);
- Negative skin friction in the upper part of the columns.

The raft-LTP-column-soil interactions lead to a specific deformation scheme with planes of equal settlements: one above the columns if the LTP is thick enough (in case of a CPRF: directly under the slab), one over the column length (neutral plane) and one under the column tip where the settlement profile is homogeneous again (Fig. 2.33 for an infinite RI grid). The load in the column increases with depth in the upper part because of the negative skin friction, reaches its maximum in the neutral plane, and then decreases through load transfer to the soil by positive skin friction and tip resistance like in the case of usual pile foundations (Fig. 2.33).

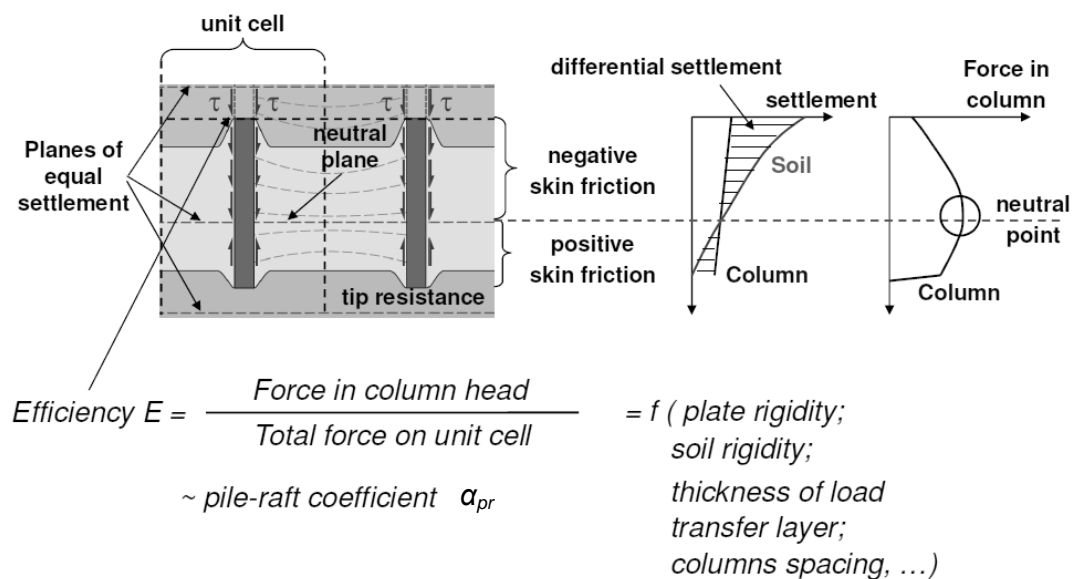


Fig. 2.33 Settlement, load-transfer behaviour and planes with equal settlements in RI grid

The maximum and differential settlements at the top of the system depend highly on the thickness of the LTP and on the slab rigidity. Fig. 2.34 shows in principle the evolution of the load efficiency and of the settlements with the LTP thickness for a granular transfer layer (Höppner 2011). The rigid case with $h = 0$ corresponds to the reference

CPRF case. From a certain LTP thickness value called critical thickness, no difference can be noticed between the rigid and the flexible case (neaning no bending moments in the slab or no differential settlements respectively).

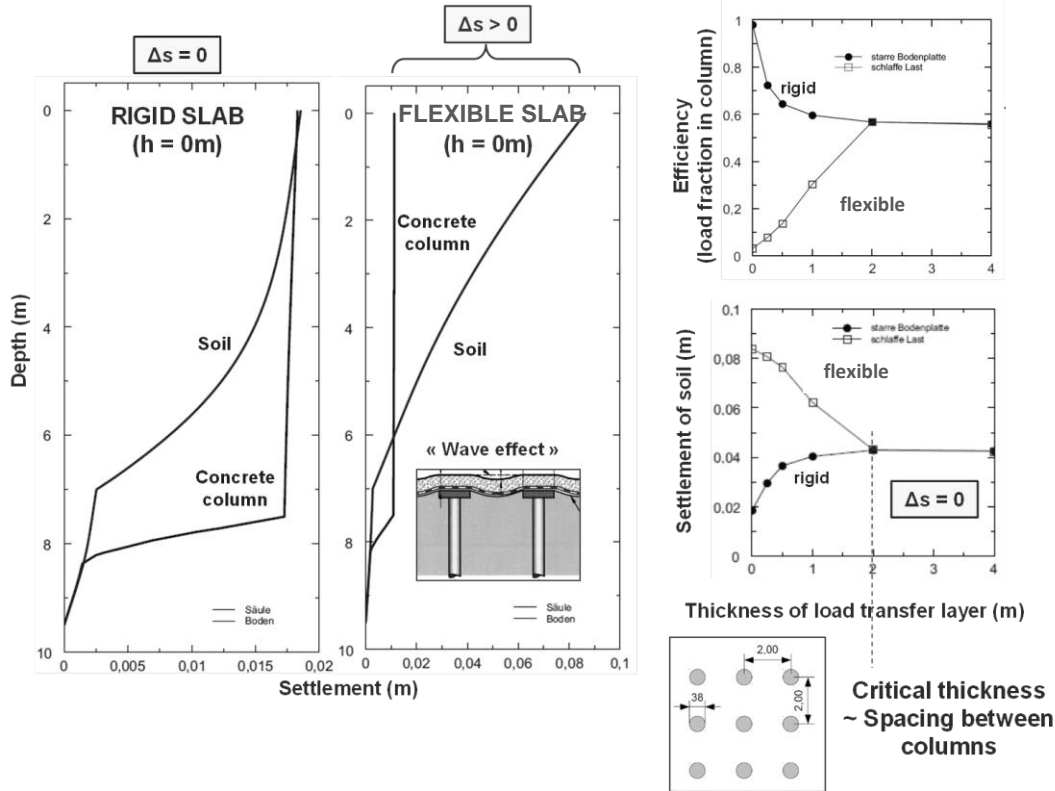


Fig. 2.34 Influence of LTP thickness and slab rigidity on efficiency and settlement behaviour adapted from (Höppner 2011)

This technique is at the boundary between soil reinforcement techniques and deep foundations. As for CPRFs, the RI design is mainly a settlement reduction problem, and all RI projects imply a detailed settlement calculation. RI systems can be used only for this purpose, in general under large slabs or embankments where no bearing capacity or slope stability problem come into question, or additionally in order to increase the bearing capacity for footings which would collapse without reinforcement. Those two philosophies are reflected in the design concept of the ASIRI recommendations: domain 1 for RI necessary for bearing capacity with safety checks similar to piles and domain 2 for RIs used as settlement reducers, for which no safety factor is required for the geotechnical resistance of the columns. The safety concept for rigid inclusion systems is detailed and compared with usual piles in chapter 2.7.

The next section presents the settlement calculation methods developed to take into account the specific behaviour of RI-systems, first the simplified and homogenization methods used in the first stages of the technique, then the different more advanced

methods developed essentially in the scope of ASIRI. Due to the specific behaviour induced by the LTP, even simplified calculation methods of the settlement of a RI system do not start from the settlement of a single column, as opposed to pile groups and CPRF presented in the previous sections. The soil behaviour is general considered based on usual methods for footing or large raft settlement calculations, that is why RI systems under single footings with limited dimensions and large RI-grids are in general distinguished.

2.5.2 RI system calculation

2.5.2.1 Simplified and equivalence methods

RI in an infinite grid

Simplified assumptions for the settlement calculation have been proposed in the CSV-guideline (DGGT 2002) for rigid column grids in Germany: here it is assumed that the whole load goes into the columns (load efficiency or load share equal to 1) and the settlement is calculated by considering the column tip as a fictive footing at depth, increased by the elastic compression of the columns, and the group effect being taken into account as well (fictive raft depending on the layers configuration in Fig. 2.35). This method is not necessarily on the safe side for the settlements, since in reality part of the load goes into the soil which is much less stiff than the columns.

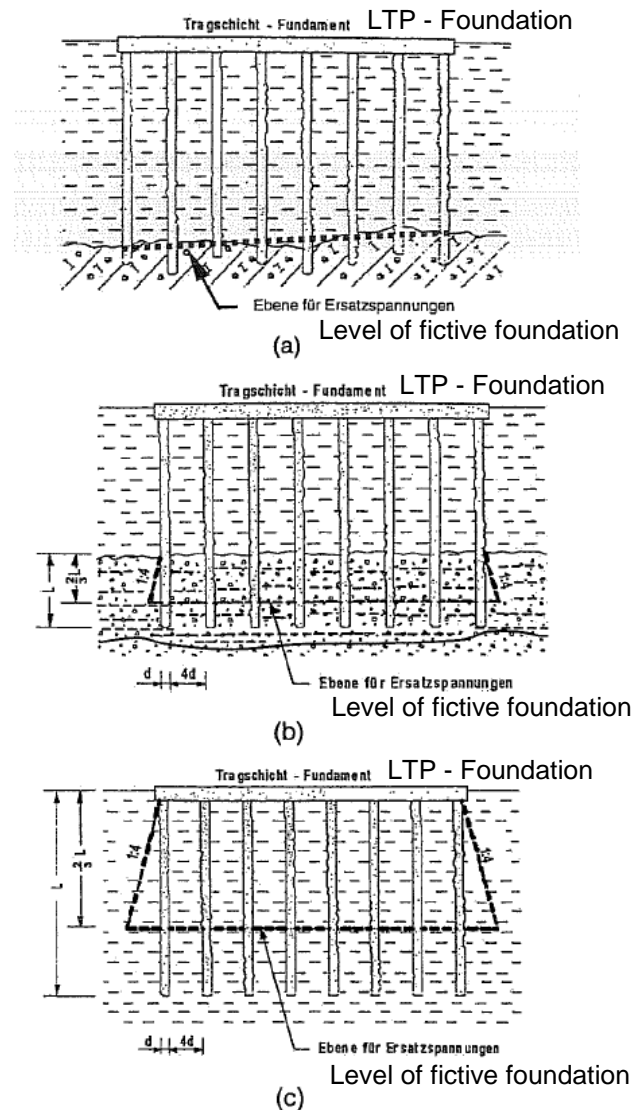


Fig. 2.35 Equivalent raft settlement calculation for groups of rigid columns (CSV-guideline, DGGT 2002)

RIs under a single footing

For single footings, Combarieu (1990) proposed a simplified interpolation method between an unimproved footing and a CPRF configuration (Fig. 31, MV1 model in ASIRI). The load-settlement behaviour of the CPRF is determined using usual methods taking the group effect into account (Fig. 2.36 – 3'). Then an equivalent soil modulus E_{oe} is calculated for the applied load as the modulus giving the same settlement for an unimproved footing. This modulus is then computed in a footing settlement calculation for the layer with columns, the LTP modulus remaining the same (Fig. 2.37). Combarieu recommends the pressuremeter method for the calculation of the raft

settlement, but theoretically the oedometer method with oedometer modulus could be used as well.

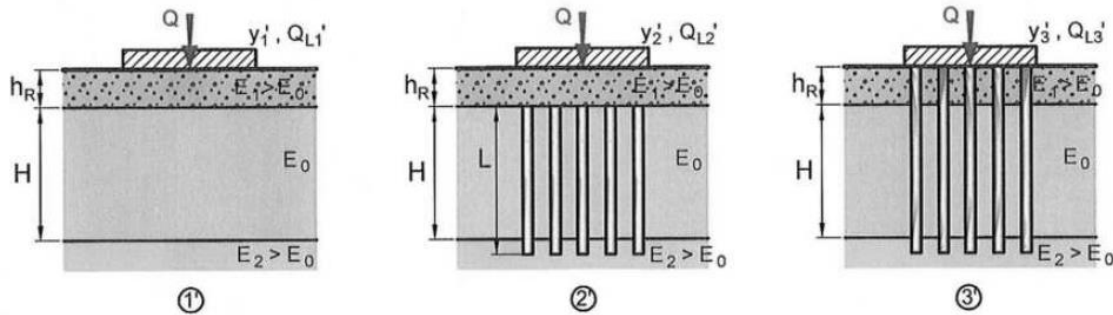


Fig. 2.36 RI system as interpolation between unimproved footing and CPRF from ASIRI (IREX 2012)

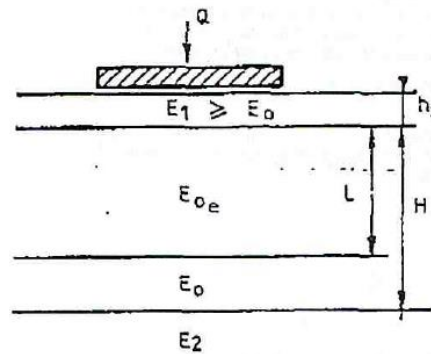


Fig. 2.37 Equivalent modulus E_{oe} for equivalent raft calculation (Combarieu 1990)

2.5.2.2 Load transfer method (LTM) with load transfer curves

RIs in an infinite grid

The load transfer method using load transfer curves (or mobilisation curves) for RI systems has been first developed for large RI grids where the soil/column interaction can be considered in a unit cell with load conservation as shown in Fig. 2.38 and (Eq. 2.51) to (Eq. 2.54) (Caira and Simon 2009). This system corresponds to the calculation method for infinite grids called “common spacing” in the English version of ASIRI (IREX 2012). The column and the soil are divided in subdivisions, in which the load changes are calculated step by step from the load transferred between the column and the soil and from the weight of possible added layers acting as a load (for example added LTP). The system with subdivisions can be calculated for example with matrix

inversion or with the unidimensional finite difference method in an iterative manner, based on the method developed originally for single piles (see Fig. 2.4 and (Eq. 2.30) to (Eq. 2.32) in section 2.2.2). The result depends on the column-pile settlement at each depth according to the chosen and computed load transfer curves. The settlement in each subsection is calculated from the load and the oedometer modulus in the soil and the Young's modulus in the column, so that this is a coupled calculation between vertical displacement and load. This means that here the soil profile does not correspond to the simple soil settlement profile in oedometric conditions under a given load at the top, but that the shape of the soil settlement profile is corrected according to the column influence. This does not correspond to the original definition of load-transfer curves which have been developed for single piles. Originally, the soil settlement was considered as a free settlement due to an external cause; this implies that the soil settlement profile shape is not corrected due to the piles (Frank et al. 1991). However, this modification of the soil settlement profile is justified for unit cell systems where strong pile-soil load transfer occurs and where the load conservation criterion must be met over the unit cell depth. The boundary conditions of uniform stress at the top for an embankment or a flexible raft, or of uniform settlement for a rigid raft, and given the mobilisation function at the column tip, the system can be solved for example by an iterative procedure. The settlement below the column tip level should be calculated separately.

According to ASIRI (IREX 2012), the group effect is automatically taken into account in a unit cell calculation.

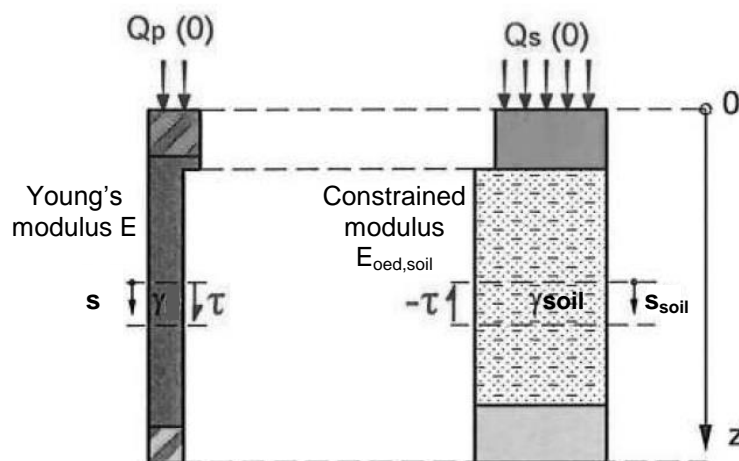


Fig. 2.38 Unit cell RI system for calculation with mobilisation functions adapted from ASIRI (IREX 2012)

$$\frac{dQ_p(z)}{dz} = \pi \cdot B \cdot \tau(s(z) - s_{soil}(z)) \left[+ \gamma \cdot \pi \cdot \left(\frac{B}{2}\right)^2 \text{ if added layers} \right] \quad (\text{Eq. 2.51})$$

$$\frac{dQ_s(z)}{dz} = -\pi \cdot B \cdot \tau(s(z) - s_{soil}(z)) \left[+ \gamma_{soil} \cdot A_s \text{ if added layers} \right] \quad (\text{Eq. 2.52})$$

$$\frac{ds(z)}{dz} = -\frac{Q_p(z)}{E \cdot \pi \cdot \left(\frac{B}{2}\right)^2} \quad (\text{Eq. 2.53})$$

$$\frac{ds_{soil}(z)}{dz} = -\frac{Q_s(z)}{E_{oed,soil} \cdot A_s} \quad (\text{Eq. 2.54})$$

With A_s : soil area

An assumption has to be made for the load transfer behaviour in the LTP (arching effect), which determines the load distribution between the soil and the columns at the level of the top of the real columns. ASIRI (IREX 2012) recommends modelling the LTP in a similar way as the column/soil described above, by considering fictive columns made of LTP material and using the same load transfer curves (Fig. 2.39). The ultimate friction values in the LTP are based on assumptions for the negative skin friction in the French standards NF P94-262 (2012) with a maximum value of $K \cdot \tan(\varphi) \cdot \sigma_v$ (K : horizontal earth pressure coefficient at rest; φ : friction angle in the LTP; σ_v : vertical stress). $K \cdot \tan(\varphi) = 1$ is recommended in granular LTPs according to ASIRI (IREX 2012). The advantage of this method is the possibility to integrate directly the LTP in the LTM model, considering in particular both the soil and the column overall stiffness under the LTP.

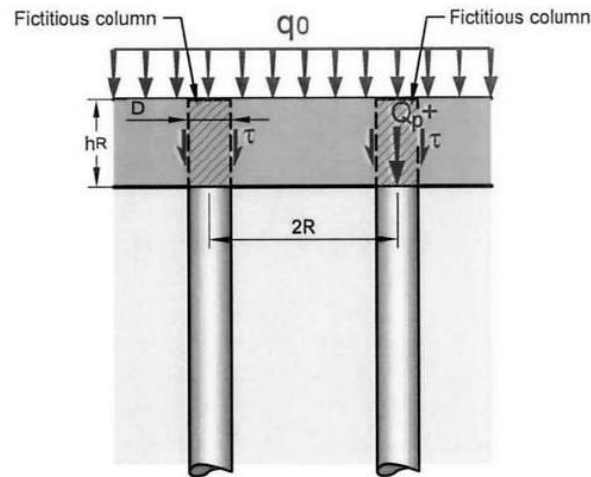


Fig. 2.39 Development of shear along the fictive columns to model the arching effect from ASIRI (IREX 2012)

An analytical expression of the load in the soil at the top of the columns according to this theory has been developed by Combarieu (1988b, 1990, 2007, 2008) (Fig. 2.40). This value is given directly by a computed equilibrium calculation of the whole system in the model presented in Fig. 2.38.

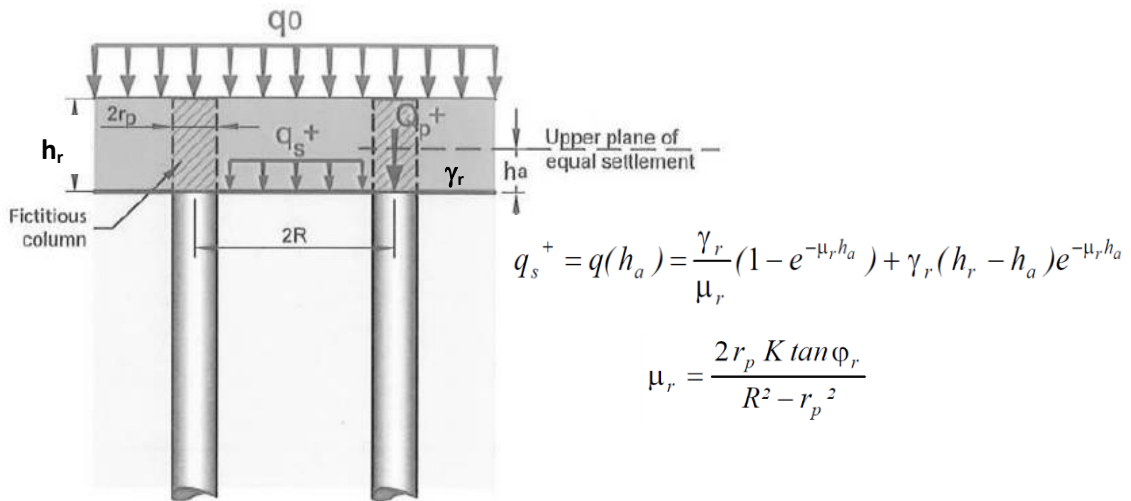


Fig. 2.40 Load in the soil at the top of the columns after Combarieu from ASIRI (IREX 2012)

Other methods exist to describe the arching effect and the corresponding load share at the top of the columns, for example the diffusion cone method for embankments and cases with flexible rafts in ASIRI (IREX 2012). Several proposals have been made in particular for cases of LTP with geogrids and geotextiles, for example after Zaeske and

Kempfert (2002) and after Kempfert et al. (2004) in the recommendations EBGEO (DGGT 2010). The latest improvements in the arching theory with geogrids and geotextiles have been made by Van Eekelen et al. (2012). These methods all rely on the simplifying assumption of infinitely stiff column behaviour.

For a LTM calculation in which the failure behaviour of the LTP material is not modelled, the resistance of the LTP against the punching of the column has to be checked. ASIRI (IREX 2012) proposes to carry out this compatibility check or consistency verification using the failure mechanism used usually to describe the ground failure under foundations after Prandtl (Fig. 2.41). Considering the boundary conditions of the bearing and structural capacity of the column, the limit stress in the soil and the load conservation, the allowable stress can be represented in a diagram as in Fig. 2.42.

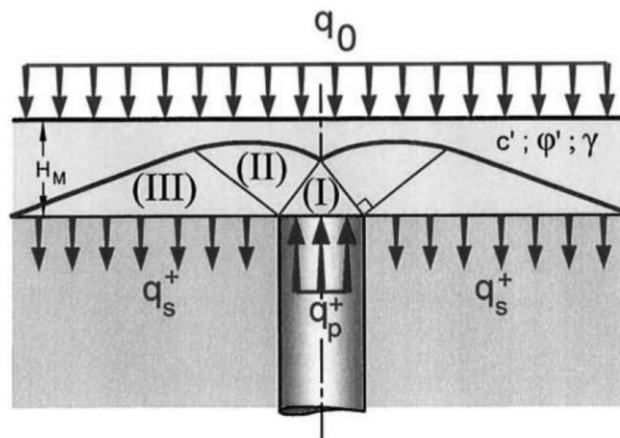


Fig. 2.41 Prandtl's failure mechanism for the compatibility check in the LTP after ASIRI (IREX 2012)

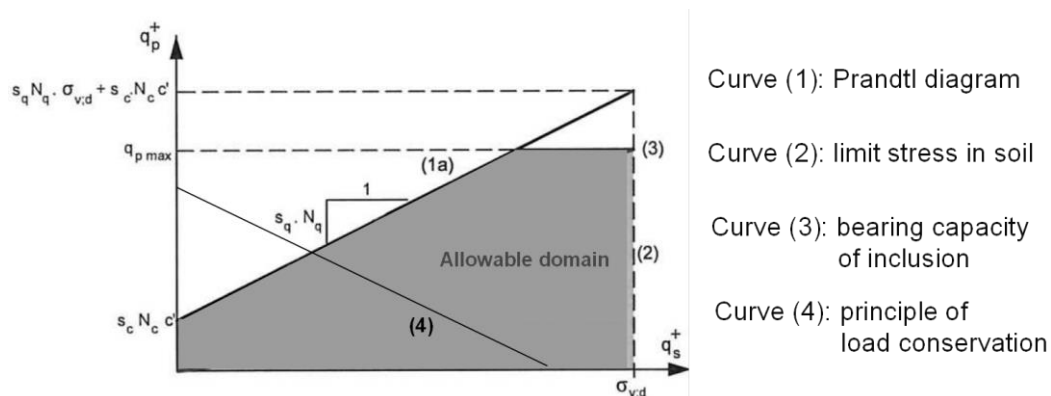


Fig. 2.42 Diagram with domain of allowable stresses in LTP, adapted from ASIRI (IREX 2012)

RIs under a single footing

Glandy and Frossard (2002), cited in ASIRI as the model MV2, proposed for single footings an iterative method similar to the case of an infinite grid. The position of the inclusions is not distinguished and only the soil settlement profile under the characteristic point of the footing is considered for the soil-column relative settlement. Glandy and Frossard proposed the use of the settlement profile with the pressuremeter method (Combarieu 1988a), but this is theoretically applicable with the oedometer method as well. In the same way as in the method for CPRF presented in 3.2.2, the shape of the soil settlement profile is considered without correction due to the presence of the piles (Fig. 2.43), as proposed by Frank et al. (1991).

According to ASIRI (IREX 2012), this model does not take into account the group effect. This should be included separately by reducing the slope of the load transfer curves.

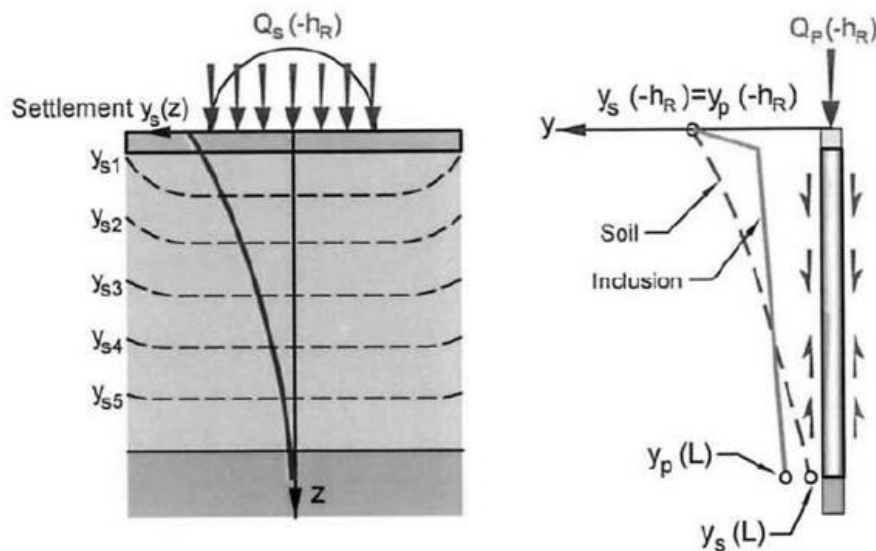


Fig. 2.43 Soil settlement profile under footing for calculation with load transfer curves from ASIRI (IREX 2012)

For single footings, ASIRI (IREX 2012) recommends a hybrid method with unit cell calculation and homogenization part called monolith method (MV3 in ASIRI). This method is quite time-consuming due to the several steps necessary. In the first step, one inclusion with the surrounding soil is calculated as if it was in an infinite grid (LTM or FEM calculation for example) (Fig. 2.44). From this calculation, an equivalent oedometric modulus E^* is calculated and used for the second step in which the soil and columns under the footing are considered as a block (Fig. 2.44). The settlement of this block is calculated as a large equivalent pile with external skin friction with the

surrounding soil. The third step corresponds to the calculation of the stresses and of the settlement profile in the inclusion. This is done by supposing a single column (real and fictive one with LTP) in a soil volume subjected to the settlement profile calculated in the second step: the load at the top of the column domain is the one corresponding to the settlement at the top from step 2 in the load-settlement curve, and the load and settlement profile in the column can be determined for the calculated load as well.

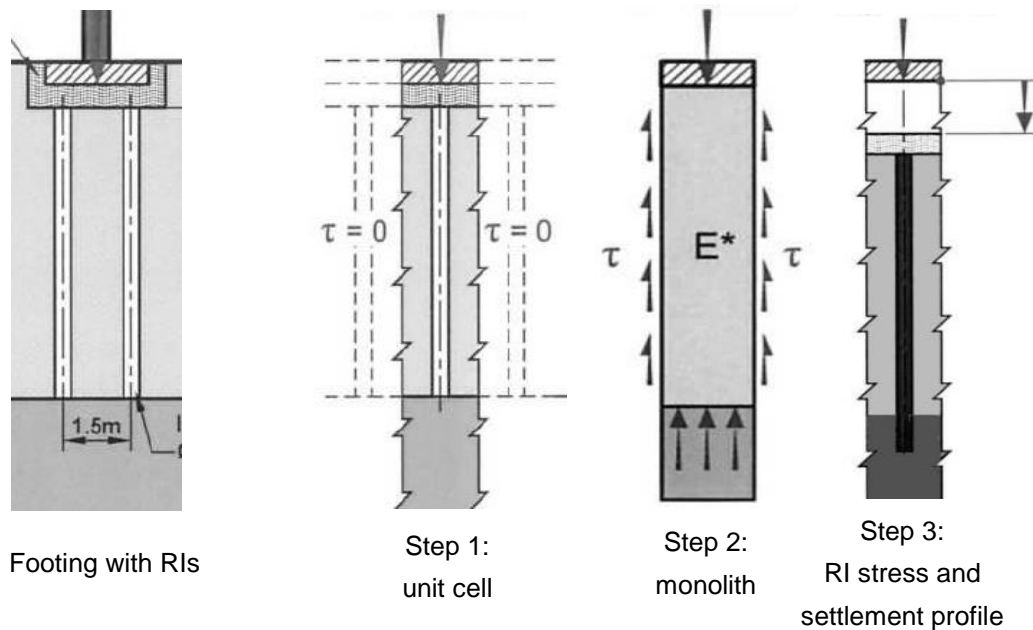


Fig. 2.44 Steps for hybrid monolith method for RIs under footing (IREX 2012)

All the presented LTM methods do not consider a plastic criterion in the LTP material. According to ASIRI (IREX 2012), a consistency check for the stresses in the LTP due to the RI hard point is always required in those cases. A proposal is made on the safe side in ASIRI based on the principle of Fig. 2.41.

2.5.2.3 Continuum methods

The elastic-plastic continuum methods, in general FEM calculation methods, present the advantage to cover directly the group effect and the plastic behaviour of the LTP.

Cases of RI grids can be modelled in an axisymmetric way. A 2D plane-strain modelling would imply that the RIs are represented as thin walls, which should be avoided if possible. The possible failure at the borders of the grid should be considered with a separate check.

Cases of RIs under single footings should be modelled in 3D. The settlement under the pile tip for the settlement-sensitive layers can be directly calculated in a 3D modelling. A 2D axisymmetric modelling of the whole footing would lead to the same representation as walls and should be avoided if possible as well.

ASIRI (IREX 2012) recommends the use of the linear elastic constitutive model for structural elements (with a necessary separated structural capacity check), and for the soil elastic-plastic models for example with Mohr-Coulomb failure criterion, or Modified Cam-clay, or Hardening soil. For the LTP, the linear elastic-perfect plastic model with Mohr-Coulomb criterion is in most cases sufficient, but more advanced models may be necessary for coarse-grained soils (Okyay 2010).

Interfaces are recommended in ASIRI (IREX 2012) by creating a fictive soil with a friction angle equal to zero and with a cohesion equal to the ultimate skin friction according to a load test or otherwise to the applicable local standards. The interface should be very stiff, that means almost no slip between soil and column for stresses smaller than the ultimate skin friction. Refining the mesh in the contact zone instead of using interfaces is another possibility, but this makes the control of the ultimate values more difficult.

ASIRI (IREX 2012) calls particular attention to the plausibility of the numerical results. The results should be controlled and the model parameters calibrated based on load test results, or at least be consistent with the local ultimate values of skin friction and tip resistance. Especially at the column tip, the soil shear parameters are not always extensively documented despite their high influence in the results.

2.6 Stone columns

2.6.1 Principle and behaviour

Granular columns differ from bonded columns in terms of column material type and column material stiffness. The pile concepts of skin friction and tip resistance are not applicable for stone columns. Different coarse-grained column material can be used like sand or gravel, but the most widespread granular columns are the stone columns, developed in the 1960s based on the vibrocompaction method. The diameter of a stone column is in general between 0.6 m and 0.8 m. Calculation methods with different levels of complexity for the load distribution and settlement behaviour have been developed mainly between 1960 and 1990.

Stone columns are in general used in a grid (considered theoretically infinite). The replacement ratio (defined as the column section area by the total unit cell area) is in general larger for stone columns than for rigid inclusions. Considerations have been made for single columns for research purposes (Kirsch 2004). Column groups under footings are relevant as well and have been studied in detail for example by Kirsch (2004) and Black et al. (2011). Kirsch (2004) studied with the software ANSYS the variation of soil modulus for a group of stone columns limited in space under a rigid slab and a levelling granular layer. The soil was modelled as an elastic-plastic material with Mohr-Coulomb failure criterion, and the surrounding soil with the Hardening Soil model. Kirsch reported that there is almost no influence of the relative column/soil stiffness and no further settlement improvement for ratios above 50, for a fixed column modulus of 100 MPa. For the special case of geotextile coated columns, the German guideline EGBEO (DGGT 2010) recommends a check of the stresses in the geotextile layers above the columns for a ratio between the subgrade reaction of the column and of the soil (different from material stiffness, see Appendix A.1) larger than 50 to 75. This reflects a distinction in the behaviour below and above this ratio.

The deformation of stone columns under service loads show a relatively important bulging of the column as opposite to rigid columns, localized in different depth depending on the foundation configuration (Fig. 2.45). The failure of the column can occur by excessive bulging deformations (Fig. 2.46 a), by a failure mechanism similar to a footing near the surface (Fig. 2.46 b) or, in particular for short or floating columns, by a monolithic punch of the column like a pile (Fig. 2.46 c).

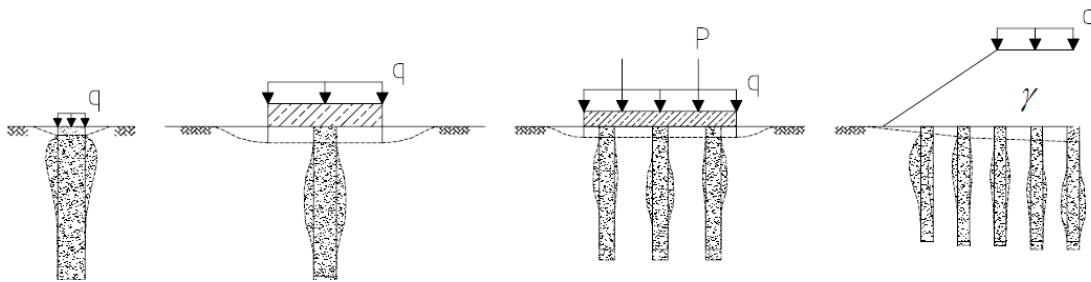


Fig. 2.45 Deformation of stone columns under service loads (Kirsch 2004)

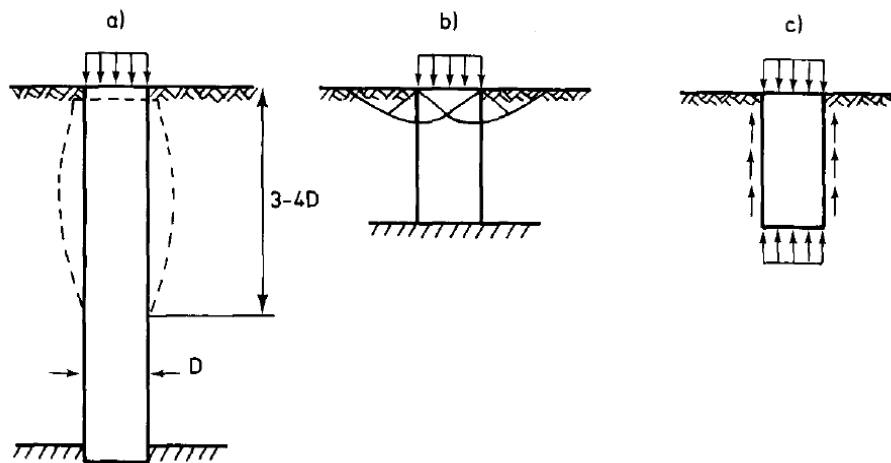


Fig. 2.46 Failure mechanisms for stone columns from Datye (1982), cited by Soyez (1985)

Unlike foundation systems, no particular safety concept is developed in general for stone columns. In many countries like in Germany, the stone column is considered as a soil volume, and thus no check of individual column bearing capacity has to be done in addition to the settlement calculation. Moreover, stone columns are in most cases applied as a large column grid, in which case no base failure of the shallow foundation can occur. For cases under single footings, the bearing capacity of the footing is checked in the same way as for unimproved footings, but with homogenized increased shear parameters for the soil and modified footing width and failure surface in order to take the column improvement into account. Different methods for the weighting of shear parameters are given by Kirsch (2004), for example in (Priebe 1995). In France, stress limitations are prescribed for the single column according to the different failure types in Fig. 2.46 (CFMS and Union Syndicale Géotechnique 2011).

Combined rigid and gravel column systems exist, for example hybrid columns with gravel head or gravel foot. Such systems are designed in practice on an individual basis with care of compatibility of deformations and safety concepts between the different column elements.

2.6.2 Deformation parameters and settlement

The first approximations made for the stone column settlement have been based on the pile settlement calculation, in spite of the considerable differences between both systems. The elastic study of Mattes and Poulos (1969), cited by Dhouib and Blondeau (2005), for compressible single piles has been used a lot in the past for this purpose

(Fig. 2.47). Vautrain proposed an analogy with the tri-axial test (Vautrain 1980). Hugues et al., cited by Soyez (1985), proposed an analogy with the cylindrical cavity expansion in the pressuremeter test.

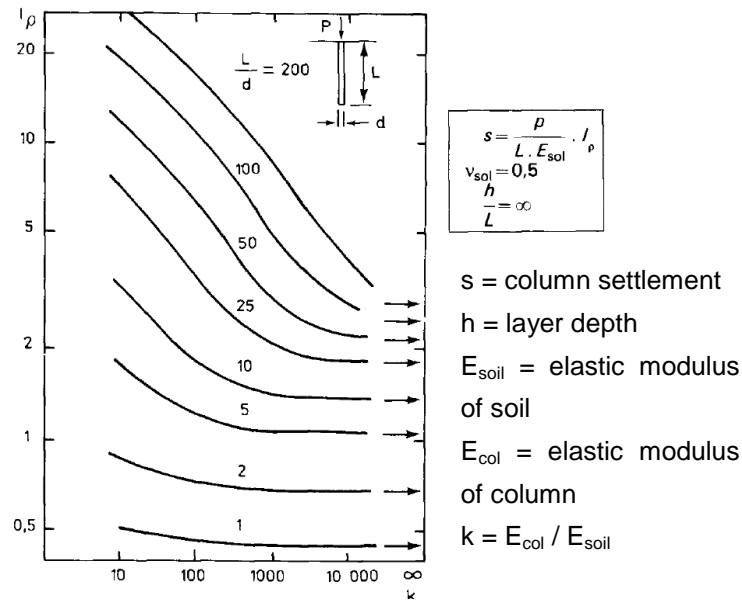


Fig. 2.47 Elastic calculation method for compressible piles from Mattes and Poulos (1969), cited by Soyez (1985): settlement factor I_p vs. column/soil stiffness ratio

Greenwood (1970) proposed a simple empirical method with only the column spacing, the undrained shear strength and the execution type as input parameters (Fig. 2.48).

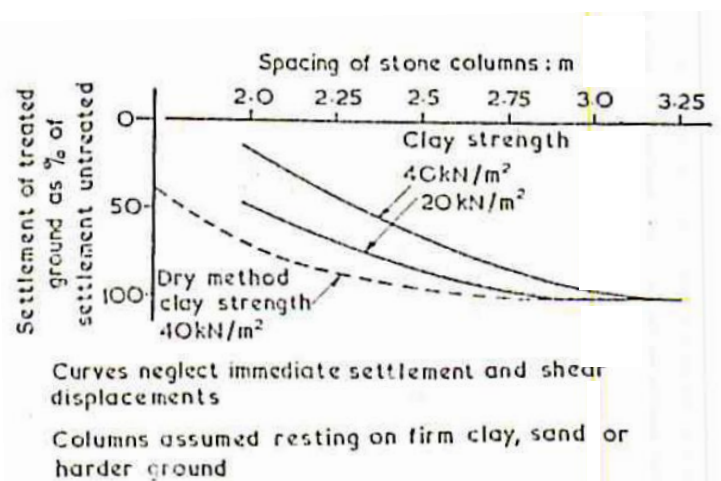


Fig. 2.48 Settlement relatively to unimproved settlement vs. stone columns spacing after Greenwood (1970)

Kirsch presents an overview of the methods in use today (Table 2.14). All of them are appropriate for column grids, but Priebe developed an interpolation method between the single column case and the grid case for column groups. The column material is always considered as elastic-plastic, whereas the soil material is modelled as an elastic material with Young's modulus by some authors, for example for the cavity expansion calculation considered by Priebe (Priebe 1976, 1978, 1988, 1995, 2003, 2004, Dhouib et al. 2004). Van Impe and De Beer (1983) consider on the contrary equivalent stone walls in plane strains. Since the reference case is the unit cell, the considered modulus for the settlement is in general an oedometric modulus.

Table 2.14 Summary of prevalent settlement calculation methods for stone columns (Kirsch 2004)

		1976- 2004	1979	1992	1981- 1985
Berechnungsverfahren nach: Calculation method after:		Priebe	Goughnour/ Bayuk	Van Impe / Madhav	Baalam / Booker
Säulenordnung configuration	Einzelssäule single column	●			
	Säulengruppe column group	●			
	Säulenraster/grid / Einheitszelle unit cell	●	●	●	●
Entwicklungsansatz method type	Empirisch empirical	●			
	Analytisch analytical	●	●	●	●
	Numerisch numerical				●
Verformungs- verhalten Säule column model	elastisch elastic				
	elasto-plastisch elastic-plastic	●	●	●	●
Verformungs- verhalten Boden soil model	elastisch elastic	●		●	
	elasto-plastisch elastic-plastic		●		●
Lagerung der Säule column	schwimmend floating	●			
	stehend on stiff layer	●	●	●	●
Unterteilung des Bodens soil	keine homogeneous			●	
	Schichten/Scheiben several layers	●	●		●

Goughnour and Bayuk (1979) proposed more advanced methods, requiring many calculation parameters. In order to improve the understanding of this method, Meier and Schanz (1998) proposed a numerical implementation of these methods.

The results of the different existing methods have been compared by Greenwood and Kirsch (1983) (Fig. 2.49), Besançon et al. (1984), Soyuz (1985) and Van Impe (2001).

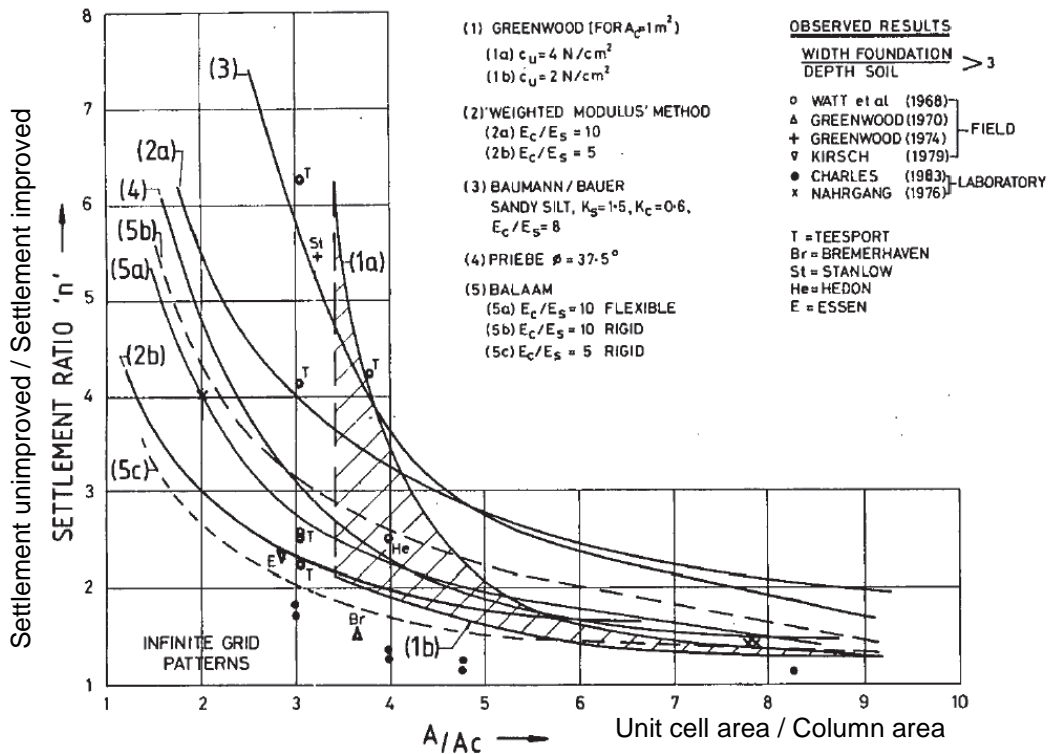


Fig. 2.49 Comparison of settlement calculation methods for stone columns (Greenwood and Kirsch 1983): settlement reduction ratio vs. area ratio

2.7 Comparison of safety concepts for usual and combined foundation systems

This chapter is the subject of conference papers by Katzenbach et al. (2011, 2013), written as a part and in the scope of the present work.

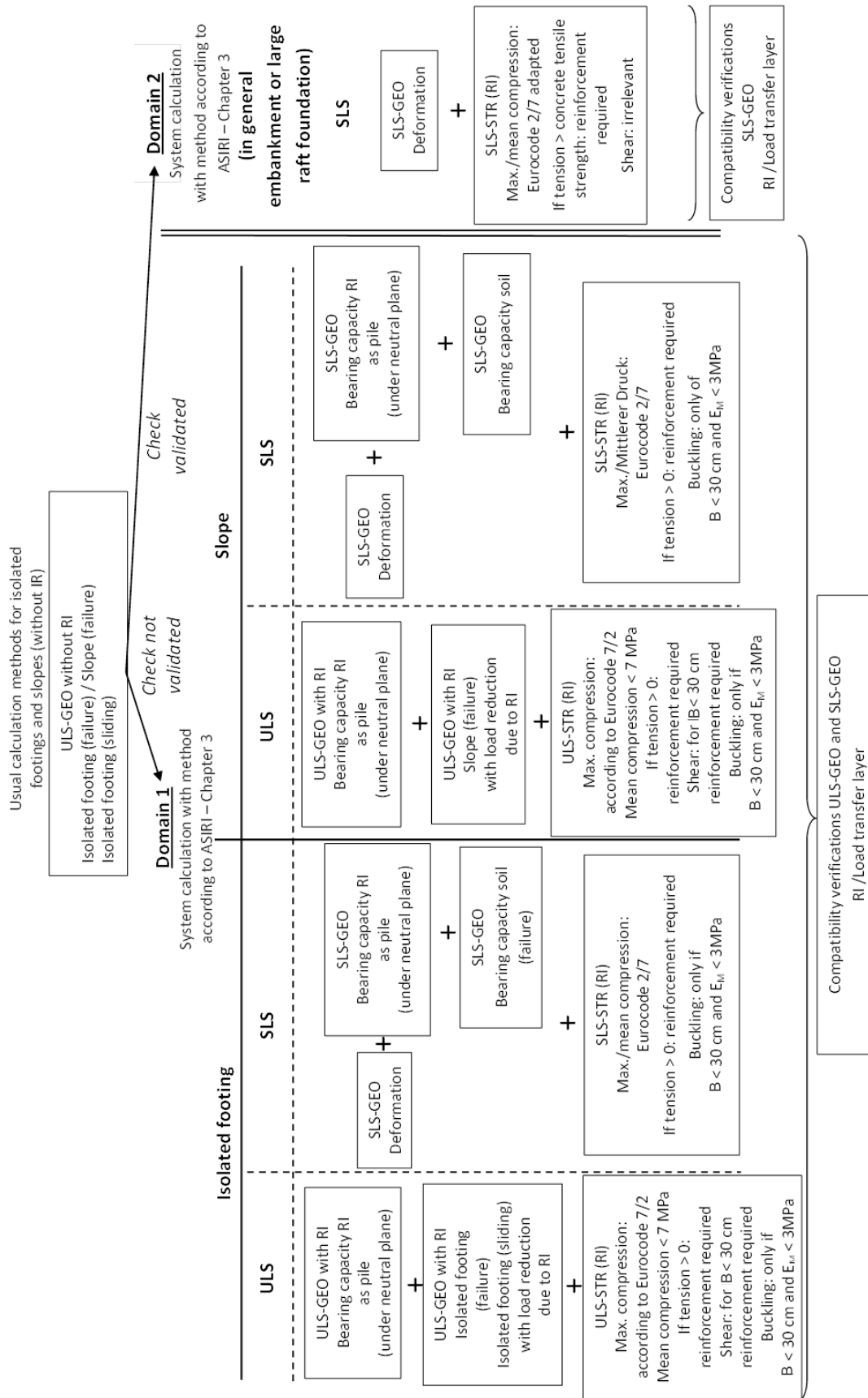
The recommended safety checks in ASIRI (IREX 2012) for the domains 1 and 2 are compared with the French and German national application standards for piling and with recommendations for similar piles or rigid columns systems only (no stone column systems), i.e. the German CPRF-guideline (Hanisch et al. 2002), or in shorter version the international CPRF-guideline (Katzenbach and Choudhury 2013), and the current

German guideline for stabilizing columns (CSV-guideline, DGGT 2002). Stone columns are rather considered as soil reinforcement and not as foundation systems without any specific safety concept, they are thus not considered in the comparison. Only the persistent load situation (BS-P in Germany) in ULS is considered here. The partial safety factors for the actions in the persistent load situation are the same in all regulations, that is 1.35 (respectively 1.5) for the permanent (respectively variable load) in the case of foundations, and 1.0 (respectively 1.3) for the slope stability. The design of usual shallow and pile foundations in France and in Germany after the Eurocode 7 has been presented in sections 2.1 and 2.2.

2.7.1.1 Safety concept for RI after ASIRI (IREX 2012)

The general safety checks workflow for RI according to ASIRI is presented in Table 2.15. First, the unreinforced system (without columns) is calculated, as a classification criterion between domain 1 and 2. Afterwards, the system is calculated with columns in terms of settlement behaviour and load distribution behaviour between the foundation elements. The loads and settlement values resulting from this calculation are considered then for the required safety checks.

Table 2.15 Chart of safety checks after ASIRI (IREX 2012)



2.7.1.2 External bearing capacity (GEO)

In ASIRI (IREX 2012), only the domain 1, where the columns are necessary for the stability, is concerned by the safety checks in the ULS (Table 2.16). The verifications correspond to those of the French application standard of the Eurocode 7 (NF P94-262 2012) for compression piles (with a diameter of usually 1 m up to 3 m), in general with the use of empirical resistance values from pressuremeter tests (Table 2.17). The favourable effect of the columns in the checks of the footing or the slope is taken into account by reducing the total load by the force taken in the columns.

Table 2.16 Partial resistance safety factors – ASIRI ULS-GEO

ULS-GEO (BS-P)	ASIRI (France)							
	Domain 1				Domain 2			
	Isolated footing		Slope	RI	Isolated footing		Slope	RI
Failure	Sliding	Failure			Sliding			
Partial safety factor for resistance	$\gamma_{R,v} \times \gamma_{R,d}$ = 1,4 x 1,2 = 1,68	$\gamma_{R,h} \times \gamma_{R,d}$ = 1,1 x 1,0 = 1,1	$\{\gamma_{\phi'} = \gamma_c\} \times \gamma_{R,d}$ = 1,25 x (1,1 bis 1,2) = 1,38 bis 1,5	$\{\gamma_b = \gamma_s\} \times \gamma_{R,d1} \times \gamma_{R,d2}$ = 1,1 x 1,15 x 1,1 = 1,39	/	/	/	/
Remark	load reduction due to RI (Slope only drained here model factor for reinforced soils depending on the sensitivity towards deformations)			like piles under the neutral plane empirical values (pressuremeter method)	no stability check	no stability check	no stability check	no stability check

Table 2.17 Partial resistance safety factors – Eurocode 7 ULS-GEO

ULS-GEO (BS-P)	Eurocode 7 Germany				Eurocode 7 France			
	Isolated footing		Slope	Piles	Isolated footing		Slope	Piles
	Failure	Sliding			Base failure	Sliding		
Partial safety factor for resistance	$\gamma_{R,v}$ = 1,4	$\gamma_{R,h}$ = 1,1	$\gamma_{\phi'} = \gamma_c$ = 1,25	$\gamma_b = \gamma_s$ = 1,4	$\gamma_{R,v} \times \gamma_{R,d}$ = 1,4 x 1,2 = 1,68	$\gamma_{R,h} \times \gamma_{R,d}$ = 1,1 x 1,0 = 1,1	$\gamma_{\phi'} = \gamma_c$ = 1,25	$\{\gamma_b = \gamma_s\} \times \gamma_{R,d1} \times \gamma_{R,d2}$ = 1,1 x 1,15 x 1,1 = 1,39
Remark			only drained here	with empirical values	with pressuremeter method		only drained here	with empirical values (pressuremeter method)

In the CPRF-guideline (Hanisch et al. 2002), no distinction is made between a use as “settlement reducer” or as “resistance increaser”. The ultimate characteristic resistance is defined here from the load-settlement curve of the global system, and divided by a safety factor to obtain the design value (Table 2.18). The bearing capacity of the piles themselves does not need to be verified, since the whole system made of the slab, the piles and the soil already has to be stable. In the CSV-guideline the bearing capacity of the single columns always has to be checked, with the additional assumption that the total applied load from the structure is taken by the columns (here diameter 12 cm up to 20 cm), which is on the safe side for the safety checks in terms of bearing capacity (but not necessarily on the safe side for the settlement calculation).

Table 2.18 Partial resistance safety factors – CPRF and CSV-guidelines ULS-GEO

ULS-GEO (BS-P)	CPRF-Guideline (Germany)			CSV-Guideline (Germany)			
	Combined pile-raft foundation		Slope	Isolated footing		Slope	Columns
	Failure	Sliding		Failure	Sliding		
Partial safety factor for resistance	$\gamma_{R,v}$ = 1,4	$\gamma_{R,h}$ = 1,1	/	/		$\gamma_{\varphi} \times \lambda_{pv}$ = 1,25 x 1,15 = 1,43	γ_{sp} = 1,25 bis 1,4
Remark	as global system		/	not taken into account		only drained here λ_{pv} against chain reaction of columns	Assumption: total load in the columns; depending on number of load tests (in execution phase)

The main differences in terms of check of geotechnical bearing capacity according to the different standards and guidelines are shown in Fig. 2.50.

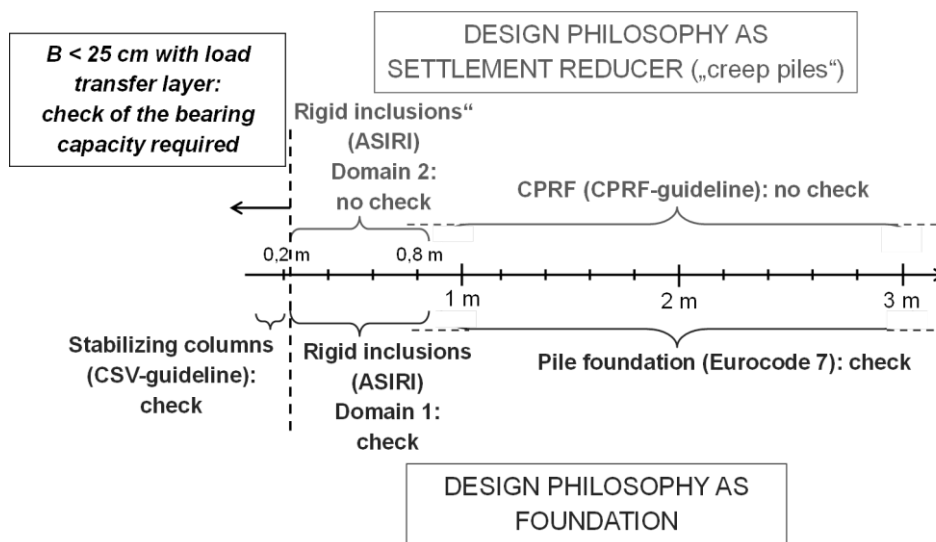


Fig. 2.50 Check of geotechnical capacity of single columns in function of column diameter according to standards and recommendations

According to the French application standards of the Eurocode 7 (NF P94-261 2013, NF P94-262 2012), safety checks for the resistance have to be carried out in the SLS as well (Table 2.20). This has been adopted in ASIRI (IREX 2012) for the domain 1 (Table 2.19). Therefore a so-called “pile creep load” has been defined in the French standards as 70 % (in the case of displacement piles) of the total resistance (reference load for the SLS). The safety against base failure of single footings also is increased in comparison with the ULS. In the domain 2, only the compatibility of the displacements has to be investigated. In the German application standards of the Eurocode 7

(Table 2.20) and in the German recommendations (Table 2.21), only the displacements have to be controlled in the SLS.

Table 2.19 Partial resistance safety factors – ASIRI SLS-GEO

SLS-GEO (BS-P)	ASIRI (France)							
	Domain 1				Domain 2			
	Isolated footing		Slope	RI	Isolated footing		Slope	RI
Failure	Sliding	Failure			Sliding			
Partial safety factor for resistance	$\gamma_{R,v} \times \gamma_{R,d}$ = 2,3 x 1,2 = 2,76	/	/	$\{\gamma_b = \gamma_s\} \times \gamma_{R;d1} \times \gamma_{R;d2} / 0,7$ = 1,1 x 1,15 x 1,1 / 0,7 = 1,99	/	/	/	/
Remark	load reduction due to RI	no stability check	no stability check	like piles 0,7: factor for "pile creep load" for displacement piles	Deformations			
	Deformations							

Table 2.20 Partial resistance safety factors – Eurocode 7 SLS-GEO

SLS-GEO (BS-P)	Eurocode 7 Germany				Eurocode 7 France			
	Isolated footing		Slope	Piles	Isolated footing		Slope	Piles
	Failure	Sliding			Failure	Sliding		
Partial safety factor for resistance	/	/	/	/	$\gamma_{R,v} \times \gamma_{R,d}$ = 2,3 x 1,2 = 2,76	/	/	$\{\gamma_b = \gamma_s\} \times \gamma_{R;d1} \times \gamma_{R;d2} / \{0,5 \text{ bis } 0,7\}$ = 1,1 x 1,15 x 1,1 / {0,5 bis 0,7} = 1,99 bis 2,78
Remark	no stability check	no stability check	no stability check	no stability check	with pressuremeter method	no stability check	no stability check	Empirical values (pressuremeter method) 0,5 bis 0,7: factor for "pile creep load" depending on the execution method
	Deformations				Deformations			

Table 2.21 Partial resistance safety factors – CPRF and CSV-guidelines SLS-GEO

SLS-GEO (BS-P)	CPRF-Guideline (Germany)			CSV-Guideline (Germany)			
	Combined pile-raft foundation		Slope	Isolated footing		Slope	Columns
	Failure	Sliding		Failure	Sliding		
Partial safety factor for resistance	/		/	/	/	/	/
Remark	Deformations as global system		/	Deformations			

2.7.1.3 Internal structural capacity (STR)

The safety factors for the maximum compression in the cross section of the rigid inclusions in the ULS and SLS are similar to those for piles in NF EN 1997-1 (2014)

(with reference to NF EN 1992-1-1 2005 and NF EN 1992-1-1/NA 2007 for the concrete). The safety factor for the resistance in ASIRI (IREX 2012) is approximately between 2 and 11 depending on the limit state, the execution type, the slenderness of the column and the quality controls. In order to avoid very small column diameters, the mean compression stress in the section is in all cases limited to 7 MPa in the ULS (domain 1). Adapted values have to be considered for domain 2 (SLS).

Although the rigid inclusions are not used as tension piles, tension stresses can develop in the section resulting from bending moments. In the domain 1, the columns have to be reinforced in the same way as piles according to NF EN 1992-1-1 (2005) and NF EN 1992-1-1/NA (2007) as soon as tension stresses appear in the section. On the other hand, in the domain 2 tensile stresses up to the characteristic value of the tensile strength of the concrete are allowed. If this value is exceeded, the columns have to be reinforced as well.

The internal resistance can be particularly endangered in the case of unreinforced columns with very small diameter. For this reason, no shear stresses are allowed in ASIRI (IREX 2012) for unreinforced columns with a diameter smaller than 30 cm (compared to 40 cm for conventional piles). Buckling effects have to be analysed also for these small diameters and for very soft soils (pressuremeter modulus E_M smaller than 3 MPa). The minimum allowed diameter in ASIRI for unreinforced columns is 25 cm.

In the CPRF-guideline (Hanisch et al. 2002) the internal resistance has to be checked in the same way as for conventional pile foundations.

According to the CSV-guideline (DGGT 2002), a safety factor of 2 has to be considered for the mean compression, in comparison with 2 to 6 for the maximum compression stress in the ULS and 7 MPa for the mean compression stress in ASIRI (IREX 2012). According to this guideline, the buckling has to be checked only in soft layers with an undrained shear strength smaller than 10 kPa. This is not in accordance with the present state of the art for slender piles: buckling effects can already appear for soils with higher undrained shear strength (DIN 1054 2010, Vogt et al. 2009).

3 Investigation of the settlement of shallow foundations

For unifying reasons in the present work between shallow and pile foundations, and in order to distinguish more easily the mobilised load from the ultimate load, the ultimate bearing capacity of a footing under vertical loads is denoted Q_{ult} from here (instead of $R_{n,k}$ in Germany and $R_{v,k}$ in France as in section 2.1). The applied vertical load is denoted Q (instead of V_k in the Eurocode 7 as in section 2.1).

3.1 Application of moduli correlations for linear elastic calculation

This chapter is partly the subject of the conference paper by Bohn et al. (2013), written as a part and in the scope of the present work.

An existing site by Keller France in Les Abymes (Guadeloupe, France), where CPTs, PMTs and oedometer tests from drill samples have been carried out close to each other, is chosen, in spite of the particularly soft soil conditions corresponding to the limit of applicability of the PMT test (Fig. 3.1). A simplified schematic representation of the soil configuration is presented in Fig. 3.2. Case (a) corresponds to a rigid single footing, loaded with a serviceability load level with no base failure risk, and case (b) represents the large raft foundation case with the same load.

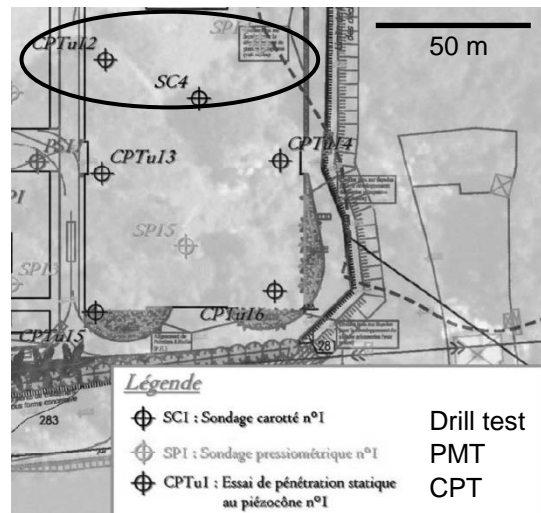


Fig. 3.1 Example site with in situ soil tests for settlement calculation of shallow foundations

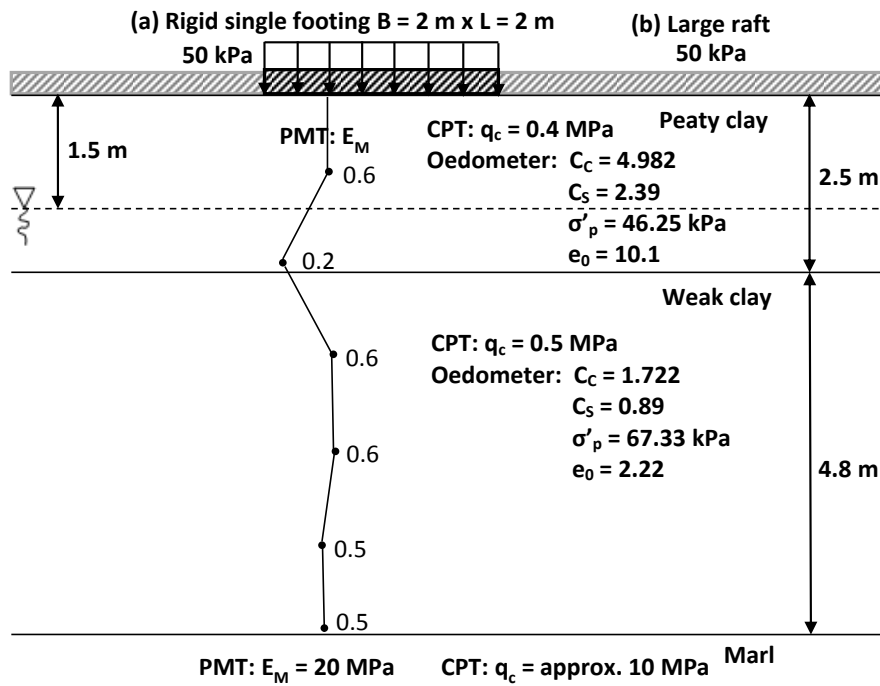


Fig. 3.2 Example site: soil configuration and shallow foundation cases

The results of the settlement calculation for both cases (a) and (b) are presented in Table 3.1. In this example where all the major important tests are available, the pressuremeter calculation method is considered as the most reliable and reference method for the footing case (see Appendix A). The oedometer method based on the oedometer test is the reference method for the raft case (see Appendix A). For the oedometer method with E_{oad} from CPTs the correlation after the Eurocode 7 EN 1997-2 (2007-2010) (DIN EN 1997-2 2010 in Germany, NF EN 1997-2 2007 in France) presented in Appendix C.2 is used.

Table 3.1 Example site: comparison of settlement calculation methods for shallow foundations and modulus calibration

Calculation method	Settlement (m)	
	(a) Footing	(b) Raft
PMT method	0.084 Reference method	0.882
Oedometer method with C_d/C_s	0.238	1.042 Reference method
Oedometer method with E_{oad} from CPT	0.017 to 0.33	0.868 to 17
Case-based correlation: calibration of E_{oad} with reference method	$E_{\text{oad}} = 2.2 \cdot E_M$	$E_{\text{oad}} = 0.6 \cdot q_c$

For the footing case, the reference PMT method gives a two to three times smaller settlement than the oedometer method, certainly because the last one does not correctly represent the actual stress-strain field with shear mechanisms under a footing. Depending on the exact organic content and water content of the soil layers, the CPT correlation method only provides a very wide range for the factor α (see Appendix C.2), between 0.4 and 8. If one considers the PMT method as the reference method, the equivalent oedometer modulus for following applications would be $2.2 \cdot E_M$ considering a calibration made on the unimproved reference case. If one would prefer to consider the extended oedometer method as the reference case, the soil moduli would be the moduli corresponding to the equivalent calculation with the swelling and the compression factors C_s and C_c .

For the raft case, the reference oedometer method and the extended PMT method give similar results. Again, the correlation from CPTs provides only a very wide and partly non-realistic range of up to 17 m. For following applications, the oedometer moduli corresponding to the oedometer test should be considered. Here one can see that this would correspond to a factor α equal to 0.6 for the CPT correlation for this soil and foundation conditions.

This leads to the following recommendations:

- for single footings, the direct pressuremeter method after Ménard is recommended if pressuremeter test results are available. If Young's moduli or oedometer moduli are necessary for following applications based on the unimproved case, they should be determined case by case by calibration with one of the two above mentioned reference methods (for example for footings $E_{\text{oad}} = k \cdot E_M$, k defined case by case). Informative annexes of standards give

indicative values for this correlation factor (see Appendix C.3). If no pressuremeter test results are available, the oedometer method may be used with oedometer test results or with the correlation $E_{\text{oed}} = \alpha \cdot q_c$ from CPTs (see Appendix C.2) but only for well-known soils;

- for large rafts, the oedometer method based on oedometer deformation parameters is recommended for large rafts or slabs. If no oedometer test results but only CPT results are available, the correlation $E_{\text{oed}} = \alpha \cdot q_c$ may be used (see Appendix C.2) but only for well-known soils. If only PMT tests are available, the correlation $E_{\text{oed}} = E_M/\alpha$ may be used (Table 2.4).

3.2 Single footing non-linear settlement behaviour

A linear elastic calculation of the settlement of a single footing is in many cases sufficient in combination with a safety check of the footing bearing capacity. This ensures a permanent load level Q small enough for the footing to remain in the initial quasi-linear domain. However, the development of combined systems like CPRF or RI systems calls for a more detailed description of the load-settlement behaviour of the footing, especially in comparison with the unreinforced case (shallow foundation alone) which may well be above the quasi-linear limit. Only very few proposals are available on this matter in the literature. Ménard proposed for the settlement calculation an increasing factor $\beta(F) = \max\left(1; \frac{2}{3} \cdot \frac{F}{F-1}\right)$ which depends on the mobilised safety factor F (see (Eq. A.38) in Appendix A.1). This formulation corresponds to a hyperbolic trend of the load-settlement curve for loads above one third of the failure load ($F \leq 3$), and a linear load-settlement curve up to this load ($F \geq 3$).

In the scope of the CPRF modelling, Combarieu (1988a) proposed a logarithmic expression of the load-settlement curve (see Appendix A.4), but this assumption has not been checked against load tests of footings. This corresponds to an exponential mobilisation curve of the footing resistance against the settlement (Eq. 3.1). Combarieu calibrated the curve parameter λ_{exp} in (Eq. 3.1) considering the settlement calculation after the pressuremeter theory of Ménard with an equality of both linear and non-linear method for a load level equal to half of the ultimate footing load (Fig. 3.3). This means that Combarieu considered that the linear settlement calculation is on the safe side for loads smaller than half of the ultimate load.

$$Q_{\text{exp}}(s) = Q_{\text{ult}} \cdot \left(1 - e^{-s/\lambda_{\text{exp}}}\right) \quad (\text{Eq. 3.1})$$

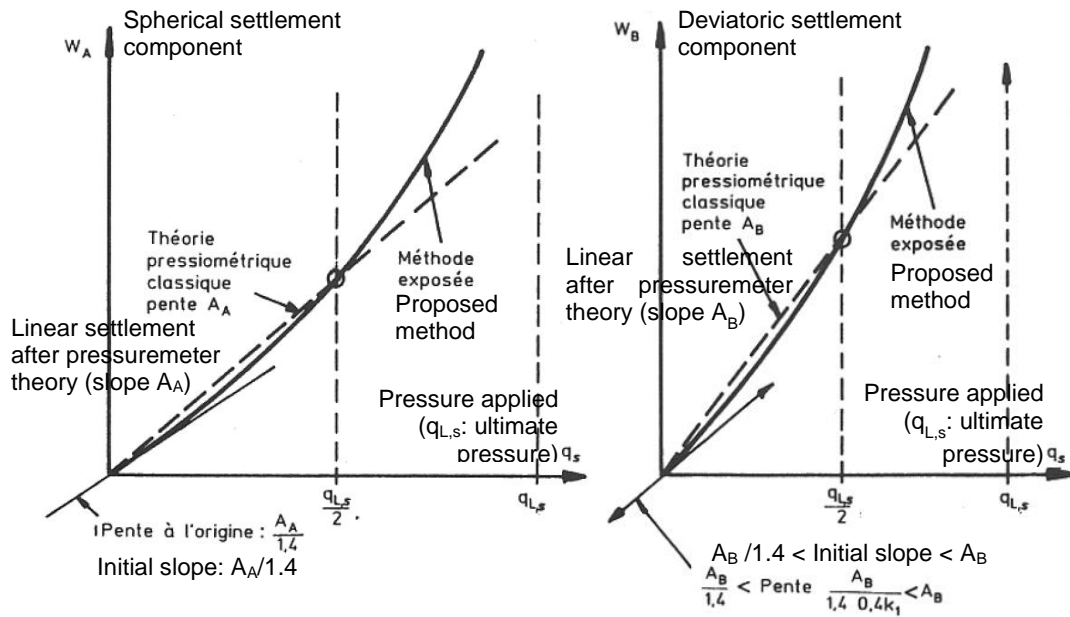


Fig. 3.3 Proposal of Combarieu (1988a) for footing load-settlement curve (spherical and deviatoric components)

Briaud (2003b, 2007) proposed a determination of the footing load-settlement curve based on the analysis of the whole stress-deformation curve of the pressuremeter test (Fig. 3.4 compared to Fig. A.18 in Appendix A.4), developed relying on measurements mainly in sands. However, this very powerful proposal is limited to regions where the pressuremeter test is well-established, and even there it may be too time-consuming for everyday projects for which only the limit pressure and the pressuremeter modulus in the quasi-linear part are considered in general.

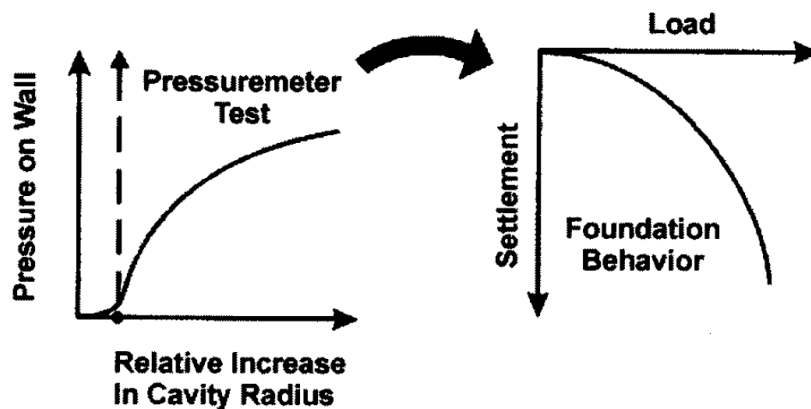


Fig. 3.4 Proposal of Briaud (2007) for footing load-settlement curve

Lutenegger and Adams (2003) propose a root mobilisation curve with a root factor between 2 and 3 (square root to cubic root). This curve presents the major inconvenient of having an infinite initial slope, leading to very high stiffness values very far from the stiffness of the usual established linear methods. In particular for the case of combined systems with columns where the load level in the footing part is small, the stiffness is preferred to remain in comparable proportion with the reference linear calculations.

In the present work, a simple non-linear load-settlement curve shape is aimed at. A hyperbolic curve shape (Eq. 3.2) is thus investigated in comparison with measurements of ten load tests from the literature with different geometries (width B, length L, embedment D), in different ground types and in different regions (Briaud 2007, Canépa and Garnier 2003).

$$Q_{hyp}(s) = \frac{s \cdot Q_{ult}}{s + \lambda_{hyp} \cdot B} \quad (\text{Eq. 3.2})$$

The dimensionless curve parameter λ_{hyp} allows for equalizing the proposed settlement with the results of usual linear calculations for the load level $Q_{ult}/3$. With this calibration choice, the initial slope of the proposed curve is 1.5 times higher than the stiffness of the reference linear method. Only the agreement of the curve shape is investigated, not the curve stiffness or the stiffness adjustment coefficient λ_{hyp} . For applications of the non-linear footing settlement behaviour in the following sections of the present work, the usual and well-established methods for footing settlement calculation (Appendix A and section 2.1) will indeed be considered for the curve calibration in the domain of small settlements, leading automatically in each case to a different λ_{hyp} factor.

The proposed methodology of assessment of the hyperbolic curve shape is the following:

- the ultimate load of the footing is defined as the maximum reachable load, determined from the measured load-settlement curve, in general by extrapolating the last part in the failure domain visually;
- the modelled hyperbolic curve is back-calculated via λ_{hyp} for an equality of the settlement s with the measurement for $Q_{ult}/3$, considered as a realistic serviceability load level. The main aspect investigated here, which is the increase of settlements for higher loads, could not be analysed in an objective way if the adjustment was made for a higher load;
- for comparison purposes with the proposal of Combarieu (1988a), the same procedure is made for the exponential expression with λ_{exp} (Eq. 3.1). Since this

shape is more abrupt than the hyperbolic one, meaning that it shows a quicker mobilisation with the settlement, an adjustment based on half of the ultimate load is made as well for the exponential case.

The hyperbolic and exponential curves are compared with the measured ones in terms of pressure q for ten footings in Fig. 3.5.

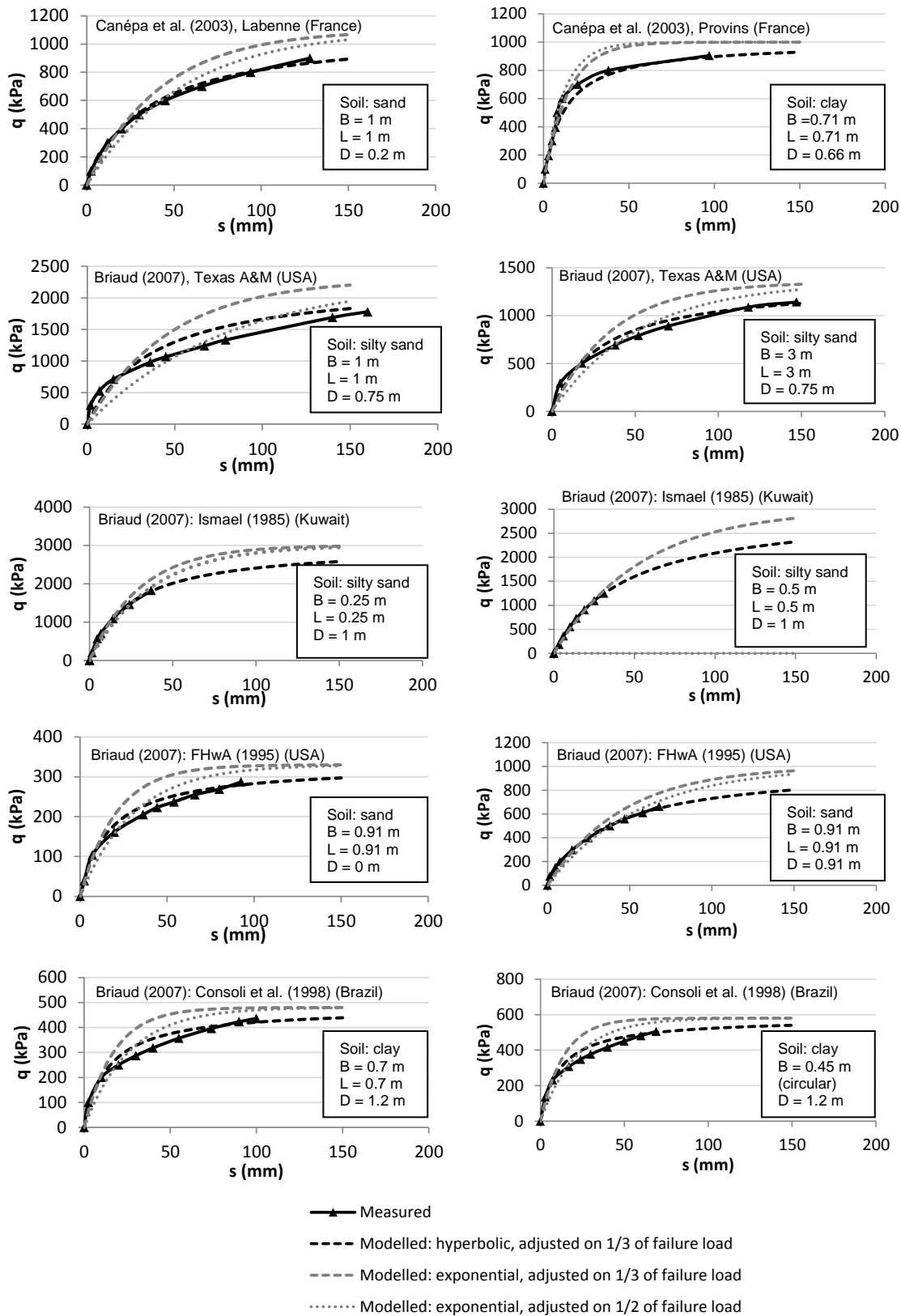


Fig. 3.5 Measured and modelled footing load-settlement curves

As stated by Briaud (2003a, 2007), the footing load-settlement curve normalized by the ultimate load and by the footing width does not depend on the size and on the embedment of the footing. This means that the load-settlement curve shape would remain the same and that the results in Fig. 3.5 would be valid for all possible different footing dimensions and embedments at least in the investigated soils. The results of Briaud (2003a, 2007) show that the footing dimensions have no influence on the ultimate area load if the soil resistance remains approximately constant in the influence zone under the footing.

The following conclusions can be drawn:

- the exponential curve type does not reproduce well the measurements for high loads, showing a too stiff behaviour, even if it is adjusted at half of the failure load;
- the hyperbolic curve shape matches almost perfectly the measured footing load-settlement curves for the whole load domain, for different footing dimensions, shapes and embedments and for different soil types.

The hyperbolic mobilisation curve shape may thus be used to represent the whole non-linear load-settlement behaviour of footings. This non-linear hyperbolic correction of the linear curve is applicable independently from the approach chosen for the linear settlement calculation used as reference for the load level $Q_{ult}/3$ (Fig. 3.6).

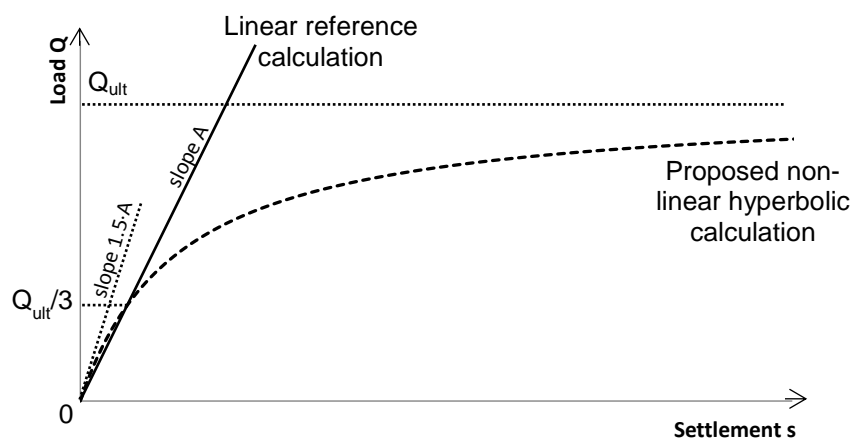


Fig. 3.6 Proposed hyperbolic mobilisation curve for single footing resistance

4 Investigation of the settlement of pile foundations

For unifying reasons in the present work between shallow and pile foundations, and in order to distinguish more easily the mobilised load from the ultimate load, the ultimate skin friction is denoted $q_{s,ult}$ from here (instead of $q_{s,k}$ in the Eurocode 7 as in section 2.2) and the mobilised skin friction q_s (instead of τ in France, as in section 2.2). In the same manner, the ultimate base resistance is denoted $q_{b,ult}$ from here (instead of $q_{b,k}$ in the Eurocode 7 as in section 2.2) and the mobilised base resistance q_b (instead of q in France, as in section 2.2).

4.1 Pile load test database

The main development proposed in the present work regards the load transfer method (LTM) in section 4.3. It is based on pile load tests with instrumentation down the pile in order to develop load transfer curves (see Table 4.1 below), and subsequently on pile load tests with measurements at the pile head only in order to check the validity of the proposed curves (see Table 4.2 below). In chapter 4.2, only one finite element method (FEM) example is presented with one test from the database. A wide range of pile types (driven, screw, bored, concrete and steel piles) of different diameters from 0.3 m to 2 m and of ground types (fine-grained and coarse-grained soils, soft rock like marl, limestone and chalk) in different geographical regions (France, Poland and Brazil) are available in the database. The tests have been provided by the French research institute Ifsttar (Burlon 2013), by the company Keller, among others for the French national project ASIRI (IREX 2012) and one test by Fernandez et al. (2014), and by Krasiński (2010, 2011, 2012a, 2012b). The load tests have been selected for their level of quality of the experimental data (with for example detailed ground investigations next to the piles).

The instrumentation consists of strain gauges or vibrating wires glued directly on reinforcement bars or of the “removable extensometer” system lowered down the pile into reservation pipes (Bustamante and Jézéquel 1975, Ifsttar example in Fig. 4.1).

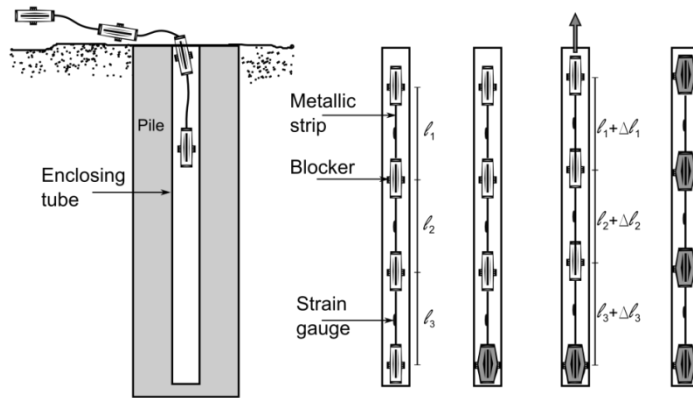


Fig. 4.1 Example of pile instrumentation with the “removable extensometer” system

From the strain measurements, the load down the pile is obtained by considering the pile as an elastic rod. The compression stiffness of the pile is the Young’s modulus multiplied by the area of the cross section. This stiffness is either estimated or measured on a pile sample. The pile tip load is extrapolated from the load profile (example in Fig. 4.2-B). The mobilisation curve is determined from the loads between two levels z or at the tip, the displacement being equal to the settlement at the pile head minus the pile shortening down to this level (example in Fig. 4.2-A and Fig. 4.2-C).

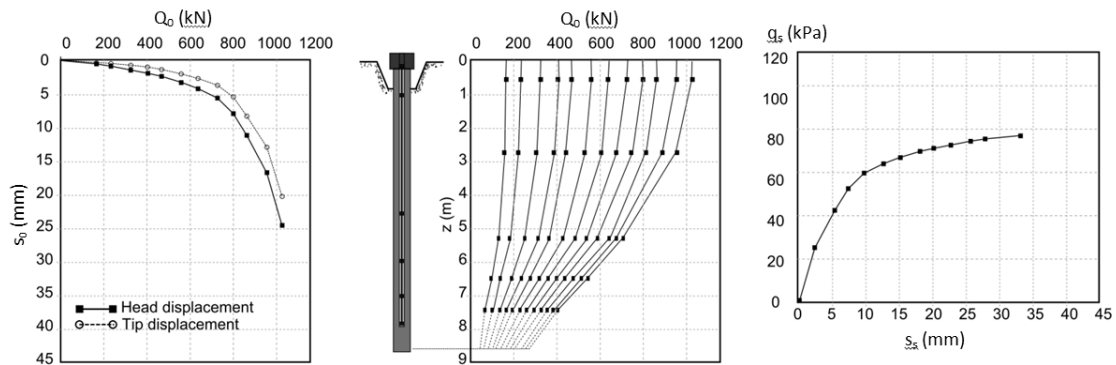


Fig. 4.2 Main results of an instrumented load test with “removable extensometer”. Left: load-settlement curve for head and tip; Middle: shaft load distribution between blockers and extrapolation for tip load; Right: skin friction load transfer curve

Table 4.1 gives information about the instrumented piles available (both concrete and steel piles are included). More details are given in Appendix D.1 and D.2. The tests Ifsttar 60 MP1, Ifsttar 166, Keller France ASIRI flot, Keller France ASIRI anc, and Keller France Manom have no utilisable measurements at the tip.

Table 4.1 Instrumented pile load tests

Source	Pile type						Total
	Non-displacement			Displacement			
	Fine-grained soil at tip	Coarse-grained soil at tip	Soft rock at tip	Fine-grained soil at tip	Coarse-grained soil at tip	Soft rock at tip	
IFSTTAR	6	0	5	7	2	4	24
Krasiński	0	0	0	0	11	0	11
Keller	4	1	0	2	6	2	15
Total	10	1	5	9	19	6	50
	16			34			

Table 4.2 gives information about the piles used for checking the developed load transfer curves (both concrete and steel piles are included). These piles are either instrumented or non-instrumented, but in any case only the load-settlement measurement at the pile head is considered here and the piles are different from the piles used for the development of load transfer curves (Table 4.1). More details about these tests are given in Appendix D.3 and D.4.

Table 4.2 Pile load tests used for checking of developed load transfer curves (mainly non-instrumented)

Source	Pile type						Total
	Non-displacement			Displacement			
	Fine-grained soil at tip	Coarse-grained soil at tip	Soft rock at tip	Fine-grained soil at tip	Coarse-grained soil at tip	Soft rock at tip	
IFSTTAR	0	0	5	0	0	5	10
Keller	5	16	0	22	17	2	62
Total	5	16	5	22	17	7	72
	26			46			

4.2 Single pile axial behaviour with the FEM and moduli correlations

4.2.1 Need of relevant correlations for single pile loading

The behaviour of the soil around an axially loaded single pile differs a lot from the behaviour of the soil under a vertically loaded shallow foundation. Fig. 4.3 shows in principle the expected p' vs. q stress paths of the soil under a large raft footing, under a single footing, around a pile and for typical soil loading cases with laboratory devices. This suggests that the usual moduli correlations, which have been developed exclusively for shallow foundation cases (see Appendix A and section 3.1), do not apply for piles. No moduli correlations for the single pile case widely established yet in current practice, in particular for numerical continuum methods.

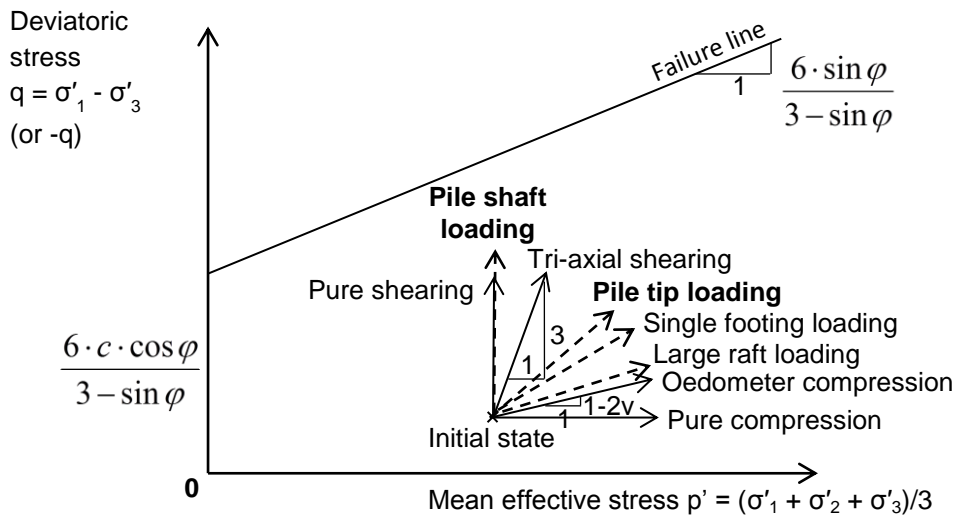


Fig. 4.3 Stress path of soil around axially loaded single pile in comparison with usual tests and shallow foundations

As a first correlation for piles, the Young's modulus used in the settlement linear formula after Randolph and Wroth (1978) can be estimated by equalizing the slope of the first part of the Frank and Zhao (1982) load transfer curves (Fig. 2.5 in section 2.2.2) with the slope from the formula after Randolph and Wroth in (Eq. 2.34) for the shaft and in (Eq. 2.35) for the tip respectively (see section 2.3.2.2). Most materials constitutive models in numerical continuum methods allow the input of a theoretical modulus of oedometer type, which is then converted in different moduli types depending on the loading level and on other model parameters. This is the case for example in the elastic-plastic model with Mohr-Coulomb failure criterion or the Hardening soil model in the software Plaxis (Plaxis 2013, Plaxis 2014). Furthermore, the correlations for shallow foundations rely in general on a modulus of oedometer type. Most of the correlations considered here rely on the pressuremeter modulus E_M as a measured soil deformation parameter, thus all correlations are converted in terms of E_M . The modulus ranges from the different correlations are then compared on the same basis in Table 4.3 and Fig. 4.4 for clays and sands. Even if the foundation does not correspond to an oedometer loading and even if no pressuremeter modulus is measured, this gives a relative comparison of the modulus to be used in each case. However, the correlation for piles has to be seen as an extreme case, since it represents only the initial stiffness.

Table 4.3 Comparison of calculation methods and oedometer modulus ranges from usual correlations for different foundation types in clay and sand

		Large raft		Single footing	Pile: initial stiffness	
		Correlation based on PMT	Correlation based on CPT	Correlation based on PMT	Shaft	Tip
		NF P 94-261 (2013): application of EN 1997-1 (2004)	EN 1997-2 (2007)	NF P 94-261 (2013) application of EN 1997-1 (2004)	Equality between methods of Frank and Zhao (1982) and Randolph and Wroth (1978) for initial stiffness	
General formula		$E_{oed} = \frac{E_M}{\alpha}$	$E_{oed} = \beta \cdot q_c$	$E = \alpha_{footing} \cdot E_M$	$E = \alpha_{pile,s} \cdot (1 + \nu) \cdot \ln \frac{2.5 \cdot L \cdot (1 - \nu)}{B/2} \cdot E_M$	$E = \frac{\alpha_{pile,b}}{4} \cdot (1 - \nu^2) \cdot \pi \cdot E_M$
Additional correlation	Clay	nothing	$E_M = 2.5 \cdot q_c$	$E_{oed} = \frac{1 - \nu}{(1 + \nu) \cdot (1 - 2\nu)} \cdot E$	$E_{oed} = \frac{1 - \nu}{(1 + \nu) \cdot (1 - 2\nu)} \cdot E$	
	Sand		$E_M = 1.25 \cdot q_c$			
Value of coefficient	Clay	$\alpha = \frac{1}{2}$ to 1	$\beta = 1$ to 8	Normally consolidated / Loose: $\alpha_{footing} = 4.5$ Overconsolidated/dense: $\alpha_{footing} = 3$	$\alpha_{pile,s} = 2$	$\alpha_{pile,b} = 11$
	Sand	$\alpha = \frac{1}{3}$ to $\frac{1}{2}$	$\beta = 3.5$ to 5		$\alpha_{pile,s} = 0.8$	$\alpha_{pile,b} = 4.8$
Approx. range of E_{oed}	Clay	1 to $2 \cdot E_M$	0.4 to $3.2 \cdot E_M$	4 to $7 \cdot E_M$ ($\nu = 0.3$ to 0.33)	For $L/B = 20$, $\nu = 0.3$ to 0.33 : $16 \cdot E_M$	$10 \cdot E_M$
	Sand	2 to $3 \cdot E_M$	2.8 to $4 \cdot E_M$		For $L/B = 20$, $\nu = 0.3$ to 0.33 : $6 \cdot E_M$	$5 \cdot E_M$

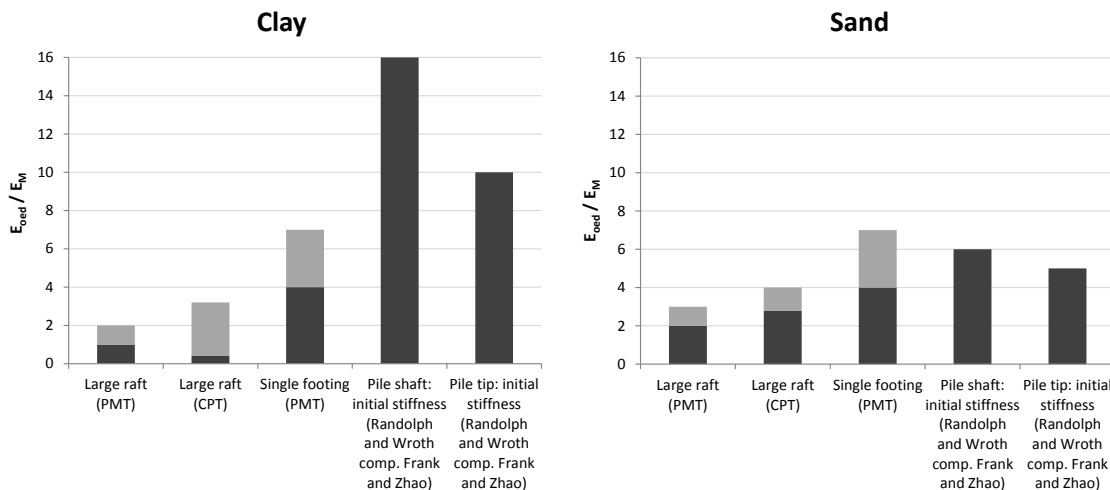


Fig. 4.4 Comparison of modulus ranges from usual correlations for different foundation types for clay and sand

Fig. 4.4 shows very large differences between the correlations for the different foundation cases for clays, with a ratio of approximately 10 between the raft case and the initial stiffness in the pile case. For sands, the different correlations give more balanced results. This trend has however to be confirmed for the stiffness under usual load levels for piles and not only for the initial pile foundation stiffness.

4.2.2 Example of moduli back-calculation for an instrumented single pile

The trend presented in the section above is now illustrated and completed by the modelling of an instrumented single pile with the finite element method (FEM), using the software Plaxis 2D version AE.02 in axisymmetric mode (Plaxis 2014). Preliminary steps leading to this analysis have been done with the support of Rostami (2013).

For the modelling of the soil layers and of the interfaces, the Hardening Soil constitutive law is chosen as a compromise between the basic elastic-plastic constitutive law with Mohr-Coulomb failure criterion and more advanced soil models. The first one presents the disadvantage of using only one modulus for a soil layer without taking into account the stress level which is not enough in particular under the pile tip. On the other side, more advanced models require an important number of measured soil parameters which are only very rarely provided in soil reports of everyday projects. This would lead to the necessity to use a non-reasonable number of correlations for all parameters. In any case, the choice of the modulus value plays a more important role than the choice of soil constitutive law and is the aim of the present section.

The main important advantage of the Hardening Soil model is the variation of modulus with the stress (Plaxis 2014). The shear hardening under deviatoric loading and the compression hardening are both represented. The relationship between the axial strain and the deviatoric stress is hyperbolic as proposed by Duncan and Chang (1970), extended with the theory of plasticity with Mohr-Coulomb failure criterion, with the soil dilatancy and with the yield cap (Fig. 4.5). The shear hardening is represented by E_{50} in terms of the principal effective stress σ'_3 (horizontal stress in the initial state defined negative in compression), with reference to the reference input stress p_{ref} (Eq. 4.1). The compression hardening is represented by E_{oed} in terms of the principal effective stress σ'_1 (vertical overburden stress in the initial state), with reference to the reference input stress p_{ref} (Eq. 4.2). The exponent m and thus the modulus variation with the stress depends on the type of soil (Benz 2007, Plaxis 2014, Vogt 2015).

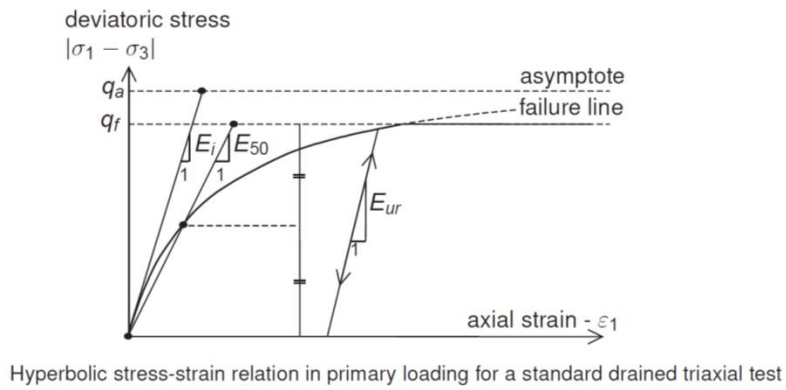


Fig. 4.5 Definition of E_{50} from deviatoric stress vs. axial strain diagram (Plaxis 2014)

$$E_{50} = E_{50}^{ref} \cdot \left(\frac{c \cdot \cos \varphi - \sigma'_3 \cdot \sin \varphi}{c \cdot \cos \varphi + p_{ref} \cdot \sin \varphi} \right)^m \quad (\text{Eq. 4.1})$$

$$E_{oed} = E_{oed}^{ref} \cdot \left(\frac{c \cdot \cos \varphi - \frac{\sigma'_3}{K_0^{nc}} \cdot \sin \varphi}{c \cdot \cos \varphi + p_{ref} \cdot \sin \varphi} \right)^m \quad (\text{Eq. 4.2})$$

The load test analysed is the instrumented test Ifsttar 35 B with a bored pile in clay (details in Appendix D.1), soil for which the correlations differences are the largest. The pile has a diameter of 0.88 m and a length of 27 m and is installed with a non-displacement technique. The model depth of 40 m has been chosen considering a minimum distance of 10 times the diameter under the pile (Fig. 4.6). The model width of is chosen approximately equal to twice the pile length corresponding roughly to the influence radius r_m defined by Randolph and Wroth (1978) in (Eq. 2.33). The ground water level is far below the pile tip level.

For the concrete material of the pile, the linear elastic constitutive law with $E = 30$ GPa as the short-duration modulus according to EN 1992-1-1 (2004-2010) (DIN EN 1992-1-1 2011 and DIN EN 1992-1-1/NA 2013 in Germany, NF EN 1992-1-1 2005 and NF EN 1992-1-1/NA 2007 in France) and with $\nu = 0.2$ is considered, since no material failure is expected for the applied loads. The non-porous drainage type in Plaxis is chosen since no pore pressures need to be calculated in the concrete (Plaxis 2014).

For the soil layers and the interfaces, the following parameters for the Hardening Soil model in drained mode are used and illustrated in Fig. 4.6:

- shear parameters c and φ of the soil: estimated average value for clay at the shaft, calibration with realistic values for clay at the tip to match the measured tip behaviour (since the plasticity under the tip plays a role in the pile tip stiffness behaviour since the beginning);
- earth pressure at rest in all soils $K_0 = 1 - \sin\varphi$ (non-displacement pile);
- the chosen m value of 0.7 corresponds to usual values for soft fine-grained soils after Benz (2007) and Vogt (2015);
- reference stress p_{ref} for the moduli equal to initial overburden stress, since the modulus of oedometer type will be back-calculated and compared afterwards with correlations based on CPT and PMT measurements at the corresponding levels (Table 4.4);
- E_{oed}^{ref} varied to best match the measured skin friction and tip resistance mobilisation curves at the level of half of the measured resistance at each level $q_{s,ult}/2$ or $q_{b,ult}/2$;
- default moduli relationships $E_{50}^{ref} = E_{oed}^{ref}$ and elastic unloading/reloading modulus $E_{ur}^{ref} = 3 \cdot E_{50}^{ref}$;
- for all the other Hardening Soil parameters, the default values are kept;
- all parameters of the soils are kept the same for the interface materials, except shear parameters c and φ : $c =$ measured ultimate skin friction $q_{s,ult}$, $\varphi = 0^\circ$ (since only the stiffness is back-calculated here). It has been checked that the soil shear resistance $\sigma_{xx} \cdot \tan\varphi + c$ is higher than the interface resistance, so that the interface resistance can be reached;
- the interface element is extended by one diameter under the pile tip, and a horizontal interface is also modelled under the pile tip for an easier analysis of the output results. Both have the parameters of the adjacent soil.

The interfaces and the pile are modelled with a coarseness factor of 0.125 with a very fine general coarseness level (Plaxis 2014). The coarseness factor in the soil is set to 1. The resulting mesh is shown in Fig. 4.6 with a detail of the pile tip zone. The mesh quality is defined in Plaxis as the ratio between the radiuses of the inner circle and of the outer circle of the element, normalized at 1.0 for the equal sided triangle (Plaxis 2014). The mesh quality is here close to 1 over the whole model.

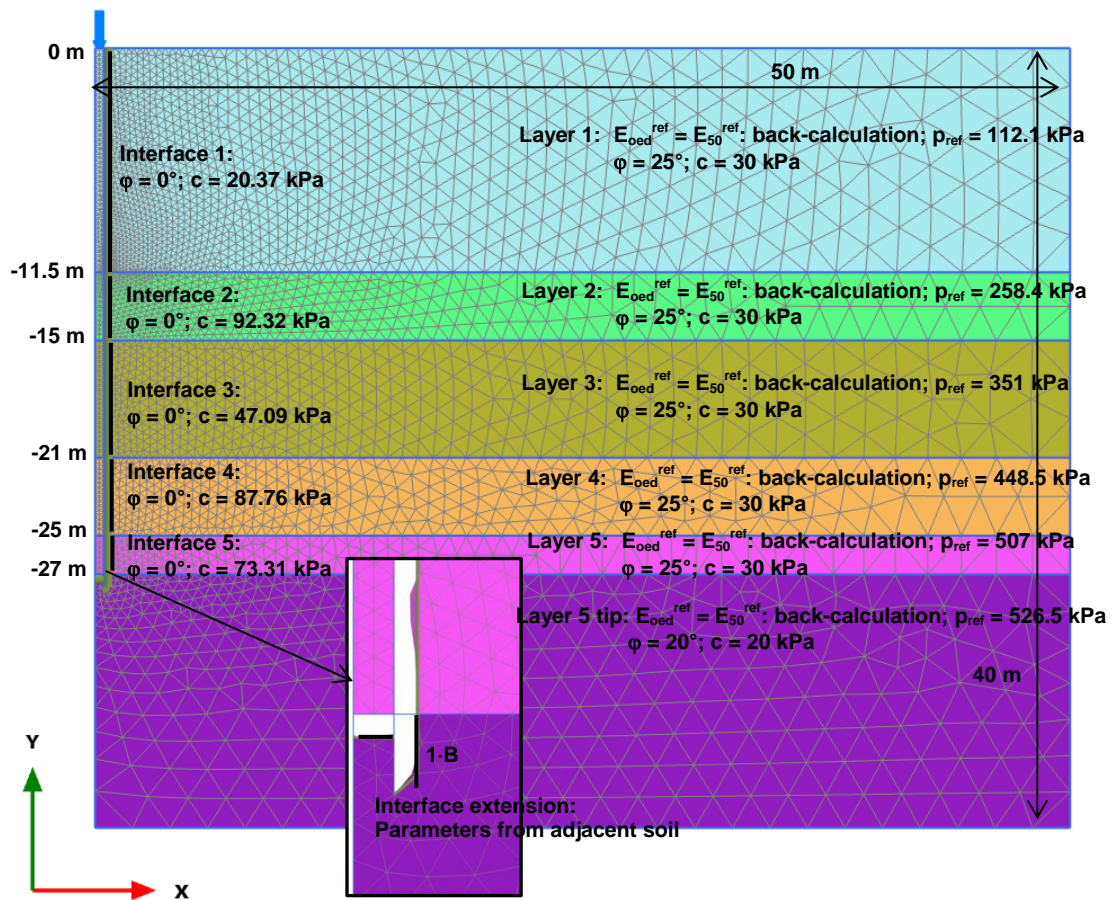


Fig. 4.6 2D-FEM-model of single pile Ifstar 35 B (layers with main parameters, pile, interfaces and mesh)

The first calculation phase is the initial phase with the calculation of the initial vertical stress from the dead weight of the soil and of the horizontal initial stress as the vertical one multiplied by K_0 (K_0 procedure in Plaxis). The second phase is the pile installation with activation of the pile concrete material and all interfaces. The last step is the loading step applied as maintained load. All calculation parameters are kept to the default values of Plaxis, except the maximum load fraction per step set to 0.05 (default 0.5) to ensure a good representation of the small stiffness domain. For a better accuracy of the results, the updated mesh option is activated for the pile installation and loading phases.

With the soil model used, the mobilisation of the pile skin friction is almost linear up to the failure stress. This means that the real mobilisation behaviour cannot be correctly modelled and a compromise has to be made with a good match either for the small or for the high load level. Fig. 4.7 on the left shows the result at the middle of the third layer (node and stress point close to each other in the interface) with the back-calculated modulus $E_{\text{oed}}^{\text{ref}} = 30$ MPa for half of the skin friction resistance in this layer. As a

comparison, the prediction after Frank and Zhao is shown in Fig. 4.7 on the right. This prediction, used for the proposed correlation of the pile initial stiffness in section 4.2.1, is very accurate in this example, but the modulus correlation based only on the initial stiffness would be too high for the FEM model.

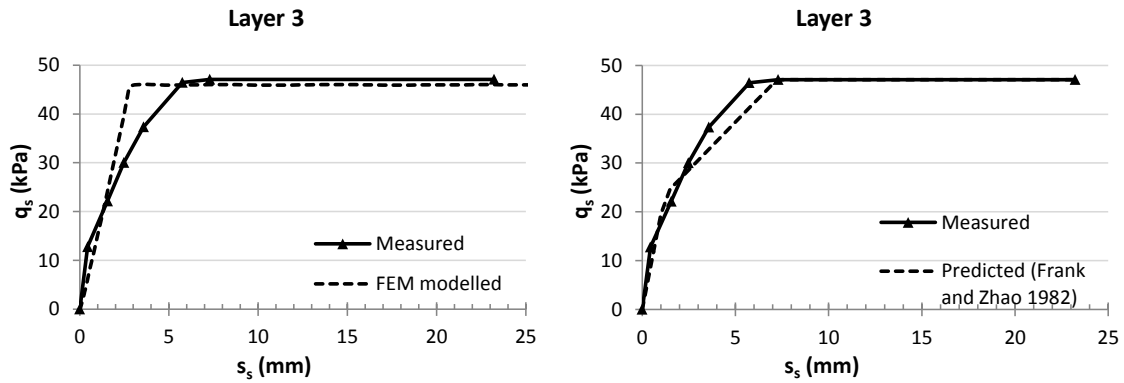


Fig. 4.7 Comparison of measured mobilisation curve of skin friction in the third layer with the back-calculated FEM model and with the Frank and Zhao (1982) prediction (instrumented load test Ifsttar 35B)

The deformations due to shearing occur mainly inside a model width equal to the length of the pile; the difference in the settlements between 30 m and 50 m far from the pile is in the order of only one thousandth to one hundredth of the total settlement.

The shape of the tip mobilisation can be modelled in a non-linear manner, since the development of local plastification or local failure also contributes to the deformation behaviour for small load levels. Since the stresses are not uniform directly under the pile tip, the tip load is determined by integration over the pile tip section of the stresses from 5 stress points situated directly under the pile tip. The pile tip behaviour cannot be modelled perfectly with c and φ values kept in a realistic range for clay. With the minimum values of $\varphi = 20^\circ$ and $c = 20$ kPa, the tip resistance is still overestimated (Fig. 4.8). More generally, the pile tip behaviour is particularly difficult to model since the precise effects of the pile execution on the soil directly under the tip remains quite unknown, for both displacement and non-displacement piles. However, the overall modelled behaviour at the pile head is very close to the measurements; this remains the main goal of any pile modelling in practice.

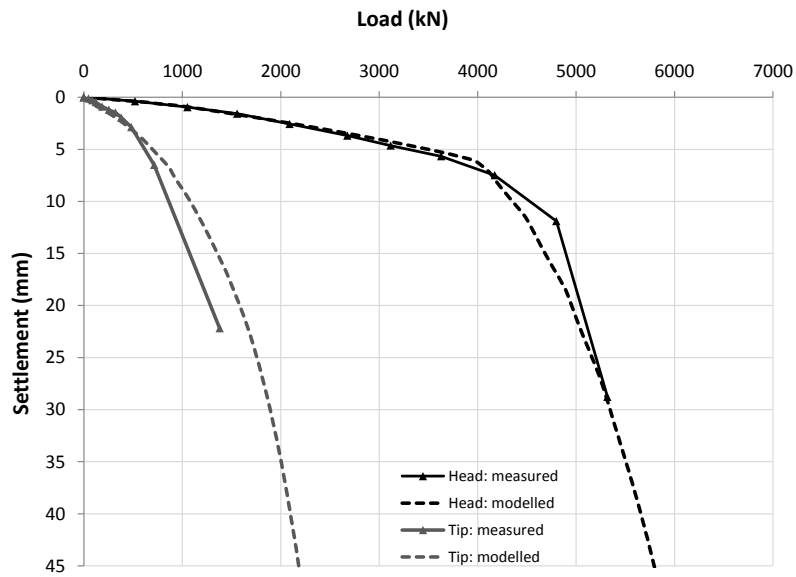


Fig. 4.8 Measured and modelled load-settlement curve after back-calculation at pile head and at pile tip (instrumented load test Ifsttar 35B)

The horizontal stress repartition across the concrete section is almost perfectly uniform except in the close vicinity of the pile tip. Profiles of pile load are determined here from the stresses located at one half of the radius (0.22 m); only the value at the tip is corrected by weighting the stresses of 5 stress points directly under the pile tip. Depending on the load level, the mobilisation of the skin friction and of the tip resistance is then more or less well represented, as shown in the pile load distribution with depth (Fig. 4.9). For example, for the load level applied during the test of 3118 kN, the mobilised skin friction is slightly underestimated in the upper layers, slightly overestimated in the next layers and the pile tip resistance is quite well represented.

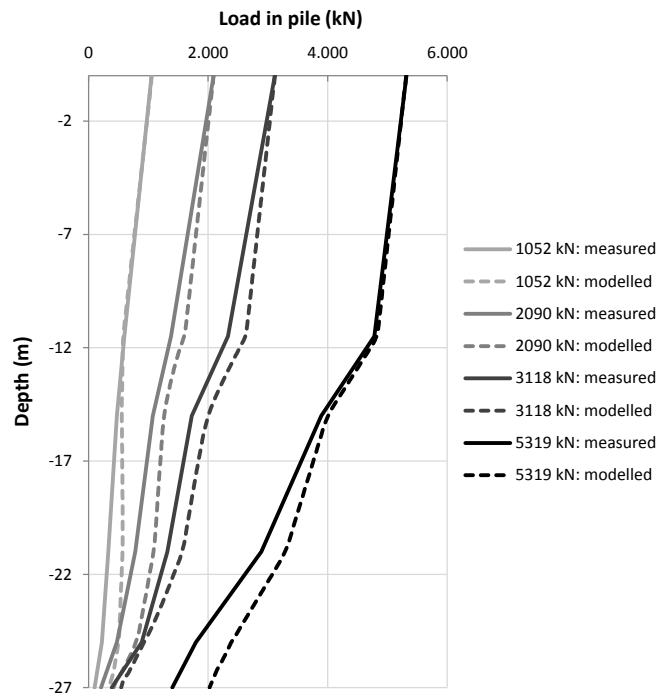


Fig. 4.9 Measured and modelled load in pile with depth (instrumented load test Ifsttar 35B)

In Fig. 4.10, the back-calculated E_{oed} moduli are compared with the correlations proposed for different foundations types based on PMT and CPT parameters (Table 4.4). As expected, the optimum modulus is in general located between the correlation for the single footing and the correlation based on the initial stiffness for the pile shaft reaction. For the pile tip, the proposed correlation in terms of initial stiffness is satisfactory, since the calibration of c and ϕ under the tip reduces automatically the pile tip stiffness for high load levels. The back-calculated modulus at the tip is close to the correlation in the same layer (last layer) for the single footing case. This reflects the well-known similarity of the pile tip with a single footing with small dimensions and with a high embedment.

Table 4.4 Results of PMT and of CPT near the Ifsttar 35 B test pile

	E_M (MPa)	p_i (MPa)	q_c (MPa)
Layer 1	3.3	0.60	2.0
Layer 2	9.5	0.98	2.5
Layer 3	8.6	1.50	3.0
Layer 4	20.0	2.30	7.0
Layer 5 and tip	28.0	2.30	10.0

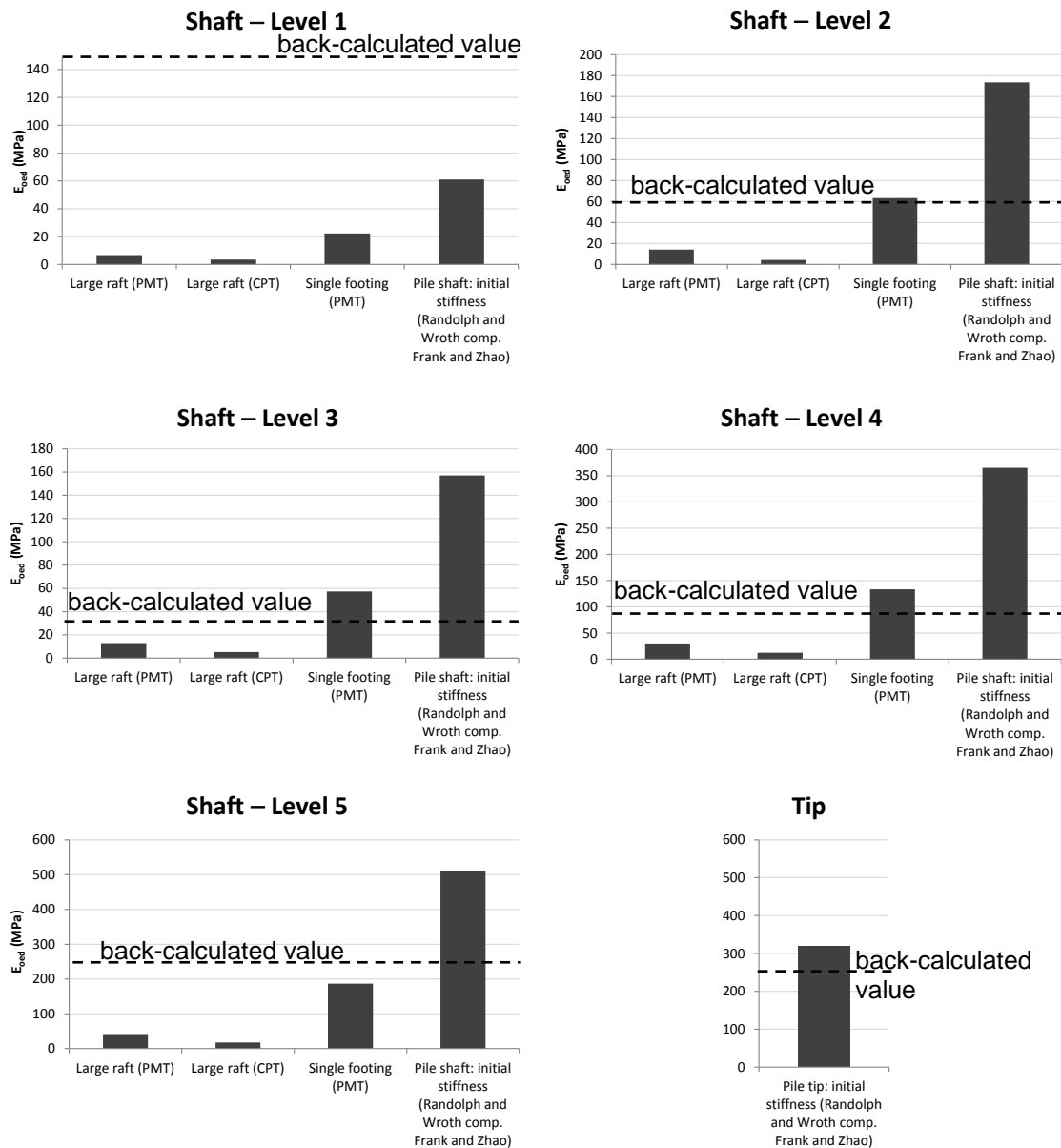


Fig. 4.10 Comparison of back-calculated moduli in each layer of the FEM model with usual correlations (instrumented load test Ifsttar 35B)

The stress paths directly at the pile shaft and directly under the pile tip (first stress point located at 0.014 m of the middle of the pile) shown in Fig. 4.11 illustrate the differences in the back-calculated moduli and confirms the expected behaviours presented in Fig. 4.3.

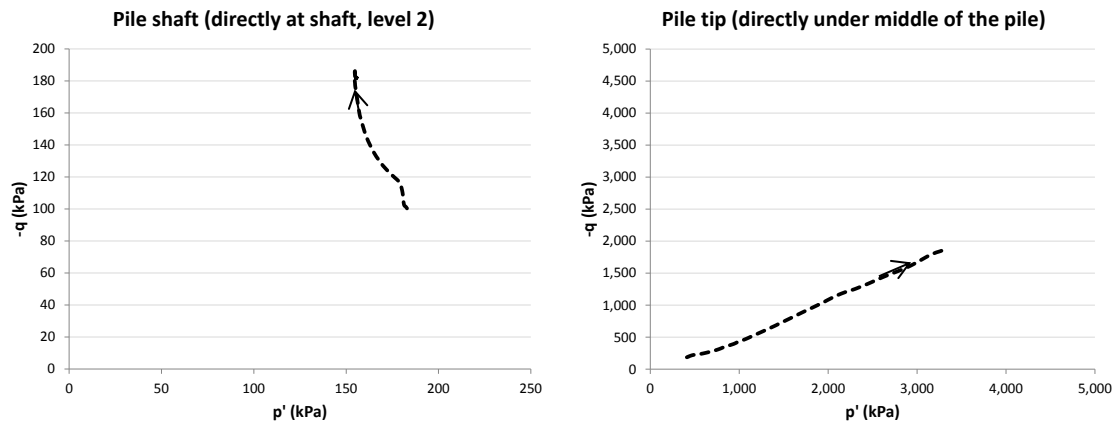


Fig. 4.11 Stress paths of stress point at the interface half way down the second layer and of stress point directly under the pile tip in the FEM model (instrumented load test Ifsttar 35B)

If the criterion of back-calculation would be rather the initial stiffness than the stiffness at half of the local resistance, the back-calculated moduli would be higher, the magnitude depending on the curvature of the curve. On the example of Fig. 4.7, the back-calculated modulus would be in that case approximately twice to 3 times higher. This is consistent with the proposed correlation in terms of initial stiffness for this example (Fig. 4.10). With the linear elastic-perfectly plastic soil constitutive law with Mohr-Coulomb failure criterion, the back-calculated moduli would be higher as well, due to the missing modulus increase with stress during the pile loading and the missing increase with depth under the pile tip level.

Depending on the single pile case to be modelled with the FEM, on the choice of the load level for which the best matching is requested and on the curvature of the real mobilisation curves in the studied soil (non-linearity), the moduli to be selected can vary a lot. Depending on the case and on the soil variability, it is even possible that moduli in the range of the correlation for rafts are obtained or moduli higher than the correlation for shaft initial stiffness like in the first layer in the studied example (Fig. 4.10). In everyday projects, no instrumented pile load tests are executed, so that the validity of the choice cannot be checked, or at most only the overall load-settlement curve at the pile head can be checked. If necessary, better modelling of the non-linear shaft behaviour would be of course possible with advanced soil constitutive laws. This would imply however much higher soil investigation costs, experienced engineers and more time-consuming designs.

For the design of combined foundation systems, the problem of the choice of the best modulus for the whole system with the FEM arises. It is in that case possibly necessary

to define different soil volumes with different deformation parameters around the pile and around or under the other foundation elements.

The FEM presents the major advantage of being a very powerful modelling tool with a high flexibility in the foundation geometry and in the diversity of output data. However, the pile non-linear behaviour and the different deformation behaviour of the foundations elements in a combined system can be modelled in a more relevant way with other methods combining theory and experience, without time-consuming meshing, calculation and analysis steps. To this end the load transfer method (LTM) will be developed in the next chapters.

4.3 Development of axial load transfer curves for LTM applications

This chapter is the subject of a submitted journal paper by Bohn et al. (submitted in January 2015), written as a part and in the scope of the present work. First steps of this analysis have been done in common work with Santos (2013a and 2013b).

4.3.1 Existing load transfer curves

Axial load transfer curves have been first developed back in the 1950's by Seed and Reese (1957), Gambin (1963), Cambefort (1964) and Coyle and Reese (1966). Different curve types with different degrees of complexity and number of soil parameters are given in the literature, based on theory, on experience or on both. They are in general developed for specific ground and pile types (API 1993, Armaleh and Desai 1987, Christoulas and Frank 1991, Everett 1991, Fleming 1992, Frank 1974, Frank 1985, Frank and Zhao 1982, Gwizdała 1996, Hirayama 1990, Kraft et al. 1981, Krasinski 2010, 2011, 2012a, 2012b, Liu et al. 2004, McVay et al. 1989, Randolph and Wroth 1978, Verbrugge 1981, Vijayvergiya 1977, Wang et al. 2012, Zhang et al. 2010).

In the following, only the curves with an acceptably simple mathematical form, requiring one soil parameter or none are further investigated (Table 4.5 and Table 4.6, with s_s and s_b : pile settlement minus soil settlement in absence of the pile, at the shaft and at the tip respectively). The proposal of EA-Pfähle (DGGT 2012) for an overall pile-load-settlement curve is not considered here because of the shortcomings already mentioned in section 2.2.1 (no consideration of pile shortening, limit settlement in skin friction defined in terms of total skin friction force). The stiffness of the load transfer curves is either derived from a measured soil deformation parameter or a fixed parameter. Frank and Zhao (1982) use the pressuremeter modulus, Randolph and Wroth (1978), Verbrugge (1981) and Fleming (1992) (only for the pile tip) use an equivalent

ground Young's modulus or oedometer modulus based for example on correlations with measured soil resistance parameters. The linear curves of Randolph and Verbrugge correspond to an elastic calculation with the use of usual correlations to determine the linear curve stiffness. Vijayvergiya (1977), Hirayama (1990), Fleming (1992) (only for the pile shaft), API (1993) and Krasinski (2010, 2011, 2012a, 2012b) consider fixed parameters, for example a limit settlement defined as the settlement for full resistance mobilisation. Most of them are explicit, meaning that all curve parameters are completely defined by the authors for a direct use; other authors propose to derive the stiffness from a case-by-case calibration procedure (Fleming 1992, Randolph and Wroth 1978).

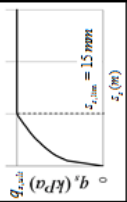
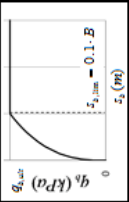
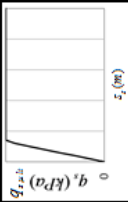
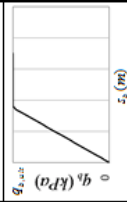
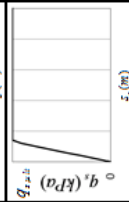
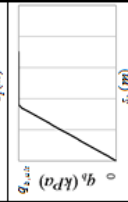
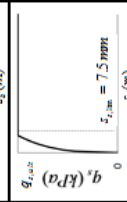
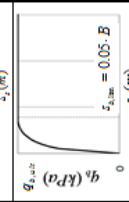
The pile diameter B has generally speaking a direct influence on the initial slope of the curve, except for some mathematical expressions with a theoretically infinite slope. The influence of the pile diameter seems to be more important for the pile tip, where the limit settlement is always defined as proportion of the diameter. Most curves reflect the fact that the pile tip requires more displacement than the skin friction to be fully mobilised. Tomlinson and Woodward (2008) report a displacement for full mobilisation of 0.3 % to 1 % of the diameter for the skin friction and of 10 to 20 % of the diameter for the tip resistance. This is why most of the load is often taken by skin friction under low load levels. Furthermore, the displacement at the pile tip is a bit smaller than at the pile head due to the pile shortening.

The empirical curves of Frank and Zhao (1982) have been well-proven by an active and effective use of them in particular in France, both for single piles and for rigid inclusions systems. Their agreement level with measurements can be thus seen as a reference here for the analysis of the different existing curves and the development of other simple load transfer curves for an international use, which would not be based on pressuremeter test results.

Table 4.5 Definition of the main simple load transfer curves (1/2)

	Mathematical expression	Curve shape	Deformation parameter	Initial slope	Ground type	Pile type	Development based on pile load tests																		
API (1993): point by point curves	Shaft <table border="1"> <tr> <th>Clay</th> <th>Sand</th> </tr> <tr> <td>$\frac{s_z}{B}$</td> <td>$\frac{q_z}{q_{b,ult}}$</td> </tr> <tr> <td>0.0016</td> <td>0.30</td> </tr> <tr> <td>0.0031</td> <td>0.50</td> </tr> <tr> <td>0.0057</td> <td>0.75</td> </tr> <tr> <td>0.0080</td> <td>1.00</td> </tr> <tr> <td>0.0100</td> <td>1.00</td> </tr> <tr> <td>0.0200</td> <td>1.00</td> </tr> <tr> <td>∞</td> <td>∞</td> </tr> </table>	Clay	Sand	$\frac{s_z}{B}$	$\frac{q_z}{q_{b,ult}}$	0.0016	0.30	0.0031	0.50	0.0057	0.75	0.0080	1.00	0.0100	1.00	0.0200	1.00	∞	∞		Limit settlement $s_{b,lim}$: 0.02·B for clay, 0.00254 m fixed for sand	Clay: $\frac{q_{z,ult}}{0.0037 \cdot B}$ Sand: $\frac{q_{z,ult}}{0.00254}$	Clay Non-carbonate sand	All	No information
	Clay	Sand																							
$\frac{s_z}{B}$	$\frac{q_z}{q_{b,ult}}$																								
0.0016	0.30																								
0.0031	0.50																								
0.0057	0.75																								
0.0080	1.00																								
0.0100	1.00																								
0.0200	1.00																								
∞	∞																								
Tip	$\frac{s_z}{B}$ $\frac{q_b}{q_{b,ult}}$ 0.002 0.25 0.013 0.50 0.042 0.75 0.073 0.90 0.100 1.00		Limit settlement $s_{b,lim}$: 0.1·B	$\frac{q_{b,ult}}{0.008 \cdot B}$																					
Fleming (1992): hyperbolic curves	Shaft $q_z = \frac{q_{z,ult} \cdot s_z}{M \cdot B + s_z}$		Parameter M (non explicit): 0.0005 for stiff soils to 0.004 for soft soils	$\frac{q_{z,ult}}{M \cdot B}$		All	4 tests																		
	Tip $q_b = \frac{q_{b,ult} \cdot s_b}{0.6 \cdot \pi \cdot \frac{B}{4 \cdot E} \cdot q_{b,ult} + s_b}$		Young's modulus E (non explicit)	$\frac{4 \cdot E}{0.6 \cdot \pi \cdot B}$																					
Frank & Zhao (1982) and Frank (1985): trilinear curves	Shaft Fine-grained: $\kappa_z = \frac{2.0 \cdot E_M}{B}$ Coarse-grained: $\kappa_z = \frac{0.8 \cdot E_M}{B}$		Pressuremeter modulus E_M	Fine-grained: $\frac{2.0 \cdot E_M}{B}$ Coarse-grained: $\frac{0.8 \cdot E_M}{B}$	Fine-grained soil Coarse-grained soil	All	Approx. 30 tests																		
	Tip Fine-grained: $\kappa_q = \frac{11.0 \cdot E_M}{B}$ Coarse-grained: $\kappa_q = \frac{4.8 \cdot E_M}{B}$		Pressuremeter modulus E_M	Fine-grained: $\frac{11 \cdot E_M}{B}$ Coarse-grained: $\frac{4.8 \cdot E_M}{B}$																					
Hirayama (1990): hyperbolic curves	Shaft $q_z = \frac{q_{z,ult} \cdot s_z}{0.0025 \cdot B + s_z}$		Fixed parameter 0.0025	$\frac{q_{z,ult}}{0.0025 \cdot B}$	Clay Non-carbonate sand	Large diameter bored piles	Several tests at one site																		
	Tip $q_b = \frac{q_{b,ult} \cdot s_b}{0.25 \cdot B + s_b}$		Fixed parameter 0.25	$\frac{q_{b,ult}}{0.25 \cdot B}$																					

Table 4.6 Definition of the main simple load transfer curves (continued, 2/2)

	Mathematical expression	Curve shape	Deformation parameter	Initial slope	Ground type	Pile type	Development based on pile load tests
Kraśński (2012): root curves	Shaft $q_s = \min \left(\left(\frac{s_s}{s_{s,lim}} \right)^{0.38} \cdot q_{s,ult} \right); q_{s,ult}$		Limit settlement $s_{s,lim}$: 0.015 m fixed	∞	Sand	Screw displacement piles	Approx. 10 tests
	Tip $q_b = \min \left(\left(\frac{s_b}{s_{b,lim}} \right)^{0.38} \cdot q_{b,ult} \right); q_{b,ult}$		Limit settlement $s_{b,lim}$: 0.1 · B	∞			
Randolph & Wroth (1978): linear curves	Shaft $q_s = \min \left(\frac{G}{B/2 \cdot \ln \left(\frac{r_m}{B/2} \right)} \cdot s_s; q_{s,ult} \right)$		Shear modulus G (non explicit)	$\frac{G}{B/2 \cdot \ln \left(\frac{r_m}{B/2} \right)}$	All	All	No
	Tip $q_b = \min \left(\frac{8 \cdot G}{\pi \cdot B \cdot (1 - \nu)} \cdot s_b; q_{b,ult} \right)$		Shear modulus G (non explicit)	Shear modulus G (non explicit)	$\frac{8 \cdot G}{\pi \cdot B \cdot (1 - \nu)}$		
Verbrugge (1981): linear curves	Shaft $q_s = \min \left(0.22 \cdot \frac{\alpha \cdot b \cdot E}{B} \cdot s_s; q_{s,ult} \right)$ with $E = 3600 + 2.2 \cdot q_e$ $\alpha = \begin{cases} 1 & \text{for bored piles} \\ 3 & \text{for driven piles} \end{cases}$ $b = \begin{cases} 1 & \text{for normally consolidated soils} \\ 2 & \text{for overconsolidated soils} \end{cases}$		Young's modulus E from CPT correlations	$0.22 \cdot \frac{\alpha \cdot b \cdot E}{B}$	Fine-grained soil Coarse-grained soil	Replacement piles Driven piles	Yes (no details)
	Tip $q_b = \min \left(\frac{\alpha \cdot b \cdot E}{0.32 \cdot B} \cdot s_b; q_{b,ult} \right)$		Young's modulus E from CPT correlations	Young's modulus E from CPT correlations	$\frac{\alpha \cdot b \cdot E}{0.32 \cdot B}$		
Vijayvergiya (1977): root curves	Shaft $q_s = \min \left(2 \cdot \sqrt{\frac{s_s}{s_{s,lim}}} \cdot \frac{q_{s,ult}}{s_{s,lim}}; q_{s,ult} \right); q_{s,ult}$		Limit settlement $s_{s,lim}$: 0.0075 m fixed	∞	Sand	Driven piles	2 tests
	Tip $q_b = \min \left(\left(\frac{s_b}{s_{b,lim}} \right)^{1/2} \cdot q_{b,ult}; q_{b,ult} \right)$		Limit settlement $s_{b,lim}$: 0.05 · B	Limit settlement $s_{b,lim}$: 0.0075 m fixed	∞		

4.3.2 Development of load transfer curves based on instrumented load tests

4.3.2.1 Analysis of existing curves

As a first step, the predicted load transfer curves shown in Table 4.5 und Table 4.6 are compared along the shaft and at the tip with the measured ones from the instrumented load tests (except for the curves of Fleming and of Randolph and Wroth which are not explicitly defined). The methodology is the following:

- all curves are applied to all pile and ground types, even if they have not been developed for them, to check for a possible extension of their domain of validity;
- the ultimate resistances taken into account are derived from the measurements. In most cases, the ultimate value is reached during the load test. Otherwise the measured curve is extrapolated by hand (often at the tip which mobilises for higher settlements). Only the curve shape and stiffness is thus investigated;
- the pile material (concrete or steel) is not considered in this investigation step since it does not influence the stiffness of the load transfer curve;
- soft rocks are considered as fine-grained soil for the curves of Frank and Zhao and of API;
- for the Verbrugge curves (1981), the consolidation state is chosen in order to obtain the better matching;
- for the API curves in clay, the ratio residual to peak resistance is chosen between 0.7 and 0.9 in order to obtain the better matching (see Fig. 4.14);
- the Frank and Zhao (1982) curves can only be used if pressuremeter test results are available (64 % of the cases) and the Verbrugge (1981) curves can only be used if CPT results are available (76 % of the cases);
- the comparison is made in a qualitative manner leading to different levels of agreement defined as excellent/good/acceptable/poor/very poor, separately for small and for large displacements (examples are given in Fig. 4.12).

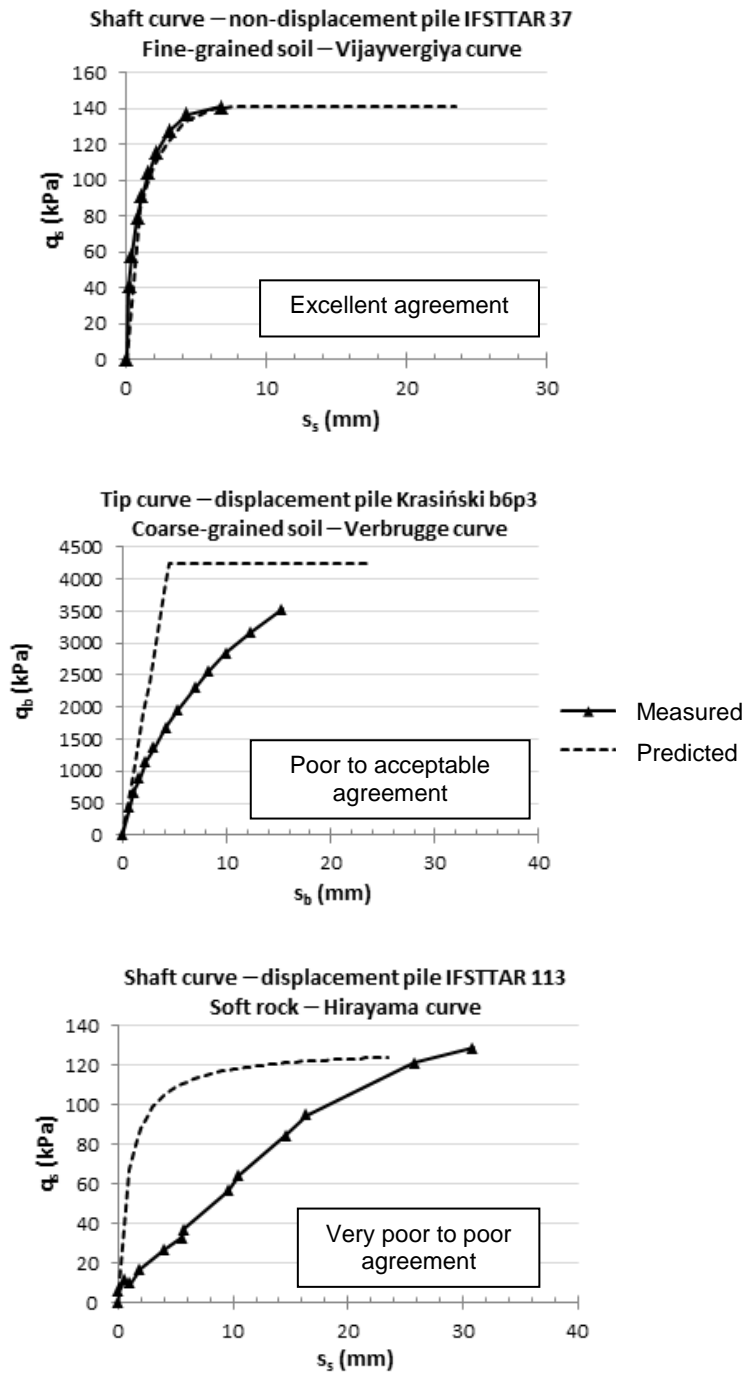


Fig. 4.12 Example of level of agreement of predicted load transfer curves

Peaks in the measurements only appear for the shaft friction. Specific pile types or ground types leading to peaks could not be identified (Fig. 4.13). Furthermore, the shape of the peaks can be very various (Fig. 4.14). The peaks seem to depend on the density or on the consolidation state of the ground. Note that peaks cannot appear in the overall load-settlement curve if “maintained load tests” are performed. Modelling peaks

is thus not a decisive point, as long as the behaviour in the initial and in the failure domain can be well reproduced.

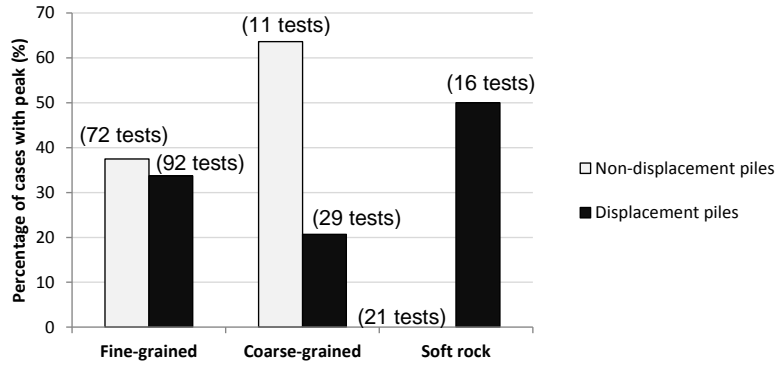


Fig. 4.13 Percentage of measured skin friction curves with peaks for different soil and pile types

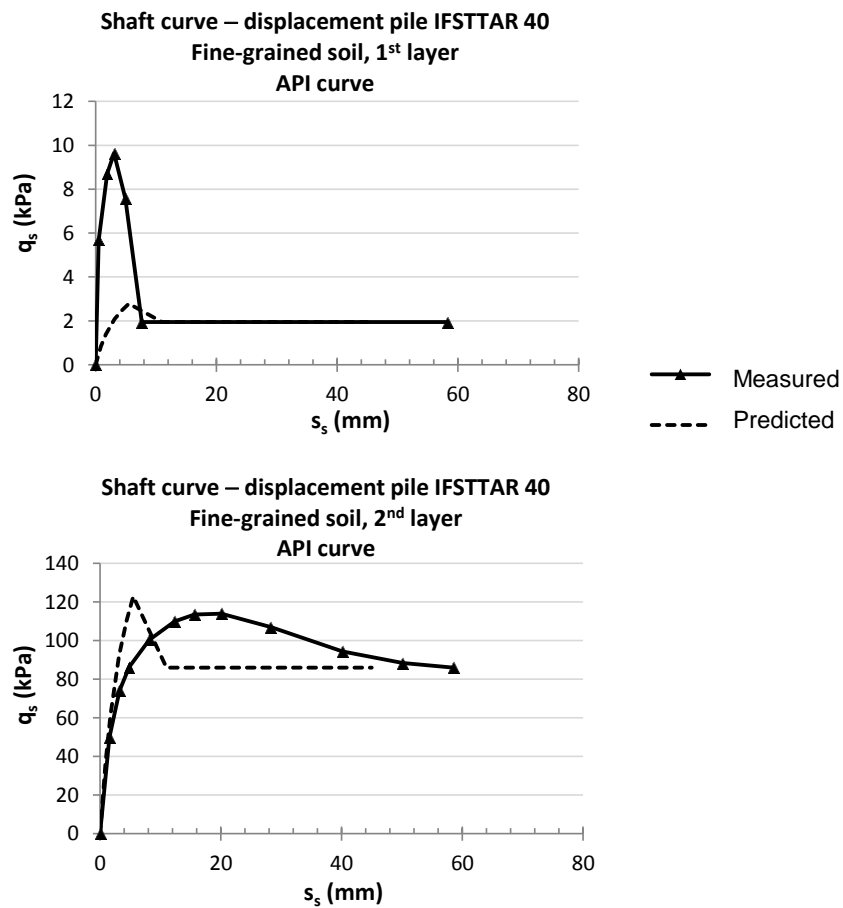


Fig. 4.14 Variability in measured and modelled peak behaviours

Fig. 4.15 gives the overall level of agreement (for small and large displacements together) between measured and predicted curves for different ground and pile types. A detailed insight into the initial stiffness domain (small displacements) as the average of the different ground and pile groups is given in Fig. 4.16. Note that the initial stiffness of the transfer curve does not necessarily require using an initial soil modulus as in the curves of Randolph and Wroth, Verbrugge or Fleming for the tip.

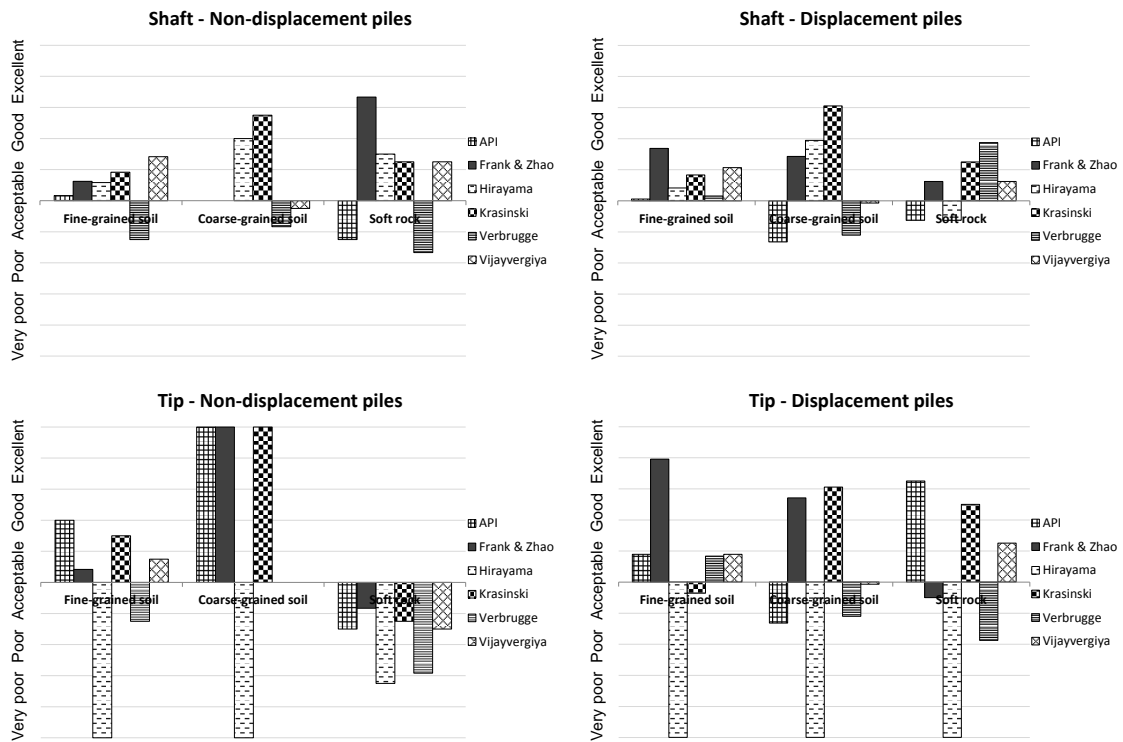


Fig. 4.15 Level of agreement of the existing load transfer curves

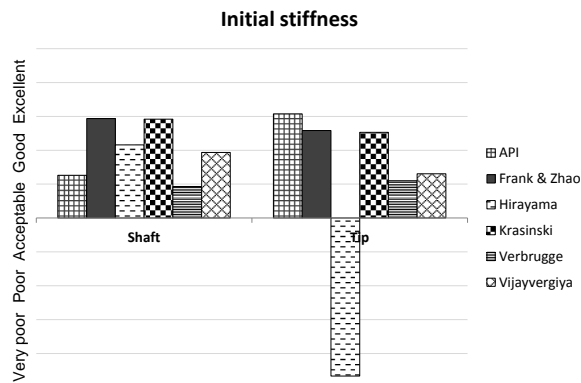


Fig. 4.16 Level of agreement of the existing load transfer curves for the initial stiffness

The conclusions of the comparison are:

- the Hirayama curve, originally developed for large diameter bored piles, is much too soft at the tip, but its hyperbolic form seems relevant with a good global agreement and a quite good initial stiffness at the shaft;
- the API curves are acceptable at the shaft and at the tip, except for the peak behaviour;
- the curves of Krasiński and Vijayvergiya (using root functions), originally developed for displacement piles in sand, show a good accordance for other ground and pile types as well, in particular in terms of stiffness in the initial domain. A limit settlement, diameter independent along the shaft and depending on the diameter B at the tip (of the order of $0.1 B$) seems relevant;
- the Verbrugge curves with Young's modulus based on a modulus correlation with the cone resistance from the cone penetration test are not satisfactory. Verbrugge himself admits that there is a very wide scatter in such correlations. Even in terms of initial stiffness, the Verbrugge curves are not as good as the other curves with fixed parameters, and imply a higher calculation effort. The question of the cone resistance dependency will be further examined in the next section;
- the Frank and Zhao curves show a good agreement, in particular in terms of initial stiffness. These curves present the decisive advantage to rely on a measured soil deformation parameter for the stiffness in the initial domain, whereas the initial stiffness of most other curves depends on the ultimate resistance (Table 4.5 and Table 4.6). This advantage cannot be reflected here where use is made of the measured ultimate values.

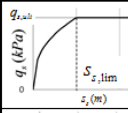
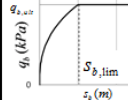
The most promising curve types seem to be the hyperbolic curves and the root curves. For the hyperbolic curves, the factor multiplying the diameter needs to be calibrated for all ground and pile types, and for the root curves the limit settlement needs to be calibrated.

4.3.2.2 Proposal of new explicit curves

Cubic root curves

The first proposed curves are cubic root curves (Table 4.7), which are similar to the Krasinski curves (exponent 1/3 instead of 0.38) and to the Vijayvergiya curve at the tip. These curves have a theoretically infinite initial slope, but in practice an initial slope will be defined for a very small initial displacement (for the so-called “elastic” range).

Table 4.7 Proposed cubic root load transfer curves

		Mathematical expression	Curve shape	Deformation parameter	Initial slope	Ground type	Pile type	Development based on pile load tests
Cubic root curves	Shaft	$q_s = \min\left(\left(\frac{s_s}{s_{s,lim}}\right)^{1/3} \cdot q_{s,ult}; q_{s,ult}\right)$		Limit settlement $s_{s,lim}$: fixed	∞	All	All	50 tests
	Tip	$q_b = \min\left(\left(\frac{s_b}{s_{b,lim}}\right)^{1/3} \cdot q_{b,ult}; q_{b,ult}\right)$		Limit settlement $s_{b,lim}$: depending on diameter	∞			

The deformation parameter $s_{s,lim}$ at the shaft and $s_{b,lim}/B$ at the tip have to be back-calculated to best match the measurements. The ultimate values are taken from the measurements like in the previous analysis of the existing curves. An example of calibration is shown in Fig. 4.17. Note that the model does not allow for peak values.

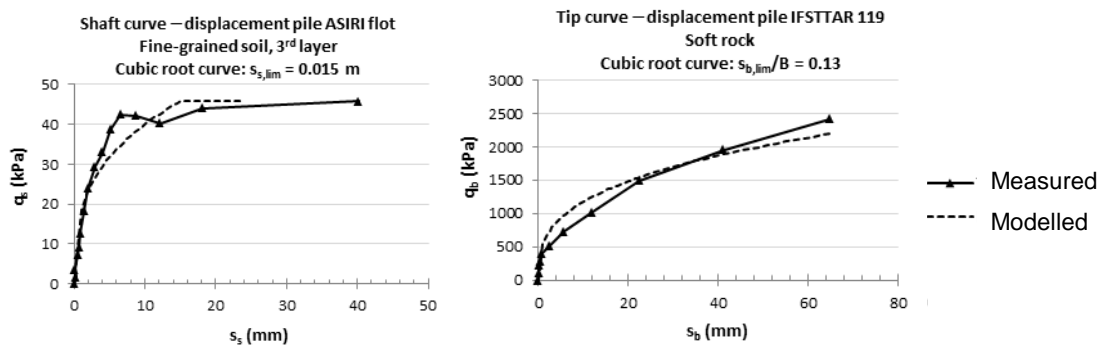


Fig. 4.17 Example of calibration of cubic root curves at shaft and at tip

From the calibration process for all the curves, representative values will be selected both for $s_{s,lim}$ and $s_{b,lim}/B$ which are applicable for all piles and all ground types. Fig. 4.18 shows the mean values of the parameters for the cubic root curves for both pile types and for all soil types. Fig. 4.19 shows all values against the cone resistance.

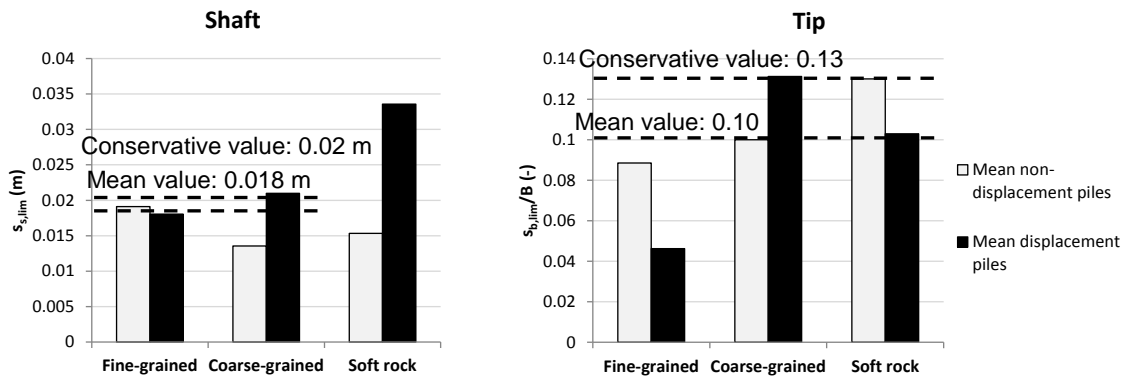


Fig. 4.18 Cubic root curves – Calibration of limit settlements $s_{s,lim}$ and $s_{b,lim}$

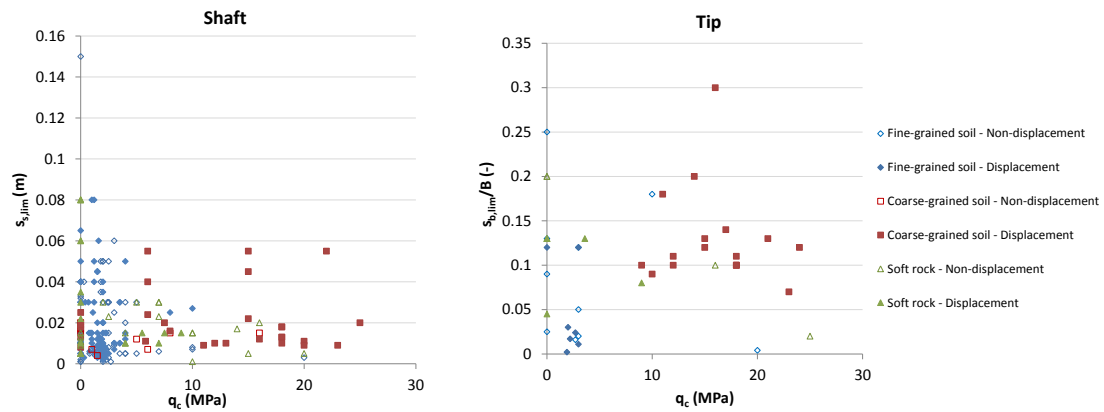


Fig. 4.19 Limit settlements $s_{s,lim}$ and $s_{b,lim}$ in function of CPT cone resistance for cubic root curves ($q_c = 0$ MPa means no CPT data)

The main conclusions of the calibration of the cubic root curves are the following:

- no correlation can be found between the parameters of the curves and the cone resistance q_c , even for a given ground type. Krasieński (2010, 2011, 2012a, 2012b) proposed s_{lim} values which are independent from q_c as well. However, it is commonly accepted that there is a correlation between q_c and the ultimate values $q_{s,ult}$ and $q_{b,ult}$. Thus in the proposed model the stiffness is indirectly correlated with q_c ;
- the scatter is higher for the shaft than for the tip with some very high values. However for the shaft and the tip most of the points are in a small range;
- coarse-grained soils results show a very small scatter, with values close to the average. Fine-grained soil and rock present more scattered values;

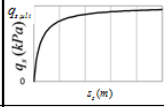
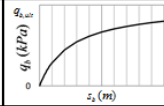
- non-displacement piles show in general slightly smaller $s_{s,lim}$ values (stiffer behaviour at the shaft) and slightly higher $s_{b,lim}/B$ values than displacement piles. Nevertheless, it is appropriate to select unique values of both parameters for both types of piles as a simplified approach;
- the curve parameters $s_{s,lim}$ at the shaft are similar for fine-grained and coarse-grained soils, and higher for soft rocks (less stiff behaviour for the shaft). However, soft rocks are in general located at the pile tip and not at the shaft. Selecting a value of $s_{s,lim} = 0.02$ m (Fig. 4.18) seems relevant, since it is conservative for the most common soils at the shaft (mean value for all pile types and for fine and coarse-grained soils only: 0.018 m). This is true for single pile loading without negative skin friction, for which larger values of the curve parameter lead to larger settlements;
- the soil type has no significant influence at the tip. The values of the parameters are slightly smaller for fine soils. All values remain located near the mean value of all pile and ground cases $s_{b,lim} = 0.10 \cdot B$. In order to remain conservative for all ground types for the single pile loading case, a value $s_{b,lim} = 0.13 \cdot B$ is proposed at this stage (Fig. 4.18);
- a project-based fitting of the curve stiffness parameters is in any case the ideal solution if the execution of instrumented pile load tests are possible in the project soil conditions.

Having selected $s_{s,lim}$ and $s_{b,lim}/B$, the cubic root curves depend only on the ultimate resistance values. This means that the decisive point, in particular for serviceability loads, is to determine the ultimate values accurately enough, if not available from an instrumented pile load test in the project conditions.

Hyperbolic curves

The second proposed curves are hyperbolic curves (Table 4.8), which are similar to the Hirayama curves ($M_s = 0.0025$ at the shaft and $M_b = 0.25$ at the tip) and to the Fleming curve at the shaft.

Table 4.8 Proposed hyperbolic load transfer curves

		Mathematical expression	Curve shape	Deformation parameter	Initial slope	Ground type	Pile type	Development based on pile load tests
Hyperbolic curves	Shaft	$q_s = \frac{q_{s,ult} \cdot s_s}{M_s \cdot B + s_s}$		Parameter M_s	$\frac{q_{s,ult}}{M \cdot B}$	All	All	50 tests
	Tip	$q_b = \frac{q_{b,ult} \cdot s_b}{M_b \cdot B + s_b}$		Parameter M_b	$\frac{q_{b,ult}}{M \cdot B}$			

The deformation parameter M_s at the shaft and M_b at the tip have to be calibrated to best match the measurements. The ultimate values are taken from the measurements like in the previous analysis of the existing curves. An example of calibration of each individual case is shown in Fig. 4.20. Note that the model does not allow for peak values.

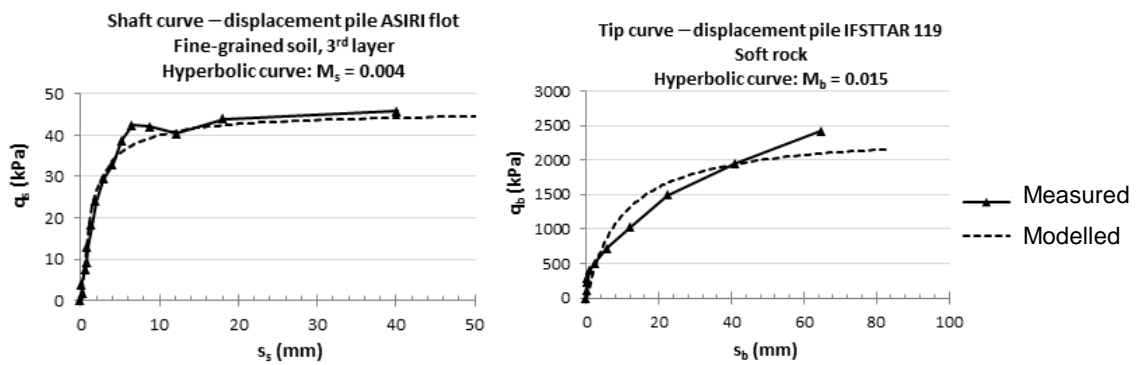


Fig. 4.20 Example of calibration of hyperbolic curve at shaft and at tip

Fig. 4.21 shows the mean values of the parameters for the hyperbolic curves for both pile types and for all soil types. Fig. 4.22 shows all values against the cone resistance.

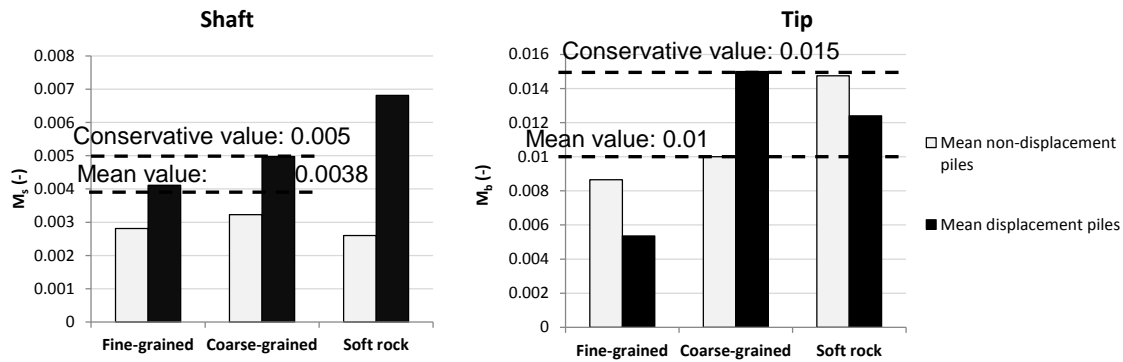


Fig. 4.21 Hyperbolic curves – Calibration of parameters M_s and M_b

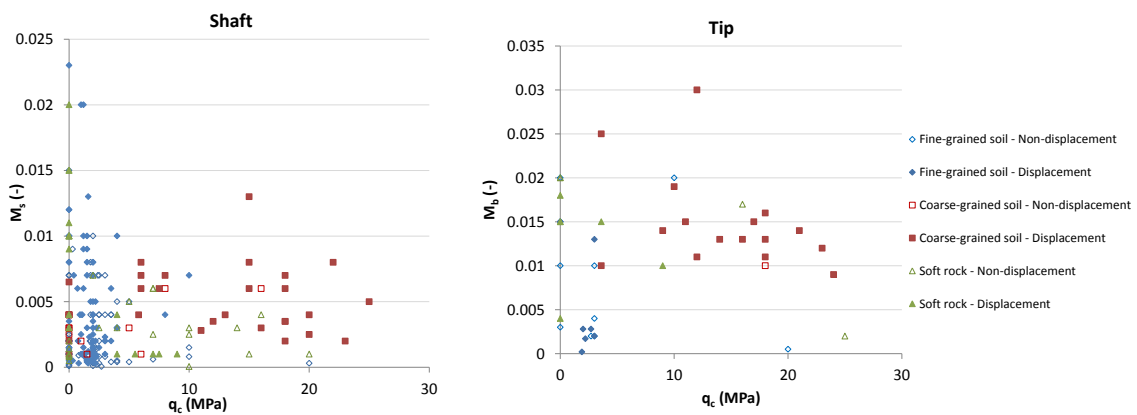


Fig. 4.22 Shaft parameter M_s and tip parameter M_b in function of cone resistance for hyperbolic curves ($q_c = 0$ MPa means no CPT data)

The main conclusions of the calibration of the hyperbolic curves are similar to those for the cubic root curves. This shows that both curve types represent similar behaviours. At this stage, the conservative parameters $M_s = 0.005$ (mean value for all pile types and for fine and coarse-grained soils only: 0.0038) for single pile loading without negative skin friction and $M_b = 0.015$ (mean value for all pile and ground types: 0.01) are proposed.

Having selected M_s and M_b , the hyperbolic curves depend only on the ultimate resistance values. This means that the decisive point, for this curve type as well, is to determine the ultimate values accurately enough. As for the cubic root curve, the execution of an instrumented pile load test is recommended in the project conditions if possible in order to fit the curve stiffness parameters and at the same time to assess the ultimate values.

Comparison of proposed curves with Frank and Zhao curves

Since only one value of the deformation parameters for all pile and ground types have been selected for both proposed curves, they do not necessarily match accurately the measurements for each pile individually. In order to check this and to compare them with the reference well-proven curves of Frank and Zhao, the procedure presented above (Fig. 4.12, Fig. 4.15 and Fig. 4.16) is applied to the proposed curves (with the measured ultimate values). Only the cases with pressuremeter parameters are considered, meaning 32 tests out of 50 (10 non-displacement piles and 22 displacement piles). The proposed curves show a similar agreement with measurements to the Frank and Zhao curves, in terms of global agreement as well as in terms of initial stiffness (Fig. 4.23). The good accuracy of the new curves shows that there is in general a correlation between the resistance and the stiffness. If the ultimate values considered would be different from the measured ones, the stiffness of the proposed curves would vary proportionally to the ultimate value considered, whereas the slope of the initial linear part of the Frank and Zhao curves would remain the same. In cases where there are no measurements of the ultimate values, the Frank and Zhao curves represent the initial domain with a high confidence owing to the direct use of a measured deformation parameter, as opposed to the proposed curves.

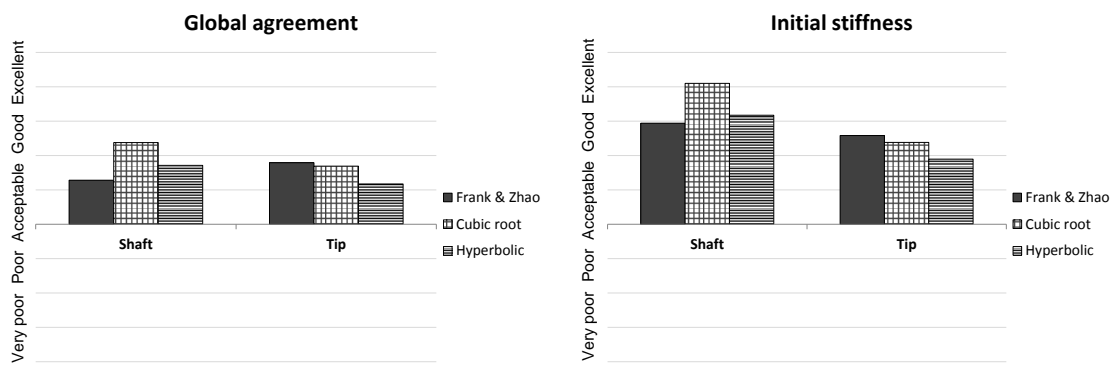


Fig. 4.23 Level of agreement of the proposed load transfer curves compared with Frank and Zhao curves (global agreement and initial stiffness)

4.3.3 Validation based on non-instrumented load tests

Since a key aspect of the validity of the proposed cubic root and hyperbolic curves is a reliable prediction of the ultimate values in practice, they are checked here only with regard to the overall load-settlement behaviour at the pile head. No instrumentation over depth (Table 4.2) and thus no measured values of local skin friction resistance and tip

resistance are considered. For the cubic root and the hyperbolic curves, the conservative stiffness parameters selected in the previous section (for single pile loading without negative skin friction) are used. The calculation is made using the single pile option of the LTM part of the KID software developed in the scope of the present work, using an iterative unidimensional finite difference method (Keller Company 2015). This calculation corresponds to the method described in section 2.2.2 with Fig. 2.4 and (Eq. 2.30) to (Eq. 2.32), without free soil settlement. The parameters necessary for the LTM calculation of a single pile are presented in Fig. 4.24. An example of calculation results (test Ifsttar 1 A1 in Appendix D.4) for a given load applied is shown in Table 4.9 and Fig. 4.25. The calculation is almost instantaneous even for a large number of subdivisions per layer (for example in general 100 subdivisions per layer in the present work). The load-settlement curve at the pile head is calculated with the proposed load transfer curves by running this calculation for different loads, as shown in Fig. 4.26.

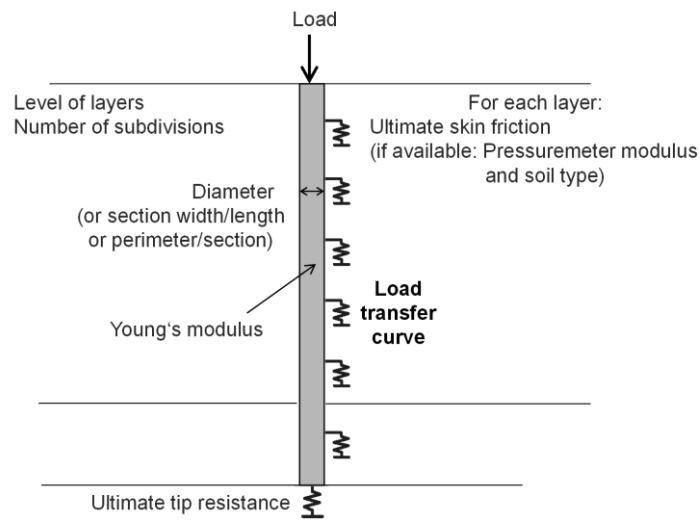


Fig. 4.24 LTM single column system with required input parameters

Table 4.9 Example of a single pile analysis with test Ifsttar 1-A1 under a given load with the LTM: input parameters

Foundation type	: Single column
Mobilisation curve	: Cubic root (conservative parameters)
Load	: 1000 [kN]
Tip resistance ult.	: 4922 [kPa]

Soil properties		Friction ult.
Top Type	[m]	[kPa]
0,00 Silt		22,5
4,00 Sand		34,2
11,00 Silt		22,5
13,00 Gravel		80,7
16,00 Chalk		56
19,00 Chalk		84,1
23,50 Chalk		79,7

Column properties				
Top Type	Column diameter	Add. resistance for diameter variation (also virtual)	Column E	No. of subdivisions
[m]	[m]	[kPa]	[kPa]	[-]
0,00 Silt	0,45	0	30000000	100
4,00 Sand	0,45	0	30000000	100
11,00 Silt	0,45	0	30000000	100
13,00 Gravel	0,45	0	30000000	100
16,00 Chalk	0,45	0	30000000	100
19,00 Chalk	0,45	0	30000000	100
23,50 Chalk	0,45	0	30000000	100

Column toe: 24 m

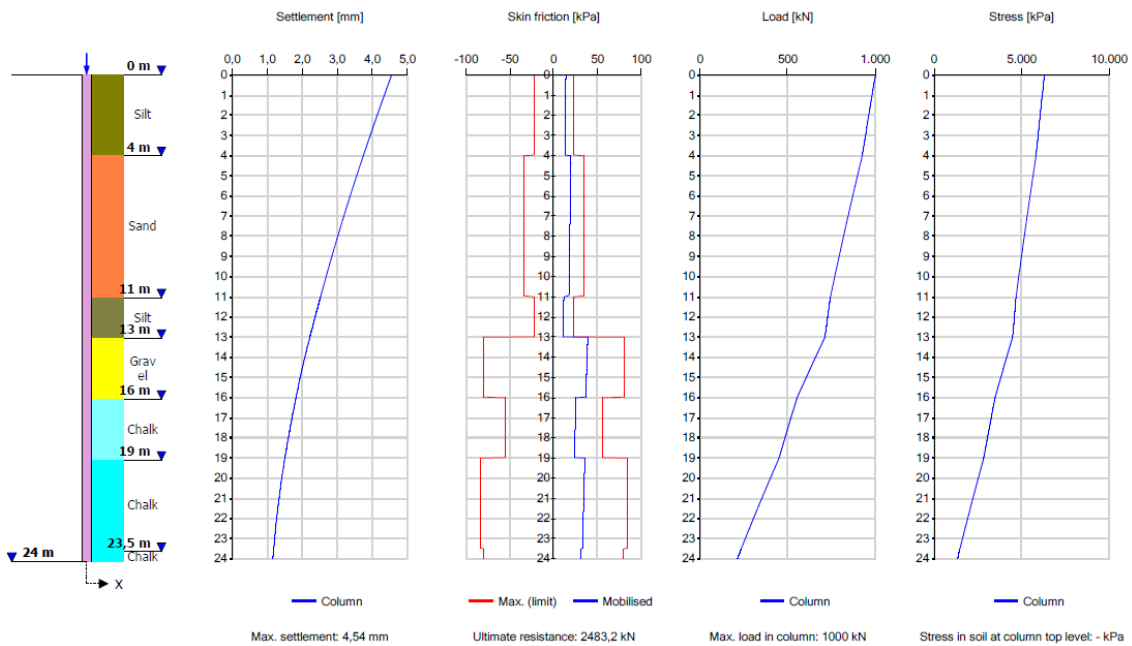


Fig. 4.25 Example of a single pile analysis with test Ifsttar 1-A1 under a given load with the LTM: output under 1000 kN

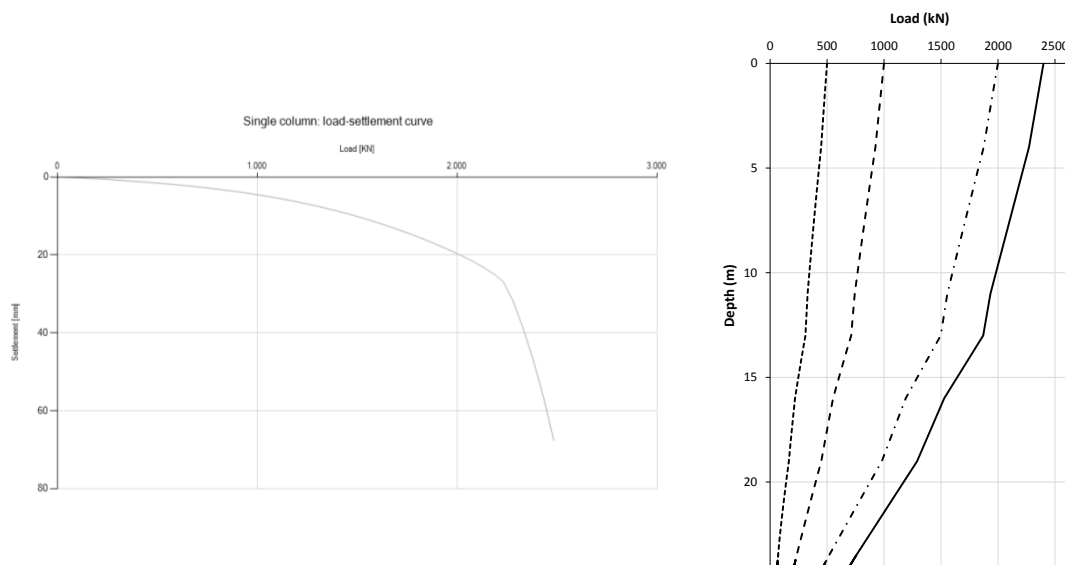


Fig. 4.26 Example of a single pile analysis with test Ifsttar 1-A1 with the LTM: load-settlement curve and load distribution along the shaft for different loads

The evaluation methodology is the following:

- the considered ultimate unit resistances are derived here as an example using the French application standard of the Eurocode 7 NF P94-262 (2012) in which both CPT rules and pressuremeter test rules are available. In priority, the CPT rules are used if CPT results are available in the database. Otherwise, the pressuremeter rules are applied (see tests with PMT only in Appendices D.3 and D.4);
- this overall calculation at the pile head requires the pile Young's modulus value, or strictly speaking the pile section stiffness (modulus multiplied by area of the pile section). This parameter has a high influence on the results for small settlements in the serviceability load level (of the order of a few millimetres). For concrete piles, the value of the short-duration pile Young's modulus after EN 1992-1-1 (2004-2010) is used since a pile load test lasts approximately a few hours. For the design of real projects, the long-duration modulus for concrete columns in soils according to NF P94-262 (2012) should be used;
- the implementation of the curves require some adaptations from a numerical point of view and for physical consistency: the cubic root curves are modified with a linear segment for displacements between 0 and 0.0001 m to avoid the infinite slope problem, and the hyperbolic curves are forced to reach the ultimate value at the point where it would be equal to 99.99 % of the ultimate resistance;

- the comparison is made quantitatively for a load equal to half of the calculated ultimate resistance load of the pile (2 examples from the pile load tests database in Fig. 4.27, see Appendices D.3 and D.4);
- the cases where the measurements stop before reaching half of the calculated pile ultimate resistance, even far from failure, cannot be considered in the comparison (tests Keller Poland 10, 25, 26, 27, 28, 129, 134, 153, 198, 199, 223, 234, 276, see Appendices D.3 and D.4). Furthermore, the extreme cases where there is a factor 2 between measured and estimated resistance (or the other way around) are excluded (Ifsttar 18 A, 29, 49 and 194). This is because it is believed that at the start the prediction is already not satisfactory because of the ultimate resistance assessment. All the above cases represent 17 pile load tests out of 72 (Table 4.2). For only 11 of the remaining tests, pressuremeter test results are available.

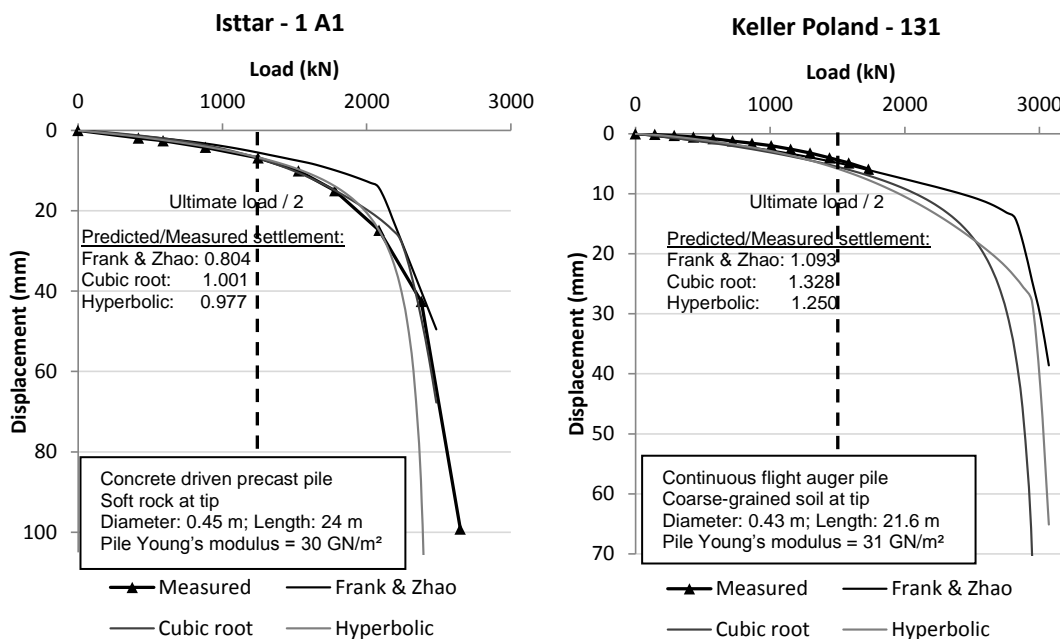


Fig. 4.27 Examples of comparison between measured and predicted load-settlement curves at pile head

The ratio between the predicted and measured settlement for both proposed curves with conservative parameters is presented in Fig. 4.28; on the left for all pile load tests and on the right only for the pile load tests where pressuremeter test results are available. The mean values as well as the values with plus or minus one standard deviation are shown.

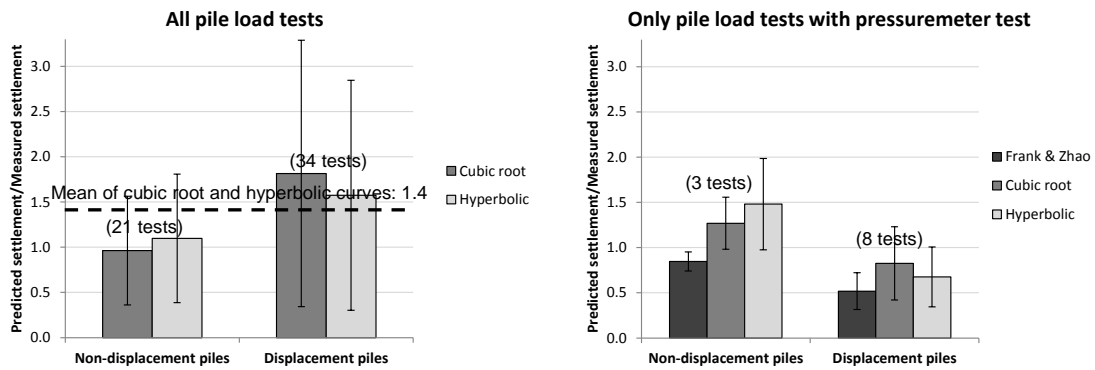


Fig. 4.28 Ratio between predicted and measured settlement for both proposed load transfer curves

The following conclusions can be drawn:

- the overall shape of both proposed curve types match very well the measured load-settlement curves;
- the agreement between the prediction and the measurement is very good, considering the low settlement values (of a few millimetres) for the load level considered and the high influence of uncertainties in the local unit resistance determination and in the pile section stiffness determination. This is part of all real projects in geotechnical engineering and explains the relatively large standard deviation values;
- the overall mean ratio for all tests between predicted and measured settlement is about 1.4, which is consistent with the conservative estimate of the parameters mentioned earlier (Fig. 4.18 and Fig. 4.21);
- the comparison with the Frank and Zhao curves is unfortunately limited, due to the very few non-instrumented load tests with pressuremeter results available. The proposed curves give settlement 50 % larger than the Frank and Zhao curves, which again shows the conservative selection of the proposed parameters. For the few investigated displacement pile cases (only 8 cases) with pressuremeter tests, the estimated settlement is smaller than the measured one, whereas for all 34 pile load tests, the ratio predicted to measured settlement is larger than 1. Thus it appears that the 8 cases where pressuremeter tests are available are not very representative of the general results;
- the cubic root and the hyperbolic curves with the proposed parameters have the same level of agreement. The hyperbolic shape may be more realistic because

the ultimate value is never reached and the initial stiffness is non-infinite. This corresponds to the proposed model for the single footing behaviour (section 3.2). However, the use of the cubic root curves does not present a problem if the domain of very small displacements is represented by a linear part in numerical applications;

- Since the conservative estimate of the parameters is reflected directly without loss of conservative margin, the use of the mean parameters $s_{s,lim} = 0.018$ m, $s_{b,lim} = 0.1$, $M_s = 0.0038$, $M_b = 0.01$ (Fig. 4.18 and Fig. 4.21) for the proposed simplified approach seems appropriate even for single piles. The use of the mean parameters would lead to a similar order of settlements as with the well-proven Frank and Zhao curves. In any case, for combined systems, use should be made of the mean parameters; in such systems, negative skin friction may appear, for which the previously selected “conservative” parameters do not apply anymore. Furthermore, for combined systems, a settlement prediction as close to reality as possible is required.

5 Application of Load Transfer Method (LTM) to combined foundation systems

5.1 Load transfer method development for combined systems

5.1.1 General aspects

Following the results in section 4, the LTM is selected in the present work as the most adequate and straightforward method for simple pile and combined foundation systems. For combined systems, the use of the LTM presents the important advantage of considering the specific behaviour of the shallow foundation on the one side and of the deep foundation on the other side (sections 3 and 4 respectively). This means that the soil deformation parameters are considered separately for each element of the combined foundation without imposing the definition of the modulus in the same way for the whole system (using the same soil constitutive law with the FEM for example). The compatibility between the elements is ensured by applying interaction conditions, depending on the foundation type.

In the scope of the present work, the LTM is implemented for different combined foundation cases as an option of the Keller internal KID software (Keller Company 2015). The calculation is made in an iterative manner with the unidimensional finite difference method, based on the basic LTM principle developed originally for single piles (see Fig. 2.4 and (Eq. 2.30) to (Eq. 2.32) in section 2.2.2). This has been done partly with the support of Nogneng (2013) and Santos (2013b). The LTM presented in 2.5.2 for combined systems (ASIRI, IREX 2012) is completed here with:

- in case of footings, the proposed non-linear hyperbolic mobilisation curve of the footing resistance (section 3.2);
- the proposed cubic root and hyperbolic load transfer curves with mean parameters for combined systems, in addition to the Frank & Zhao curves (section 4.3);
- a proposal for the calculation of the settlement of the layers below the pile tip level in the case of combined systems, if necessary.

5.1.2 Large slabs or embankments: unit cell calculation

For flexible loadings (embankment or flexible slabs) or rigid slabs, the load is applied to the soil and to the columns directly or through a LTP, over a uniform grid of columns which is assumed to be infinite. This assumption is legitimate for the calculation down to the column tip for ratios between column length and slab width typically smaller than 1.5. This system can be analysed considering a unit cell made of one column and of the corresponding soil. The total load is considered to remain constant over the depth of the unit cell. In the flexible slab calculation type, the applied stress is considered to be uniform at the top of the system. In the rigid slab calculation type, the settlement is considered to be uniform at the top of the system. New layers (for example an LTP) not replacing a previously existing layer can be considered as an additional load, which is applied progressively over the thickness of the new layers. The settlement of the soil is calculated using the constrained modulus E_{oed} and the stress in each sub-layer is the result of the load applied on the soil at the top and also of changes due to the load transfer to and from the column. For rigid slabs, an equal settlement of column and soil at the upper limit of the system is considered as a boundary condition. This system corresponds to the calculation method for infinite grids translated as “common spacing” in the English version of ASIRI (IREX 2012) and presented in section 2.5.2. The principle of the embankment or rigid slab system is presented together with the required input parameters in Fig. 5.1 as an extension of the basic case for single pile already presented in 4.3.3 (Fig. 4.24). The calculation is almost instantaneous even for a large number of subdivisions per layer (for example in general 100 subdivisions per layer in the present work).

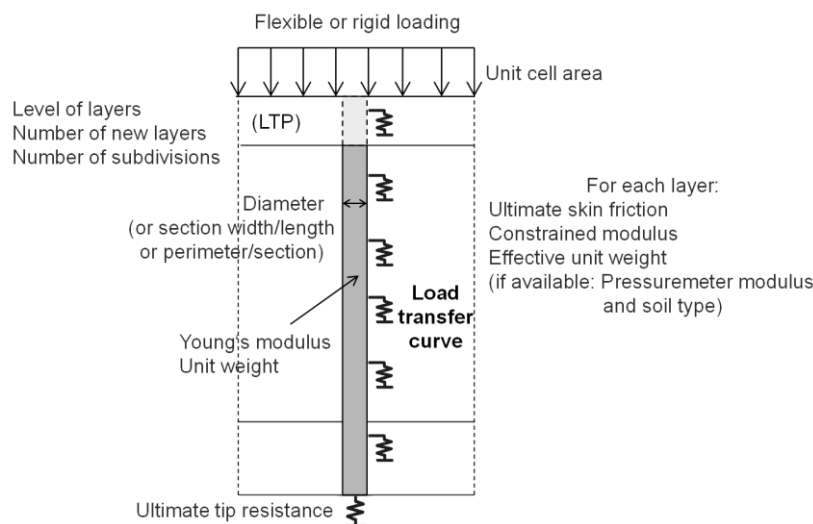


Fig. 5.1 Unit cell for large slabs or embankments with required input parameters

The calculation gives a settlement profile over depth for the column and for the soil, a distribution of positive and negative skin friction and a distribution over the depth of the load and stress in the column and in the soil. Several examples and a comparison between the rigid and flexible loading cases are given in section 5.2.

In the floating columns case (columns embedded in a relatively soft layer), the settlement below the column tips should be calculated separately as the unidimensional settlement of the layers down to the critical depth. In accordance with the original definition of load transfer curves, the soil settlement to be considered is the free soil settlement in the absence of the pile (Frank et al. 1991). Thus the load to be considered for the settlement calculation below the column tip is the stress in the soil at the top of the system (known from the LTM calculation carried out down to the column tip), without considering the stress variations in the soil due to the column over the column depth. This load is supposed to remain constant with depth in the grid considered to be infinite. This assumption is reasonable for a thickness of the layers below the column tip down to the stiff substratum typically smaller than 1/5 of the slab width. Otherwise, a correction considering the diffusion of the soil load below the column tip level is necessary.

For comparison the “unimproved” settlement can be calculated, with a critical depth defined as the depth where the constant applied stress falls below 20 % of the overburden pressure.

In the rigid slab case, the bending moments can be estimated in a simplified way at the centre and at the edge of the unit cell according to the elastic plate theory. The plate is considered to be circular, fixed at the edge and loaded by constant area loads. The partial area loads applied on the plate are the load applied at the top of the slab, the soil reaction directly under the slab from the LTM calculation, and the reaction of the column considering a diffusion of the column reaction in the load transfer platform (Fig. 5.2). The column reaction is calculated for the given diffusion slope with the load conservation theory (total load applied at the top equal to the sum of the total soil reaction and the total diffused column reaction). The moments at the centre of the plate and at the edge are calculated according to (Eq. 5.1) and (Eq. 5.2). A typical value of the diffusion slope is 0.4.

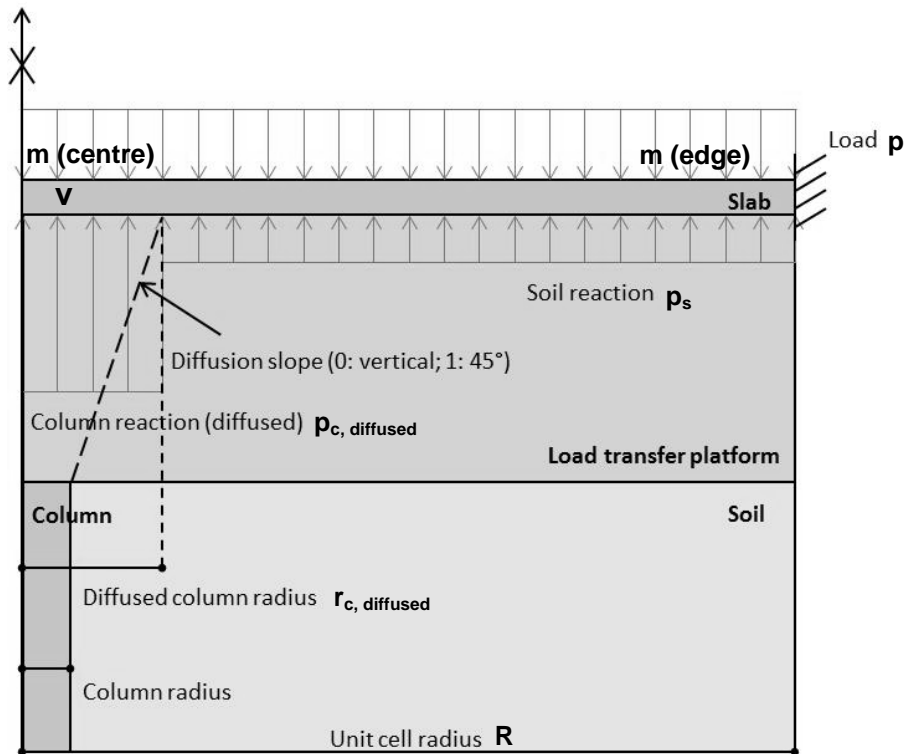


Fig. 5.2 System for calculation of slab bending moments m after plate theory

$$m(\text{centre}) = \frac{-(p_{c,diffused} - p_s) \cdot R^2}{16} \cdot \left(\frac{r_{c,diffused}}{R}\right)^2 \cdot (1 + \nu) \cdot \left(\left(\frac{r_{c,diffused}}{R}\right)^2 - 4 \cdot \ln\left(\frac{r_{c,diffused}}{R}\right)\right) + \frac{(p - p_s) \cdot R^2}{16} \cdot (1 + \nu) \quad (\text{Eq. 5.1})$$

$$m(\text{edge}) = \frac{-(p_{c,diffused} - p_s) \cdot R^2}{8} \cdot \left(\frac{r_{c,diffused}}{R}\right)^2 \cdot \left(\left(\frac{r_{c,diffused}}{R}\right)^2 - 2\right) - \frac{(p - p_s) \cdot R^2}{8} \quad (\text{Eq. 5.2})$$

5.1.3 Single footings: oedometer and pressuremeter method

Single footings apply the load to a limited area of soil reinforced by a given number of columns with or without a LTP. This configuration corresponds to cases where the ratio between the column length and the foundation width is typically larger than 1.5. The different positions of the columns under the footing are not distinguished in the present modelling. The single footing is considered as rigid, which means that the boundary

condition at the top of the system is the equality of the settlement of the soil and of the columns. Due to the limited dimensions of the footing, the load diffusion over the depth has to be considered in the soil. In accordance with Frank et al. (1991), the shape of the stress and settlement profile for the load share of the soil is considered not to be influenced by the presence of the columns. The reference settlement and the stress propagation shape in the soil are calculated under the characteristic point, corresponding to the point where the settlements are equal for a fully flexible and fully rigid footing. The equations of stresses under the characteristic point are given for example in DIN 4019 (2015). Either the elastic oedometer method down to the critical depth, based on the stress distribution of Boussinesq (1885), cited by Vogt (2015), or the pressuremeter method based on the approach of Ménard (Combarieu 1988a) shown in Fig. 5.3 can be used. In the oedometer method, the critical depth for the soil load share in the improved case is calculated on the safe side from the unimproved case as the depth where the stress from the total applied area load falls below 20 % of the overburden pressure. In the pressuremeter method, the critical depth is fixed at 8 times the footing width for all load levels (Fig. 5.3). The selected settlement calculation is considered as the reference calculation for the hyperbolic footing settlement behaviour according to chapter 3.2. This system corresponds to the calculation method for footings on inclusions MV2 in ASIRI (IREX 2012) presented in section 2.5.2. The shape of the stress distribution in the soil over depth is calculated based on the theory of elasticity for both oedometer and pressuremeter methods.

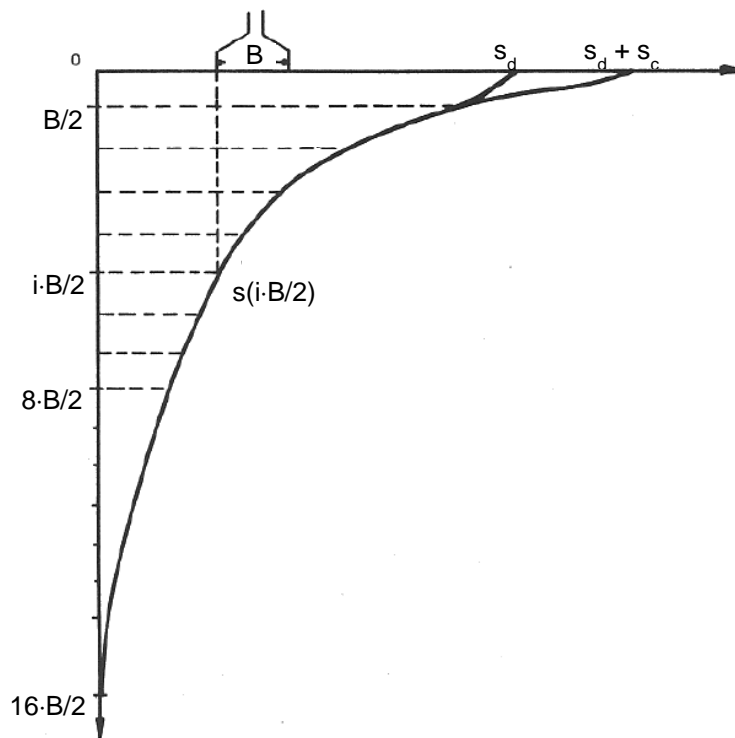


Fig. 5.3 Soil settlement profile under a single footing according to the pressuremeter theory (Combarieu 1988a)

The working principle of the single footing system is shown in Fig. 5.4 together with the required input parameters. The calculation is almost instantaneous even for a large number of subdivisions per layer (for example in general 100 subdivisions per layer in the present work).

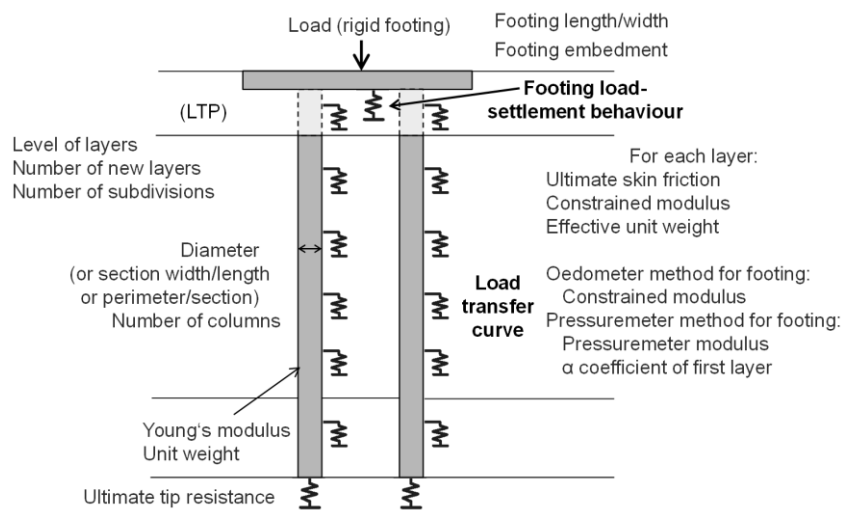


Fig. 5.4 LTM Single footing with oedometer method or pressuremeter method with required input parameters

The calculation gives a settlement distribution over the depth for the column and for the soil, a distribution of the positive and, if existing, of the negative skin friction and the mobilisation of the limit values, a distribution of the load and of the stress in one column and in the soil. Different footing examples with and without a LTP are presented in the next section 5.2).

The additional settlement of the system below the column tip level corresponds to the settlement of the footing in the layers below the column tip level under the load in the soil at the top of the system (known from the LTM calculation carried out down to the column tip).

For comparison the “unimproved” settlement can be calculated down to the critical depth.

5.2 Comparison and transition between CPRF and RI systems based on reference cases with measurements

5.2.1 Infinite grid system

5.2.1.1 Reference RI infinite grid case with measurements

The reference case for the infinite grid analysis is the full-scale monitored field test of a slab on non-displacement inclusions with a load transfer platform conducted in Saint-Ouen-l’Aumône, France in the scope of the ASIRI programme (IREX 2012) French national project (Briançon and Simon 2010). Fig. 5.5 shows a sketch of the test slab with the soil parameters (E is here the oedometer modulus), together with another test slab without columns. The slabs have an area of $8\text{ m} \times 8\text{ m}$ area and a thickness of 0.17 m . The 0.5 m load transfer platform (LTP) is made of highly compacted granular material. The bottom 0.25 m of the LTP served as a working platform for the installation of the columns. The loading of the slabs is made with a 4 m embankment (78 kPa). The settlement at the top of the system results from both the load applied at the top and the dead weight of the LTP. For the reinforced section with soil reinforcement, 4 by 4 columns of diameter 0.42 m have been installed in a 2.5 m square grid. Since the column spacing is approximately equal to 6 times the column diameter, no group effect should occur. The columns are embedded 50 cm in the sandy substratum. It appeared that the soil profile is quite different under the unimproved slab from under the slab with columns, so that the modelling of the unimproved case is not relevant here for the calibration of the soil parameters for the slab with columns.

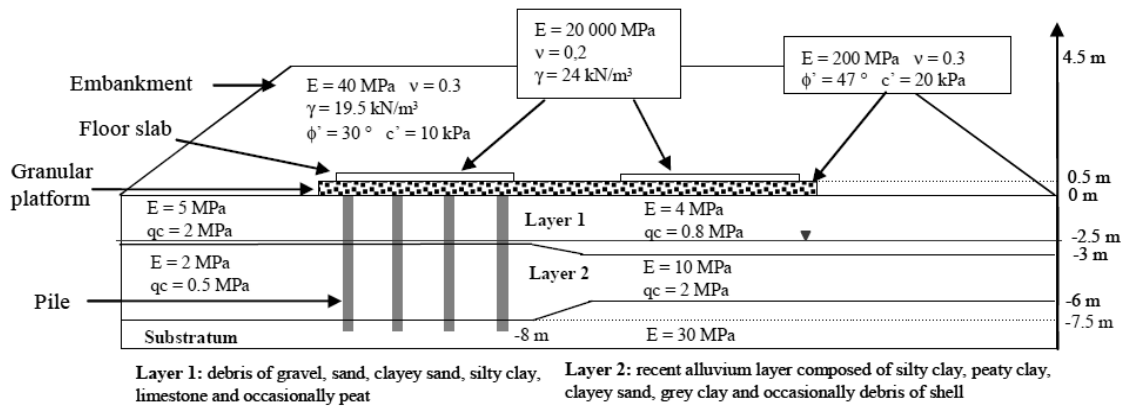


Fig. 5.5 Cross section of monitored RI field test for ASIRI in Saint-Ouen-l'Aumône with main soil and foundation parameters (Briançon and Simon 2010)

The central inclusion of the system with the surrounding soil can be modelled as a unit cell in an infinite grid (ratio pile length to slab width equal to 1). For the LTM modelling with the Frank and Zhao curves, the PMT moduli of the different layers are necessary. These are estimated according to the PMT measurements made approximately 20 m from the test slab (Briançon 2007) and considering the oedometer moduli in Fig. 5.5 estimated by Briançon and Simon (2001), in combination with the usual correlations for large slabs given in Appendix C.3. The skin friction values in the layers 1 and 2 are taken from the measurements made on a single inclusion at the same site without embedment in the substratum (Nunez et al. 2010). For the substratum, the skin friction and the tip resistance are estimated based on the measured limit pressure of approximately 1 MPa (Briançon 2007) using the French method described in 2.2.2. In the LTP, the Young's modulus of the virtual column is calculated according to the theory of elasticity with the given oedometer modulus (Poisson's ratio of 0.3), and a pressuremeter modulus is estimated with the usual correlation for large slabs given in Appendix C.3 with $\alpha = 1/4$. The ultimate skin friction in the LTP is determined as the vertical stress in the middle of the layer multiplied by $K \cdot \tan(\phi) = 1$ (section 2.5.2.2). The LTP is considered as an additional load (meaning for the calculation one new layer in the system from the top). The Young's modulus of the column is taken equal to 20 GPa as a value between short-duration and long-duration concrete modulus for concrete columns in soils according to EN 1992-1-1 (2004-2010), ASIRI (IREX 2012) and NF P94-262 (2012). All parameters used in the LTM calculation for the central unit cell are summarized in Table 5.1.

Table 5.1 LTM parameters for infinite grid system of the ASIRI field test

Load	:	78 [kPa]			
Tip resistance ult.	:	2000 [kPa]			
No. of layers considered as load	:	1 [-]			
Unit cell area	:	6,25 [m ²]			
Soil properties					
Top Type	Eoed modulus	Pressure			
[m]	[kPa]	modulus			
		Friction ult.			
		γ eff. soil			
		Fine soil			
-0,50 LTP	200000	50000	83	20	
0,00 Layer1	5000	3300	20	20	x
2,50 Layer2	2000	1300	60	10	x
7,50 Substratum	30000	10000	100	10	
Column properties					
Top Type	Column	γ column	Add. resistance for	Column E	No. of
[m]	diameter	diameter variation (also virtual)	resistance for	subdivisions	
	[m]	[kN/m ³]	[kPa]	[kPa]	
-0,50 LTP	0,42	23	0	150000	100
0,00 Layer1	0,42	23	0	20000000	100
2,50 Layer2	0,42	23	0	20000000	100
7,50 Substratum	0,42	23	0	20000000	100
Foundation level:			-0,5 m		
Column toe:			8 m		

Since the slab is very thin (17 cm), the system is calculated both with a rigid slab and with a flexible slab. The settlement of the layers below the column tip is negligible due to the quickly increasing stiffness of the substratum with depth. The LTM calculation results as a rigid slab are shown in Fig. 5.6 with the Frank and Zhao curves. The results are compared to the calculation results with the cubic root and with the hyperbolic curves with the proposed simplified approach using fixed mean stiffness parameters for the rigid slab case (Fig. 5.7 and in Fig. 5.8).

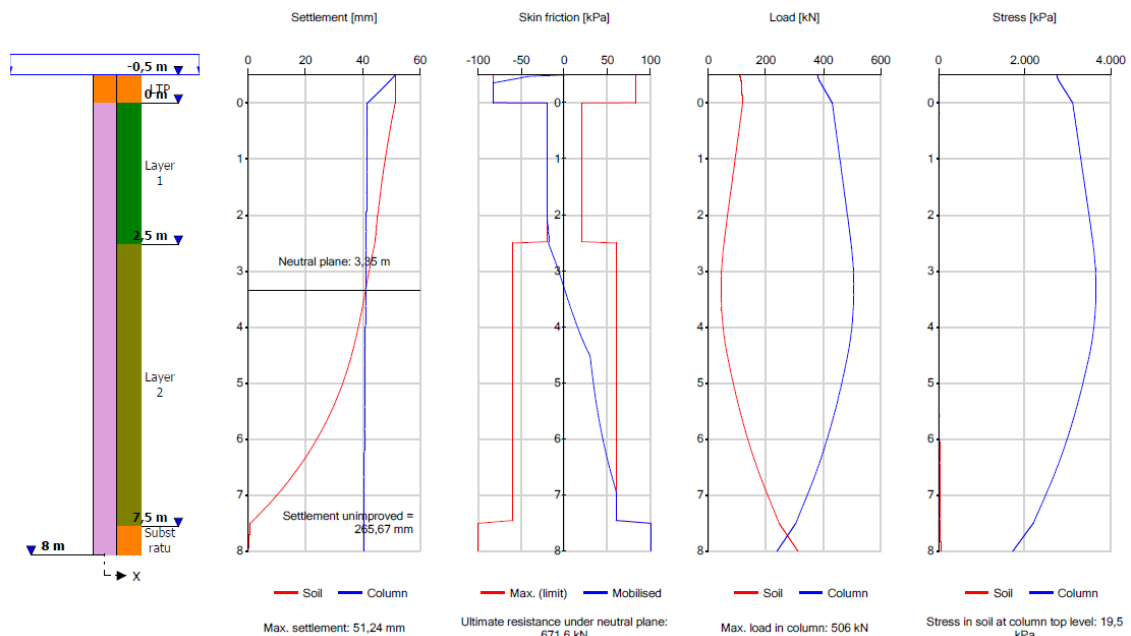


Fig. 5.6 Results of LTM calculation of infinite grid system of the ASIRI field test with a rigid slab with Frank and Zhao load transfer curves

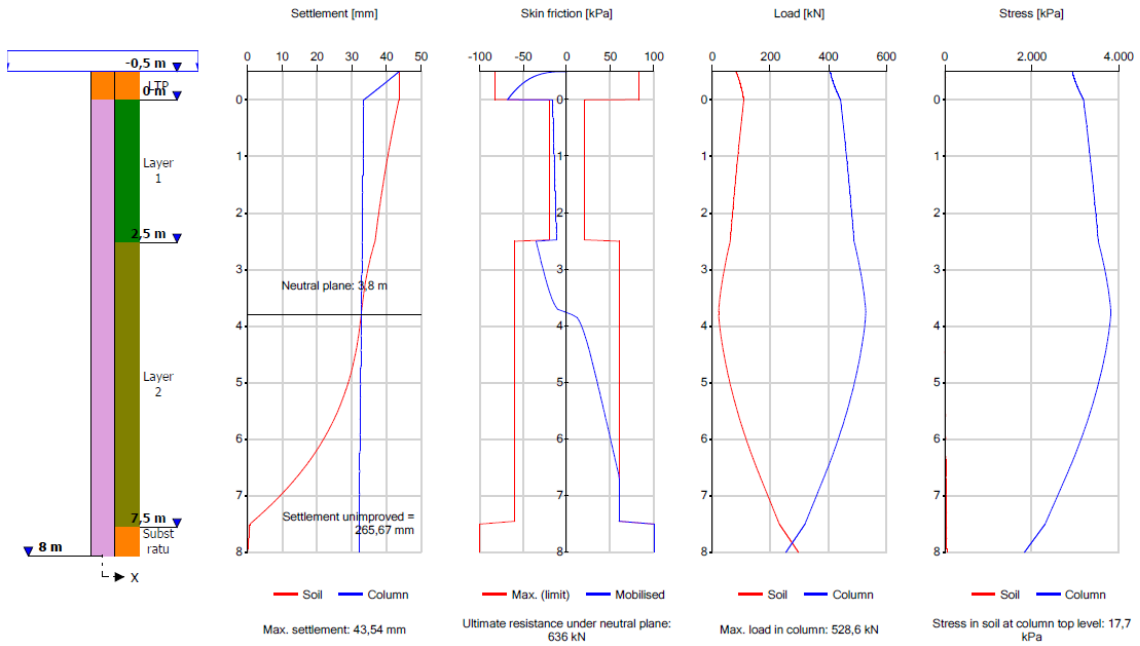


Fig. 5.7

Results of LTM calculation of infinite grid system of the ASIRI field test with a rigid slab with proposed cubic root load transfer curves

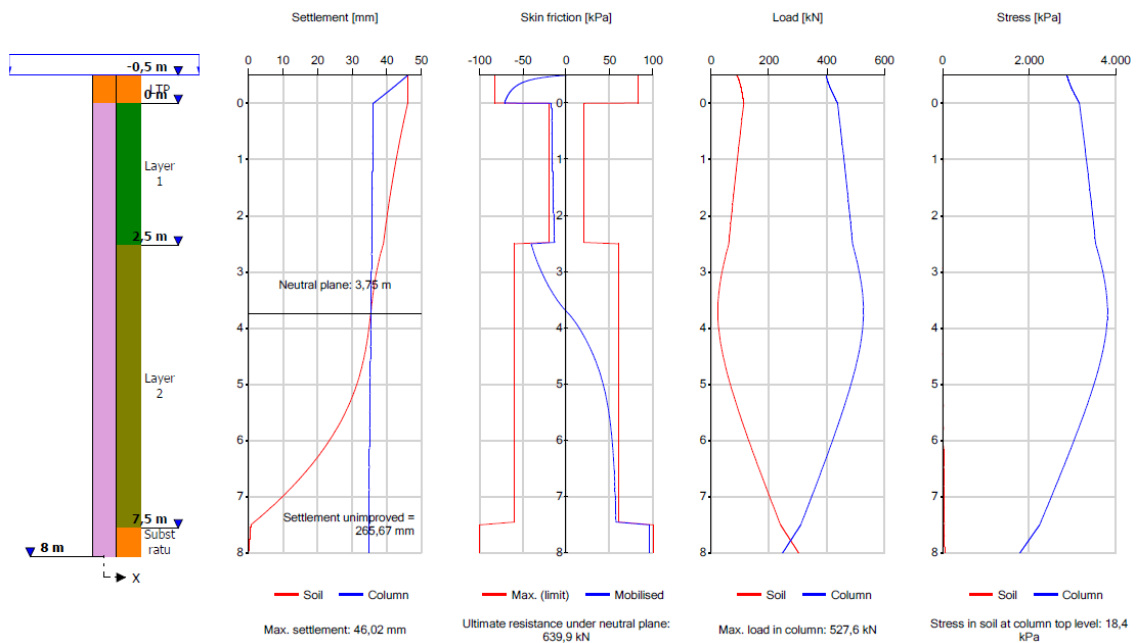


Fig. 5.8

Results of LTM calculation of infinite grid system of the ASIRI field test with a rigid slab with proposed hyperbolic load transfer curves

The calculation with the proposed cubic root and hyperbolic curves gives similar results to those with the Frank and Zhao curves, with a settlement at the top of the system of 4.4 to 5.1 cm, a maximum column load of 500 to 530 kN (93 to 96 % of the total applied load) and a neutral plane position at 3.3 to 3.9 m. The load transfer in the LTP is similar with all 3 approaches.

The LTM calculation results for the flexible slab are shown in Fig. 5.9 with the Frank and Zhao curves.

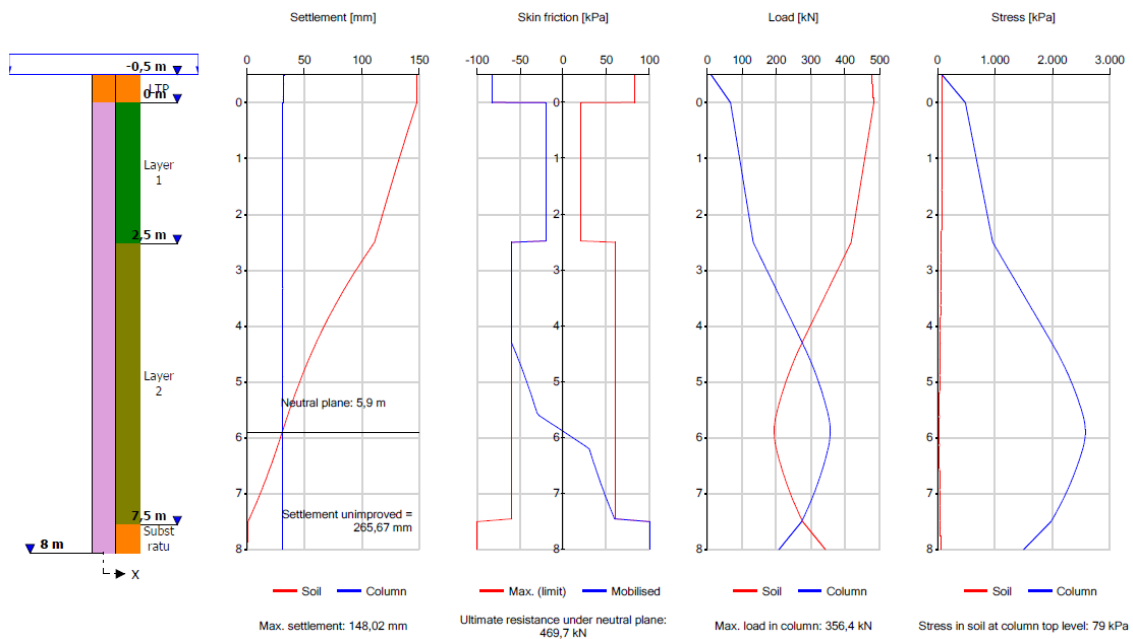


Fig. 5.9 Results of LTM calculation of infinite grid system of the ASIRI field test with a flexible slab with Frank and Zhao load transfer curves

The calculation for a flexible slab shows much larger settlements of 15 cm with a very high differential settlement of 12 cm at the top of the system. The maximum column load is smaller than in the rigid case, with 356 kN (65 % of the total load). The neutral plane is deeper than in the rigid case.

Briançon and Simon (2010) report a measured pressure at the pile head of 1800 kPa and a differential settlement at the column head level of 23 mm in the diagonal of the central unit cell one year after the full loading (Fig. 5.10). Most of the differential settlement happens in relatively close vicinity of the column (19 mm at 0.5 m of the column edge). The total settlements have not been measured.

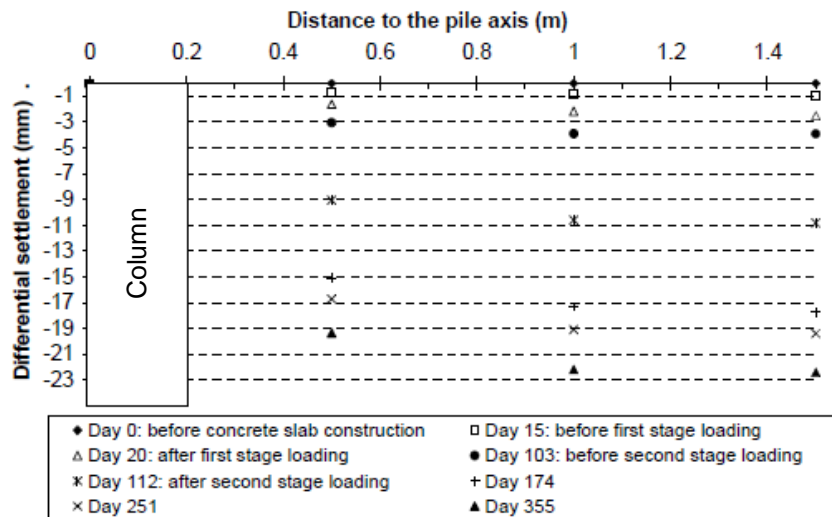


Fig. 5.10 Differential settlement measured in central unit cell of ASIRI field test (Briançon and Simon 2010)

Table 5.2 gives the values of the predicted pressure at the column head and of the differential settlement at the column head level in comparison with the measurements. The measurements lie between the values of the rigid and of the flexible case, but remain closer to the rigid case. This is in good agreement with the expectations since the slab is particularly thin and thus not fully rigid. These results assess the good agreement of the predictions.

Table 5.2 Comparison of measurements with predictions for the ASIRI field test

	Measurement (Briançon and Simon 2010)	Rigid slab LTM calculation Frank and Zhao curves	Rigid slab LTM calculation Cubic root curves	Rigid slab LTM calculation Hyperbolic curves	Flexible slab LTM calculation Frank and Zhao curves
Pressure at column head (kPa)	1800	3111	3190	3159	485
Differential settlement at column head level (mm)	23	10	10	10	117

For the following parameter studies, the case with rigid loading will be considered as reference case.

5.2.1.2 Variation of load

The behaviour of the rigid inclusion system under load variation is examined. All the parameters of the reference case remain the same, in particular the LTP thickness of 0.5 m. The area load at the top of the system is varied between 0 and 200 kPa (total area

load between 10 and 210 kPa considering the additional load of 10 kPa due to the LTP). All following calculations are made with the Frank and Zhao load transfer curves in order to take advantage of the PMT test results available. For the different load levels, the settlement, the column load share, the position of the neutral plane and the column load at the neutral plane compared to the column maximum resistance under the neutral plane are represented in Fig. 5.11, Fig. 5.12 and Fig. 5.13, respectively. For all load levels, it is checked that the stress in the LTP is allowable (see Fig. 2.41 in section 2.5.2.2).

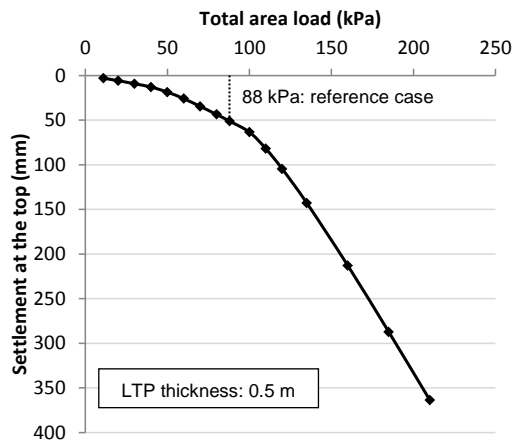


Fig. 5.11 Surface load-settlement based on ASIRI reference case with Frank and Zhao load transfer curves (infinite grid, rigid loading)

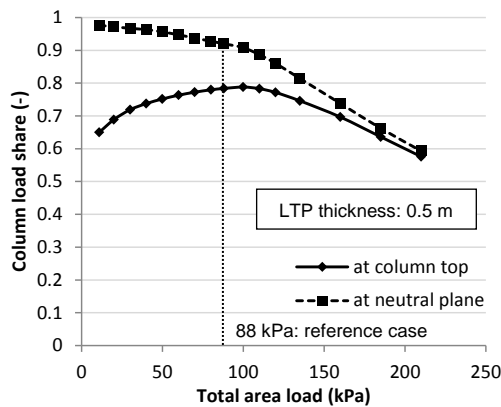


Fig. 5.12 Column load share vs. area load based on ASIRI reference case with Frank and Zhao load transfer curves (infinite grid, rigid loading)

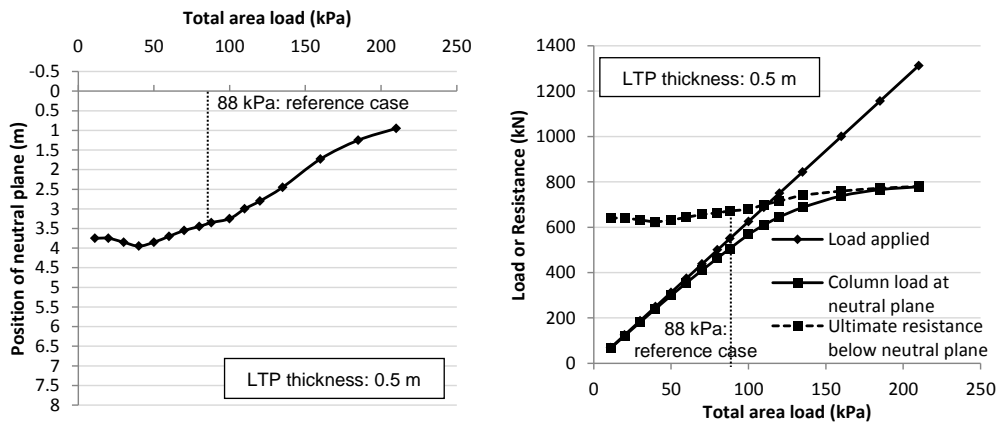


Fig. 5.13 Neutral plane variations vs. area load based on ASIRI reference case with Frank and Zhao load transfer curves (infinite grid, rigid loading)

The settlement increases non-linearly with the load for area loads lower than 120 kPa. Then the settlement increase is proportional to the load increase. This reflects the fact that first the non-linear column settlement behaviour is governing. Then the settlement grows in a regular proportion theoretically up to infinite loads according to the theoretical linear one-dimensional oedometer behaviour of the soil in the unit cell (notwithstanding the influence of the load exchanges with the column over the depth). These two different modes are also visible in Fig. 5.12 and Fig. 5.13. The neutral plane moves up due to the higher column settlements with regard to the soil. The column load share at the column top decreases faster after 120 kPa, where a peak of the column share at the neutral plane occurs. The mode change corresponds to the moment where the column maximum load gets close to the resistance under the neutral plane and where the additional load has to be thus transferred to the soil in the system equilibrium.

The load-settlement behaviours of the column in the RI system (load at the top of the RI), of the soil in the RI system and of the whole RI system are represented together with the load-settlement behaviour of the single column in Fig. 5.14. As for a CPRF system (see Fig. 2.20 in section 2.4.1), the stiffness of the column in the system is reduced compared to the single column. However, the bearing capacity is not increased since the ultimate skin friction is taken from the single column case and thus no group effects and no confinement effects are represented here. The single column behaves significantly stiffer than the RI system for small loads, but the bearing capacity is smaller than the one of the whole RI system.

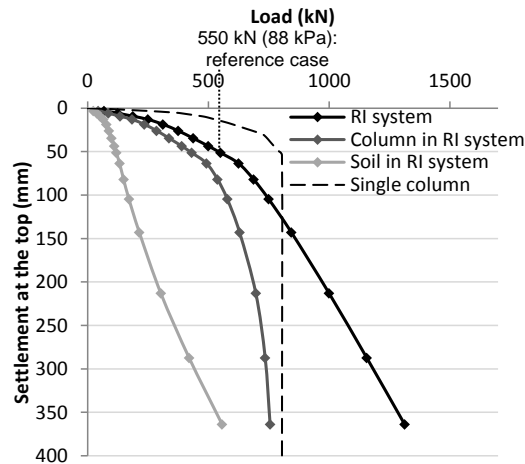


Fig. 5.14 Load-settlement behaviour based on ASIRI reference case with Frank and Zhao load transfer curves (infinite grid, rigid loading) compared to single column case

5.2.1.3 Variation of LTP thickness

The study of the variation of the LTP thickness highlights at the same time the transfer mechanisms involved in the LTP in RI systems and the transition with the CPRF case which corresponds to a LTP thickness equal to zero. The total load level at the base of the LTP is kept constant; this means that the applied load at the very top has to be reduced for larger LTP thickness values. The constant load level is chosen as 120 kPa. This load corresponds to the value at the transition between the two modes in the reference case studied above and is large enough to allow for high LTP thickness values. The determination of the ultimate skin friction in the LTP is made in the same manner as in the reference case. Test calculations have shown that one single average value over the whole LTP height is sufficient, since the results are very close to the case with a graduated increase of skin friction with depth in the LTP.

The evolution with the LTP thickness of the settlement at the top, of the column load share, of the position of the neutral plane and of the resistance under the neutral plane are presented in Fig. 5.15, Fig. 5.16 and Fig. 5.17 respectively. The settlement at the top of the system results from both the load applied at the top and the dead weight of the LTP.

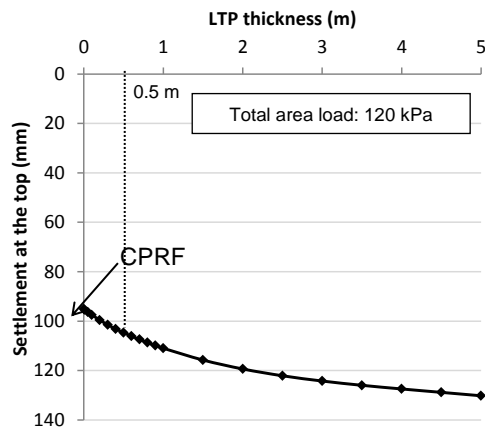


Fig. 5.15 Settlement at the top vs. LTP thickness based on ASIRI reference case with Frank and Zhao load transfer curves (infinite grid, rigid loading)

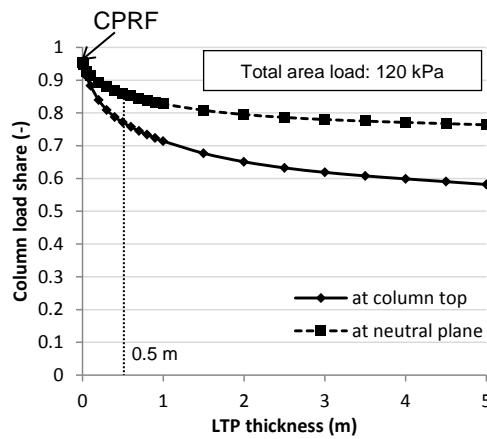


Fig. 5.16 Column load share vs. LTP thickness based on ASIRI reference case with Frank and Zhao load transfer curves (infinite grid, rigid loading)

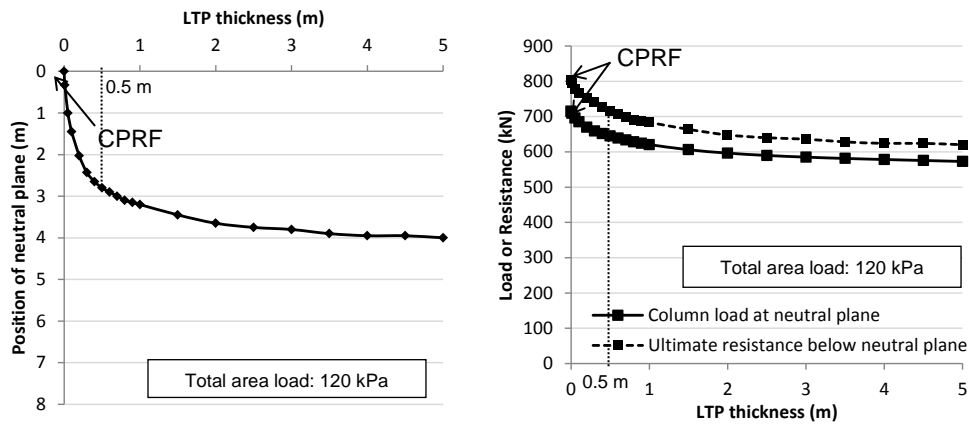


Fig. 5.17 Neutral plane variations vs. LTP thickness based on ASIRI reference case with Frank and Zhao load transfer curves (infinite grid, rigid loading)

The settlement increases slightly with the LTP thickness, whereas the column load share decreases and the position of the neutral plane moves down.

The CPRF case is characterized by a maximum column load share, a neutral plane located at the top of the system and a maximum load in the column situated at the top of the column. For the selected 120 kPa top load, the column load is close to the ultimate column geotechnical resistance below the neutral plane; such a situation would be allowed only in domain 2 according to the ASIRI recommendations (IREX 2012).

5.2.1.4 Comparison between rigid and flexible slab cases

The study of the flexible slab case in comparison with the rigid slab case gives information about the mechanisms in the LTP as well as about the moment to be expected in the slab in the rigid case, both for the CPRF and for the RI system. In Fig. 5.18, Fig. 5.19 and Fig. 5.20, the same parameters as in section 5.2.1.3 above are presented together for the flexible and rigid slab cases.

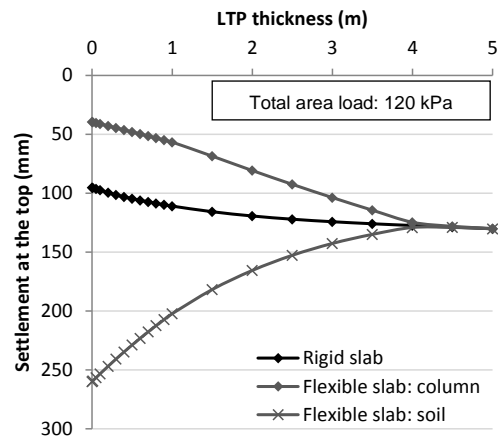


Fig. 5.18 Settlement at the top vs. LTP thickness based on ASIRI reference case with Frank and Zhao load transfer curves (infinite grid, rigid and flexible loading)

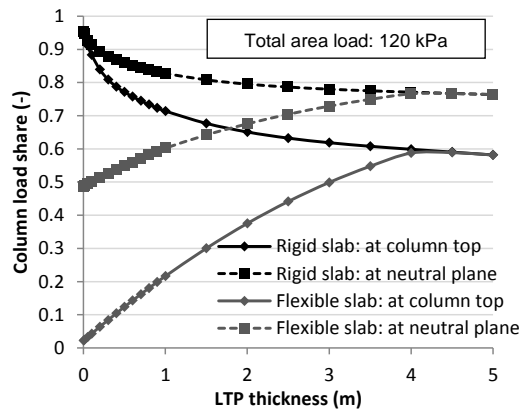


Fig. 5.19 Column load share vs. LTP thickness based on ASIRI reference case with Frank and Zhao load transfer curves (infinite grid, rigid and flexible loading)

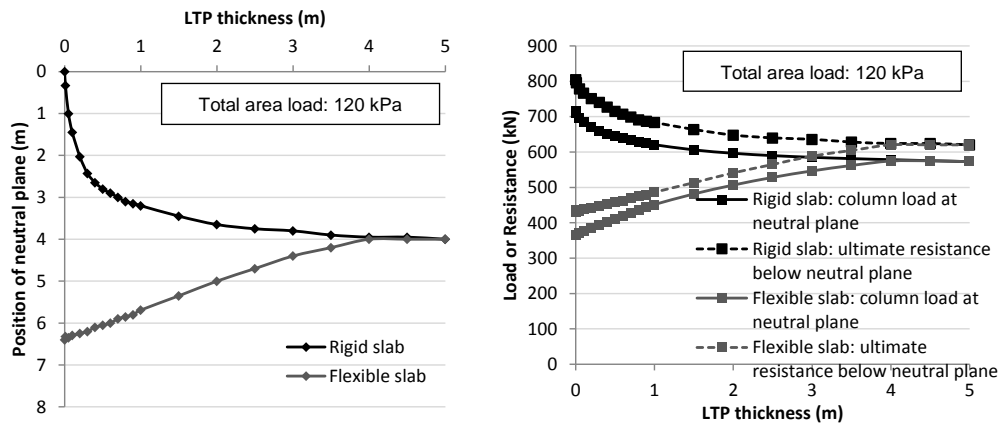


Fig. 5.20 Neutral plane variations vs. LTP thickness based on ASIRI reference case with Frank and Zhao load transfer curves (infinite grid, rigid and flexible loading)

In the flexible case, a differential settlement appears and increases if the LTP thickness decreases. The column load share is smaller and the neutral plane is deeper in the flexible case. From a certain value of the LTP (or embankment) thickness, the settlement at the top is uniform and both systems do not differ anymore. Similar findings have been made by Höppner (2011, Fig. 2.34). This LTP thickness is equal to 4 m in the present case for a column spacing of 2.5 m, whereas Höppner finds a limit thickness equal to the column spacing in a different example. The limit thickness depends highly on the soil and column parameters as well as on the selected load level which determines the ultimate skin friction value in the LTP.

High stresses appear in the rigid slab for low LTP thickness values and for the CPRF case in order to withstand the differential settlement which would appear in the flexible case. The moments in the rigid slab are estimated as described in section 5.1.2, with a Poisson's ratio equal to 0.2 in the slab and a diffusion slope equal to 0.4 (Fig. 5.21). The effects in the slab become smaller if the LTP thickness increases. The extreme case of a pile foundation would lead to even larger moments. For a LTP thickness larger than 3 to 4 m, the moment becomes negligible, reflecting the absence of differential settlements at the top above the critical LTP thickness.

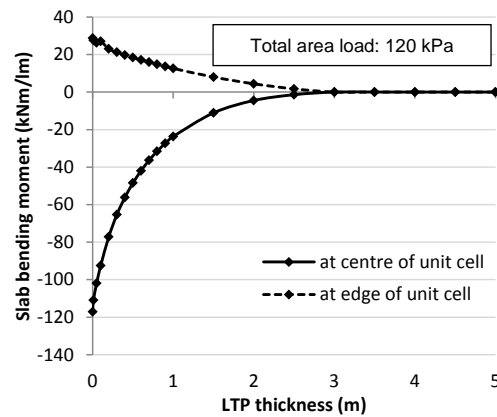


Fig. 5.21 Bending moment at the edge and at the centre of the unit cell based on ASIRI reference case with Frank and Zhao load transfer curves (infinite grid, rigid loading)

5.2.2 Single footing system

5.2.2.1 Reference CPRF case with measurements

The reference case for the combined foundation system with single footing is the CPRF full-scale field test at Merville, France presented by Borel (2001). The system is made of a circular footing with a radius of 1 m and an embedment of 0.80 m and only one open-ended driven hexagonal box sheet pile formed by two U sections with a length of 12.17 m under the footing base level, a perimeter of 1.64 m and a section area of 0.166 m² in a silty and clayey soil (Fig. 5.22). The ground water level is located at 1.5 m to 1.9 m depth under ground level. The load-settlement curve of the whole CPRF, the load in the soil under the footing and the load in the pile have been measured.

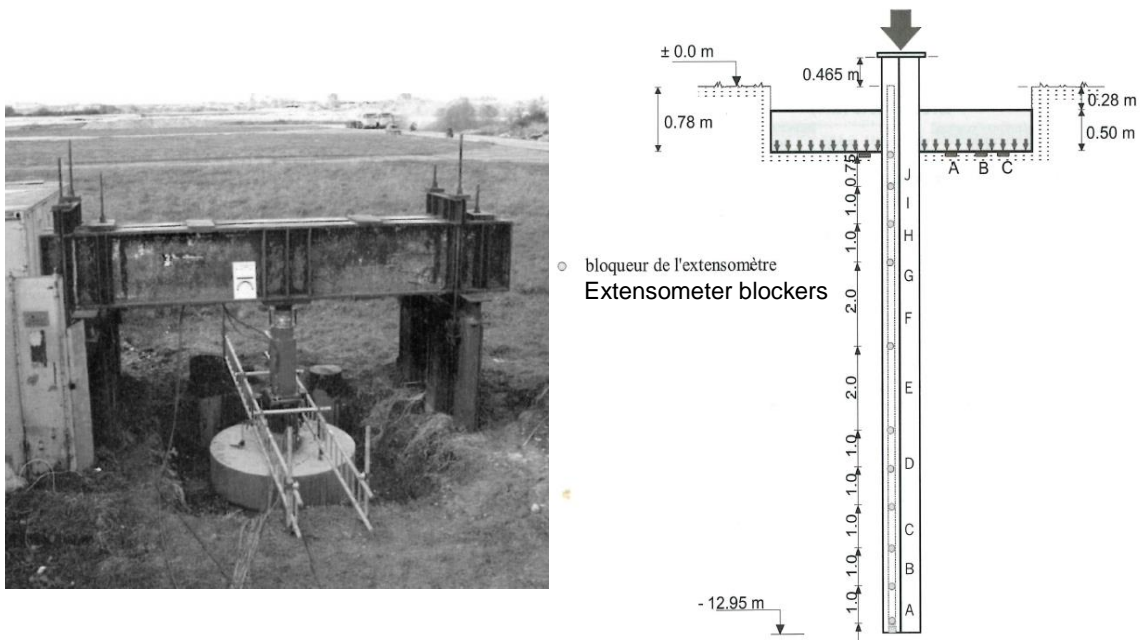


Fig. 5.22 Test site picture and cross section of monitored CPRF field test in Merville (Borel 2001)

Borel modelled the system using the software FONMIX developed by Combarieu (1988a). This method corresponds to the principle of the method MV2 described in ASIRI (IREX 2012) and in section 2.5.2.2, for the special case without LTP. The load-settlement behaviour of the footing has been modelled with the non-linear logarithmic pressuremeter method proposed by Combarieu (1988a, see Fig. 3.3 section 3.2). The load transfer curves used are the ones of Frank and Zhao. The footing ultimate load has been estimated equal to 1033 kN. The skin friction and tip resistance values have been taken from a static load test conducted on the single open-ended sheet pile (with 50 kPa skin friction from 6 m down to 10 m under the footing, 70 kPa below 10 m and 2200 kPa tip resistance). The confining effect of the footing on the pile skin friction in the CPRF has been ignored. The soil layers have been discretized in layers of thickness equal to one radius of the footing (1 m) and values of the pressuremeter modulus is given for each of them. The pile Young's modulus considered is equal to 21 GPa.

All parameters from the FONMIX calculation are kept for the LTM calculation proposed here. The only differences in the calculations here are the modelling of the footing as an equivalent square footing and a hyperbolic non-linear footing load-settlement behaviour (instead of a logarithmic one). All parameters used for the LTM calculation with the pressuremeter method are summarized in Table 5.3.

Table 5.3 LTM parameters for CPRF with rigid footing field test in Merville after FONMIX calculation by Borel (2001)

Tip resistance ult.	:	2200 [kPa]
Foundation length	:	1,77 [m]
Foundation width	:	1,77 [m]
Foundation embedment	:	0,78 [m]
Number of columns	:	1 [-]
Calculation footing	:	non-linear
Bearing capacity footing	:	1033 [kN]
Alpha coefficient (1st layer)	:	0,67 [-]
Soil properties		
Top Type	Pressure	modulus Friction ult. γ eff. soil Fine soil
[m]	[kPa]	[kPa] [kN/m ³]
0,00 Silt	5960	0 20 x
1,78 Clay	7880	0 10 x
2,78 Clay	9800	0 10 x
3,78 Clay	11720	0 10 x
4,78 Clay	13640	0 10 x
5,78 Clay	15560	50 10 x
6,78 Clay	17480	50 10 x
7,78 Clay	19400	50 10 x
8,78 Clay	21320	50 10 x
9,78 Clay	23240	70 10 x
10,78 Clay	25160	70 10 x
11,78 Clay	27080	70 10 x
12,78 Clay	28000	70 10 x
Column properties		
Top Type	Section perimeter	γ column Add. resistance for Column E No. of subdivisions
[m]	[m] [m ²]	[kN/m ³] [kPa] [kPa] [-]
0,00 Silt	1,64 0,17	23 0 21000000 100
1,78 Clay	1,64 0,17	23 0 21000000 100
2,78 Clay	1,64 0,17	23 0 21000000 100
3,78 Clay	1,64 0,17	23 0 21000000 100
4,78 Clay	1,64 0,17	23 0 21000000 100
5,78 Clay	1,64 0,17	23 0 21000000 100
6,78 Clay	1,64 0,17	23 0 21000000 100
7,78 Clay	1,64 0,17	23 0 21000000 100
8,78 Clay	1,64 0,17	23 0 21000000 100
9,78 Clay	1,64 0,17	23 0 21000000 100
10,78 Clay	1,64 0,17	23 0 21000000 100
11,78 Clay	1,64 0,17	23 0 21000000 100
12,78 Clay	1,64 0,17	23 0 21000000 100
Column toe:	12,95 m	

The results of the FONMIX calculation and the measurements for different load levels are compared with the results of the present LTM calculation in the following section.

5.2.2.2 Variation of load

In the LTM footing calculation with the pressuremeter method, the depth of the settlement profile in the soil and thus the critical depth for the calculation of the system is independent from the load level and fixed at 8 times the footing width for usual service loads (see Fig. 5.3 in section 5.1.3). In the present case, the critical depth is approximately equal to the column tip depth, so that no additional soil settlement occurs below the pile tip.

The results in terms of load-settlement curve and pile load share with the load applied from Borel (2001) and from the LTM calculation with the Frank and Zhao curves, with

the cubic root curves and with the hyperbolic curves (with the proposed mean fixed stiffness parameters) are compared to the measurements in Fig. 5.23 and Fig. 5.24.

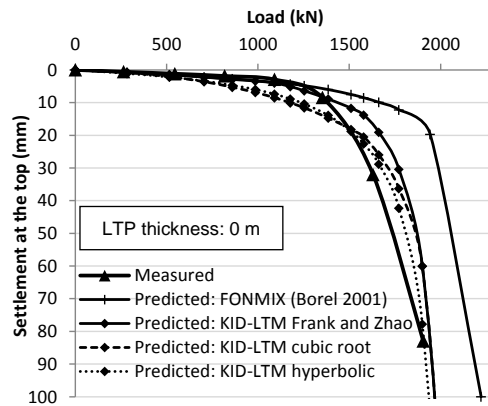


Fig. 5.23 Settlement with load in CPRF field test from Borel (2001): measurements and predictions with FONMIX and with proposed LTM calculation

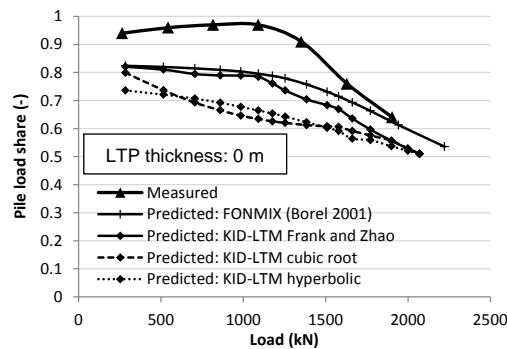


Fig. 5.24 Pile load share with load in CPRF field test from Borel (2001): measurements and predictions with FONMIX and with proposed LTM calculation

As an example, the detailed LTM results for the intermediate load level applied of 1091 kN are shown in Fig. 5.25. Under this reference load, the ultimate resistance of the pile is almost completely mobilised. Above this load, the slope of the load-settlement curve gets sharper due to the fact that the additional load is taken by the soil under the footing.

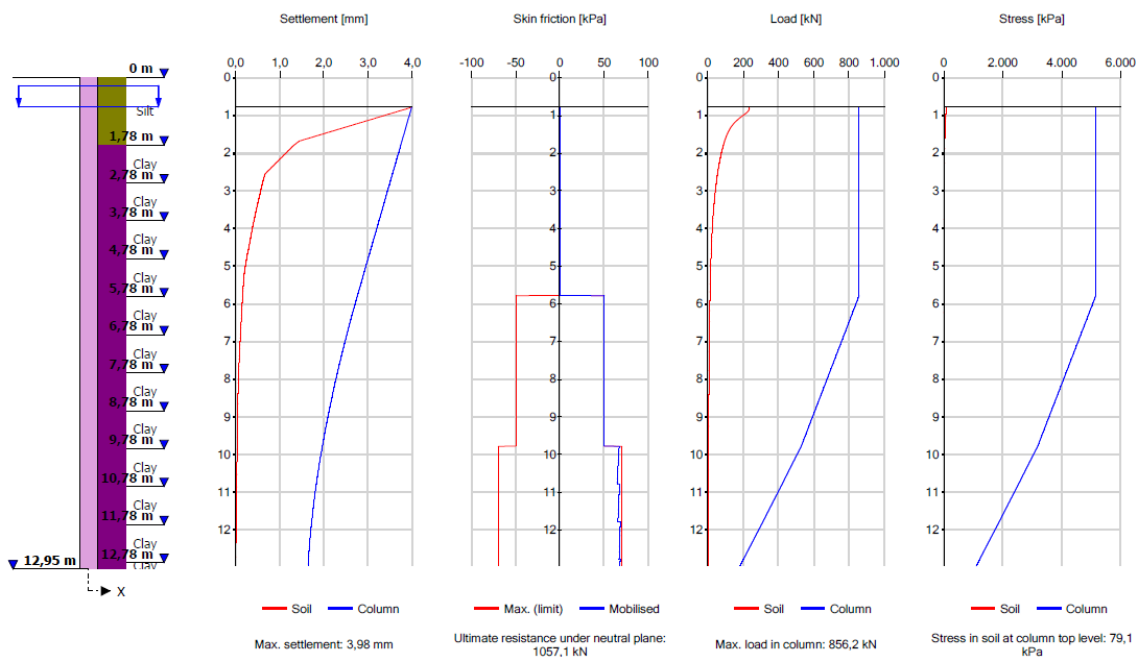


Fig. 5.25 Results of LTM calculation of CPRF with rigid footing field test from Borel (2001) with Frank and Zhao load transfer curves for intermediate load level of 1091 kN

The load-settlement curve is very well predicted up to 1300 kN by the FONMIX and by the LTM calculations with the Frank and Zhao curves. Above this load level, the predictions are stiffer than the measurements, in particular for the FONMIX solution in which the more “abrupt” exponential load transfer curve for the footing is implemented (section 3.2). The modelling with the proposed cubic root and hyperbolic curves shows a good overall agreement, even if the initial stiffness is underestimated. All predictions underestimate the pile load share in particular for small loads, but the FONMIX and LTM models using the Frank & Zhao curves are closer to the reality.

The load-settlement behaviours of the column in the CPRF, of the soil in the CPRF and of the whole CPRF system are represented together with the load-settlement behaviour of the single column in Fig. 5.26. In this particular case with no skin friction in the upper layers, the column in the CPRF behaves like the single column. The bearing capacity of the single column is smaller than the one of the whole CPRF system. For the reference load of 1091 kN for example, the settlement of the single column would be theoretically infinite, whereas the settlement of the CPRF is only around 4 mm.

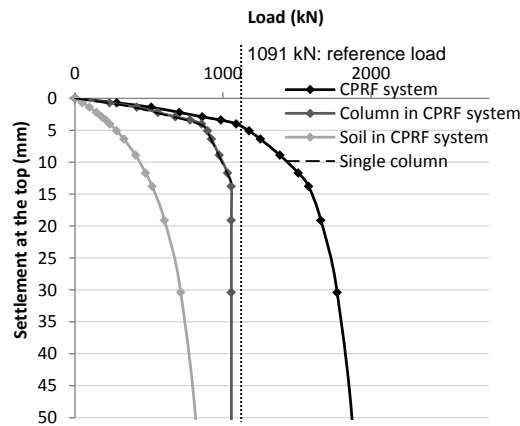


Fig. 5.26 Load-settlement behaviour based on Borel (2001) reference case: with Frank and Zhao load transfer curves compared to single column case

5.2.2.3 Variation of LTP thickness

The study of the variation of the LTP thickness with a footing highlights at the same time the transfer mechanisms involved in the LTP in RI systems on footings and the transition with the CPRF case (which corresponds to a thickness equal to zero). The total load level is kept constant; the LTP is not considered as additional load since it replaces existing soil in general in the case of footings. The constant load level is chosen equal to 1091 kN (intermediate load level in the reference case). The ultimate skin friction in the LTP is determined as the vertical stress in the middle of the layer multiplied by $K \cdot \tan(\varphi) = 1$ (section 2.5.2). The LTP thickness is varied in a realistic range for footings of 0 to 1 m. For the Young's modulus and for the PMT modulus of the LTP, realistic values are chosen: 60 MPa and 20 MPa, respectively. All following calculations are made with the Frank and Zhao load transfer curves in order to take advantage of the PMT test results available. For the selected load level, it is checked that the stress in the LTP is allowable (see Fig. 2.41 in section 2.5.2.2).

The evolution with the LTP thickness of the settlement, of the column load share, of the level of the neutral plane and of the resistance under the neutral plane is presented in Fig. 5.27, Fig. 5.28 and Fig. 5.29. The settlement at the top of the system results from both the load applied at the top and the dead weight of the LTP.

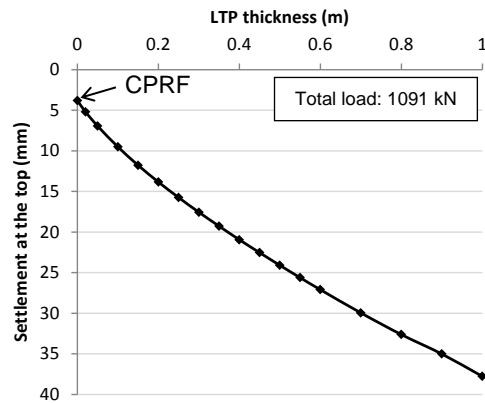


Fig. 5.27 Settlement at the top vs. LTP thickness based on Borel (2001) reference case with Frank and Zhao load transfer curves (rigid footing)

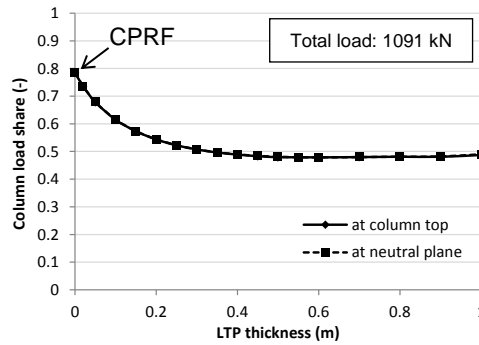


Fig. 5.28 Column load share vs. LTP thickness based on Borel (2001) reference case with Frank and Zhao load transfer curves (rigid footing)

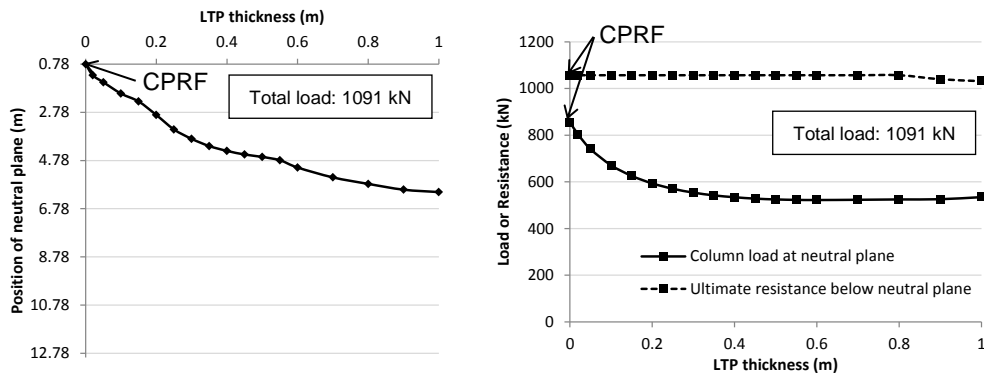


Fig. 5.29 Neutral plane variations vs. LTP thickness based on Borel (2001) reference case with Frank and Zhao load transfer curves (rigid footing)

The settlement increases sharply with the LTP thickness of the footing, whereas the column load share decreases and remains nearly constant after a thickness of 0.4 m. After 0.4 m, the column maximum load is roughly equal to half of the resistance below the neutral plane; this would allow a design in domain 1 according to ASIRI (IREX 2012). The CPRF case is characterized by a maximum column load share and a neutral plane located at the top of the system. In this particular case with no skin friction above a level around 6 m, the resistance under the neutral plane is almost not varying and the load at the column top is equal to the load at the neutral plane.

5.2.3 High-rise building example

5.2.3.1 Reference case with measurements

The CPRF technique has been extensively used and monitored for very challenging high-rise buildings in Frankfurt, Germany in the overconsolidated Frankfurt clay (Lutz 2002, Reul 2000, Richter and Lutz 2010). One example is treated here, in order to highlight the CPRF mechanisms in such exceptional structures with high loads. The possibility of a transition to a RI system is examined in a purely theoretical way. Such very complex cases would call for detailed continuum analyses in practice, considering horizontal loads, edge effects and necessary constructive measures.

Outside of France, pressuremeter testing is not of common practice for the estimation of the soil modulus and a fortiori of load transfer curves. The parametric study based on this typical high-rise building example is thus treated in the present work as if no pressuremeter tests were available for the definition of the load transfer curves. However, in the Frankfurt region, pressuremeter tests with unloading and reloading have been exceptionally carried out, in particular in order to estimate the relation between the soil stiffness under first loading and reloading (Mader 1989, Wind 1992a, Wind 1992b). The use of the pressuremeter test for this purpose is not of common practice; only first steps in this direction have been done by Combarieu and Canépa (2001). The reloading stiffness is particularly interesting considering the generally large embedment of high-rise buildings in the Frankfurt soil. The first loading and reloading pressuremeter moduli seem to be considered by Reul directly equal to the oedometer moduli (Fig. 5.30). This simplification seems justified for overconsolidated clays since according to NF P94-261 (2013), a value of α equal to 1 is considered for the correlation between pressuremeter and oedometer-type modulus for such soil types ((Eq. C.10) in Appendix C.3).

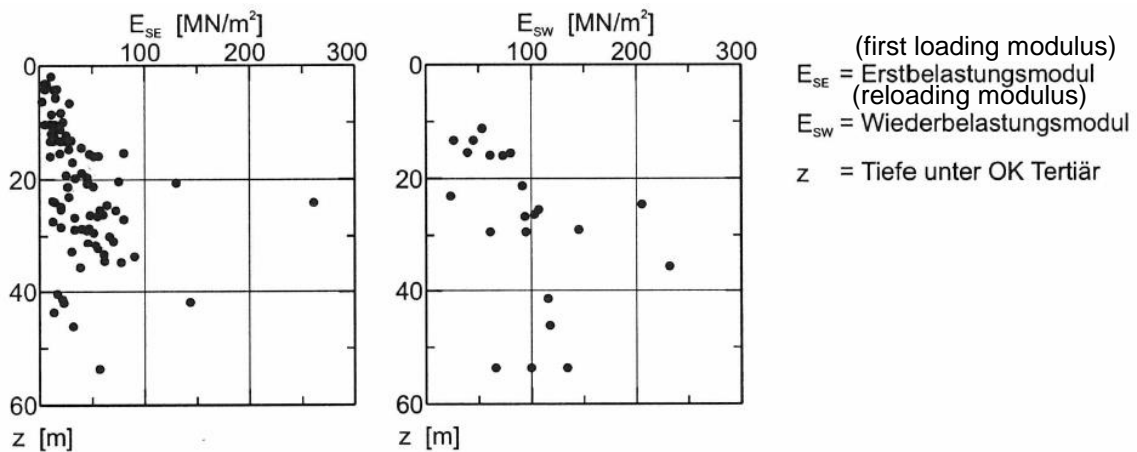


Fig. 5.30 Distribution of the soil modulus of oedometer type of the Frankfurt clay evaluated from pressuremeter tests along the depth z (Reul 2000)

For his FEM calculations of high-rise buildings in the Frankfurt clay, Reul (2000) chose to consider a simplified profile of Young's modulus based on back-calculations in the Frankfurt clay and on the reloading pressuremeter modulus (Fig. 5.31).

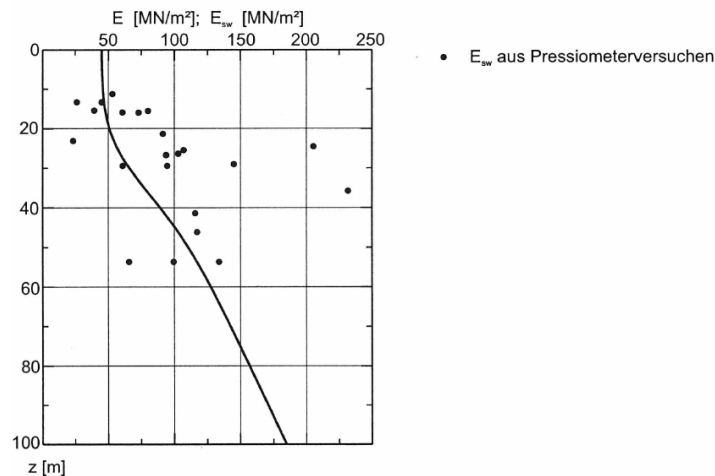


Fig. 5.31 Simplified distribution of Young's modulus compared to pressuremeter reloading modulus (Reul 2000)

The example treated is the skyscraper Westend 1 in Frankfurt of more than 200 m height, which presents the advantage of having a relatively simple foundation geometry (Reul 2000). The 3 m to 4.65 m thick rectangular slab of dimensions 64.4 m \times 47.3 m is founded on 40 piles of diameter 1.3 m and a unique length of 30 m, regularly distributed over the slab area. Since the pile spacing is equal on average to 5 to 6 times the pile diameter, group effects on the settlements are not considered. The system is presented in

vertical cross section and in plan view with the monitoring system in Fig. 5.32. The incompressible Frankfurt chalk layer begins at a depth of 68 m. The total load from the structure is 956.9 MN (314.1 kPa). The ground water is located near the surface.

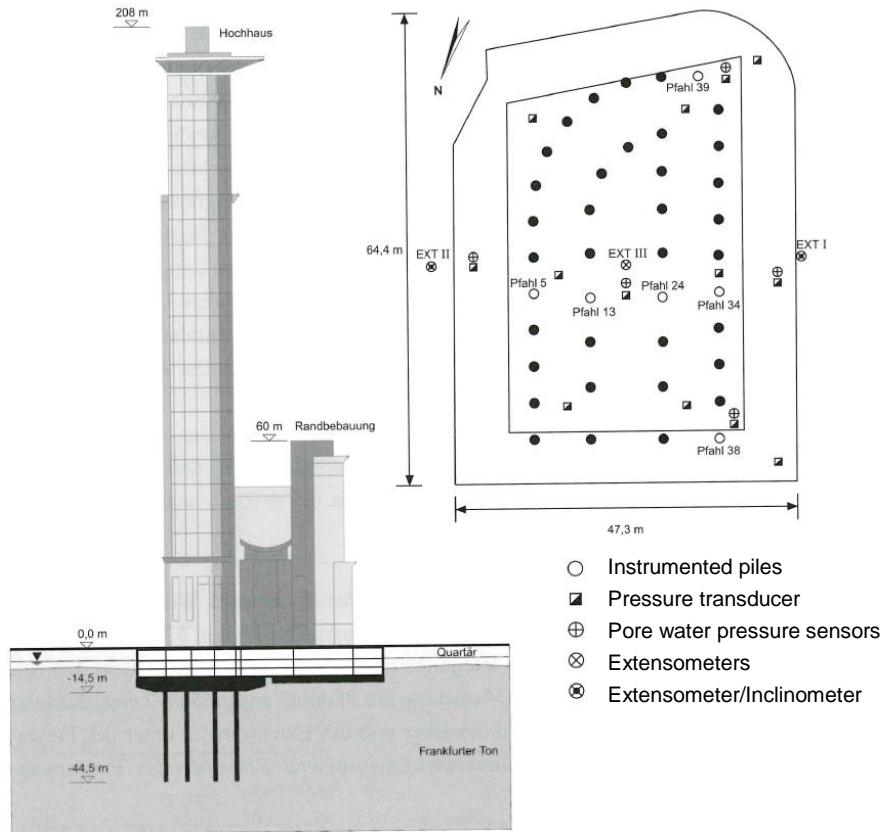


Fig. 5.32 Vertical cross section and plan view of monitored CPRF foundation of high-rise building Westend 1 in Frankfurt (Reul 2000)

The central pile with surrounding soil can be modelled as a unit cell in an infinite grid (ratio between pile length and slab width equal to 0.63). Furthermore, the measurements show that the behaviour of the piles at different positions of the slab have a similar behaviour with similar loads in the piles (Fig. 5.33). This leads to the conclusion that the global system can be modelled quite well with the assumption of an infinite grid under a rigid slab, at least down to the pile tip level.

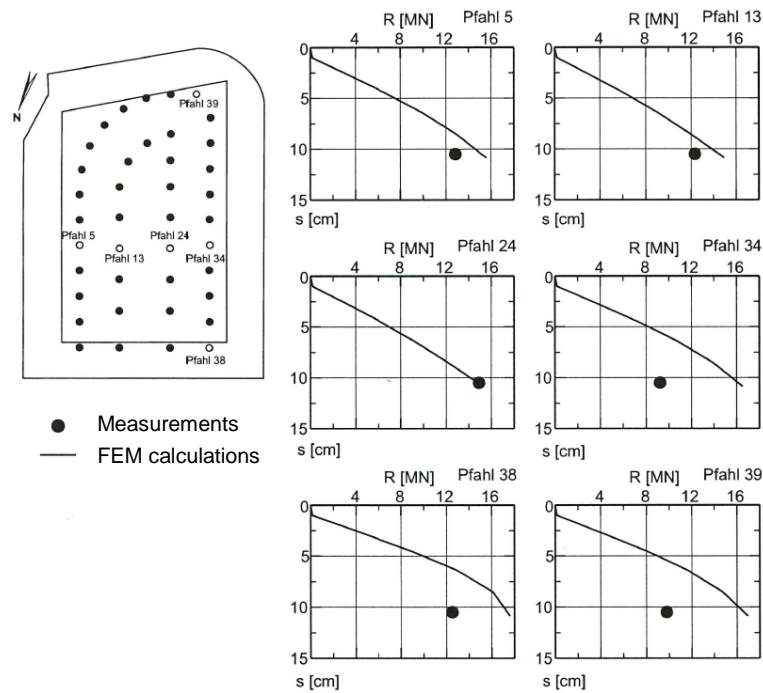


Fig. 5.33 Pile load vs. settlement for different pile locations for CPRF Westend 1 (Reul 2000)

The additional settlement under the pile tips cannot be calculated without load diffusion in this case. The depth of the stiff chalk layer (68 m meaning 23.5 m from the pile tip) is namely not small compared to the foundation width. Thus the additional settlement is calculated here as described in 5.1.2, using the calculated stress in the soil at the top of the system in the LTM model and considering load diffusion down to 68 m.

The choice is made here to determine the soil modulus of oedometer type from the first loading pressuremeter moduli (Fig. 5.30) as in the pressuremeter theory, considering $\alpha = 1$ (see Appendix C.3). This gives a oedometer modulus of 65 MPa over the pile length (14.5 m to 44.5 m depth) and of 50 MPa between the pile tip level and the stiff chalk layer (44.5 m to 68 m depth). Considering existing experience in Frankfurt clay and measurements on instrumented piles at different sites in the same soil and at similar depths, an average ultimate skin friction of 85 kPa and an ultimate tip resistance of 1500 kPa can be assumed for this foundation. The Young's modulus of the pile is taken equal to 22 GPa as in the FEM calculation of Reul (2000). All parameters used in the LTM calculation with the rigid slab option are summarized in Table 5.4.

Table 5.4 LTM parameters for CPRF Westend 1 as infinite rigid slab

Load	:	314,1 [kPa]				
Tip resistance ult.	:	1500 [kPa]				
No. of layers considered as load	:	0 [-]				
Unit cell area	:	76,1 [m ²]				
Soil properties						
Top Type		Eoed modulus	Friction ult.	γ eff. soil		
[m]		[kPa]	[kPa]	[kN/m ³]		
14,50 Frankfurt clay		65000	85	10		
Column properties						
Top Type		Column diameter	γ column	Add. resistance for diameter variation (also virtual)	Column E	No. of subdivisions
[m]		[m]	[kN/m ³]	[kPa]	[kPa]	[-]
14,50 Frankfurt clay		1,3	23	0	22000000	1000
Foundation level:	14,5 m					
Column toe:	44,5 m					

The calculations are made with both cubic root and hyperbolic load transfer curves with the proposed mean fixed parameters (Fig. 5.34 and Fig. 5.35). For comparison purposes in the reference case, the calculation is made with the Frank and Zhao curves as well, with a pressuremeter modulus of 65 MPa over the pile length and 50 MPa at the pile tip (Fig. 5.36). Under the applied load, the pile resistance is already almost completely mobilised. This is typical for a CPRF, for which the safety concept is based on the stability of the global system and not on the bearing capacity of the single piles (see section 2.4). For the applied load, the critical depth is located at a depth of 56 m, for a soil stress at the top of approximately 170 kPa and a soil stress at 56 m of approximately 110 kPa. The resulting additional soil settlement below the pile tip level is equal to 35 mm. The results of all 3 load transfer curve approaches are very similar.

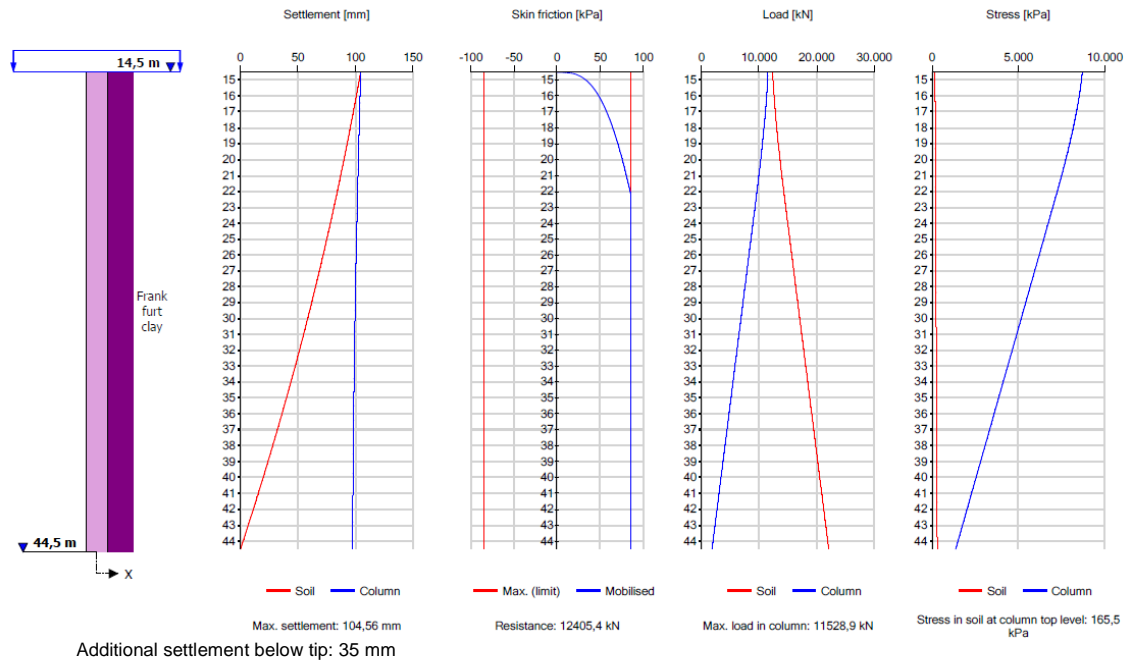


Fig. 5.34 Results of LTM calculation of CPRF Westend 1 as infinite grid system with a rigid slab with cubic root load transfer curves

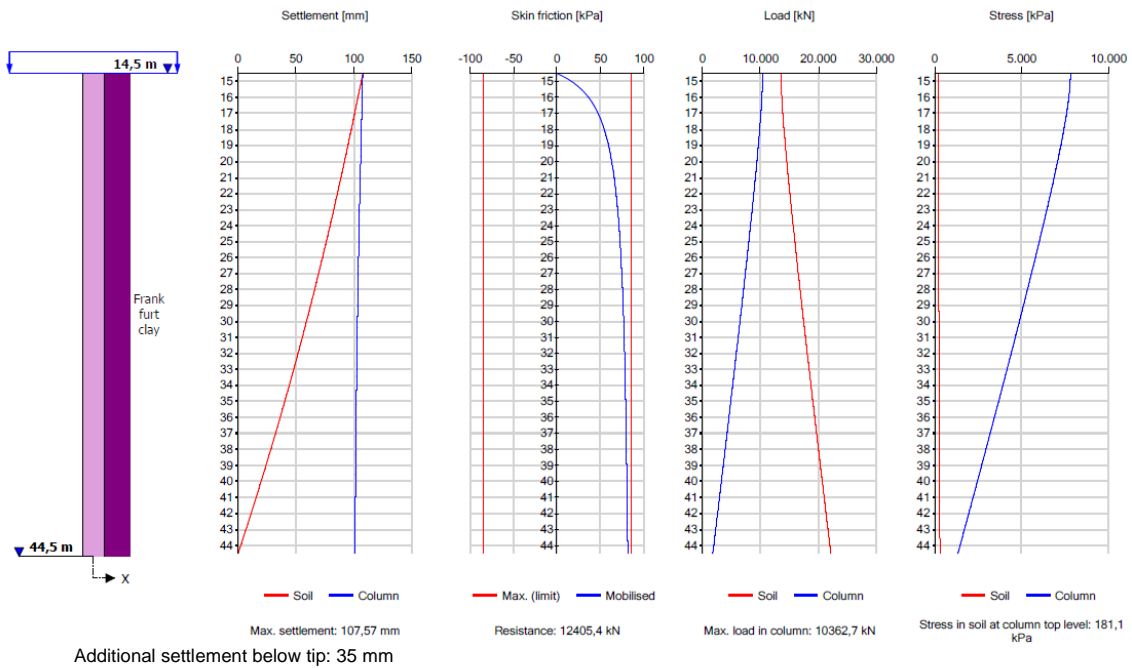


Fig. 5.35 Results of LTM calculation of CPRF Westend 1 as infinite grid system with a rigid slab with hyperbolic load transfer curves

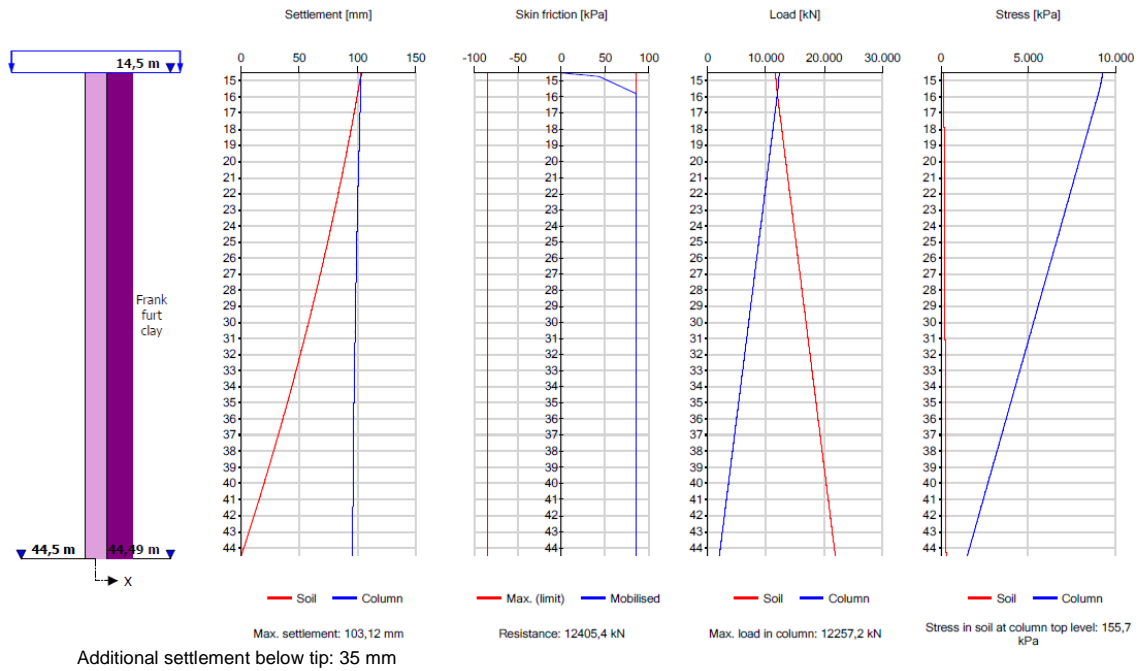


Fig. 5.36 Results of LTM calculation of CPRF Westend 1 as infinite grid system with a rigid slab with Frank and Zhao load transfer curves

Reul (2000) reports a measured settlement of 12 cm and a measured pile-raft coefficient (load share in the pile) of 0.5 from the pile loads in Fig. 5.33. The settlement share of the soil under the pile tip level is between 30 and 50 % of the settlement at middle of the footing (Fig. 5.37). This denotes the typical transfer of the load to larger depths through the piles for floating foundations. An important settlement part remains under the pile level, but this settlement is limited by the smaller remaining depth down to the stiff chalk layer.

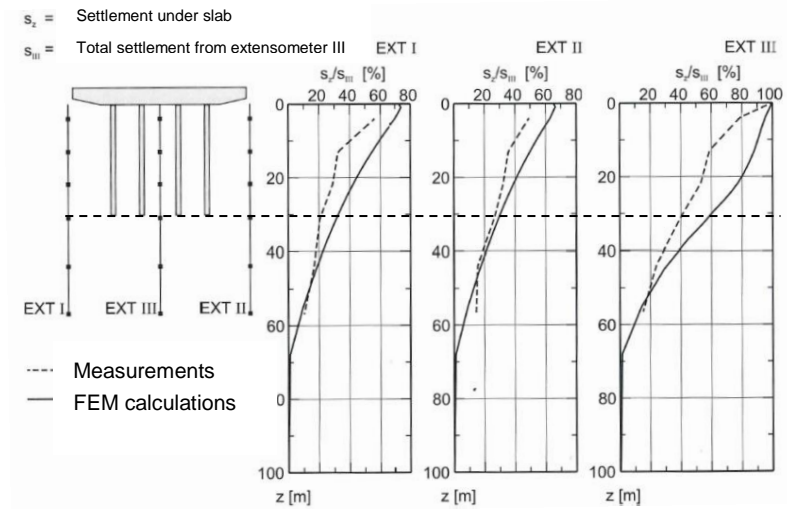


Fig. 5.37 Measured settlement distribution along the depth of CPRF Westend 1 (Reul 2000)

Table 5.5 presents the values of the predicted pile load share, of the total settlement and of the settlement share under the pile tip in comparison with the measurements. The LTM calculations made with the cubic root and hyperbolic curves overestimate slightly the settlements and underestimate slightly the soil settlement share below the pile tip.

Table 5.5 Comparison of measurements with predictions for the CPRF Westend 1

	Measurement (Reul 2000)	LTM calculation Cubic root curves	LTM calculation Hyperbolic curves	LTM calculation Frank and Zhao curves
Total settlement (mm)	120	140	143	138
Soil settlement share below pile tip (-)	0.3 to 0.5	0.23	0.22	0.25
Pile load share (-)	0.5	0.48	0.43	0.51

5.2.3.2 Variation of load

The previous calculations are repeated for different load levels, always considering the additional settlement under the pile tip down to the critical depth in the same way as previously. The results in terms of load-settlement curve, of settlement share below pile tip and of pile load share are presented in Fig. 5.38, Fig. 5.39 and Fig. 5.40 with both cubic root and hyperbolic curves.

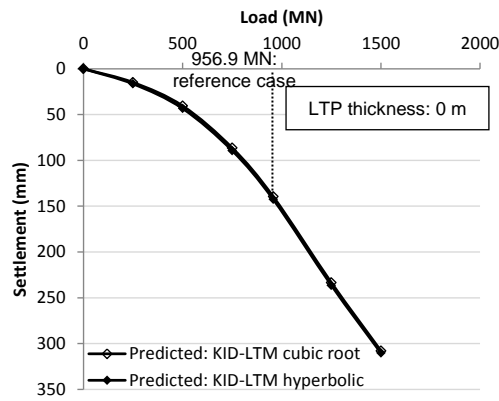


Fig. 5.38 Settlement at the top vs. load based on Westend 1 reference case with cubic root and hyperbolic load transfer curves (infinite grid, rigid loading)

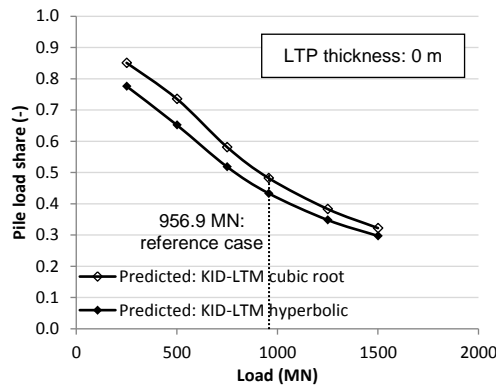


Fig. 5.39 Settlement share below pile tip vs. load based on Westend 1 reference case with cubic root and hyperbolic load transfer curves (infinite grid, rigid loading)

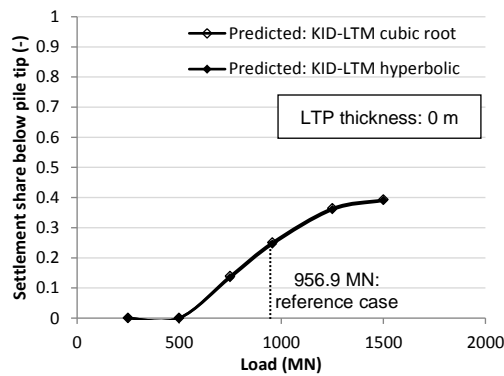


Fig. 5.40 Pile load share vs. load based on Westend 1 reference case with cubic root and hyperbolic load transfer curves (infinite grid, rigid loading)

The cubic root and the hyperbolic load transfer curves give very similar results, except for the pile load share. It is smaller in the hyperbolic case. The pile load share decreases strongly with the load, highlighting the load transfer from the piles to the soil under the slab in the case of larger settlements.

The load-settlement behaviours of the piles in the CPRF, of the soil in the CPRF and of the whole CPRF system are represented in Fig. 5.41, together with the load-settlement behaviour of the single piles (pile foundation), as an example here only with the cubic root load transfer curves. As usual for a CPRF system (see Fig. 2.20 in section 2.4.1), the stiffness of the pile in the system is reduced compared to the single pile. However, the bearing capacity is not increased since the ultimate skin friction is taken here from the single pile case and thus no group effects and confinement effects are represented. For the reference load of 956.9 MN for example, the settlement of the single pile would be theoretically infinite, whereas the settlement of the CPRF would be around 140 mm.

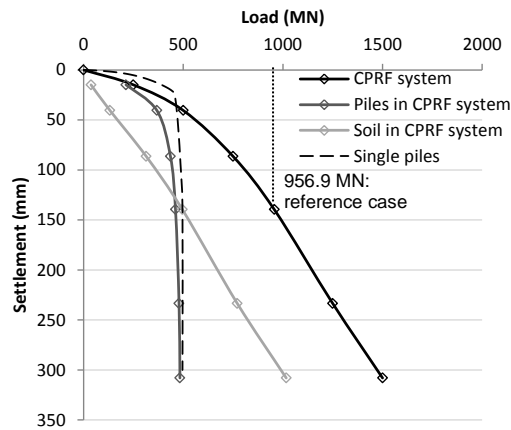


Fig. 5.41 Load-settlement behaviour based on Westend 1 reference case: with cubic root load transfer curves (infinite grid, rigid loading) compared to single column case

5.2.3.3 Variation of LTP thickness

The addition of a LTP in the foundation system of the Westend 1 high-rise building is presented here on a purely theoretical basis in order to represent the advantages of using a LTP in the case of vertical loads. Horizontal loads, effects at the edge of the slab and other particularities or possible constructive measures for high-rise buildings are ignored here. No wide experience, if any, of rigid inclusion systems under high-rise buildings exists in engineering practice at the moment. Even for the large column diameter (much higher than for usual RI systems with 1.3 m), the LTP thickness is kept in the usual range of 0 to 1 m. Higher thickness values could trigger unknown additional effects in the load transfer mechanisms in the LTP under a rigid slab. The total load level is kept equal to the one of the reference case (956.9 MN); the LTP is not considered as an additional load since it replaces existing soil here. The ultimate skin friction in the LTP is determined as the vertical stress in the middle of the layer multiplied by $K \cdot \tan(\phi) = 1$ (section 2.5.2). The LTP is considered to be made of ballast with a Young's modulus and a oedometric modulus of 70 MPa and 100 MPa, respectively (Poisson's ratio between 0.3 and 0.33). For the selected load level, it is checked that the stress in the LTP is allowable (see Fig. 2.41 in section 2.5.2.2). The additional settlement below the column tip level varies with the LTP since the stress in the soil at the top considered in the calculation (see section 5.1.3) gets larger than in the CPRF case.

The influence of the LTP thickness on the settlement, on the column load share, on the position of the neutral plane and on the resistance under the neutral plane is presented in Fig. 5.42, Fig. 5.43 and Fig. 5.44.

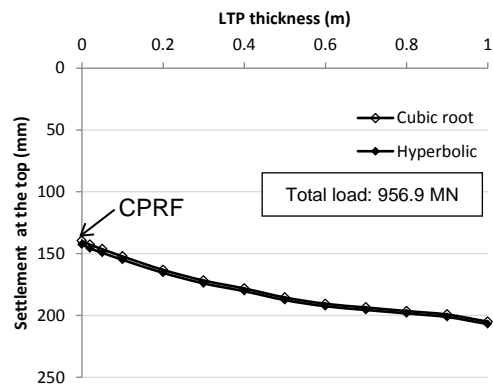


Fig. 5.42 Settlement at the top vs. LTP thickness based on Westend 1 reference case with cubic root and hyperbolic load transfer curves (rigid loading)

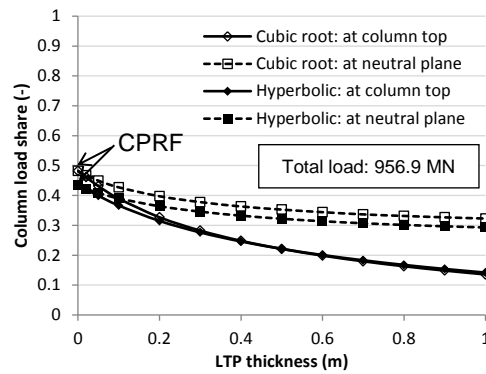


Fig. 5.43 Column load share vs. LTP thickness based on Westend 1 reference case with cubic root and hyperbolic load transfer curves (rigid loading)

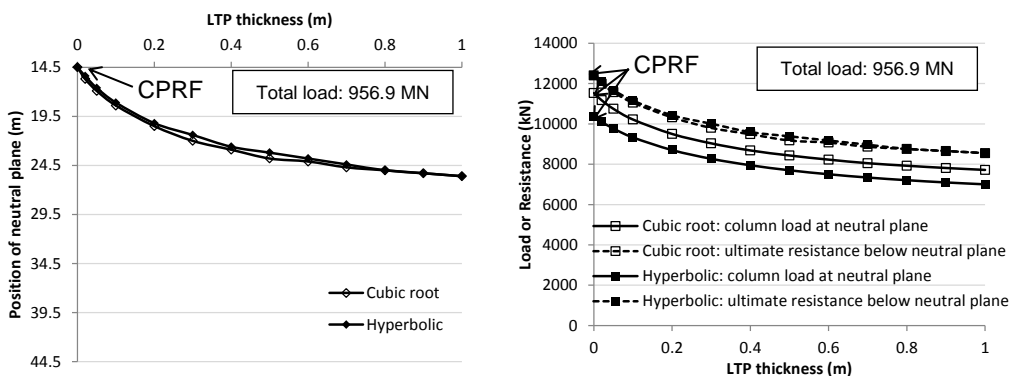


Fig. 5.44 Neutral plane variations vs. LTP thickness based on Westend 1 reference case with cubic root and hyperbolic load transfer curves (rigid loading)

Since the LTP thickness remains small compared to the system depth, the settlement increase with the LTP thickness remains small. The difference between the load at the column top and at the neutral plane is significant in this example. The differences in the column load share at the top between the cubic root and the hyperbolic cases for the CPRF case disappear for a LTP thickness larger than 0.2 m. However, a certain difference remains for the load at the neutral plane level.

The moments in the rigid slab are estimated as described in section 5.1.2, with a Poisson's ratio equal to 0.2 in the slab and a diffusion slope equal to 0.4 (Fig. 5.45) With a LTP thickness of 1 m, a reduction of the maximum load in the column of approximately one third is achieved compared to the CPRF case. At the same time the moments in the slab are reduced with a factor of 3. This allows for a significant optimization of the design of the structural elements, with only a relatively small settlement increase.

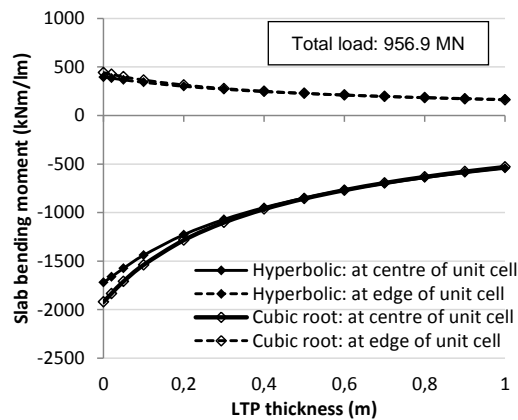


Fig. 5.45 Bending moment at the edge and at the centre of the unit cell based on Westend 1 reference case with cubic root and hyperbolic load transfer curves (rigid loading)

5.3 Comparison of LTM with FEM for theoretical single footing combined system

5.3.1 General modelling aspects

All FEM calculations made for this chapter, with Plaxis 3D 2013.01 (Plaxis 2013), have been performed and analysed jointly with Ackermann (2015b).

introduced under the tip of the columns, and at the top of the columns in the case with a LTP.

The unreinforced column material is defined as follows:

- the elastic-plastic model with Mohr-Coulomb failure criterion is used with a Poisson's ratio $\nu = 0.2$. Since no pore pressures need to be calculated in the concrete, the drainage type is set to non-porous (Plaxis 2014). The column unit weight is 22 kN/m^3 ;
- the oedometric modulus is $E_{\text{oed,column}} = 22200 \text{ MPa}$ (Young's modulus 20000 MPa);
- the friction angle is set to 37° , which is a common value for concrete. The cohesion is determined considering a compressive strength of 10 MPa as shown in Fig. 5.47 and (Eq. 5.3) to (Eq. 5.6) and is thus equal to 2500 kPa ;
- the tensile strength is set to 0.5 MPa (5% of the compressive strength).

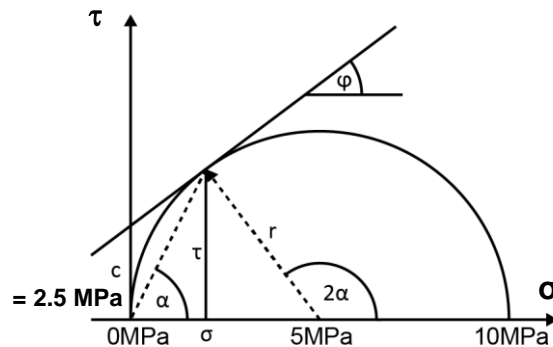


Fig. 5.47 Mohr-Coulomb failure criterion for modelled concrete

$$\alpha = 45^\circ + \frac{\varphi}{2} \quad (\text{Eq. 5.3})$$

$$\tau = r \cdot \sin(90^\circ - \varphi) \quad (\text{Eq. 5.4})$$

$$\sigma = r \cdot (1 - \cos(90^\circ - \varphi)) \quad (\text{Eq. 5.5})$$

$$c = \tau - \sigma \cdot \tan \varphi = \text{approx. } 2.5 \text{ MPa} \quad (\text{Eq. 5.6})$$

The footing material is modelled with the same material as the columns, but the footing unit weight is set to zero; the whole load is chosen to be applied as an external load.

An interface is inserted around the footing as well, with $R_{\text{inter}} = 0.67$ in order to represent the shearing between the soil and the concrete of the footing.

The mesh is generated using the very fine global coarseness (Plaxis 2013). All soil and column parameters which are not equal to the Plaxis default values are given in Fig. 5.48. The m value of 0.7 corresponds to usual values for the Hardening Soil Model for soft fine-grained soils after Benz (2007) and Vogt (2015). All model dimensions, local mesh coarseness values and the resulting mesh for the case without columns, with columns without LTP and with LTP are shown in Fig. 5.48, Fig. 5.49 and Fig. 5.50, respectively. The mesh is not optimized in terms of reduction of the number of elements and thus of the calculation time; the goal in this theoretical example is to model the system as finely as possible. The mesh quality is defined in Plaxis as the ratio between the radiuses of the inner circle and of the outer circle of the mesh element, normalized at 1.0 for the equal sided tetrahedron in the 3D case (Plaxis 2013). Due to the size of the model and the large number of elements, the mesh quality could not be kept close to 1.0 over the whole model; some elements next to the footing, at the side interface between soil and columns or in the soil directly next to the columns have a mesh quality only very locally down to 0.2. This remains still acceptable and the results remain reliable.

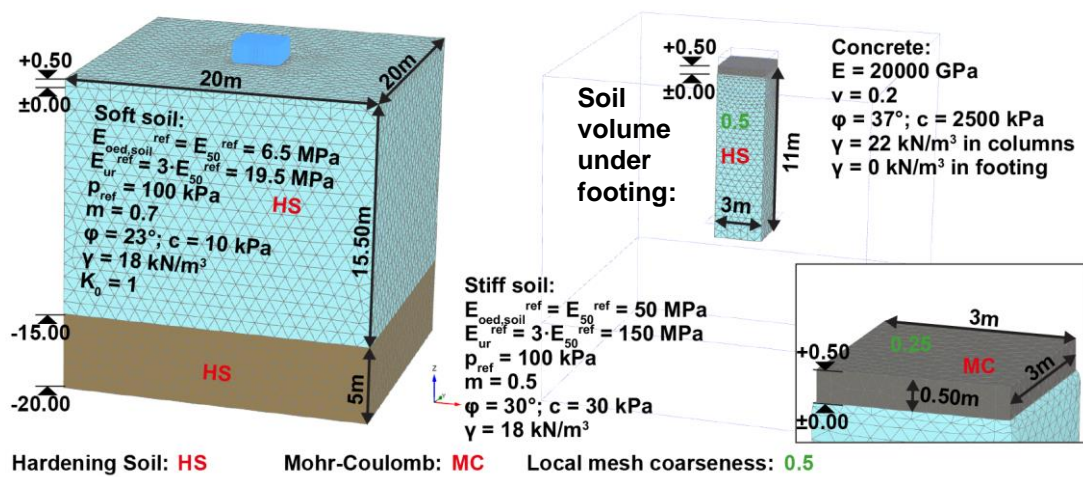


Fig. 5.48 3D FEM model of footing without columns

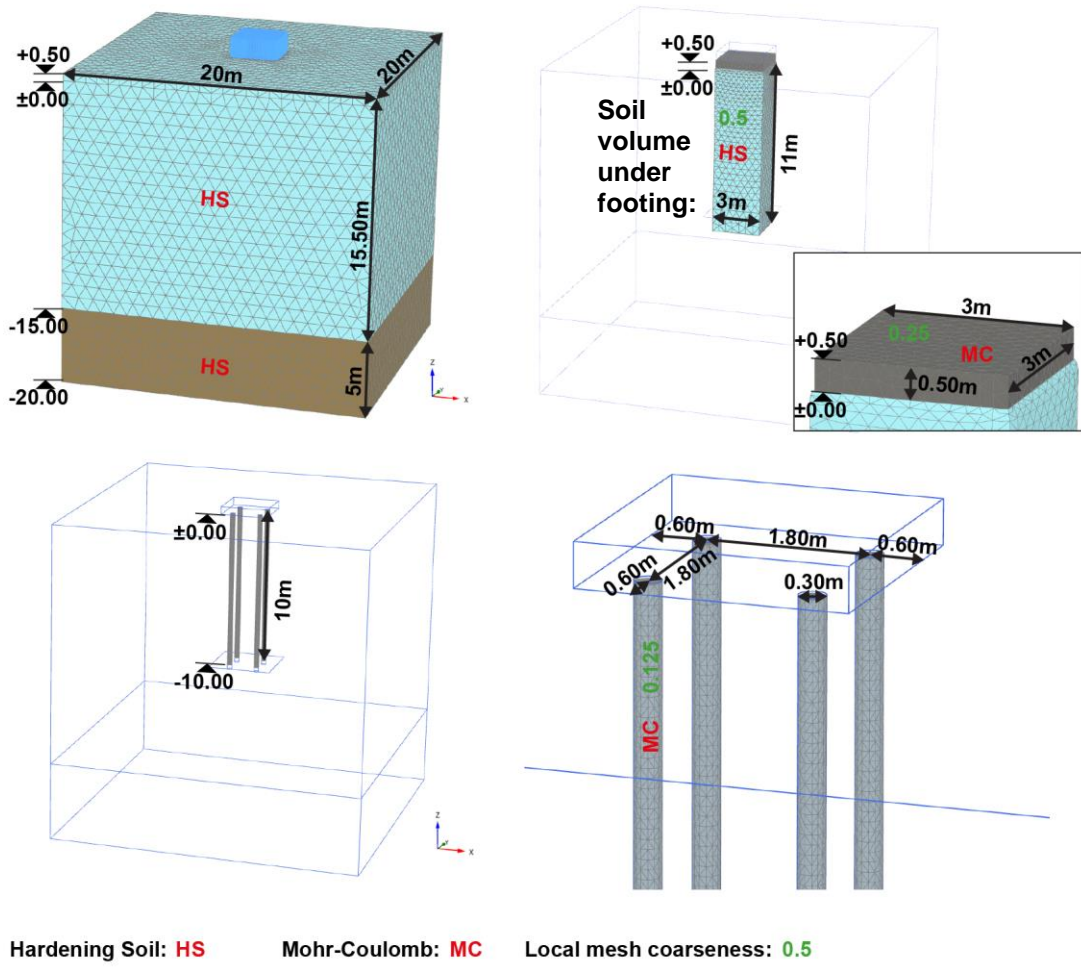


Fig. 5.49 3D FEM model of footing with columns without LTP

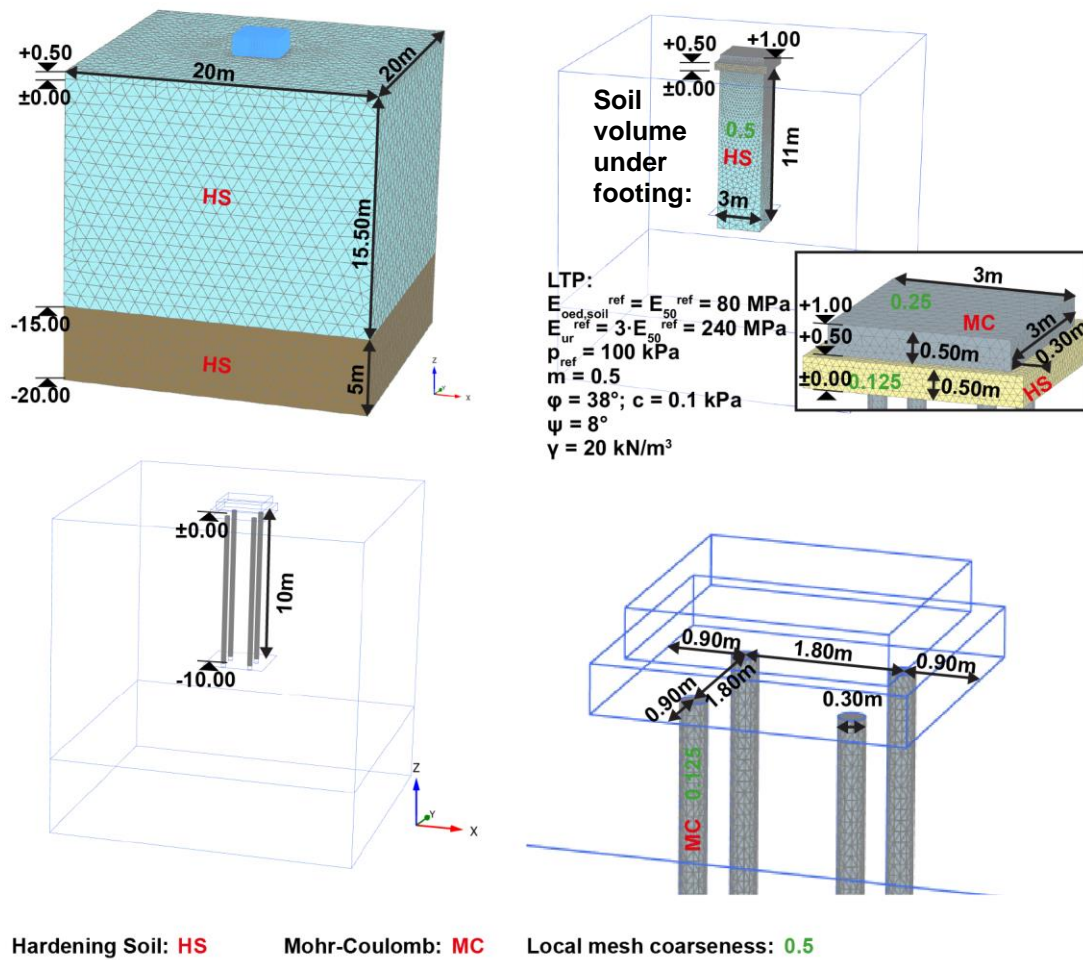


Fig. 5.50 3D FEM model of footing with columns with LTP

The first calculation phase is the initial phase with K_0 procedure and the original soil layers (Plaxis 2013). The second phase is the installation of the columns and of the footing with activation of the concrete material and of all interfaces. After this phase, the displacements are reset to zero. During the last step, the total load is applied. All calculation parameters are kept equal to the default values. For a better accuracy, the updated mesh option is activated for the second and last steps.

The LTM calculations correspond to the method for footings described in section 5.1.3. The cubic root and the hyperbolic load transfer curves with the mean values of parameters for combined systems are considered. The skin friction and the tip resistance used in the LTM analysis are determined as average values in one meter steps from the axisymmetric FEM study of the single column (more details are given in section 6.2 below).

5.3.2 Calibration on case without columns

The load-settlement behaviour of the single footing without columns is investigated with the FEM in comparison to the hyperbolic method proposed in section 3.2 (Fig. 3.6). The hyperbolic method is based here on the oedometer reference settlement calculation for one third of the ultimate footing load. As shown in Fig. 5.51, the footing load-settlement curve with the FEM does not show a typical failure behaviour, even for very large deformations (much higher than the usual reference settlement of 10 % of the footing width, 300 mm). The footing failure load to be used for the LTM is thus estimated with methods based on the shear parameters (c , φ) as approximately 4500 kN. The hyperbolic curve with the reference Hardening Soil oedometer modulus defined as 6500 kPa for a reference horizontal stress of 100 kPa (Fig. 5.48) does not lead to a satisfactory stiffness in the domain of service loads (loads smaller than half of the failure load). This denotes that in the footing influence zone, the stresses are generally smaller than the reference stress of 100 kPa. The modulus used in the LTM is thus back-calculated to reach a good agreement in the domain of service loads. This adjustment leads to a soil modulus of 4300 kPa to be used in the LTM calculations (Fig. 5.51).

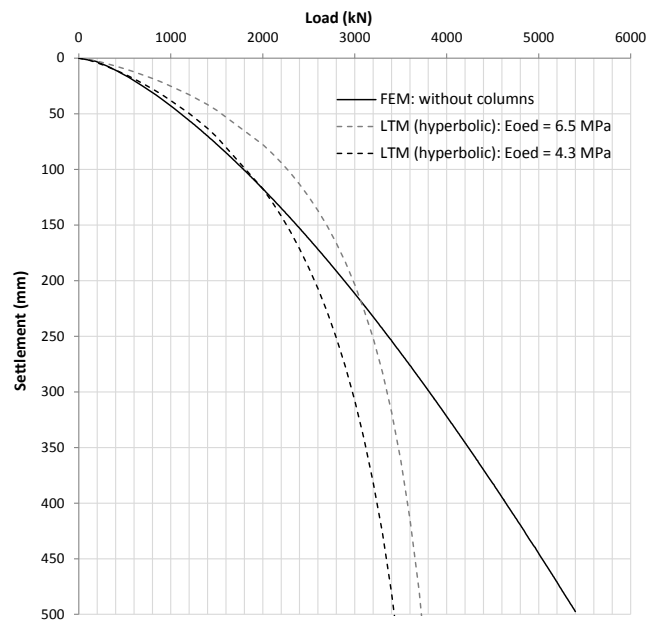


Fig. 5.51 Footing load-settlement curves with 3D FEM and LTM

The load proposed at this stage for the study of the combined CPRF and RI systems is 2000 kN (or 222 kPa, less than one half of 4500 kN), in the service load domain. The combined CPRF or RI system works thus as a settlement reducer and no check of the bearing capacity of the single columns is required (CPRF-guideline design or domain 2 in ASIRI, see section 2.7). The settlement of the system without columns under this load is uniform and equal to approximately 12 cm.

The pressure under the characteristic point directly under the footing is slightly smaller than the average pressure applied on the footing and stress peaks appear at the edge of the footing, as expected for a rigid footing (Fig. 5.52). The elastic stress distribution under a rigid footing is given for example by Vogt (2015). For the selected load level, the FEM and the LTM model show a very good agreement in terms of additional stresses due to the load (total stresses minus initial stresses) and in terms of settlements under the characteristic point of the footing (Fig. 5.53 and Fig. 5.54).

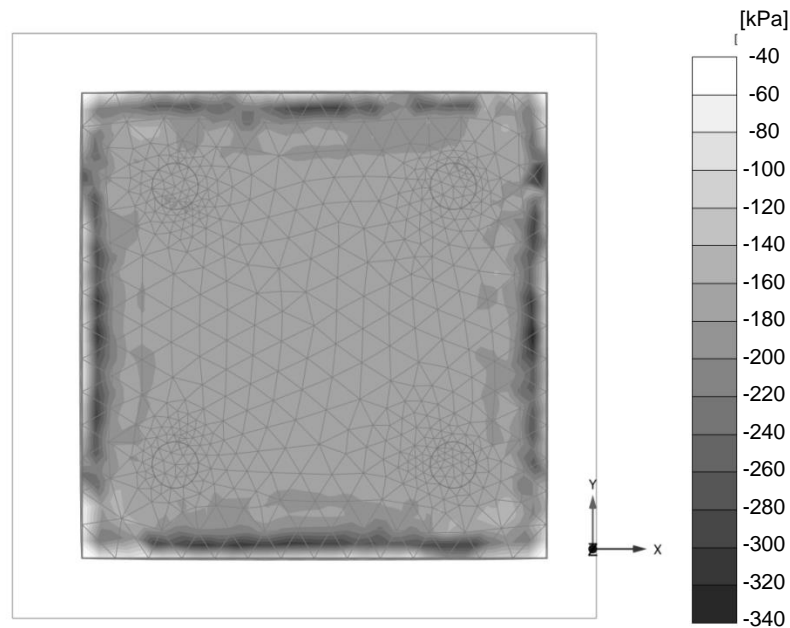


Fig. 5.52 Vertical stresses over bottom surface of the footing with 3D FEM for case without columns

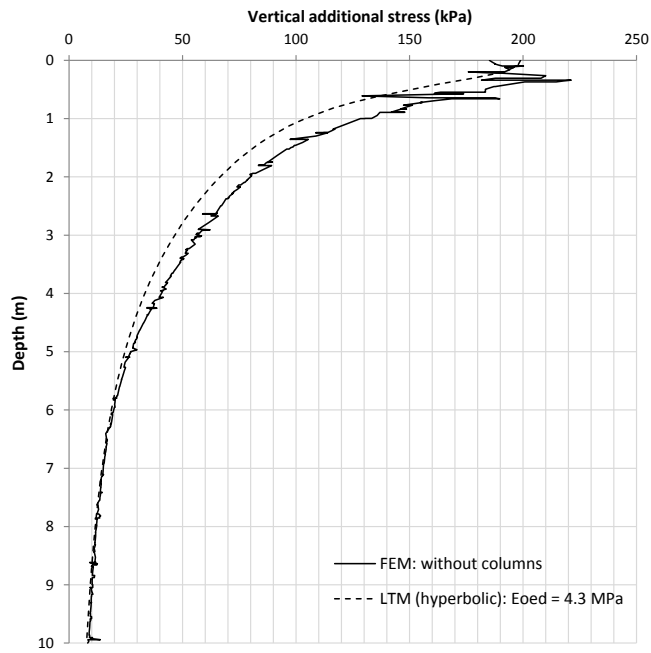


Fig. 5.53 Profiles of vertical stress due to load with 3D FEM and LTM without columns

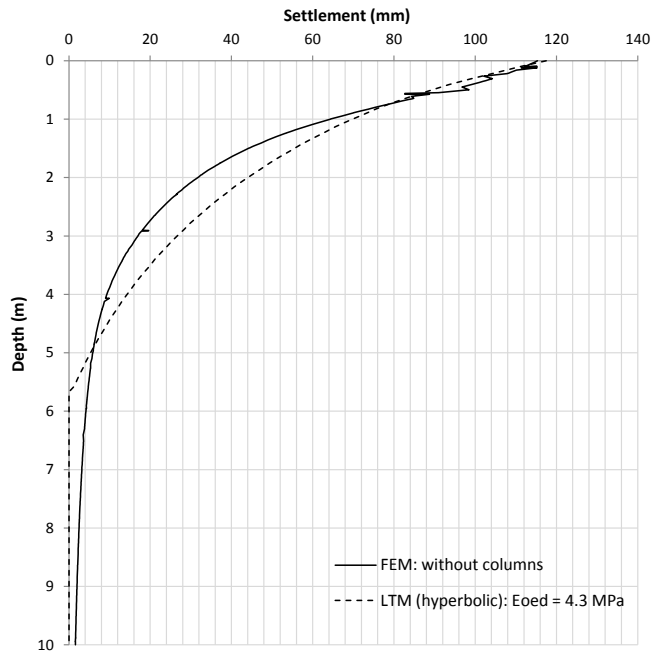


Fig. 5.54 Settlement profiles with 3D FEM and LTM without columns

5.3.3 Comparison in CPRF case

The 3D FEM calculation of the CPRF case allows for a detailed representation of the interactions in the system. The stress distribution in various sections is shown in Fig. 5.55, Fig. 5.56 and Fig. 5.57. As expected, the load is concentrated in the columns. The 3D FEM analysis shows that stress peaks occur at the edge of the columns at the inner side of the footing (Fig. 5.55). However these peaks are very local and the stress remains below or of the order of the compressive strength of the concrete.

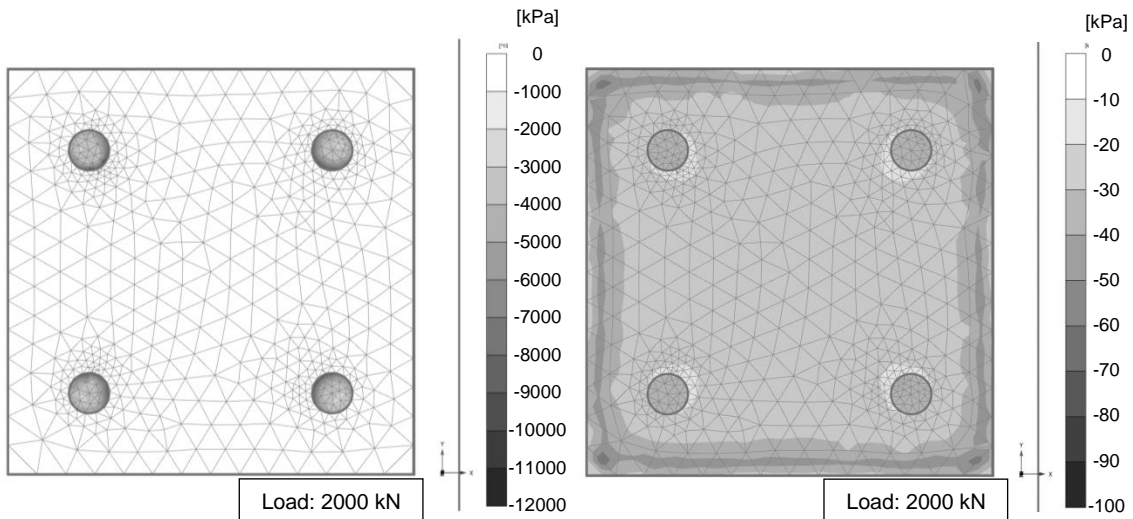


Fig. 5.55 Vertical stresses over bottom surface of the footing with 3D FEM for CPRF case (right: only soil stresses; in Plaxis: compression negative)

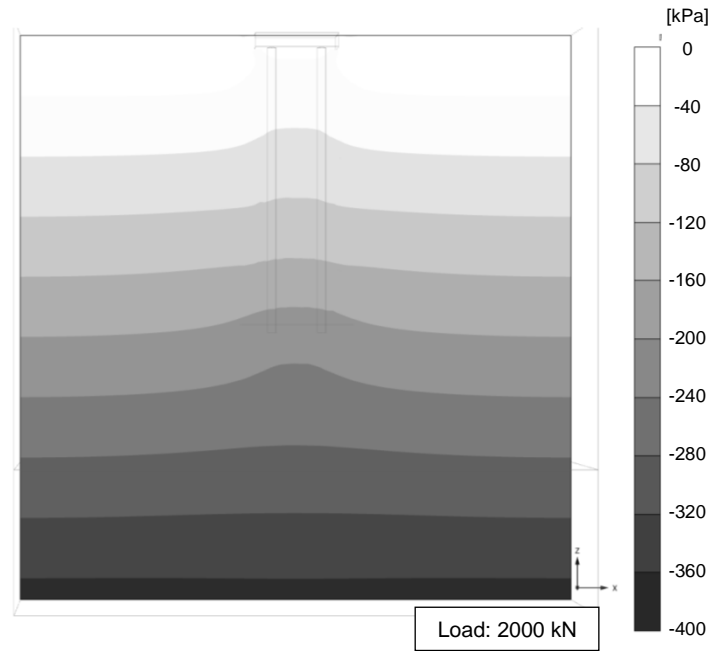


Fig. 5.56 Vertical stresses in section A-A (see Fig. 5.46) with 3D FEM for CPRF case (in Plaxis: compression negative)

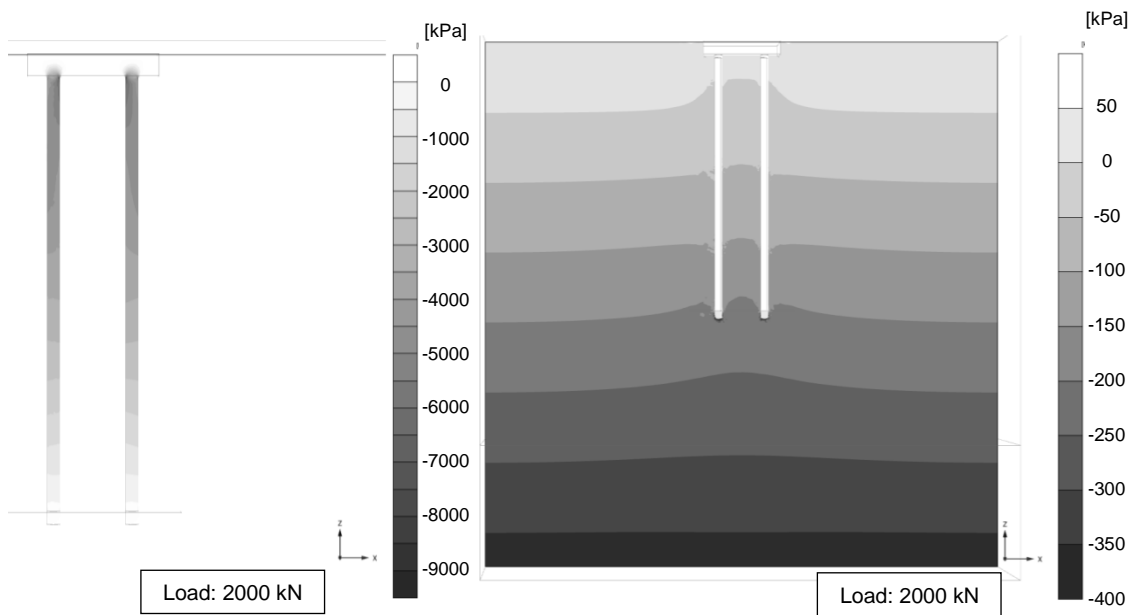


Fig. 5.57 Vertical stresses in section B-B (see Fig. 5.46) with 3D FEM for CPRF case (left: only column stresses; right: only soil stresses; in Plaxis: compression negative)

The settlements under the footing are almost perfectly uniform (Fig. 5.58 and Fig. 5.59). The difference in settlements between the column and the soil shown in Fig. 5.59 reflects the activation of positive skin friction typical of a CPRF. Only small differences are noticed in the skin friction mobilisation on the inner side and on the outer side of the

columns (not shown), thus an average skin friction profile is considered in the following comparison with the LTM.

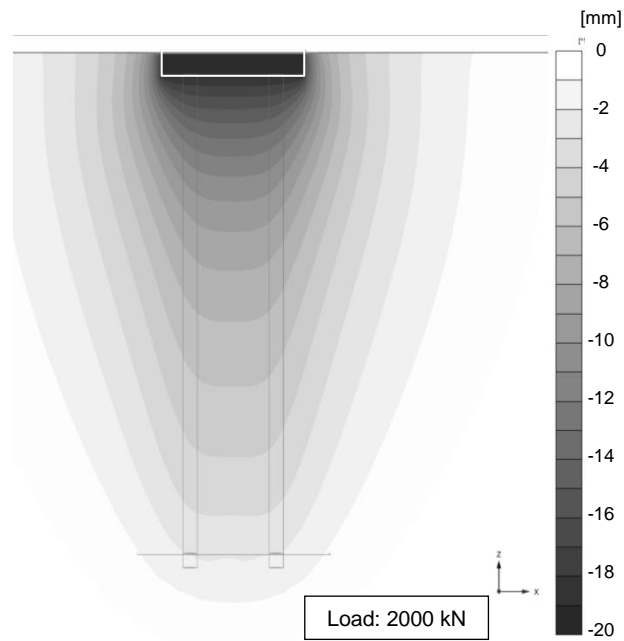


Fig. 5.58 Vertical displacement in section A-A (see Fig. 5.46) with 3D FEM for CPRF case

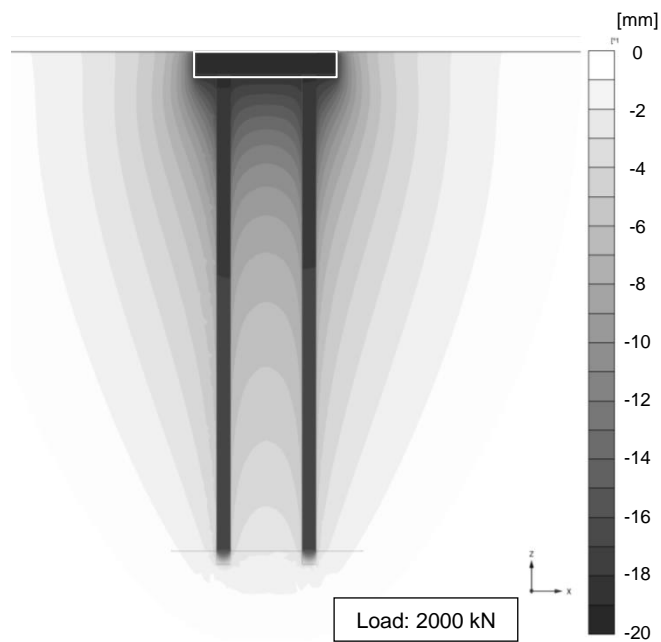


Fig. 5.59 Vertical displacement in section B-B (see Fig. 5.46) with 3D FEM for CPRF case

The results are similar for all 4 columns due to symmetry reasons. In the following comparison with the LTM, only the results for the column located in the corner of the positive x and y axes are presented.

The parameters for the LTM calculations are shown in Table 5.6.

Table 5.6 LTM parameters for CPRF case

Load	:	2000 [kN]						
Tip resistance ult.	:	940 [kPa]						
Foundation length	:	3 [m]						
Foundation width	:	3 [m]						
Foundation embedment	:	0,5 [m]						
Number of columns	:	4 [-]						
Calculation footing	:	non-linear						
Bearing capacity footing	:	4500 [kN]						
Soil properties								
Top Type		Eoed modulus	Friction ult.	γ eff. soil				
[m]		[kPa]	[kPa]	[kN/m ³]				
-0,50 soft clay		4300	12,1	18				
1,00 soft clay		4300	16,7	18				
2,00 soft clay		4300	21,5	18				
3,00 soft clay		4300	26,4	18				
4,00 soft clay		4300	31,5	18				
5,00 soft clay		4300	36,7	18				
6,00 soft clay		4300	42	18				
7,00 soft clay		4300	47,1	18				
8,00 soft clay		4300	52,4	18				
9,00 soft clay		4300	54,3	18				
Column properties								
Top Type		Column diameter	γ column	Add. resistance for diameter variation (also virtual)	Column E	No. of subdivisions		
[m]		[m]	[kN/m ³]	[kPa]	[kPa]	[-]		
-0,50 soft clay		0,3	22	0	20000000	100		
1,00 soft clay		0,3	22	0	20000000	100		
2,00 soft clay		0,3	22	0	20000000	100		
3,00 soft clay		0,3	22	0	20000000	100		
4,00 soft clay		0,3	22	0	20000000	100		
5,00 soft clay		0,3	22	0	20000000	100		
6,00 soft clay		0,3	22	0	20000000	100		
7,00 soft clay		0,3	22	0	20000000	100		
8,00 soft clay		0,3	22	0	20000000	100		
9,00 soft clay		0,3	22	0	20000000	100		
Column toe:		10 m						

The results of the FEM and of the LTM calculation in terms of settlements of column and of soil at the characteristic point and in terms of skin friction mobilisation are presented in Fig. 5.60. The settlement is similar with both methods for the given parameters. As expected, the settlement profile in the soil is different with the FEM, since the LTM does not consider the presence of the columns in the shape of the soil settlement profile. The ultimate skin friction in the interface in the single column case with FEM in axisymmetry (more details in the section 6.3.2 below) is presented together with the ultimate skin friction in the interface in the CPRF system. The ultimate skin friction in the CPRF case is slightly higher due to confinement stresses in the soil between the columns. Both in the FEM and LTM cases, it appears clearly that the mobilised skin friction is equal to zero at the very top of the system due to the equality of the settlement between the soil and the column under the rigid footing. It increases then with depth and reaches the maximum value at a quite small depth, meaning that the ultimate skin friction force in the system is almost reached. This is

typical of a CPRF system where a safety factor is not necessarily applied on the bearing capacity of the single piles (see section 2.7).

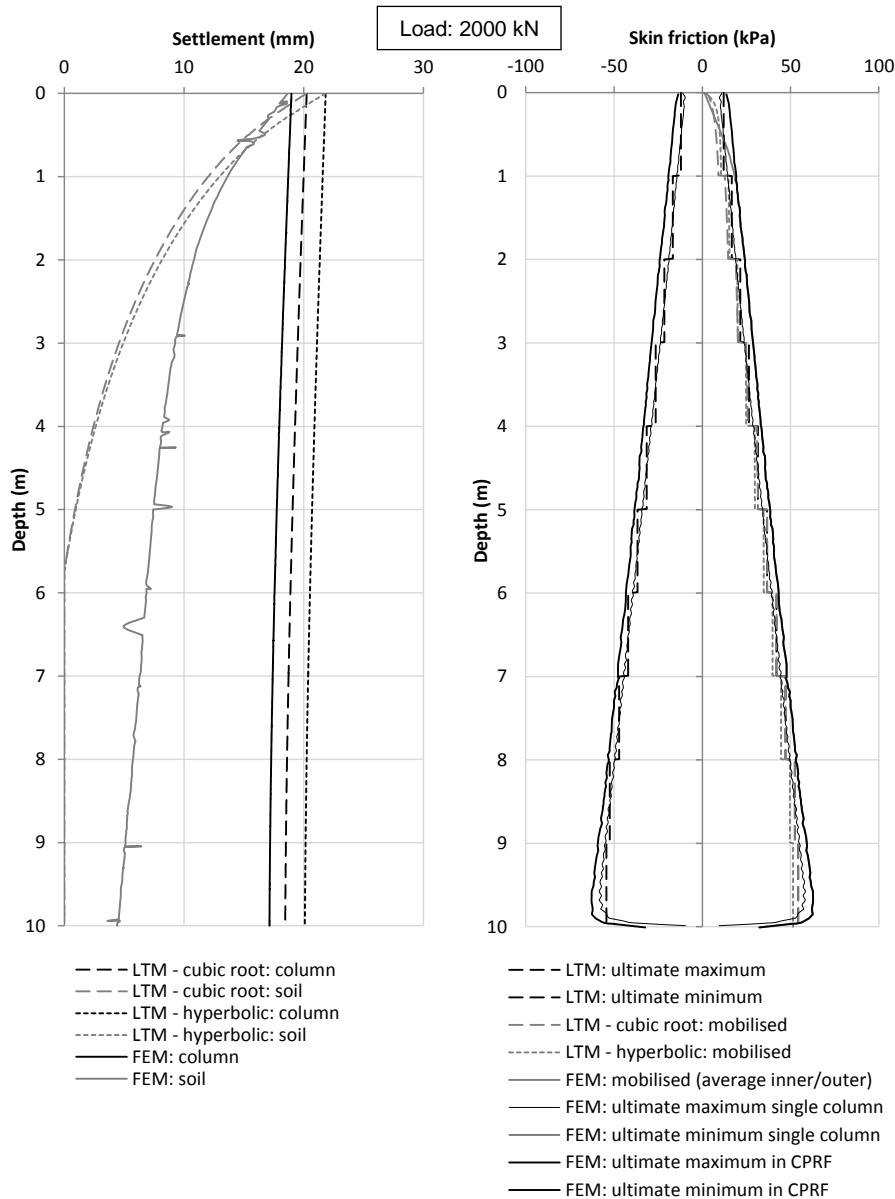


Fig. 5.60 Comparison of LTM and 3D FEM results for CPRF case: settlement and skin friction mobilisation (depth 0 m: column head position)

The additional stresses coming from the load (total stresses minus initial stresses) in the column and in the soil under the characteristic point are presented for both calculation methods in Fig. 5.61. The average stress in the column section is calculated with the option of structural forces calculation of the Plaxis version 3D.AE (Plaxis 2015). The load share at the top of the columns is equal to 76 %. The additional stress in the soil

below the characteristic point with the FEM shows a quite irregular distribution over depth. This is due to the proximity of the characteristic point to the column with the fully mobilised interface for the applied load (Fig. 5.60). The LTM predicts larger stresses in the soil than the FEM in the first meters, but the results become similar at larger depths. The column stresses are very similar with the LTM and with the FEM. The global agreement is good, in particular in terms of the shape of the profiles.

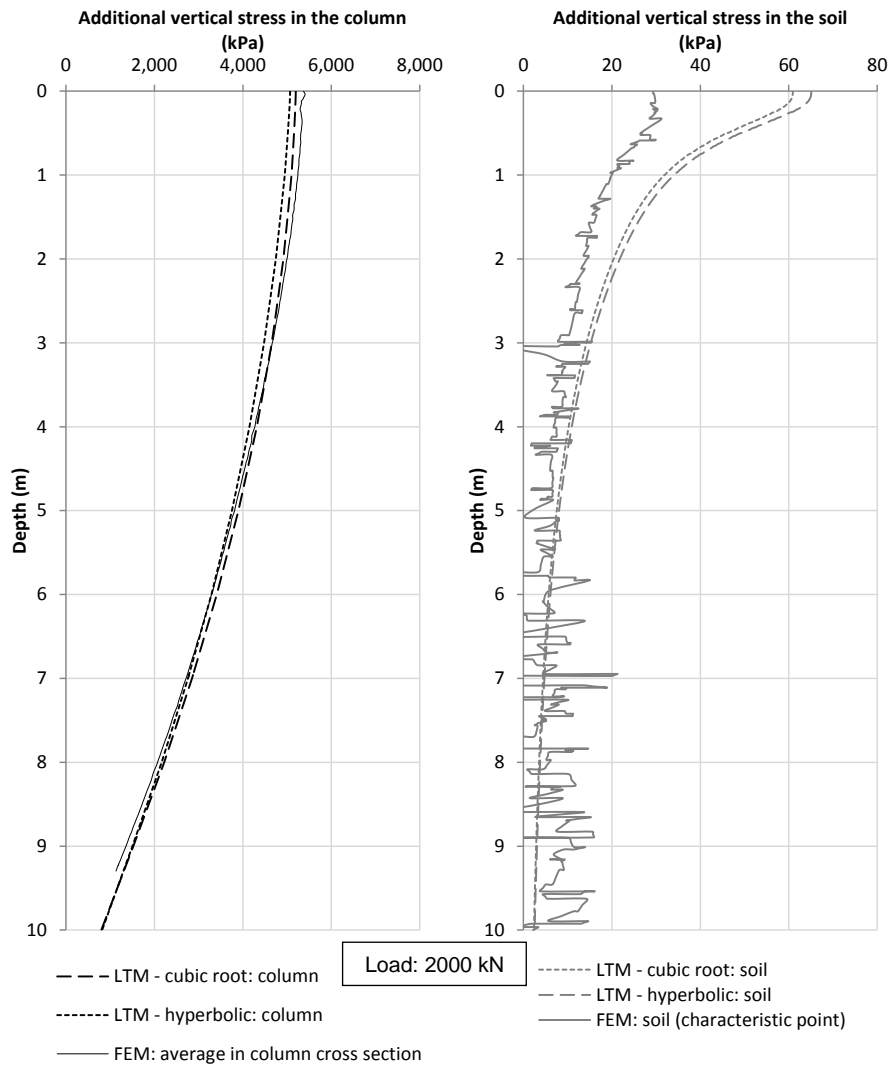


Fig. 5.61 Comparison of LTM and 3D FEM results for CPRF case: additional stress in the column and in the soil due to the load applied (depth 0 m: column head position)

In order to assess the footing behaviour in the CPRF, the load-settlement curve of the soil in the CPRF is compared with the previous curves determined without columns (Fig. 5.62). For this purpose, the exact load in the soil is calculated by subtracting the

load in the columns (determined by integration over the column section) to the total load applied, here in 5 load steps up to the final load of 2000 kN. The soil shows a similar behaviour as in the unimproved case for small loads. For loads higher than 120 kN in the soil, the soil under the footing shows a less stiff behaviour. This may be explained by the load transferred by the columns to the soil at depth.

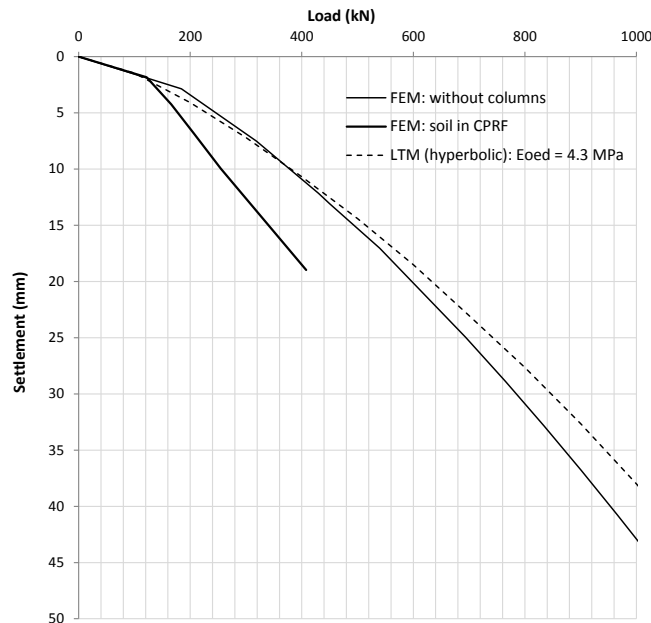


Fig. 5.62 Footing load-settlement curve in CPRF with 3D FEM compared with load-settlement curves without columns

Even if the unfavourable effect of the columns on the load-settlement curve of the soil under the footing is not taken into account with the LTM, the LTM results are very close to the 3D FEM results and the settlement prediction remains slightly more conservative than with the 3D FEM for the given parameters. In this example, the reliability of the proposed cubic root and hyperbolic curves (with fixed mean stiffness parameters) to model the soil-column interactions in a CPRF is confirmed.

5.3.4 Comparison in RI case

The 3D FEM calculation of the RI case allows for a detailed representation of the interactions in the system, in particular of the load transfer in the LTP. For the proposed load of 2000 kN (222 kPa), the failure points distribution (Hardening Soil Model, see section 4.2.2) shows a global failure of the LTP (Fig. 5.63). The settlement still remains moderate with 3 to 4 cm with this load. Nevertheless, in order to allow for a comparison with the LTM which only represents failure mechanisms at the interface of the virtual

columns in the LTP, a load of 1350 kN (150 kPa) is selected. For 1350 kN, the settlement of the footing without columns is approximately 66 mm (Fig. 5.51). For this load, the failure points remain located directly above the columns and under the edge of the footing (Fig. 5.63).

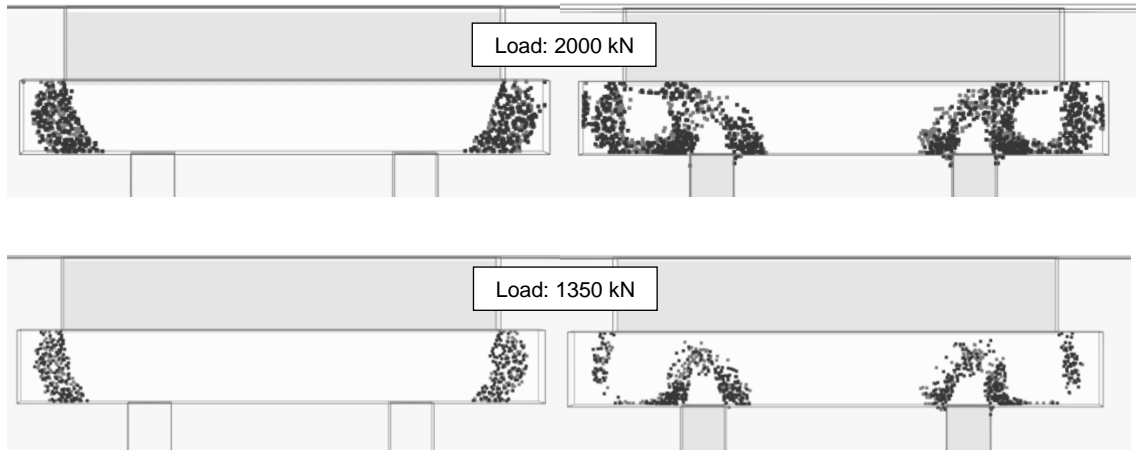


Fig. 5.63 Failure points in LTP (RI case) with 3D FEM (left: in section A-A; right: section B-B after Fig. 5.46)

The stress distribution is shown in various sections in Fig. 5.64, Fig. 5.65, Fig. 5.66 and Fig. 5.67. The load is concentrated in the columns; however the load share at the top of the columns is smaller than in the CPRF case (around 47 % compared to 76 %). Even for the smaller load, the settlement is still slightly larger than in the CPRF case (around 22 mm). The stress distribution in the columns (Fig. 5.66) is not uniform over the column (horizontal) cross section, reflecting a different skin friction mobilisation between the inner and the outer diagonal side of the columns (Fig. 5.68), difference which is more significant than in the CPRF case. This is partly due to the deeper position of the columns compared to the footing base. The position of the neutral plane can be determined thus only approximately from the column stresses or from the skin friction.

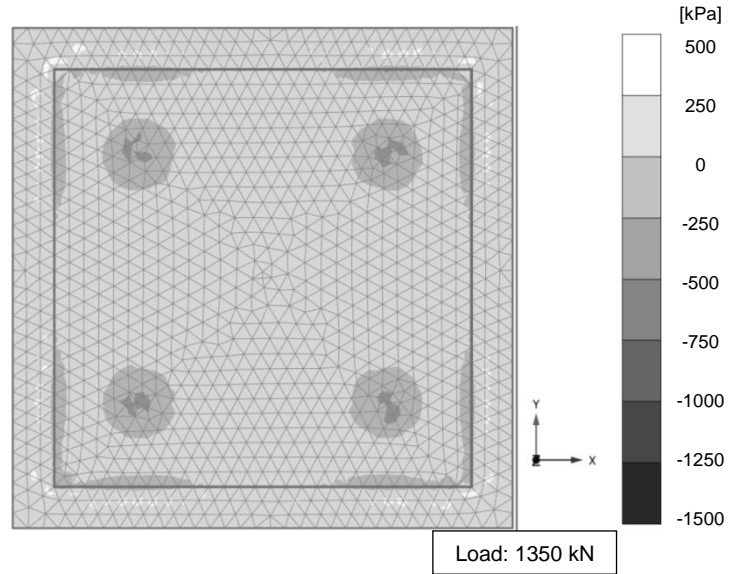


Fig. 5.64 Vertical stresses over bottom surface of the footing with 3D FEM for RI case (in Plaxis: compression negative)

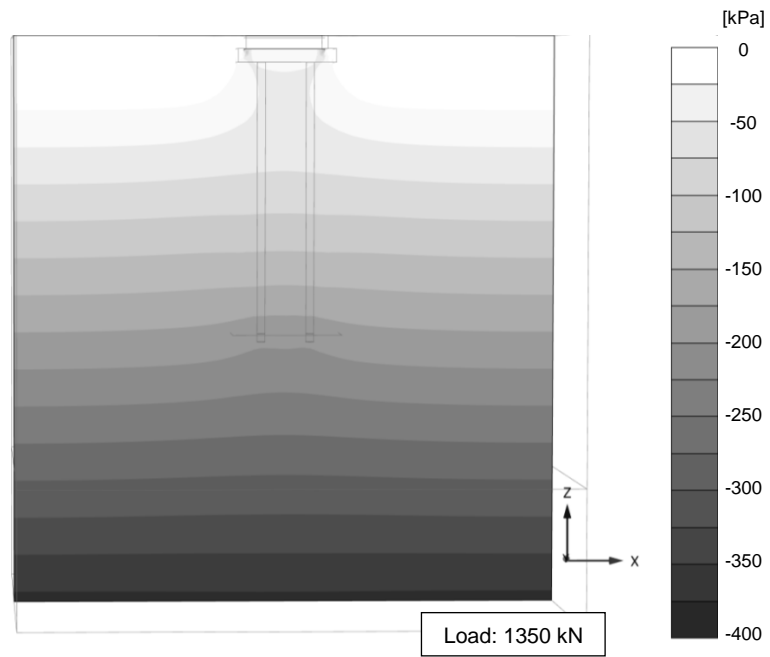


Fig. 5.65 Vertical stresses in section A-A (see Fig. 5.46) with 3D FEM for RI case (in Plaxis: compression negative)

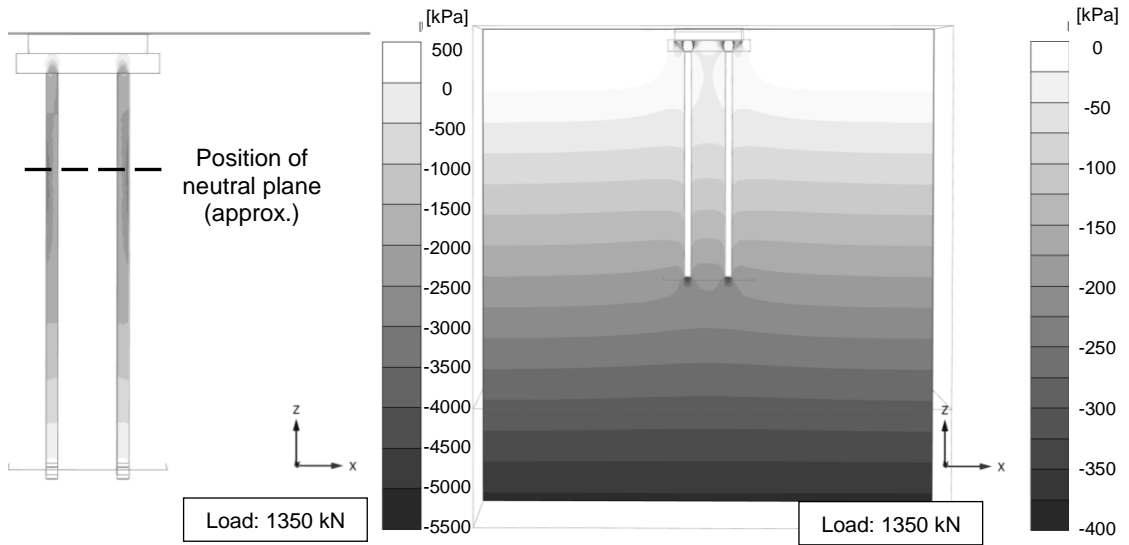


Fig. 5.66 Vertical stresses in section B-B (see Fig. 5.46) with 3D FEM for RI case (left: only column stresses; right: only soil stresses; in Plaxis: compression negative)

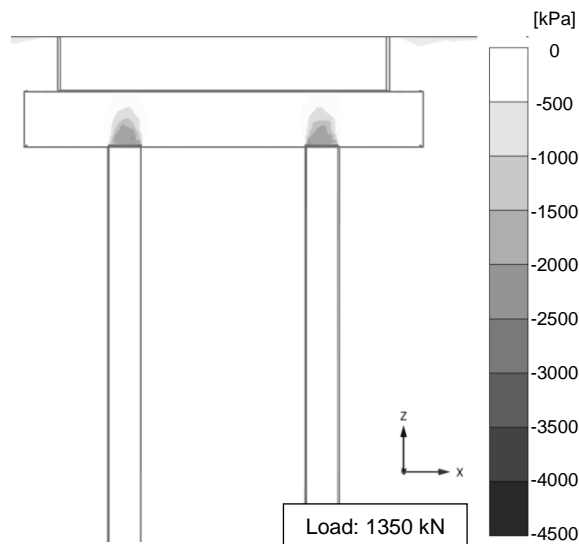


Fig. 5.67 Detail of vertical stresses in LTP in section B-B (see Fig. 5.46) with 3D FEM for RI case (in Plaxis: compression negative)

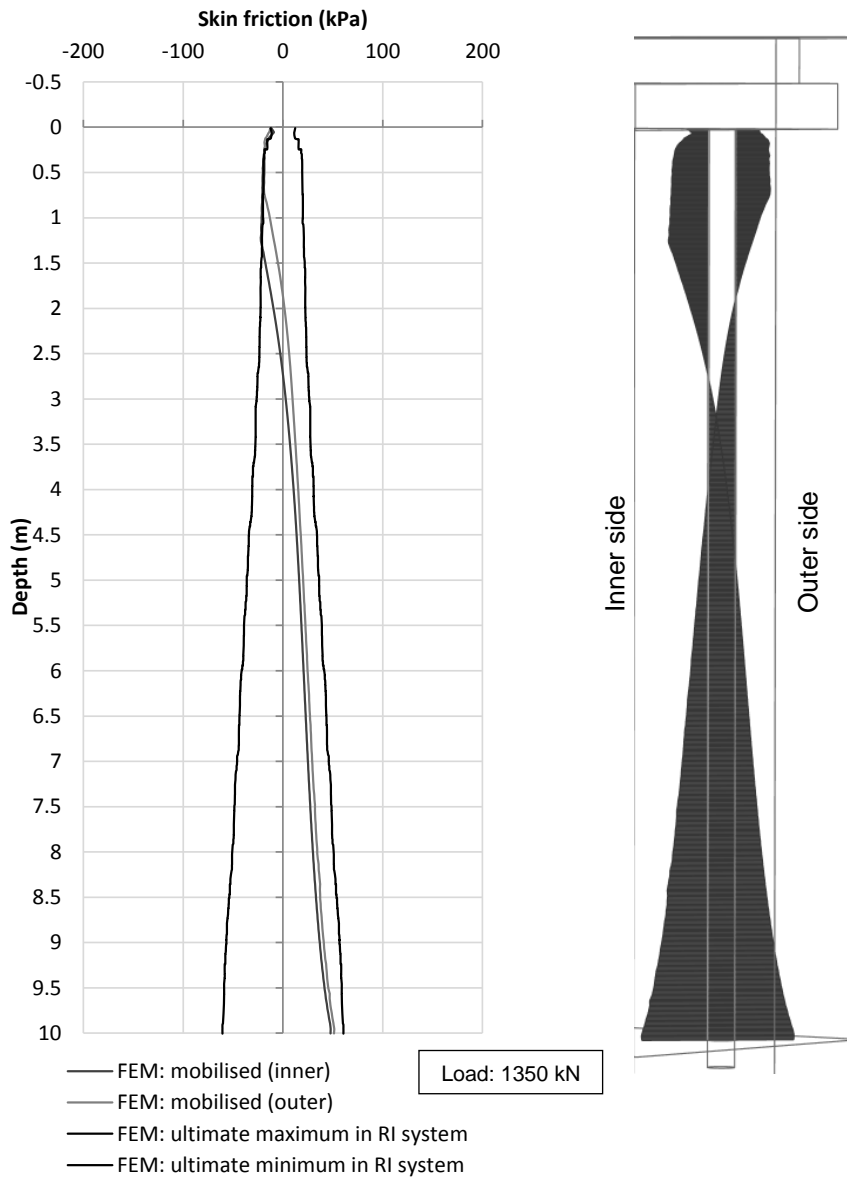


Fig. 5.68 Skin friction mobilisation with 3D FEM for RI case

The settlement under the footing is almost perfectly uniform (Fig. 5.69, Fig. 5.70 and Fig. 5.71). The difference in settlements between the column and the soil shown in Fig. 5.71 reflects the activation of negative skin friction at the top and of positive skin friction at the bottom, typical of a RI system. The neutral plane is located at 2 to 2.5 m from the top of the columns (depending on the analysis in terms of settlements between soil and column, of skin friction or on column load).

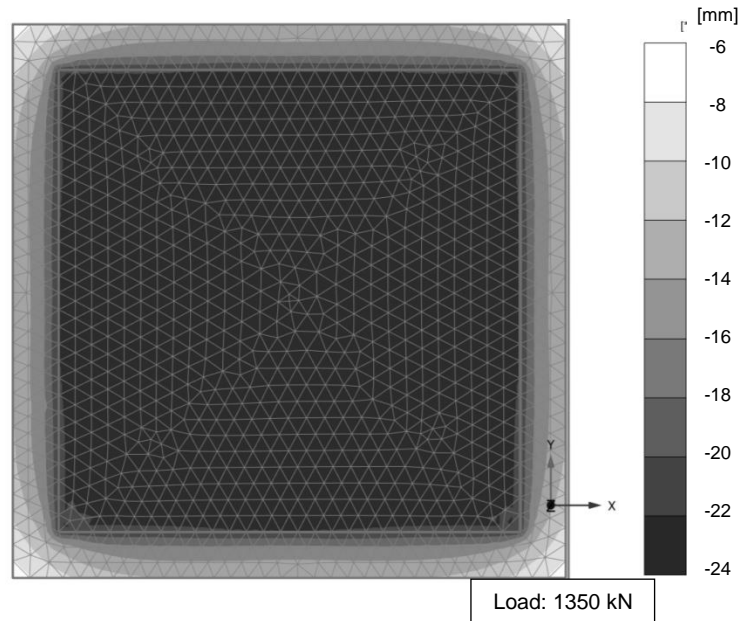


Fig. 5.69 Vertical displacement over bottom surface of the footing with 3D FEM for RI case

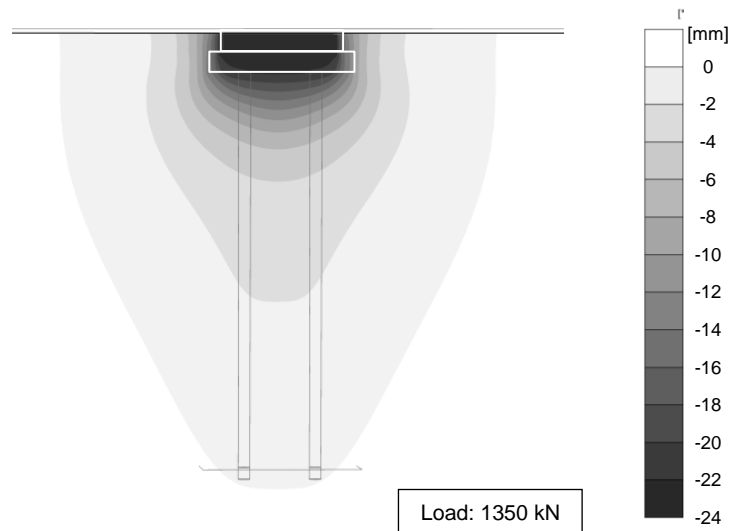


Fig. 5.70 Vertical displacement in section A-A (see Fig. 5.46) with 3D FEM for RI case

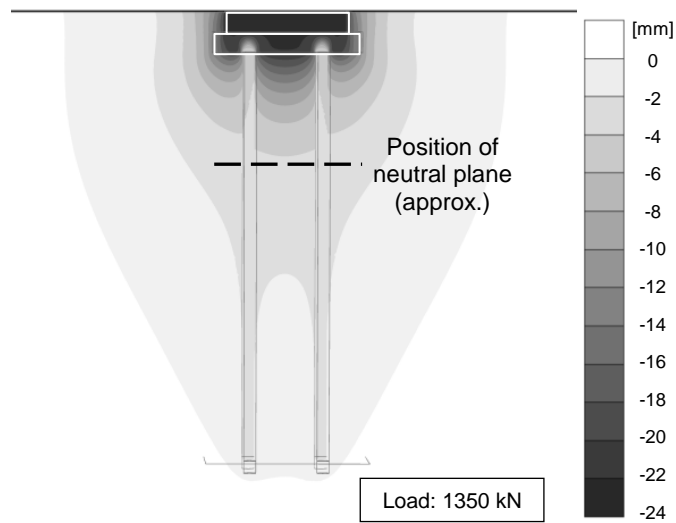


Fig. 5.71 Vertical displacement in section B-B (see Fig. 5.46) with 3D FEM for RI case

The load transfer and arching occurring in the LTP is presented in terms of directions of principal stresses in Fig. 5.72.

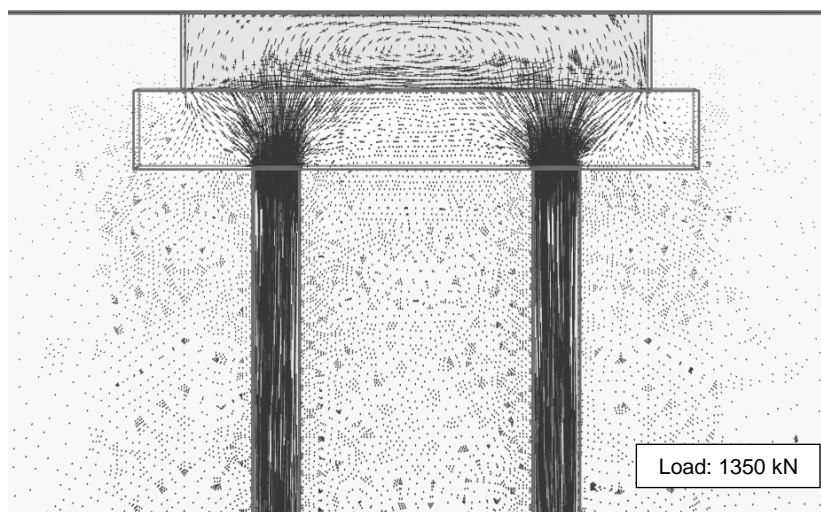


Fig. 5.72 Directions of principal stresses in section B-B (see Fig. 5.46) with 3D FEM for RI case

The results are similar for all 4 columns due to symmetry reasons. In the following comparison with the LTM, only the results for the column located in the corner of the positive x and y axes are shown.

The parameters for the LTM calculations are given in Table 5.7. The skin friction in the LTP is determined in the usual manner from the vertical stresses in the LTP (stress in the middle of the LTP: 155 kPa). The Young's modulus in the LTP is estimated considering a usual ratio of approximately 0.7 with the constrained modulus of 80 MPa (Poisson's ratio between 0.3 and 0.33).

Table 5.7 LTM parameters for RI case

Load	:	1350 [kN]			
Tip resistance ult.	:	940 [kPa]			
Foundation length	:	3 [m]			
Foundation width	:	3 [m]			
Foundation embedment	:	0,5 [m]			
Number of columns	:	4 [-]			
Calculation footing	:	non-linear			
Bearing capacity footing	:	4500 [kN]			
Soil properties					
Top Type		Boed modulus	Friction ult.	γ eff. soil	
[m]		[kPa]	[kPa]	[kN/m ³]	
-1,00 LTP		80000	155	20	
0,00 soft clay		4300	12,1	18	
1,00 soft clay		4300	16,7	18	
2,00 soft clay		4300	21,5	18	
3,00 soft clay		4300	26,4	18	
4,00 soft clay		4300	31,5	18	
5,00 soft clay		4300	36,7	18	
6,00 soft clay		4300	42	18	
7,00 soft clay		4300	47,1	18	
8,00 soft clay		4300	52,4	18	
9,00 soft clay		4300	54,3	18	
Column properties					
Top Type		Column diameter	γ column	Add. resistance for diameter variation (also virtual)	Column E
[m]		[m]	[kN/m ³]	[kPa]	[kPa]
-1,00 LTP		0,3	20	0	56000
0,00 soft clay		0,3	22	0	20000000
1,00 soft clay		0,3	22	0	20000000
2,00 soft clay		0,3	22	0	20000000
3,00 soft clay		0,3	22	0	20000000
4,00 soft clay		0,3	22	0	20000000
5,00 soft clay		0,3	22	0	20000000
6,00 soft clay		0,3	22	0	20000000
7,00 soft clay		0,3	22	0	20000000
8,00 soft clay		0,3	22	0	20000000
9,00 soft clay		0,3	22	0	20000000
Column toe:		10 m			

The results of the FEM and of the LTM calculation in terms of settlements of column and of the soil at the characteristic point and in terms of skin friction mobilisation are presented in Fig. 5.73. In the FEM results, the mobilised skin friction represented is an average between the inner and the outer diagonal side. The settlement is slightly larger with the LTM for the given parameters. As expected, the settlement profile in the soil is different with the FEM, since the LTM does not consider the presence of the columns in the shape of the soil settlement profile. The ultimate skin friction in the interface in the single column case with FEM in axisymmetry (more details in the section 6.3.2 below) is shown together with the ultimate skin friction in the interface in the RI system. The ultimate skin friction in the RI case is slightly higher due to confinement stresses in the soil between the columns. At the top of the columns, the negative skin friction is fully mobilised. In the FEM calculation, the comparison of the settlement of the column and the soil at the characteristic point gives a neutral plane at a position of 2.1 m below the

column head whereas the average skin friction gives a neutral plane at approximately 2.3 m. In the LTM calculation, the neutral plane is located at approximately 2.9 m.

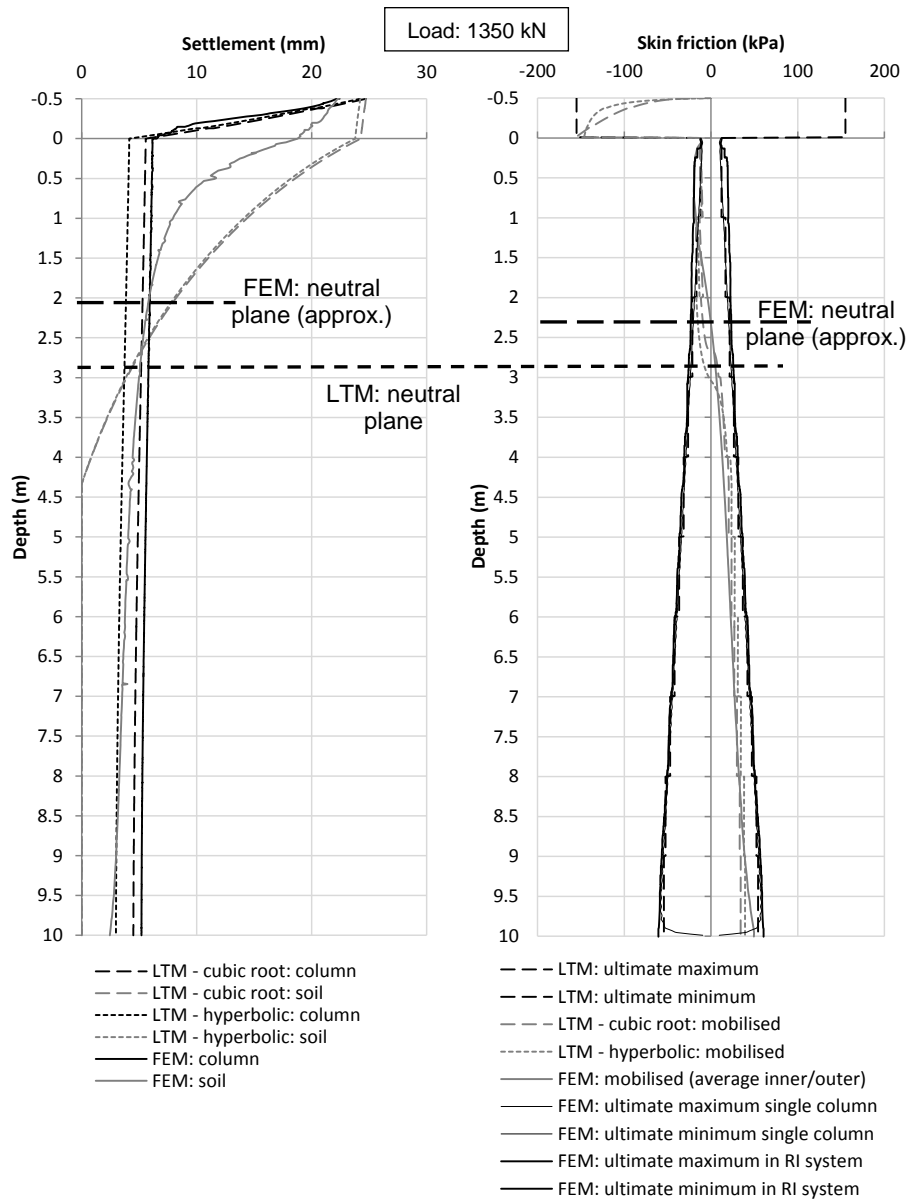


Fig. 5.73 Comparison of LTM and 3D FEM results on RI case: settlement and skin friction mobilisation (depth 0 m: column head position)

The additional stresses coming from the load (total stresses minus initial stresses) in the column and in the soil under the characteristic point are presented for both calculation methods in Fig. 5.74. The average stress in the column section is calculated with the option of structural forces calculation of the Plaxis version 3D.AE (Plaxis 2015).

As stated in section 2.5.2, the validity of LTM calculations in terms of stresses in the LTP at the top of the columns has to be checked after ASIRI (2012), as no plasticity criterion is represented in this method beside the non-linear mobilisation of the skin friction at the side of the virtual columns (here almost full mobilisation with high relative settlements at the LTP base). The check according to ASIRI (see Fig. 2.41, modified for the footing case) gives an allowable stress of around 1000 kPa for the LTM. The calculated stress here is significantly higher, around 2600 kPa. Following ASIRI (2012), the modulus in the LTP should be reduced in order to take into account failure zones. However, even with unrealistically small moduli, the allowable stress criterion cannot be fulfilled. Furthermore, the settlement with the original parameters does not seem to be underestimated as it is slightly larger than in the FEM case. This leads to the conclusion that the check recommended in ASIRI for footings may be too conservative.

The column stress profile in the column is very similar with the LTM and the FEM methods. With the FEM, the stresses in the soil under the characteristic point show high variations in the LTP, reflecting the failure zones (see Fig. 5.63). This cannot be directly compared with the average soil stresses represented by the LTM stress profile in the LTP. Below the level of the column heads, both methods give similar results for the soil stresses.

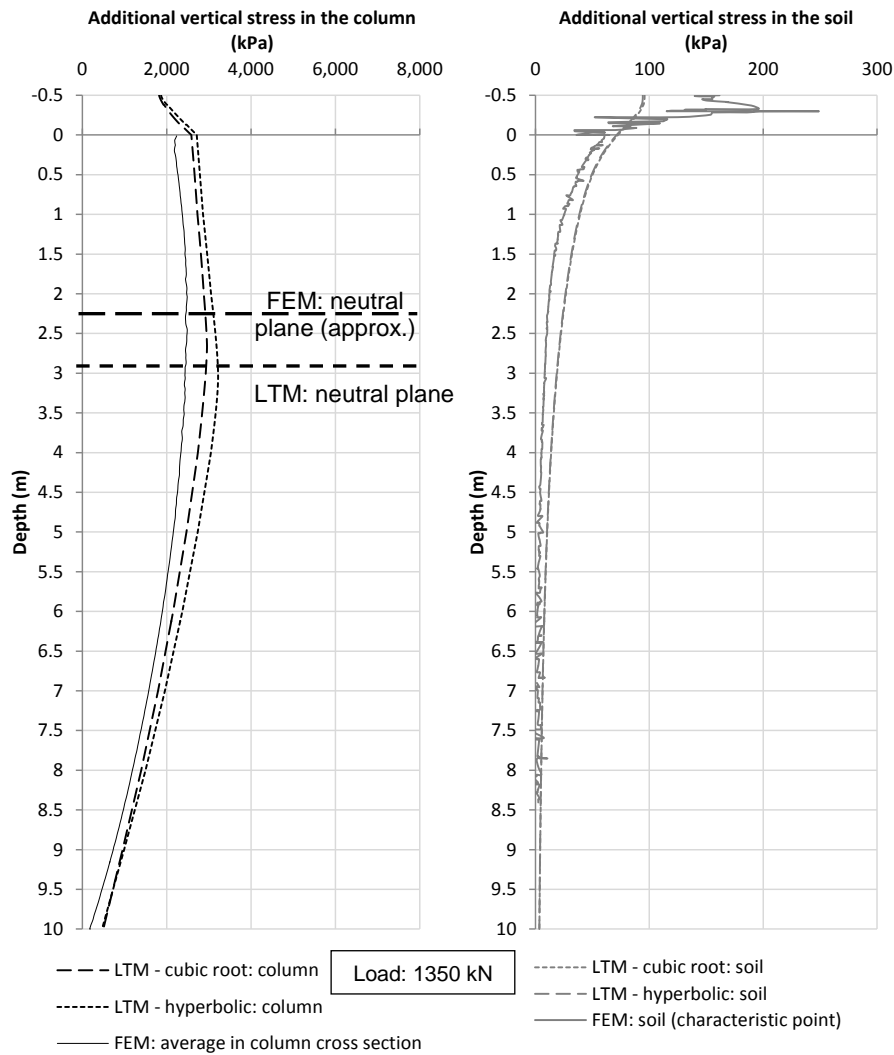


Fig. 5.74 Comparison of LTM and 3D FEM results in RI case: additional stress in the column and in the soil due to the load applied (depth 0 m: column head position)

The LTM results are very close to the 3D FEM results for this RI system example. The settlement prediction is slightly more conservative with the LTM than with the 3D FEM for the given parameters. The load transfer in the LTP with the model of fictive columns leads to a similar stress at the top of the columns as with the 3D FEM. In this example, the reliability of the proposed cubic root and hyperbolic curves (with fixed mean stiffness parameters) to model the soil-column interactions in a RI system is confirmed.

6 Sensitivity investigation

6.1 Influence of column material in a unit cell system

6.1.1 General modelling aspects

The column material has an important influence on the column-soil behaviour and on the global behaviour of combined systems. As already indicated in sections 2.5 and 2.6, bonded columns (e.g. concrete columns) and coarse-grained columns behave differently (Wehr and Sondermann 2011). The goal of the present section is to illustrate this difference and to distinguish between the influence of the column modulus and the influence of the column material (bonded or coarse-grained). Furthermore, this investigation can be used for assessing the effects of an imperfection in the column material properties over the whole column height. Similar analyses are presented in conference papers by Bohn (2012, 2013b), written as a part and in the scope of the present work.

Only few publications exist on this subject and they are all related to a specific column material type. Sabatini et al. (2012) examined the effect of unmixed clay zones in deep soil mixing columns. Kirsch (2004) studied the variation of the soil modulus for a group of stone columns (see section 2.6). Han and Gabr (2002) and Gangakhedkar (2004) focused on bonded columns (see section 2.5).

The investigation is performed here with the finite element method (FEM), using the software Plaxis 2D version AE.02 in axisymmetric mode (Plaxis 2014). Since it is expected that the column material has an influence mainly on the load distribution between the column and the soil and on the differential settlement in combined systems, the unit cell case with a LTP is chosen. A purely theoretical unit cell example with a column in a soft fine-grained soil (without ground water) and with LTP under a rigid plate is considered (Fig. 6.1). The soil and LTP parameters are the same as in section 5.3. The floating column has a diameter of 0.5 m (realistic for both concrete and stone columns) and a length of 10 m. It is assumed that the installation is made with a displacement technique both for the bonded and for the coarse-grained column types. This is modelled for all column types using $K_0 = 1$ in the soil in the initial calculation phase. The diameter of the unit cell is 3 m. A stiffer cohesive layer is located 5 m below the column tip. The model extends down to 20 m. The area load applied on the unit cell is equal to 40 kPa. The LTP is 0.5 m thick and is considered as an additional load (unit weight 20 kN/m³), thus the total load amounts to 50 kPa.

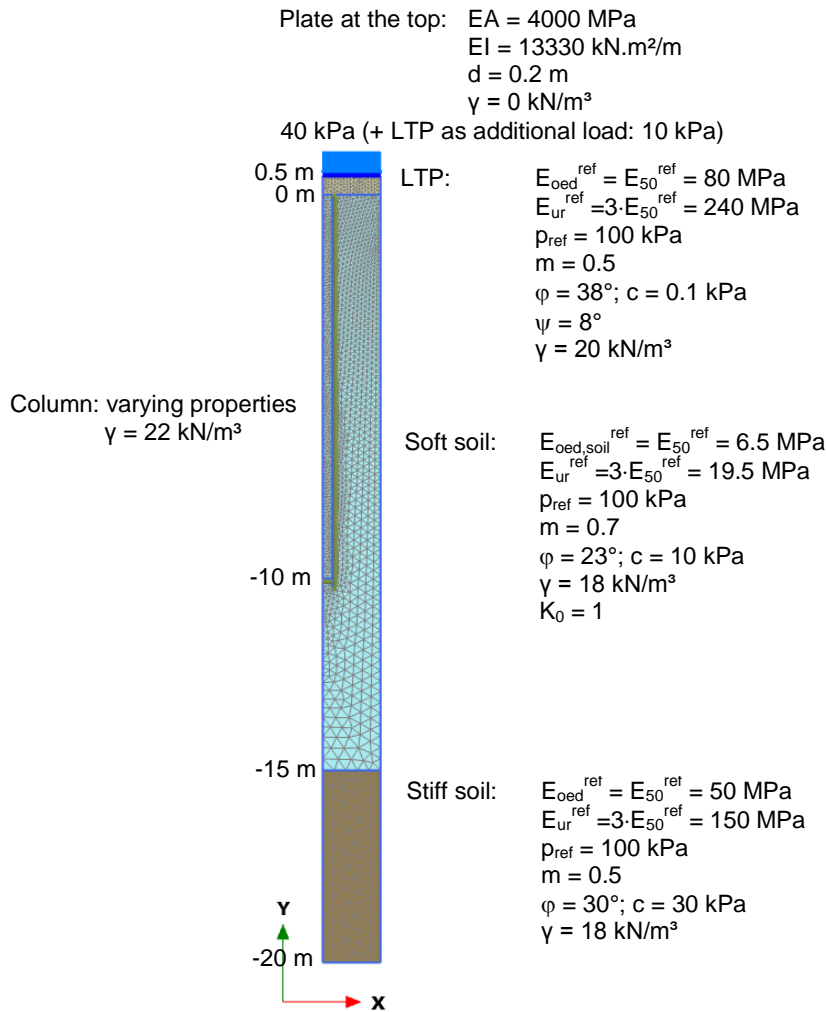


Fig. 6.1 Axisymmetric FEM-model for column material variation (layers with main parameters and mesh)

The bonded column type is modelled as follows:

- the isotropic linear elastic model is used with Poisson's ratio $\nu = 0.2$. Since no pore pressures need to be calculated in the bonded material, the drainage type is set to non-porous (Plaxis 2014). The column unit weight is 22 kN/m^3 ;
- the oedometric modulus is varied from the concrete reference case defined here with $E_{\text{oed,column}} = 22200 \text{ MPa}$ (Young's modulus 20000 MPa) down to the typical oedometric modulus for stone columns of 120 MPa . The modulus of usual concrete and usual lightweight concrete shows very small variations with the compressive strength f_c as shown in (Eq. 6.1), (Eq. 6.2) and Fig. 6.2. The value of 120 MPa value would rather correspond for example to lightweight concrete with expanded polystyrene spheres as presented by Le Roy et al. (2005), to very

weak lime-cement columns as stated by Moseley and Kirsch (2004), or simply to a rubber material;

- no structural failure occurs, given the fact that even the weakest material modelled here still has a sufficient compressive strength. It is around 0.5 MPa for weak lime-cement (Moseley and Kirsch 2004). Thus the isotropic linear elastic model is appropriate;
- the side interface is defined from the adjacent soil with a R_{inter} factor for the column/soil shear equal to 0.67. The interface is extended by one diameter under the column tip, and a horizontal interface is introduced under the column tip. Both have the parameters of the adjacent soil with no reduction of the shear parameters ($R_{inter} = 1$).

$$E = 22 \cdot ((f_c + 8)/10)^{0.3} \cdot \frac{(\rho/2200)^2}{1 + \varphi} \text{ after EN 1992-1-1 (2004-2010)} \quad (\text{Eq. 6.1})$$

(ρ : concrete density in kg/m^3 ; φ : creep factor)

$$E = 3700 \cdot f_c^{1/3} \text{ after ASIRI (IREX 2012)} \quad (\text{Eq. 6.2})$$

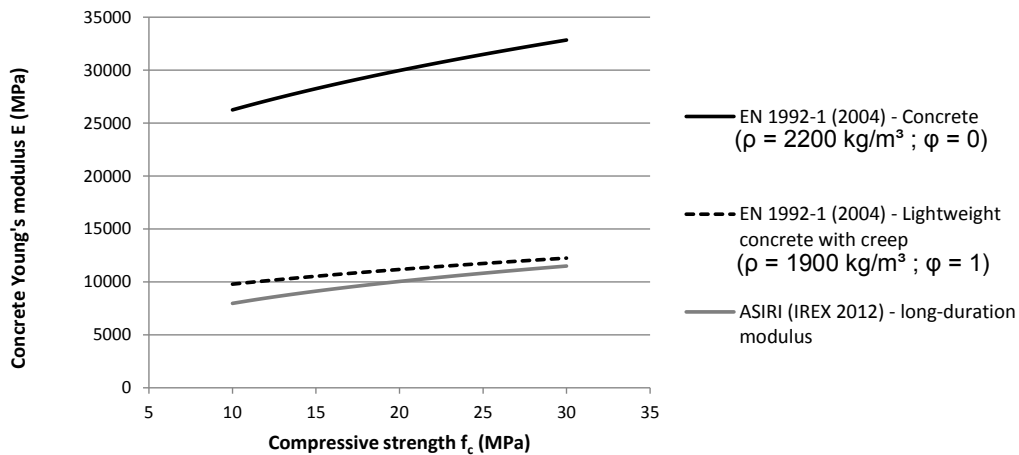


Fig. 6.2 Young's modulus vs. compressive strength for usual concrete and lightweight concrete

The coarse-grained column type is modelled as follows:

- the elastic-plastic model with Mohr-Coulomb failure criterion is used in drained mode with $\nu = 0.33$, $\varphi = 45^\circ$, $c = 0.1 \text{ kPa}$ (for numerical stability), $\psi = 15^\circ$ and a unit weight of 22 kN/m^3 . This constitutive law allows for a soil modulus

constant with depth. This is useful for coarse-grained columns, for which the modulus corresponds to a reloading modulus given the execution method;

- the oedometric modulus is varied from the stone column reference case with $E_{\text{oed,column}} = 120$ MPa up to a maximum gravel oedometric modulus of 500 MPa.

The global coarseness of the mesh is set to very fine with a coarseness factor of 0.5 in the soil and 0.125 in the column, in the interfaces and in the LTP (Plaxis 2014). The resulting mesh is shown in Fig. 6.1. The mesh is not optimized in terms of reduction of the number of elements and thus of the calculation time; the goal in this theoretical example is to model the system as finely as possible. The mesh quality is here close to 1 over the whole model.

The first calculation phase is the initial phase with K_0 procedure with the original soil layers (Plaxis 2014). The second phase is the column installation with activation of the column material and of the interfaces in the case of the bonded column. After this phase, the displacements are reset to zero. The last step is the loading step in which the LTP and the load are activated. All calculation parameters are kept to the default values, except for the maximum load fraction per step set to 0.05 (default 0.5) and the activation of the updated mesh option for the second and last steps for a better accuracy.

The following output parameters are analysed:

- uniform settlement at the top of the LTP (top of the system with rigid plate);
- settlement of the column at the column top (LTP base level);
- settlement of the soil at the edge of the model (LTP base level);
- column load share at the column head level (integration of the vertical stresses over the circular column top section).

6.1.2 Concrete column and stone column reference cases

In the concrete reference case, the total settlement at the top is 29 mm, the differential settlement between column and soil at the LTP base is 10 mm and the column load share is 0.58. In the stone column reference case, the settlement at the top is larger with 68 mm, the differential settlement is only 2 mm and the column load share is smaller with 0.13. The differences in the behaviour in both cases is reflected by the vertical stresses in the system with a more important load concentration in the concrete case

(Fig. 6.3) and by the horizontal deformations with a significant bulging at a quite shallow depth for the stone column (Fig. 6.4), as already indicated by Kirsch (2004) in Fig. 2.45. For the load applied here, failure points appear in the LTP at the top of the concrete column and at the interface at the top and at the bottom, whereas they appear in the stone column itself at relatively shallow depth (Fig. 6.5).

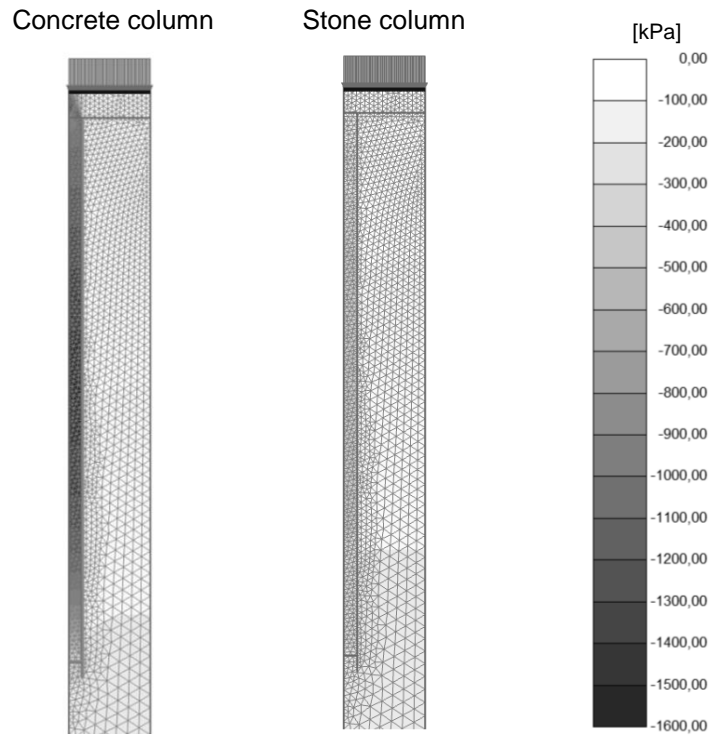


Fig. 6.3 Comparison of vertical stresses between concrete column and stone column reference cases (in Plaxis: compression negative)

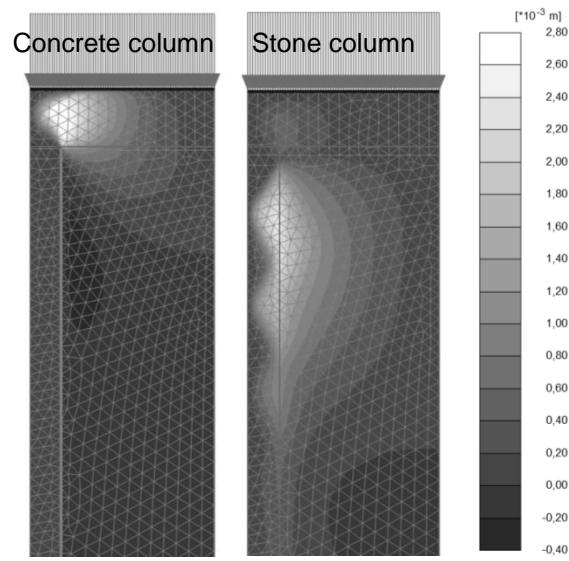


Fig. 6.4 Comparison of horizontal deformations between concrete column and stone column reference cases

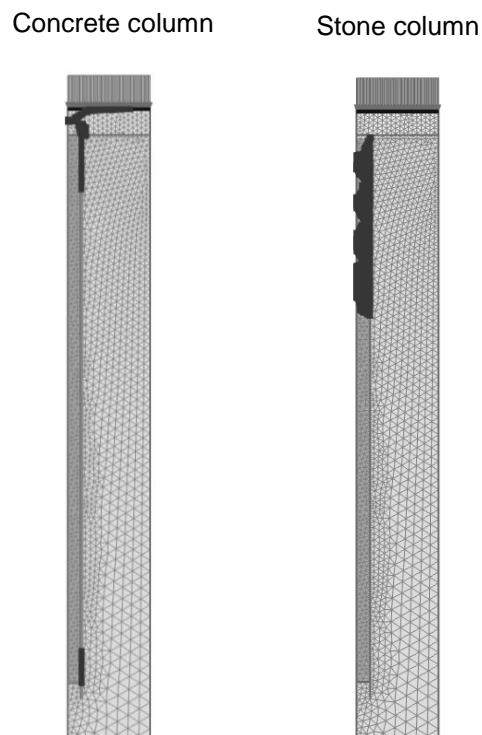


Fig. 6.5 Comparison of failure points between concrete column and stone column reference cases

The stiffer reaction of the concrete column in comparison with the stone column is reflected by the maximum and minimum bending moments in the plate which are 2.5 to 3.5 times more important than in the stone column case.

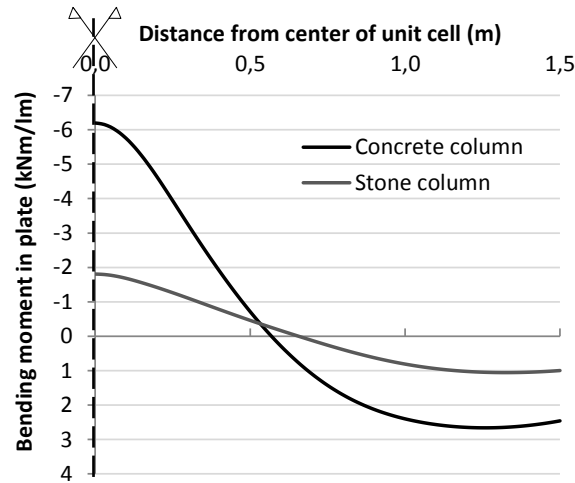


Fig. 6.6 Bending moments in the plate vs. distance to centre of the unit cell for the concrete column and for the stone column reference cases

6.1.3 Variation of column modulus and material type

The results of the material variations in terms of settlement at the top, settlements at the LTP base level and in terms of column load share at the column head are presented in Fig. 6.7, Fig. 6.8 and Fig. 6.9 respectively for both column types. Preliminary tests made with different soil modulus values led to the conclusion that the modulus ratio between the column and the soil is the governing factor for the general behaviour (Bohn 2012). The results are thus presented here in function of the modulus ratio between the column and the soil. The coarse-grained column cases with the largest $E_{\text{oed,column}}$ of 400 MPa and 500 MPa ($E_{\text{oed,column}}/E_{\text{oed,soil}}^{\text{ref}} = 62$ and 77) could be calculated up to the full load only with deactivation of the updated mesh option. This may be explained by a contradiction between high values of $E_{\text{oed,column}}$ and the assumption $K_0 = 1$. Anyhow this shows the limit of the selected model for coarse-grained columns.

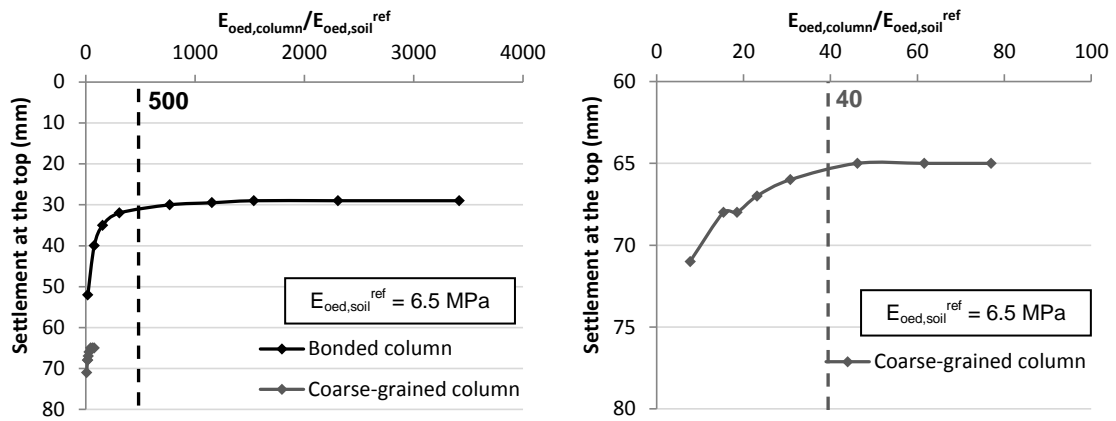


Fig. 6.7 Settlement at the top vs. modulus ratio column to soil for bonded and coarse-grained column ($E_{oed,soil}^{ref} = 6.5 \text{ MPa}$)

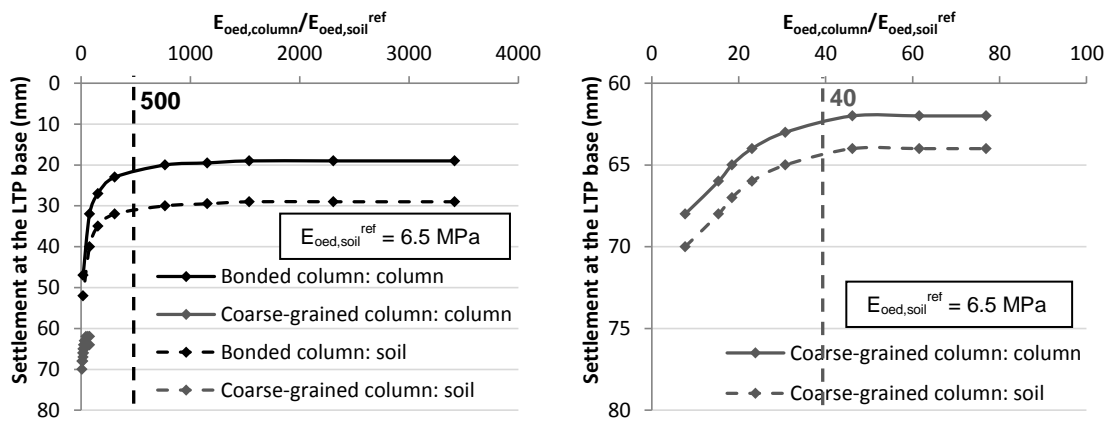


Fig. 6.8 Settlement at the LTP base level vs. modulus ratio column to soil for bonded and coarse-grained column ($E_{oed,soil}^{ref} = 6.5 \text{ MPa}$)

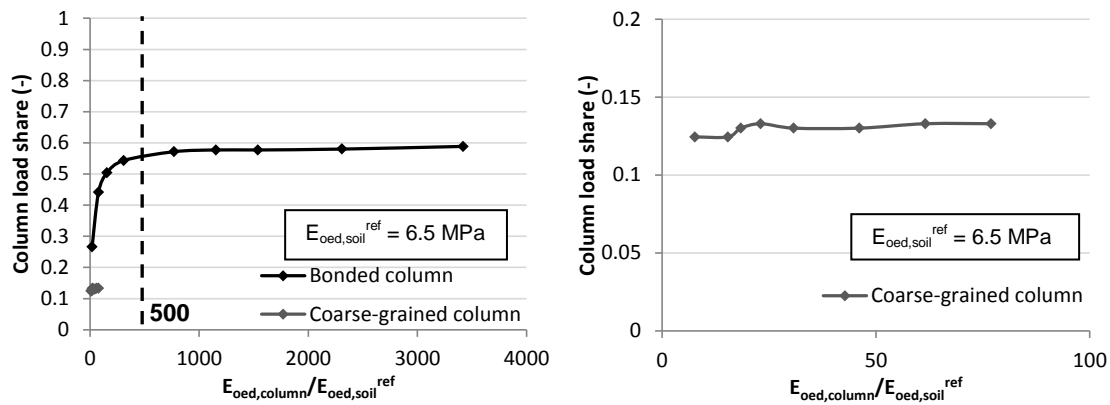


Fig. 6.9 Column load share at the column head vs. modulus ratio column to soil for bonded and coarse-grained column ($E_{oed,soil}^{ref} = 6.5 \text{ MPa}$)

The bonded column and the coarse-grained column behave differently, even for the same values of modulus. The coarse-grained column type shows larger settlements, lower differential settlements at the LTP base level and a lower column load share than the bonded column. Both column types present two different behaviour modes. Above a moduli ratio of approximately 500, the behaviour of the bonded column is almost independent from the moduli ratio. This value can be seen as an optimum, as long as the corresponding compressive strength of the material is sufficient. Below this value, the total settlement increases quickly whereas the differential settlement at the LTP base level and the column load share decrease. An exceeding of the structural capacity (breaking) of the column material may happen as well, depending on the material used. For the coarse-grained column, no change in the behaviour is noted above a moduli ratio of approximately 40 in the studied case. This ratio can be seen as an optimum value with the smallest possible moduli ratio for the maximum settlement improvement in typical cases, at least in the studied example.

6.2 Influence of geometrical imperfections on a single column

6.2.1 General modelling aspects

This chapter is partly the subject of conference papers by Bohn (2013a, 2013b) and by Trunk et al. (2014), written as a part and in the scope of the present work. All FEM calculations for this chapter have been performed and analysed jointly with Ackermann (2013, 2014a, 2014b, 2015a, 2015b).

Even if some investigations about imperfections of usual piles exist in the literature (Alber 2007b, Van Weele 1999), specific problems for recent systems using unreinforced small-diameter piles or rigid columns have not yet been extensively studied. The assumed particular sensitivity of such columns is however taken into account today by specific safety factors or increased control measures (EN 1997-1 2004-2009-2013, DGGT 2002, IREX 2012).

Imperfections of diameter, necking and bulging, inclination, curvature and eccentricity are investigated. Length variations are not considered, since the only significant problem that may happen is a notable bearing capacity decrease if a planned embedment in a stiffer layer is not reached. In order to highlight the particularities of each geometrical imperfection, which are quite complex, the single column case is selected. This presents the advantage that the results apply for single non-steel reinforced pile foundations too. The effects of these imperfections in the single column case will be later used for assessing the case of imperfections in combined systems.

The investigations are made first by means of simple analytical methods and then by means of FEM calculations for each imperfection case. The diameter imperfections, necking and bulging are calculated with Plaxis 2D version AE.02 in axisymmetric mode (Plaxis 2014). The inclination, curvature and eccentricity are modelled with Plaxis 3D version 2013.01 (Plaxis 2013).

An unreinforced circular rigid column or pile in a soft fine-grained soil is considered here, with the general simplified case of a vertical load applied directly on the pile. The simple case under consideration is presented together with the few parameters needed for the analytical study in Fig. 6.10. The reference diameter considered is 30 cm, which is a common value for soil reinforcement columns. However, different diameters are considered up to 90 cm in the analytical study and up to 60 cm in the FEM analysis, in order to assess the possible particularities of small-diameter columns.

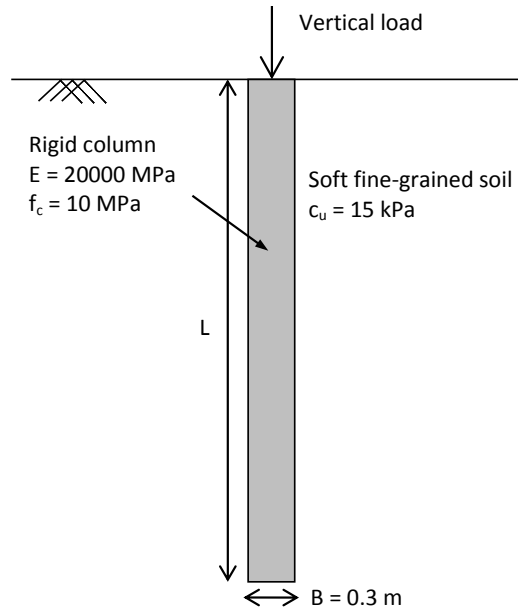


Fig. 6.10 Reference single column for analytical study

The soil and column parameters for the FEM calculation are those already presented in sections 5.3 and 6.1. Effects of imperfections in terms of structural failure are represented here with the elastic-plastic model (with a failure criterion) in the column. Further improvements in modelling the column material, in particular under tension stresses, may be appropriate. First steps in this direction representing the crack development in the column material are proposed by Schweiger et al. (2014).

The mesh coarseness is the same as in section 6.1, except for the soil volume far from the pile with a coarseness factor of 1. This leads to larger elements due to the fact that the model width chosen for the single column case is equal to 10 m (2D mesh in Fig. 6.11) and thus is larger than for the unit cell case. The mesh is not optimized in terms of reduction of the number of elements and thus of the calculation time; the goal in this theoretical example with imperfections is to model the system as finely as possible. According to the finding in 4.2.2, a model width equal to the length of the column is sufficient for single column cases. The mesh quality is defined in Plaxis as the ratio between the radiuses of the inner circle and of the outer circle of the element, normalized at 1.0 for the equal sided triangle or tetrahedron (Plaxis 2013, Plaxis 2014). The mesh quality is here close to 1 over the whole model.

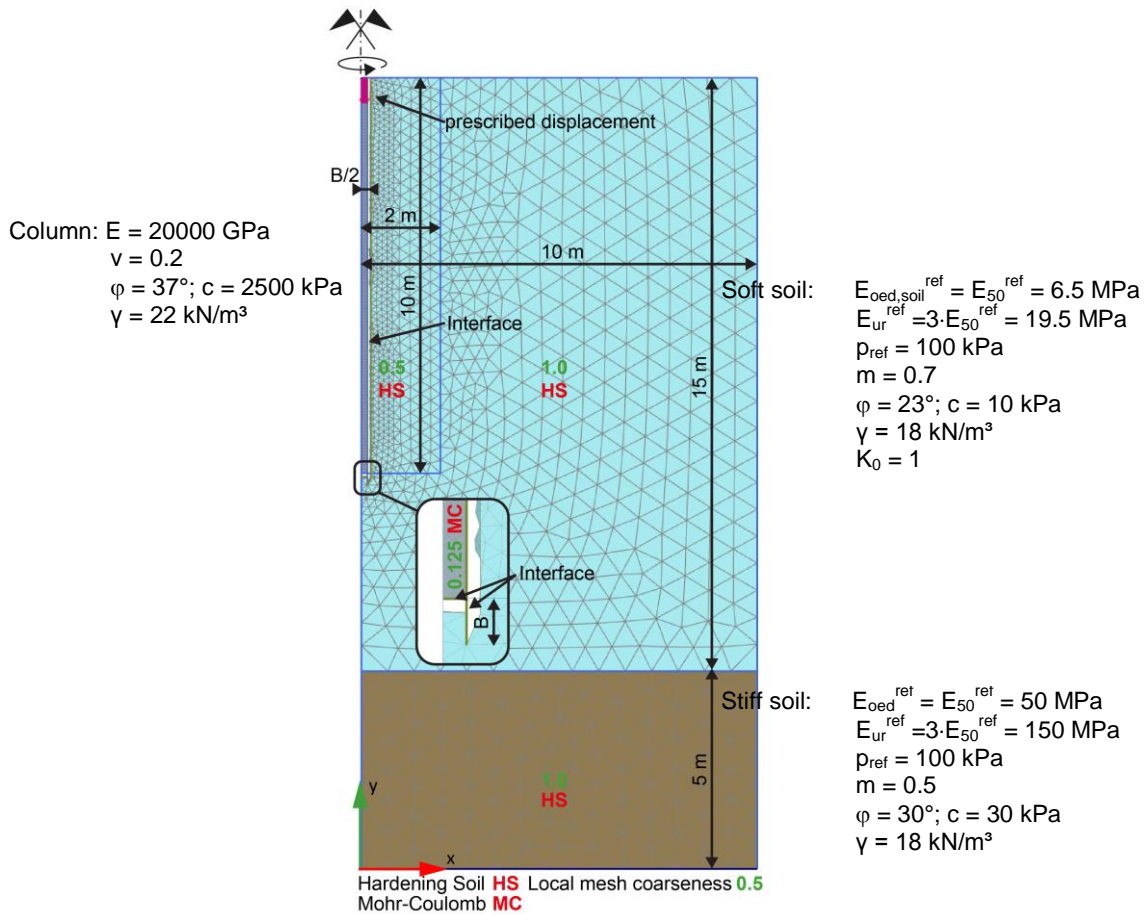


Fig. 6.11 Single column axisymmetric FEM reference model

The first calculation phase is the initial phase with K_0 procedure with the original soil layers (Plaxis 2014). The second phase is the column installation with activation of the column material and of the interfaces. After this phase, the displacements are reset to zero. The last steps are the loading steps in which the imposed displacement or the maintained load (depending on the imperfection type) are activated. This is made in 3 steps: settlement of 1 %, 2 % and 10 % of the column diameter or load of 50 %, 70 % and 100 % of the bearing capacity (defined as the resistance for a settlement of 10 % of the planned diameter). The Plaxis default calculation parameters have been partly modified. The tolerated error is set to 0.005 (default 0.01) for all loading or imposed displacement phases in order to represent failure mechanisms more accurately. In the imposed displacement case, the maximum load fraction per step is set to 0.05 for the first two phases and to 0.1 for the last phase (default 0.5). In the maintained load case, the maximum load fraction per step is set to 0.1 for the first two loading steps and kept to 0.5 for the last step. For a better accuracy and in order to better represent the large deformations occurring near the pile close to failure, the updated mesh option is used in all cases with and without imperfections for the column installation and loading phases.

For the 3D FEM reference model, the same parameters and settings have been considered, leading automatically to much more elements in the model (2849 in the axisymmetric reference model and 138233 in the 3D one). Only the height of the soil volume with the coarseness factor equal to 0.5 is extended by one meter under the column tip in the 3D case in order to reach a mesh quality as good as in the axisymmetric case. The cylindrical volume of the column is modelled using the extruding function of Plaxis with a cross section defined from arc segments of 5° , leading to a very smooth surface. It is checked that the axisymmetric and 3D models give very close results for the reference cases.

The influence of the different geometrical imperfections is analysed in terms of effects on the bearing capacity and on the structural capacity. In the FEM model, the bearing capacity is defined as the resistance for a settlement of 10 % of the planned diameter (nominal diameter). Above this settlement value, the results of the FEM calculation are considered not to be reliable anymore. As the usual global safety factor is about 2 for single piles (as presented in section 2.7), the load level is selected as 50 % of the bearing capacity in order to be in the usual serviceability range. The design structural capacity is considered in a simplified way to be equal to 50 % of the compressive strength for single piles considering the order of global safety for concrete according to EN 1992-1-1 (2004-2010). As in ASIRI (IREX 2012) for inclusions in the domain 1 (see section 2.7), no tension is allowed in the column section.

6.2.2 Diameter reduction over whole column length

Usual piles have in general a diameter of 1 to 2 m, while EN 14199 (2015) indicates diameters smaller than 30 cm for micropiles, ASIRI (IREX 2012) mentions 25 to 80 cm for rigid inclusions and the CSV-guideline (DGGT 2002) values of 12 to 20 cm. For the decrease of the diameter, tolerances are not mentioned in the applicable standards and recommendations. For inclusions, diameter increases should be avoided, since this could lead to increased attracted load and negative skin friction force in the upper part of the columns (maximum tolerated increase of 30 % according to ASIRI).

A diameter decrease corresponds to a loss of shaft surface and of and cross section surface of the pile over the whole length (Fig. 6.12).

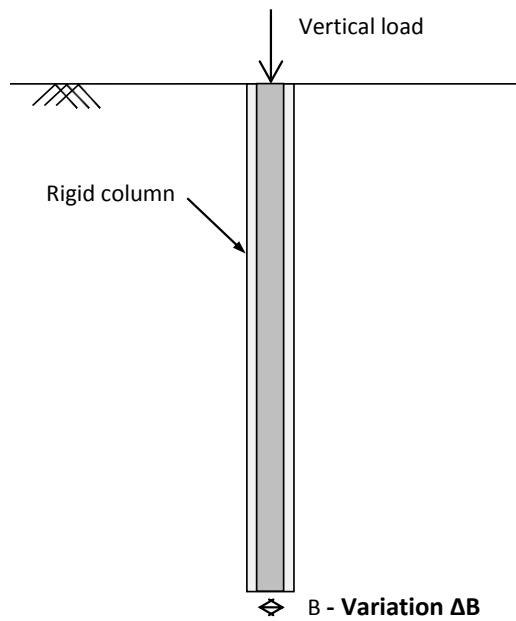


Fig. 6.12 Diameter imperfection for analytical study

This has an impact on the skin friction resistance, as well as on the tip and structural resistances. By simple analytical calculations of the area involved, the loss of resistances for different diameters is presented in Fig. 6.13 for a diameter reduction over the whole length of 1 and 10 cm. For nominal diameters of more than 80 cm, the resistance loss remains lower than 20%. The consequences become much higher with smaller diameters, reflecting a high sensitivity to diameter imperfections.

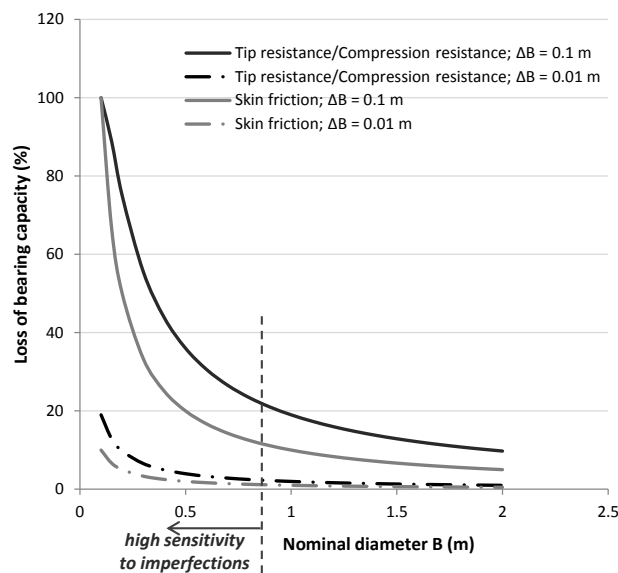


Fig. 6.13 Loss of resistance due to diameter variation over whole height from analytical study

A diameter decrease causes theoretically a diminution of the buckling load as well, if combined with a certain small initial curvature which always exists in practice. However, in the case of non-steel-reinforced mortar or concrete, this theoretical buckling load is generally much higher than the load exceeding the structural resistance (see below section 6.2.5). This means that for the column studied here, the buckling is not the decisive failure mode.

With regard to the axisymmetric FEM calculations, the load-settlement curves calculated with the 2D FEM model for different diameters are calculated with imposed displacements up to a settlement of $B/10$ (Fig. 6.14). The bend in the curves corresponds to the full mobilisation of the skin friction. For the case of the column with 30 cm diameter, the total skin friction resistance is around 320 kN and the tip resistance around 60 kN.

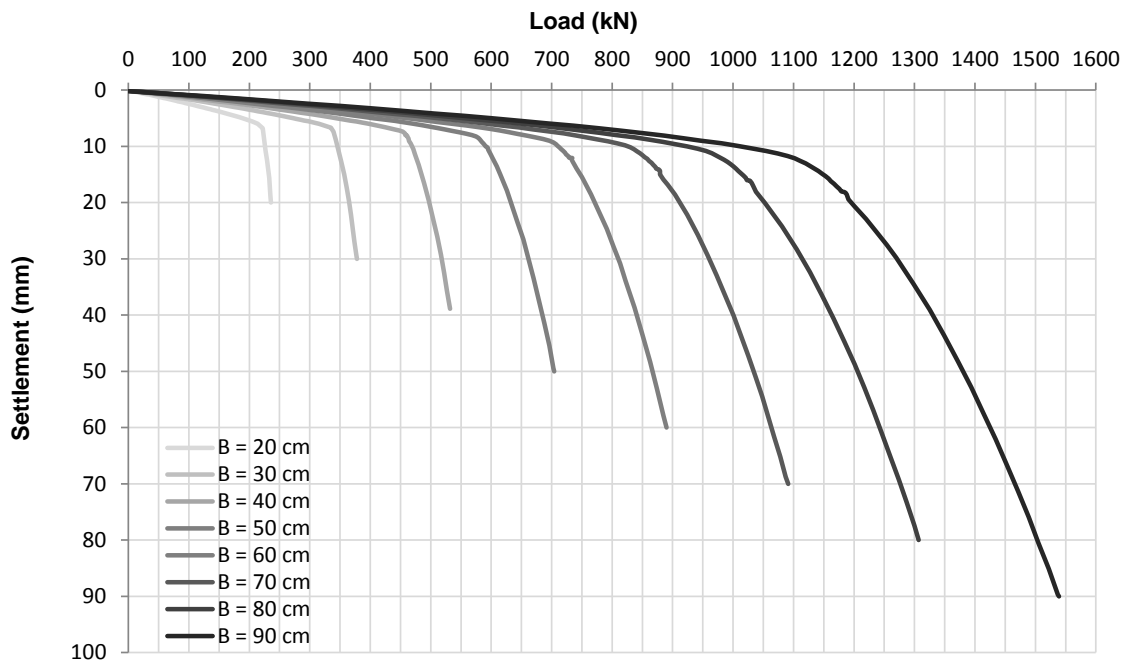


Fig. 6.14 Load-settlement curves for different diameters from axisymmetric FEM analysis

For diameter reductions of 10 cm, the results are presented together with the analytical results in Fig. 6.15: the loss lies between the analytical results for skin friction and tip resistance and remains closer to the skin friction case. This confirms that the resistance of the column comes mainly from skin friction (floating column). The settlement increase under the load level in the serviceability range (50 % of bearing capacity) is shown in Fig. 6.16. It becomes significant for diameters smaller than 50 cm with an increase of settlement of 20 to 50 %.

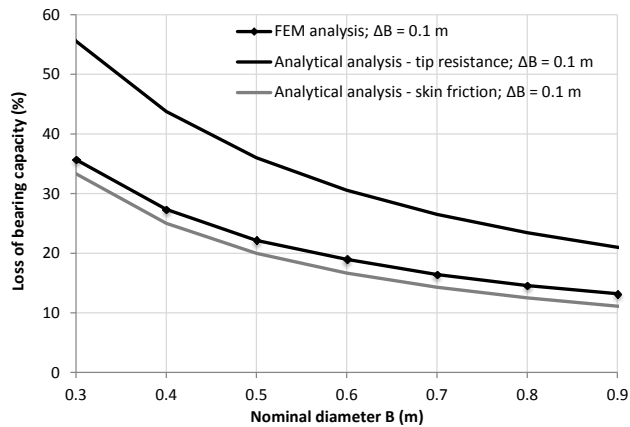


Fig. 6.15 Loss of bearing capacity due to a diameter reduction of 10 cm from axisymmetric FEM analysis compared to analytical results

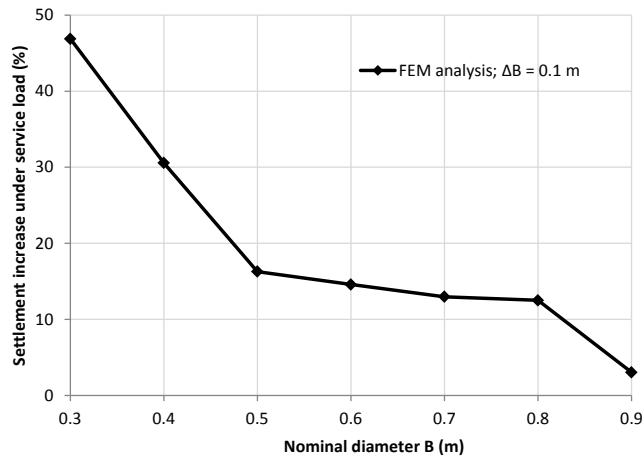


Fig. 6.16 Settlement increase under service load due to a diameter reduction of 10 cm from FEM analysis

The effect of a diameter reduction over the whole length is thus, as expected, a reduction of bearing capacity and structural capacity, with a significant settlement increase under the service load for diameters smaller than 50 cm.

6.2.3 Necking and bulging

The effect of necking and bulging imperfections cannot be represented correctly by simple analytical calculations. A necking would however in any case lead to a reduction of the structural bearing capacity, as shown in Fig. 6.13.

The details of the necking and bulging imperfections at 3 different depths ($0.25 \cdot D$, $0.5 \cdot D$ and $0.75 \cdot D$) for the FEM modelling are given in Fig. 6.17. The value of the diameter reduction or increase is equal to $\Delta B = 0.05$ m for the columns with 30 cm, 40 cm and 60 cm planned diameter.

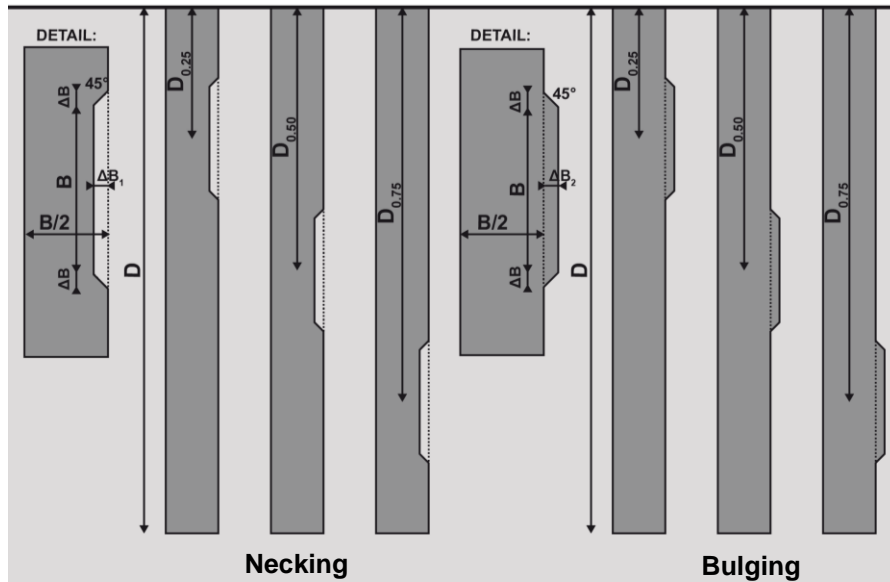


Fig. 6.17 Necking and bulging imperfection for axisymmetric FEM analysis

For this imperfection type, the interface is redefined following locally the shape of the necking or bulging. The calculation is made with imposed displacements up to a settlement of 10 % of the nominal diameter.

As expected, the main issue with the necking is an increase of stresses in the column and thus a possible failure in terms of structural capacity. The case with 30 cm planned diameter is the only case where the whole column cross section fails, leading to an abort of the calculation. This calculation is thus carried forward with the isotropic linear elastic model in the column in order to see the development of the stresses (Fig. 6.18). The increase of the stresses occurs first at the corner of the necking zone as shown in Fig. 6.18.

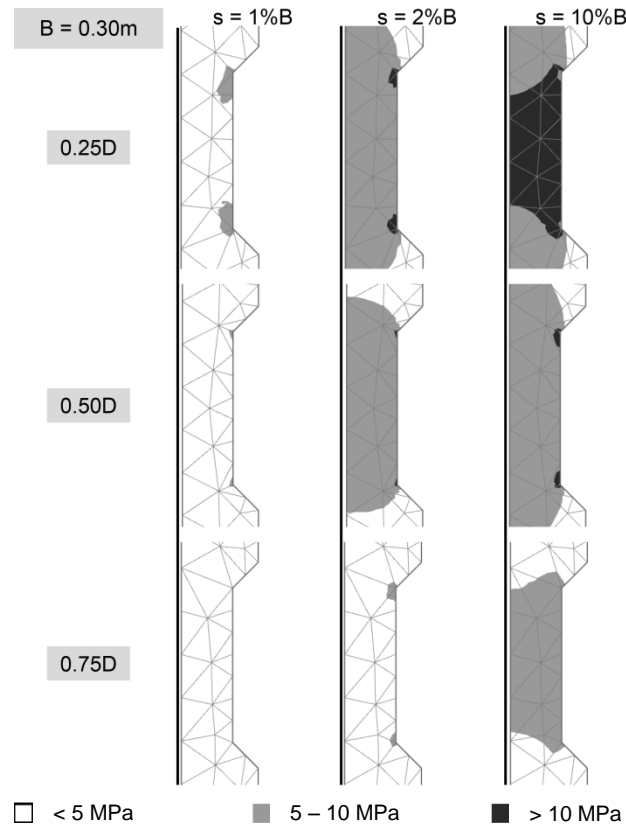


Fig. 6.18 Vertical stress in necking zone from axisymmetric FEM analysis for $B = 30\text{ cm}$

The stress level for the different planned diameters (30, 40 and 60 cm) and for the different positions of the necking is presented in Table 6.1.

Table 6.1 Stress level at the corner of the necking for different planned diameters and necking position from axisymmetric FEM analysis

		Settlement level								
		0.30 m*			0.40 m			0.60 m		
		1% B	2% B	10% B	1% B	2% B	10% B	1% B	2% B	10% B
Position	0.25·D	5-10 MPa	> 10 MPa	> 10 MPa	5-10 MPa	5-10 MPa	> 10 MPa	5-10 MPa	5-10 MPa	5-10 MPa
	0.50·D	< 5 MPa	5-10 MPa	5-10 MPa	< 5 MPa	5-10 MPa	5-10 MPa	< 5 MPa	5-10 MPa	5-10 MPa
	0.75·D	< 5 MPa	< 5 MPa	< 5 MPa	< 5 MPa	< 5 MPa	< 5 MPa	< 5 MPa	< 5 MPa	< 5 MPa

< 5 MPa
 5 - 10 MPa
 > 10 MPa

Tension stresses

* linear elastic calculation

The load-settlement curves of the linear elastic calculated column (column with higher concrete quality for example) for example with a planned diameter of 30 cm with necking and with bulging are presented in Fig. 6.19. For all diameters, the settlement

behaviour remains the same as without imperfections for usual service loads. Both bulging and necking lead to an increase of the column bearing capacity. This effect is more important for larger depths of the imperfection. The increase of bearing capacity for the bulging case can be explained by the larger shaft surface and thus by the larger total skin friction. The increase of bearing capacity in the necking case is at first unexpected. It can be explained by an increase of the soil stresses due to the column pressing on the soil in the necking corner. This leads to a vertical reaction in the necking corner and to a higher skin friction in the whole necking zone. This effect is reflected by the directions of the principal stresses shown in Fig. 6.20, similar in the bulging and in the necking case. This favourable effect may explain the increased bearing capacity of piles with helical shape (for example Atlas piles described in EA-Pfähle, DGGT 2012). However, it acts only very locally and would not be that pronounced or would lead to a decrease of bearing capacity if the necking extended over a larger height.

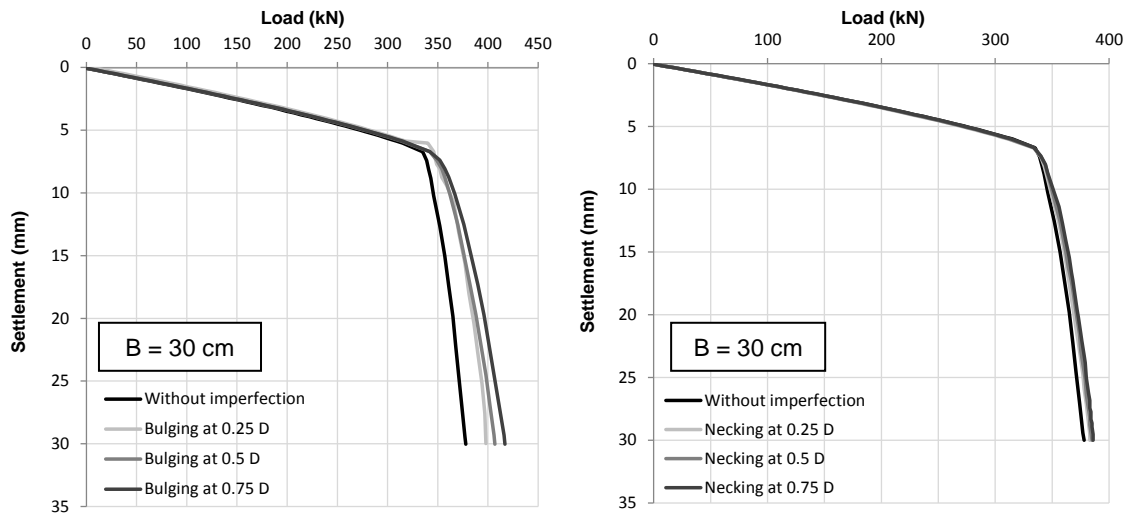


Fig. 6.19 Load-settlement curves with bulging and necking from axisymmetric FEM analysis for $B = 30$ cm

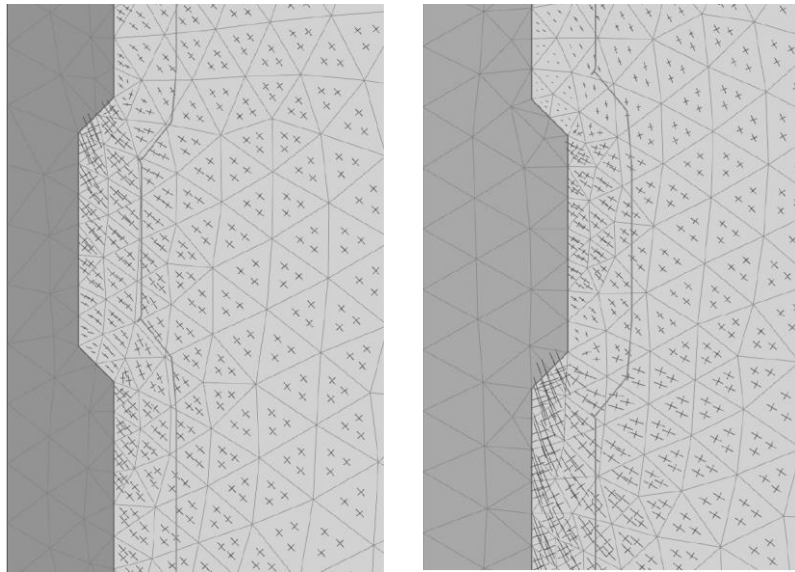


Fig. 6.20 Directions of principal stresses in the soil with bulging and necking from axisymmetric FEM analysis for $B = 30$ cm

The increase of bearing capacity is presented for the different column diameters in Fig. 6.21.

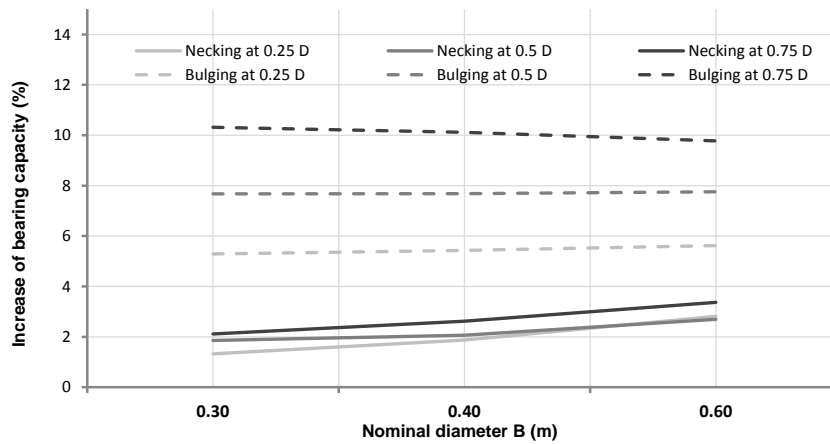


Fig. 6.21 Increase of bearing capacity with bulging and necking from axisymmetric FEM analysis

The only critical case is thus the necking in terms of structural failure. Both bulging and local necking lead to a slightly increased bearing capacity due to a stress concentration in the imperfection zone. A necking over a large height would lead to a similar effect to a diameter reduction over the whole column length (see section 6.2.2).

6.2.4 Inclination

The inclination tolerance for vertical piles is 2 % for bored piles after EN 1536 (2010) and for micropiles after EN 14199 (2015) and 4 % for displacement piles after EN 12699 (2015). ASIRI (IREX 2012) and the CSV-guideline (DGGT 2002) prescribe a maximum value of 2 % for rigid inclusions.

The effect of an unintentional inclination can be represented by an additional transversal load (Fig. 6.22). For the conciseness of the following calculations, the moment $M(z)$ is taken here as being positive for tension at the “right” side of the column (z defined here along the column axial axis).

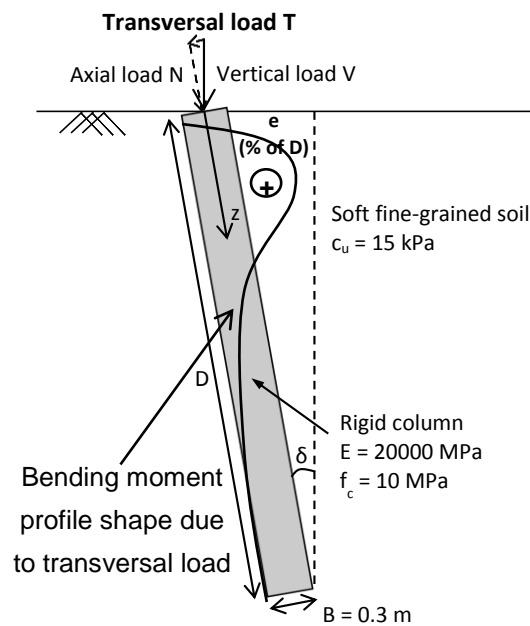


Fig. 6.22 Inclination imperfection with parameters for analytical study

The system is calculated analytically after Winkler (in Philipponnat and Hubert 2000) for an embedded rod with elastic support in the case with free head and horizontal load. (Eq. 6.3) gives the bending moment along the column following Winkler’s theory. The shear force is in general not damaging.

$$M(z) = H \cdot l_0 \cdot e^{-\frac{z}{l_0}} \cdot \sin\left(\frac{z}{l_0}\right) \quad (\text{Eq. 6.3})$$

$$\text{With: } l_0 = \sqrt[4]{\frac{4 \cdot E \cdot I}{K_f}} \text{ (transfer length)}$$

The resulting maximum moment M is located not very far from the column top (Fig. 6.22), at a depth of $\frac{\pi}{4} \cdot l_0$, equal to 1.8 m in the present case. The axial load at this shallow depth is assumed to be equal to the one at the column head. The reaction modulus is estimated as $K_f = 80 \cdot c_u = 1200$ kPa (Vogt et al. 2009). The maximum moment is equal to $M_{\max} = M\left(\frac{\pi}{4} \cdot l_0\right) \cong T \cdot l_0 \cdot 0.32$. Considering that $\tan \delta = T/N$ and $\sin \delta = e/D$ (δ is the inclination angle), then $T = N \cdot \frac{e/D}{\cos(\arcsin e/D)}$. Thus the relationship between the maximum moment and the axial load for a given inclination e/D is $M_{\max} = N \cdot \frac{e/D}{\cos(\arcsin e/D)} \cdot l_0 \cdot 0.32$. Note that $\cos(\arcsin(e/D))$ varies from 0.9950 to 0.9999, for e/D varying from 1 % to 10 %.

The minimum normal stress at the edge of the section σ_{\min} depends on the ratio between the moment and the normal axial load at the given level as in (Eq. 6.4) and (Eq. 6.5). Tension appears as soon as the ratio between M and N (equivalent load eccentricity) reaches 1/8 of the diameter. In the example studied here, this happens for an inclination of approximately 5 % (Fig. 6.23).

$$\sigma_{\min} = \frac{N}{A} - \frac{M \cdot B/2}{I} \quad (\text{Eq. 6.4})$$

$$\sigma_{\max} = \frac{N}{A} + \frac{M \cdot B/2}{I} \quad (\text{Eq. 6.5})$$

With $A = \pi \cdot \frac{B^2}{4}$ (cross section area) and $I = \pi \cdot \frac{B^4}{64}$ (moment of inertia)

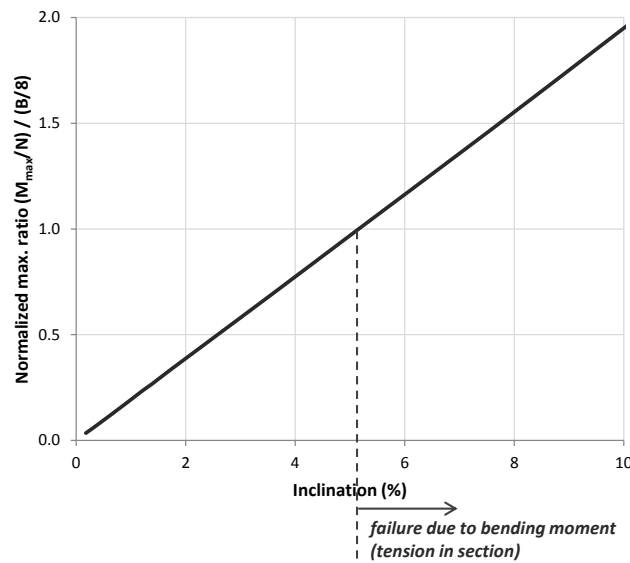


Fig. 6.23 Load section vs. normalized lever arm from analytical study

Inclination levels between 1 % and 10 % are investigated with the 3D FEM (Fig. 6.24). The surfaces at the top and at the bottom of the column remain horizontal, as it would be expected in reality. If the calculation would be made with imposed displacements, the vertical stresses over the cross section would not be uniform due to the asymmetric reaction of the system. The choice made here is thus to impose a vertical uniform stress loading, up to a total load corresponding to a settlement of the column centre equal to 10 % of the diameter in the reference case (without imperfection).

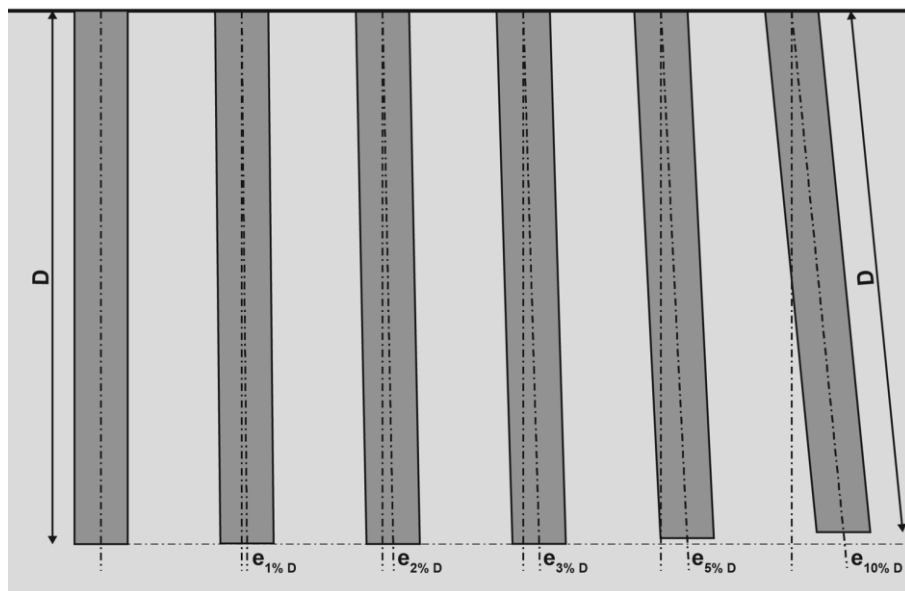


Fig. 6.24 Inclination imperfection for 3D FEM analysis

The inclination leads to a small increase of the bearing capacity, as shown for example for the column with 30 cm diameter in Fig. 6.25. This can be explained by a soil supporting (“passive”) effect on the “left” side (the side working against an overturning of the column), as reflected by the increase of the interface normal stress and skin friction (Fig. 6.26 and Fig. 6.27). The case with a nominal diameter of 30 cm and 10 % inclination could not be calculated up to the full bearing capacity since the entire column section had cracked. For all the other cases, the load-settlement behaviour remains almost the same as in the case without imperfection in the service load range. For the maximum load applied, the settlement difference between the edge and the centre of the column at the top remain below 1 mm for all inclination levels under consideration.

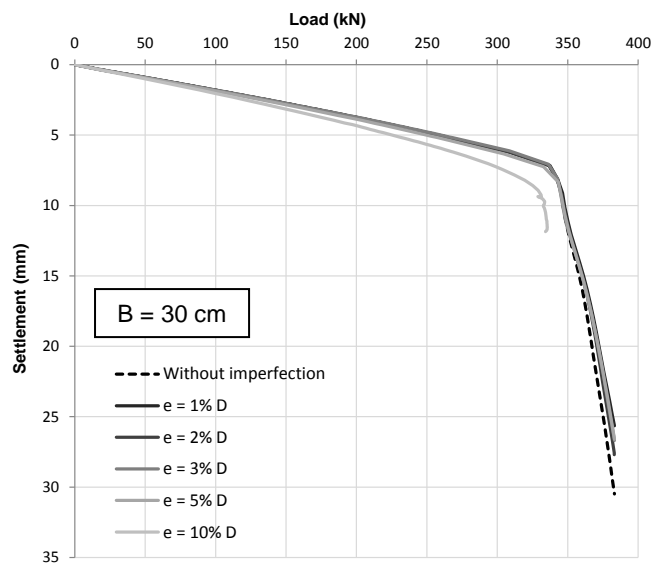


Fig. 6.25 Load-settlement curves with column inclination from 3D FEM analysis for B = 30 cm

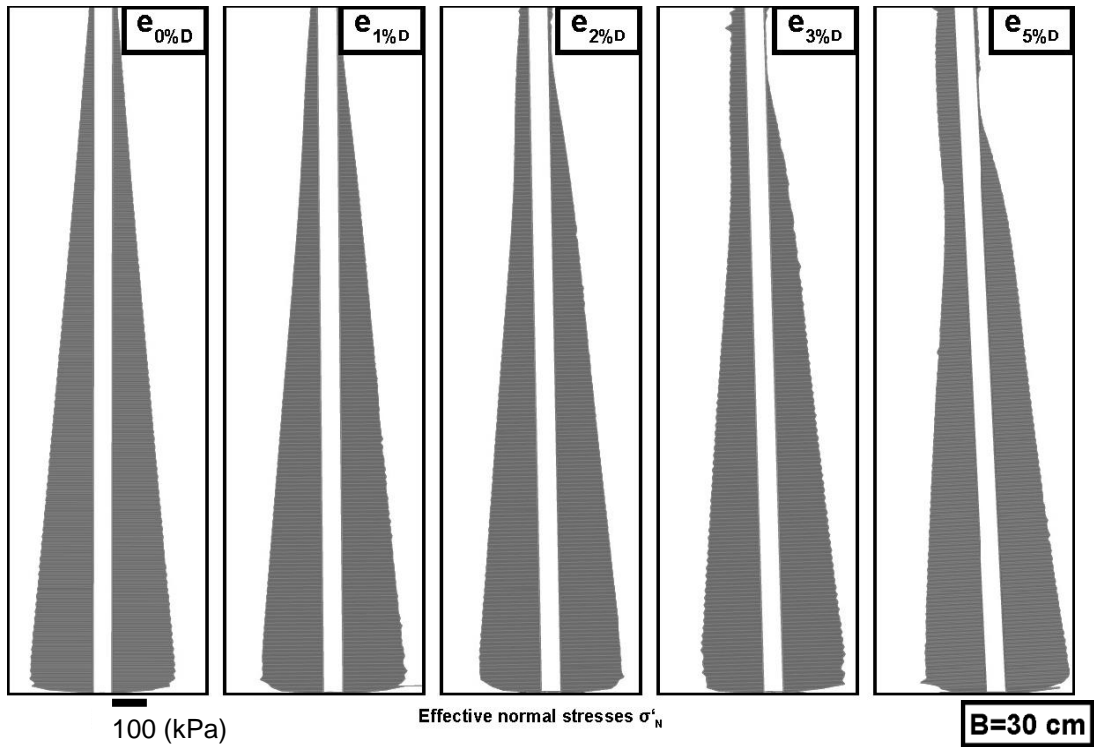


Fig. 6.26 Normal stress in the interface around the inclined columns under the maximum applied load from 3D FEM analysis for $B = 30$ cm

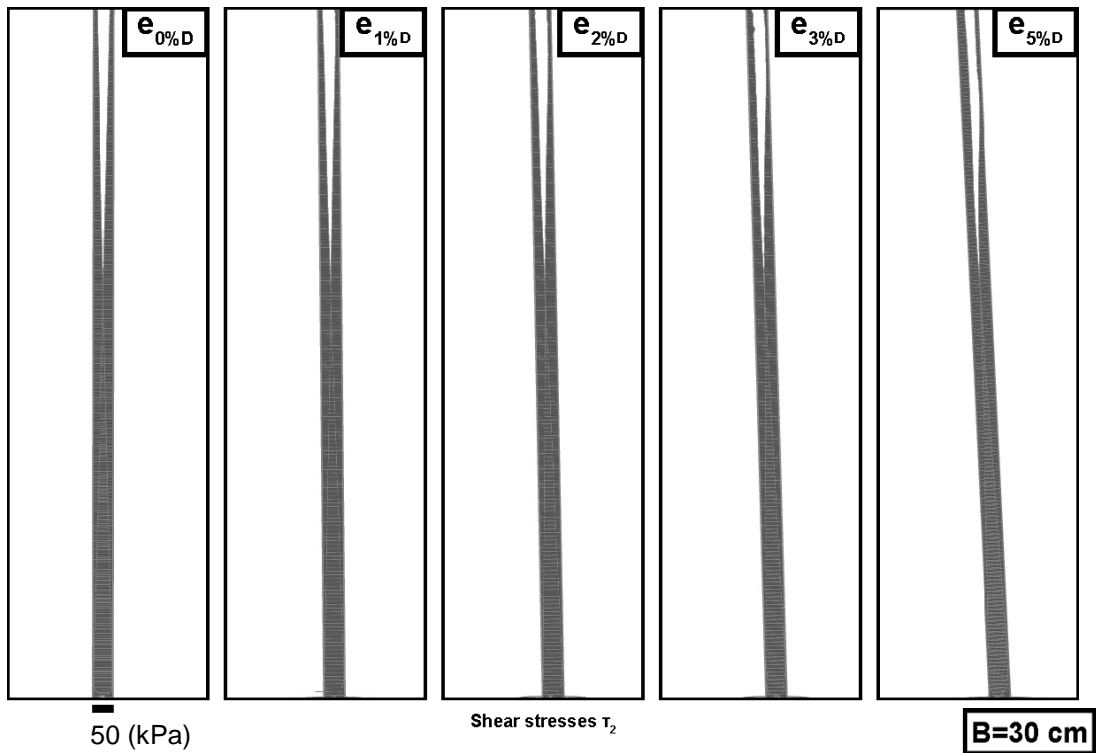


Fig. 6.27 Skin friction in the interface around the inclined columns under the maximum applied load from 3D FEM analysis for $B = 30$ cm

The vertical stresses development is shown for the 30 cm column in Fig. 6.28. The bending moment is calculated additionally using the structural forces option of the Plaxis 3D.AE version (Plaxis 2015). The moment distribution with depth is consistent with the moment distribution of the analytical calculations. For the 30 cm column with an inclination of 5 %·D, the maximum moment calculated with the FEM (16.5 kNm at 1.5 m depth) is very close to the result with the analytical method of $M_{\max} = M\left(\frac{\pi}{4} \cdot l_0\right) \cong T \cdot l_0 \cdot 0.32 \cong 14 \text{ kNm}$. As in the analytical method, tension stresses appear for the inclination of 5 %·D.

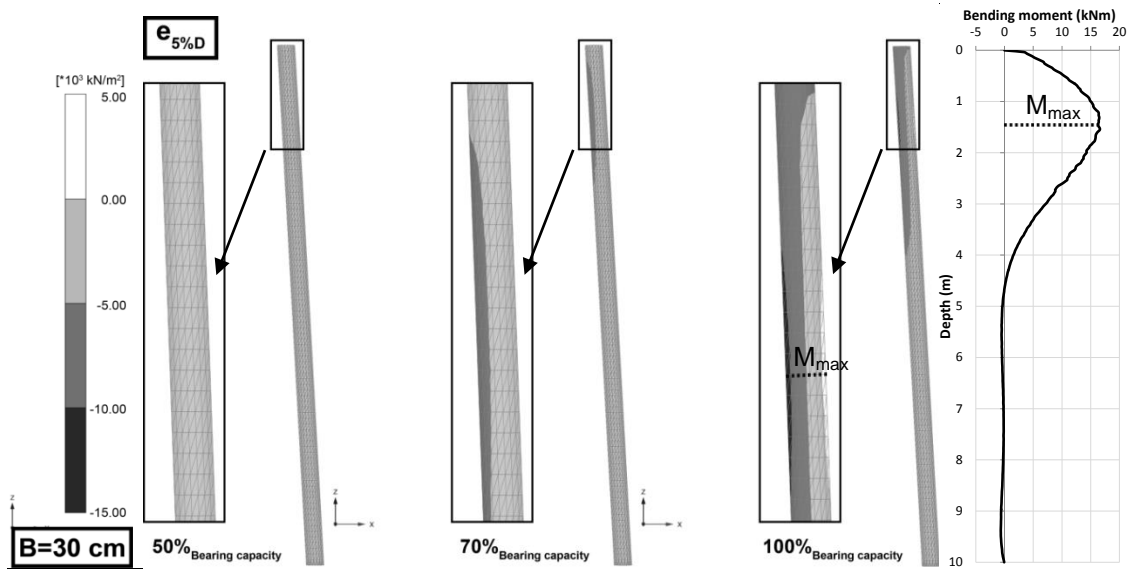
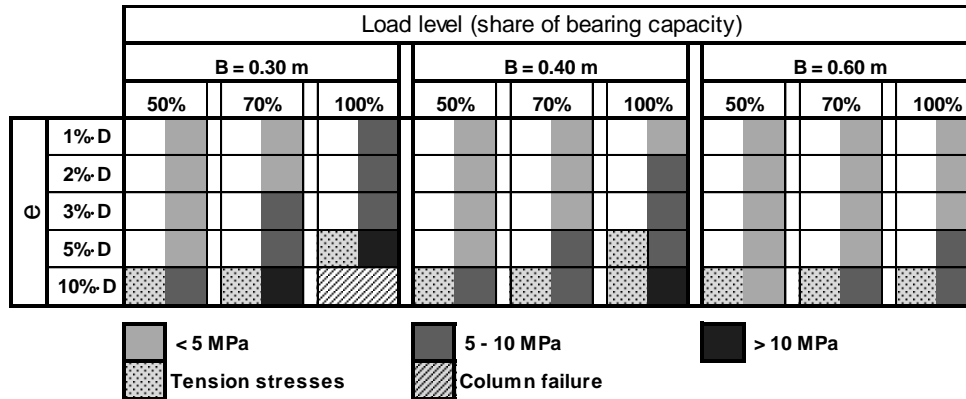


Fig. 6.28 Vertical stress (in Plaxis: compression negative) and bending moment in the inclined column from 3D FEM analysis for B = 30 cm

In Table 6.2, the stress level is presented for different column diameters and inclination levels. It can be seen that for inclinations higher than 5 %, tension stresses or high compressive stresses appear. This effect is more significant for smaller column diameters.

Table 6.2 Stresses at the edge of the column section for different diameters, settlement levels and inclination imperfections from 3D FEM analysis



In any case, an inclination up to 3 % of the length can be tolerated by the column. This corresponds to a high maximum deflection of 50 % to 100 % time the column diameter for $D = 10$ m. It is very unlikely that such an inclination level is reached in practice.

6.2.5 Curvature

For usual pile diameters, the soil support ensures in general the stability against buckling, even for relatively soft soils and with an initial curvature (Fig. 6.29). EN 1997-1 (2004-2009-2013) prescribes a buckling check for slender piles passing through very weak soils, specifying that this is in general not necessary for $c_u > 10$ kPa. However, this check should be made even for higher undrained shear strength values considering the current state of the art (Vogt et al. 2009). ASIRI (IREX 2012) prescribes a verification for diameters smaller than 30 cm and for a soil pressuremeter modulus smaller than 3 MPa (approximately $c_u = 30$ kPa) over a minimum height of 5 diameters.

Theoretical calculations of the buckling load for micropiles with the second order theory considering the soil lateral support are proposed by Sovinc (1981), Meek (1996), Wimmer and Ofner (2006) and Vogt et al. (2009). Pichler (2014) proposed a finite element analysis of the buckling of micropiles, however in a simplified form in 2D plane strain. In the scope of the FOREVER project (IREX 2004), Youssef (1994) proposed in addition a determination of the so-called “prebuckling” effect for micropiles. This corresponds to the effect of the initial curvature on the internal forces before the theoretical buckling load is reached. With respect to buckling considerations, unreinforced concrete columns differ from micropiles (the section of which is mainly made of steel): larger diameter, smaller compressive strength and negligible tension

resistance. A calculation of the additional internal forces due to the initial curvature in unreinforced concrete columns is proposed by Alber (2007a, 2013). These methods consider the horizontal soil support, but none of these represent the vertical soil support under the curved column head (as in the inclination case in 6.2.4). The methods of Vogt et al. (2009) and of Alber (2007a, 2013) can be applied for the study of the reference unreinforced concrete column (with 30 cm diameter), for different initial curvature imperfections (Fig. 6.29). The shape of the curvature in Fig. 6.29 corresponds to one possible case where the half-wave would be equal to the full column length. The buckling profile depends on the system parameters and on the calculation assumptions. Second order calculation methods consider that the initial imperfection is located at the most unfavourable position for the corresponding column geometry and for the corresponding support properties.

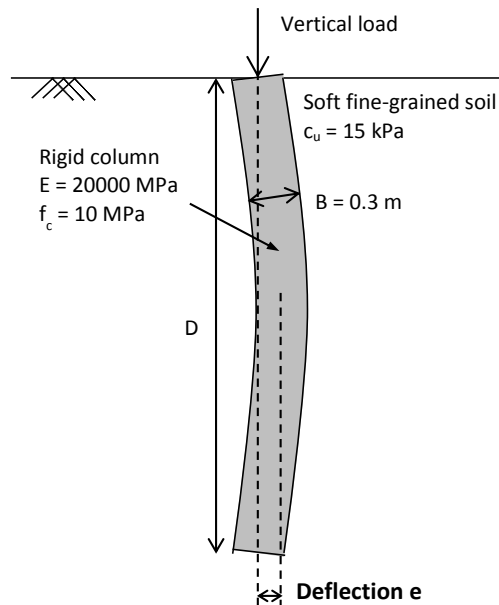


Fig. 6.29 Curvature imperfection with parameters for analytical study

The main differences between both methods are the following:

- Vogt et al. (2009) consider an infinitely long pile as a simplification since the buckling length develops in most cases independently from the boundary conditions for embedded columns, whereas Alber (2007a, 2013) considers the real finite column length;
- Alber (2007a, 2013) limits the calculation to the domain of elastic soil reaction, whereas Vogt et al. (2009) allows for an elastic-plastic soil reaction.

For both approaches, the soil reaction modulus is calculated as $80 \cdot c_u = 1200 \text{ kPa}$. The horizontal limit displacement for an elastic soil reaction estimated as $B/10$ is not exceeded in both cases. The decisive buckling mode corresponds to a half-wave length of half the total column length with the method of Alber. The half-wave length varies between 5 m and 6.5 m with the method of Vogt et al. (2009) considering an infinite total column length. The most unfavourable position of the deflection is thus located at approximately one quarter of the column length. The reduction of the normal load with depth due to skin friction is not considered. The theoretical buckling loads for both methods are presented with the normalized deflection or alternatively with the curvature radius (Eq. 6.6) together with the geotechnical bearing capacity (see section 6.2.2) in Fig. 6.30. The buckling load is smaller with the method of Vogt et al. (2009). However the geotechnical bearing capacity is always much smaller than the calculated buckling loads; thus the geotechnical failure is the decisive failure mode for the selected parameters.

$$e = r - \sqrt{r^2 - \left(\frac{D}{2}\right)^2} \quad (\text{Eq. 6.6})$$

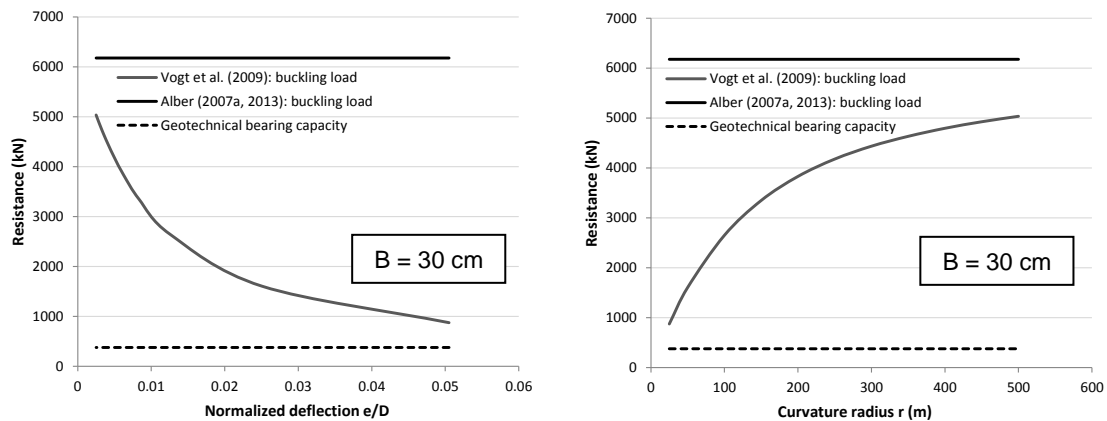


Fig. 6.30 Buckling load and geotechnical bearing capacity in function of curvature imperfection for $B = 30 \text{ cm}$

The “pre-buckling” stresses due to the initial imperfection after Alber are presented in Fig. 6.31 for a vertical service load applied of 189 kN corresponding to half of the geotechnical bearing capacity. For the service load, the effect of the initial deflection on the stresses leads to a cracking in the column material for deflections larger than approximately 1.5 % of the column length or a curvature radius smaller than 100 m.

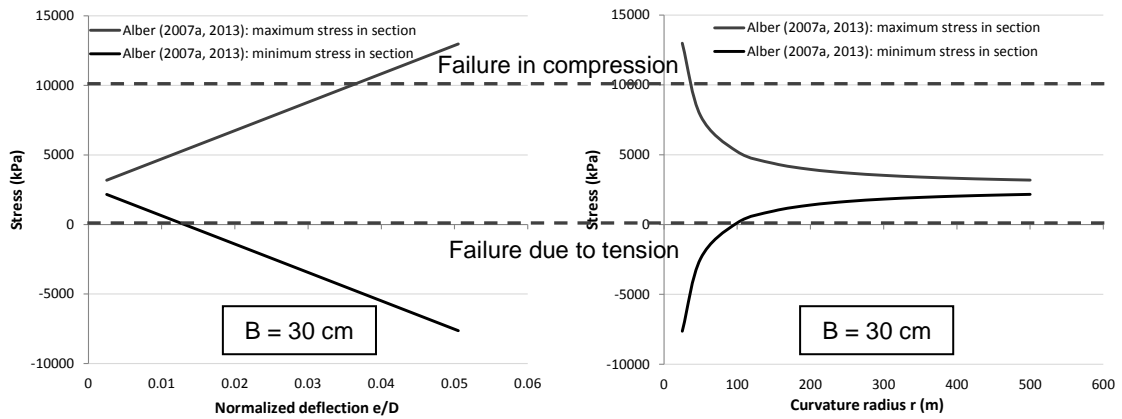


Fig. 6.31 Stresses in section in function of curvature imperfection for service load of 189 kN (half of bearing capacity) for B = 30 cm

The 3 cases modelled with the 3D FEM method are shown in Fig. 6.32. If the calculation would be made with imposed displacements, the stresses would not be uniform due to the asymmetric reaction of the system. The choice made here is thus to impose a vertical uniform stress loading, up to a total load corresponding to a settlement of the centre equal to 10 % of the diameter in the reference case (without imperfection). The inconvenient of the single-order FEM used is that buckling effects with different buckling shapes cannot be modelled.

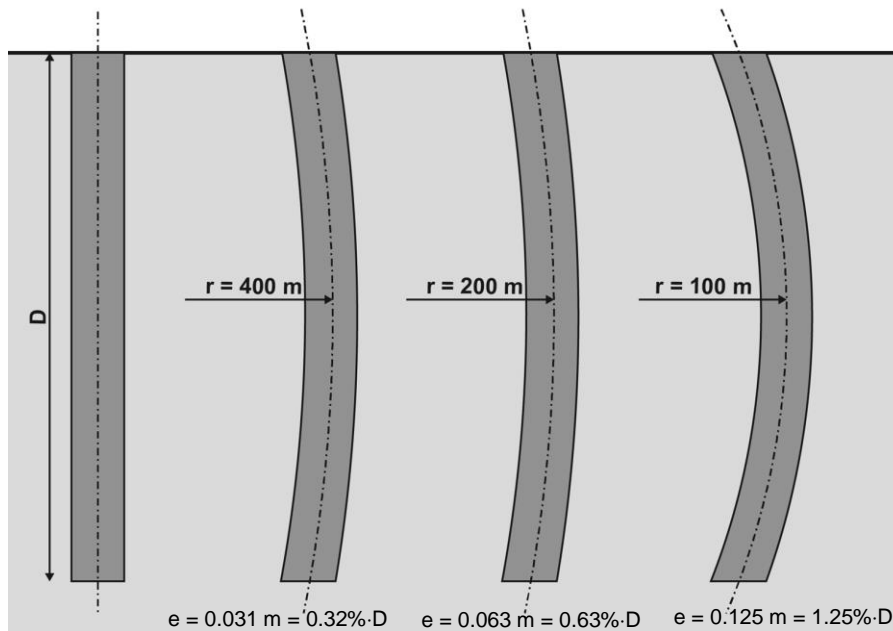


Fig. 6.32 Curvature for 3D FEM analysis

For the modelling of this complex column shape, the discretization angle of the circular column section has to be increased to 10° (linked to the Plaxis meshing possibilities). The column is modelled along its length by 4 polyline segments with the same curvature radius. The interface prolongation at the pile tip is modelled as one separated segment.

The influence of the curvature on the load-settlement behaviour is almost negligible as shown in Fig. 6.33 for the column with 30 cm diameter. The slight increase in bearing capacity can be explained by a soil support effect in the upper part of the column similarly to the inclination case. For the maximum load applied, the settlement difference between the edge and the centre of the column at the top remain below 0.5 mm for all curvature levels under consideration.

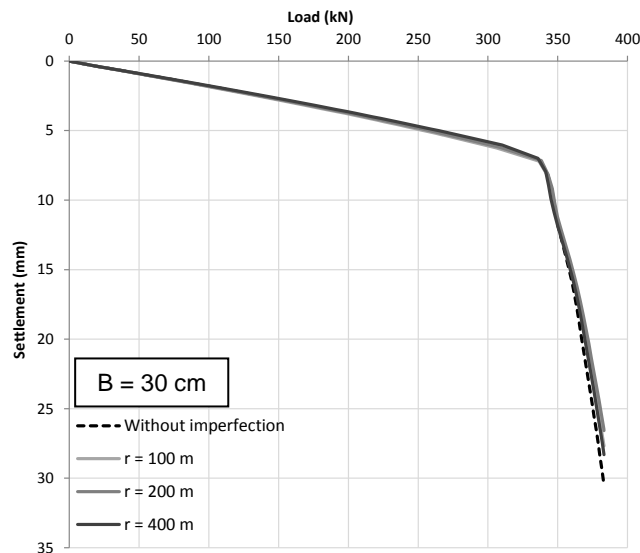


Fig. 6.33 Load-settlement curves with column curvature from 3D FEM analysis for $B = 30$ cm

With the FEM, the maximum moment is found near the top of the column, similarly to the inclination case (section 6.2.4), as presented in Fig. 6.34 for the highest curvature of 100 m. However, for the modelled curvature radiuses, no tension force appears. The shape of the moment curve is similar to the one for the inclination case; only the moment values are not as high (no tension forces).

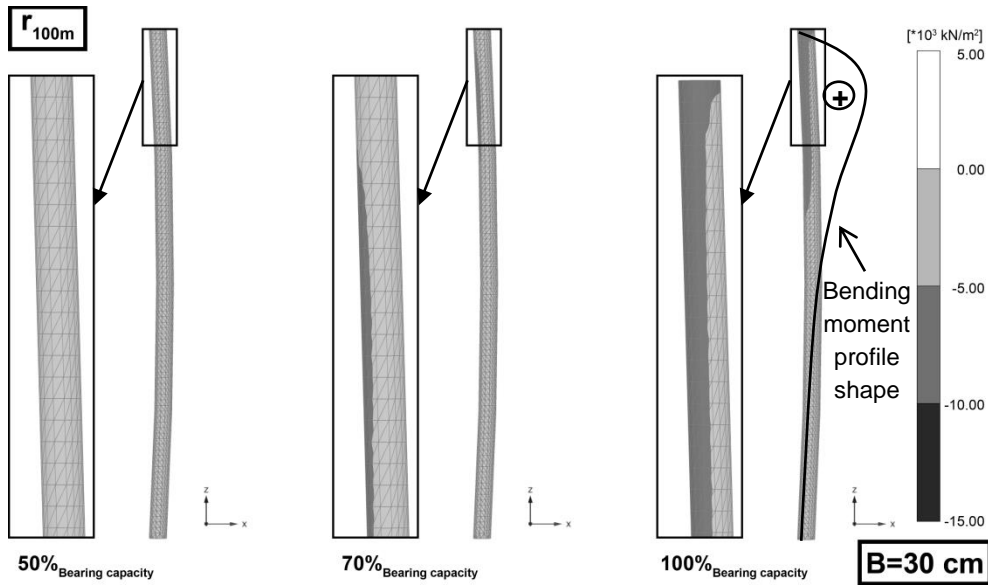


Fig. 6.34 Vertical stress in the curved column from 3D FEM analysis for $B = 30$ cm (in Plaxis: compression negative)

For all modelled cases, the stresses remain smaller than the compressive strength of 10 MPa (Table 6.3).

Table 6.3 Stresses at the edge of the column section for different diameters, settlement levels and curvatures from 3D FEM analysis

		Load level (share of bearing capacity)												
		B = 0.30 m			B = 0.40 m			B = 0.60 m						
		50%	70%	100%	50%	70%	100%	50%	70%	100%				
r	100 m													
	200 m													
	400 m													

	< 5 MPa		5 - 10 MPa		> 10 MPa
	Tension stresses				

Both theoretical and FEM calculations reflect a critical point located at quite shallow depth. However, the theoretical calculation considers neither a vertical soil support nor a reduction of axial load in the column with depth. The FEM calculations performed present the inconvenient of not taking on board second order effects. Nevertheless, considering the strong attenuating effect from the soil with depth like in the inclination case, the conclusion is that the upper part of the column is the most impacted. This is particularly damaging for inclination radiuses smaller than 100 m (deflection larger than 1.25 % of the column length meaning 2.5 % of the half column length).

6.2.6 Load eccentricity

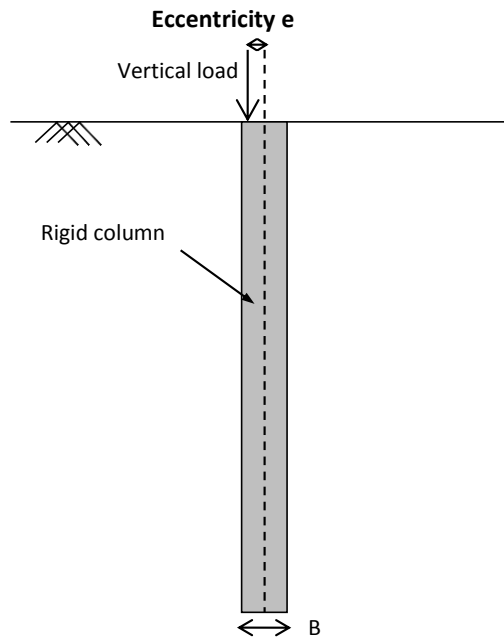


Fig. 6.35 Load eccentricity for analytical study

The tolerated axis offset or load eccentricity (Fig. 6.35) is 10 to 15 cm for bored piles depending on the pile diameter (EN 1536 2010) and 10 cm for displacement piles (EN 12699 2015), and 10 cm as well for micropiles (EN 14199 2015) or in the CSV-guideline (DGGT 2002). ASIRI (IREX 2012) recommends values of 5 to 10 cm under footings, where the load is quite concentrated and thus an offset has more consequences in terms of bending moments, and 20 cm under large loading areas where the vertical load can redistribute in the column mesh.

An eccentricity at the top is much more damaging than a curvature deep in the soil, because the full lever arm is applied on the top without any attenuating effect of the supporting soil. Independently from the load level, an eccentricity larger than $B/8$ leads to tension and thus in general to the cracking of the top of the unreinforced column.

For the 3D FEM analysis, load eccentricities of $B/20$ to $B/7$ are investigated (Fig. 6.36). The eccentricity is represented with a load which is increasing linearly. The system is calculated up to a load corresponding to a settlement of 10 % of the diameter in the reference case (without imperfection).

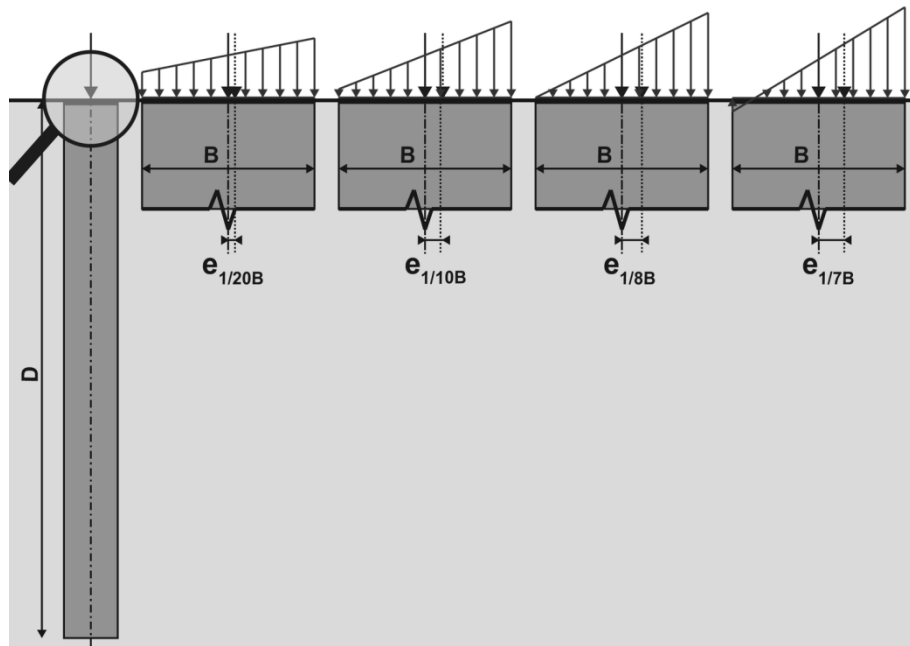


Fig. 6.36 Load eccentricity for 3D FEM analysis

No influence of the load eccentricity can be noted on the load-settlement curves (Fig. 6.37). This reflects a similar mobilisation of skin friction and tip resistance with and without eccentricity, denoting that the stresses redistribute most probably already at the very top of the column. For the maximum load applied, the settlement difference between the edge and the centre of the column at the top remain below 0.6 mm for all eccentricity levels under consideration.

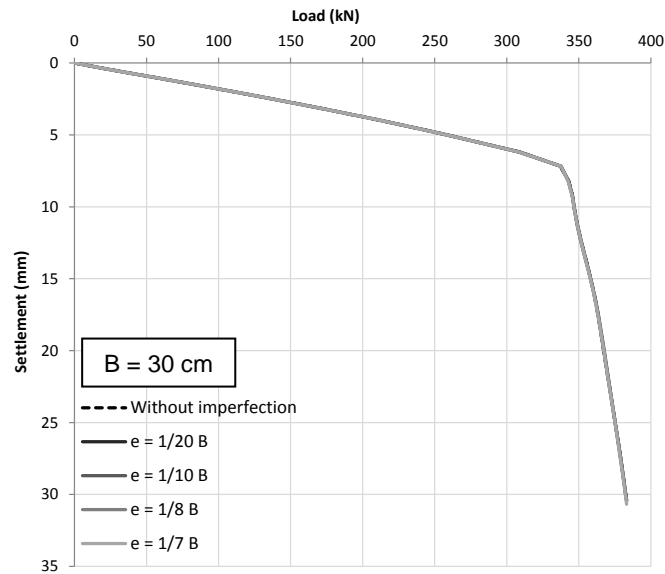


Fig. 6.37 Load-settlement curves with load eccentricity from 3D FEM analysis for $B = 30$ cm

As expected, tension stresses appear at the edge of the column for an eccentricity larger than $1/8$ of the diameter (Fig. 6.38). For the same eccentricity and for high loads, in the case of the column with 30 cm diameter, the compression stresses exceed the compressive strength on the other side of the column.

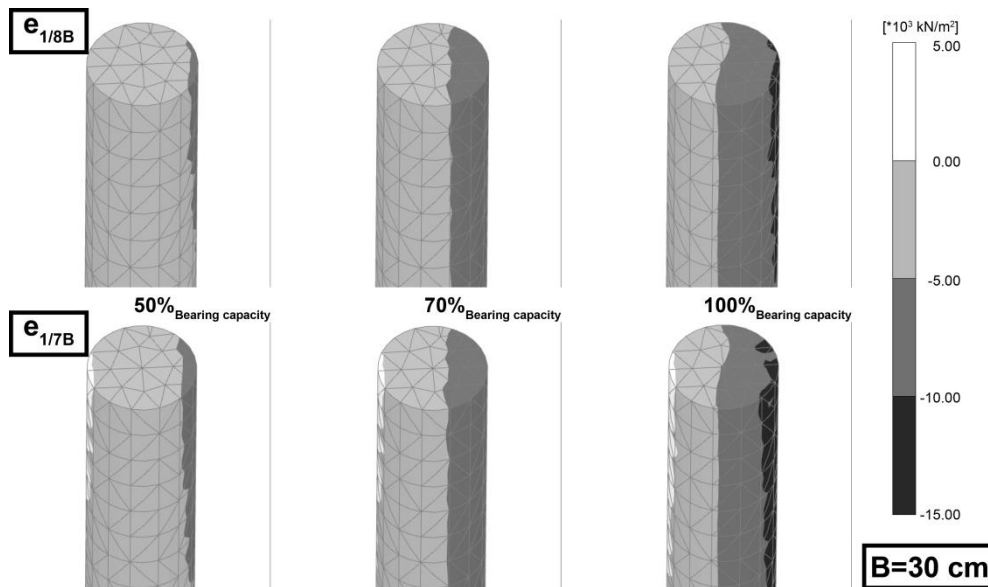
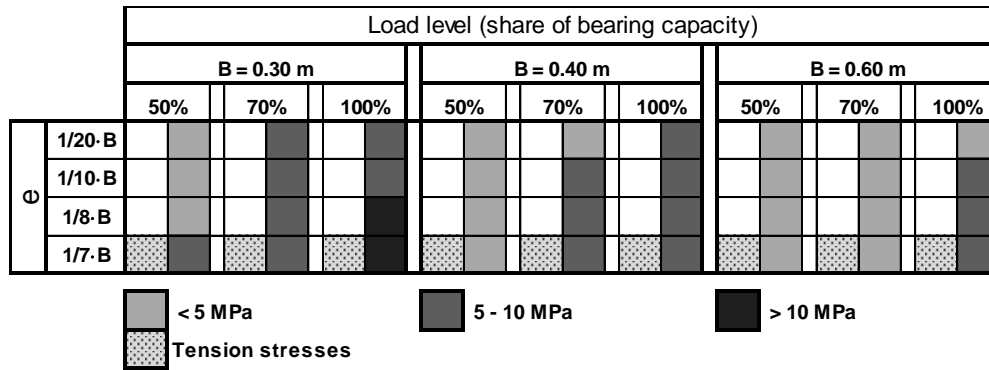


Fig. 6.38 Vertical stress at the top of the eccentric-loaded column from 3D FEM analysis for $B = 30$ cm (in Plaxis: compression negative)

The results are summarized for all diameters in Table 6.4. For all diameters, tension appears for an eccentricity of $B/7$ independently from the load level.

Table 6.4 Stresses at the edge of the column section for different diameters, settlement levels and load eccentricities from 3D FEM analysis



In conclusion, the load eccentricity has mainly a local effect with an exceeding of the allowable stresses at the column head for eccentricities larger than $1/8$ (0.125) of the diameter. The overall load-settlement behaviour is not affected, meaning that the soil resistance remains mainly vertical.

6.3 Comparison and recommendations

6.3.1 Column material imperfections

Following the study of the unit cell, and as expected, the column material type and modulus have a decisive influence on the load distribution and on the differential settlement between the column and the soil in combined systems. The trends shown in 2.5 and 2.6 are confirmed (Table 6.5). The present study extends the published results by considering bonded and coarse-grained columns together. It is shown here that bonded and coarse-grained column material cannot be considered, calculated and designed in the same manner. In the case of bonded columns, there is no influence of the modulus for a modulus ratio between column and soil higher than 500. This denotes quite a monolithic behaviour governed by positive skin friction and tip resistance with only vertical displacements of the column under vertical loads. Considering the present study and the results of Kirsch (2004), an optimum modulus ratio of generally 40 to 50 is found for coarse-grained columns.

Table 6.5 Influence of column material type and modulus according to the present study and to the published results

	Type of column	Load level	Modulus varied	Qualitative change noticed for:		
				$E_{oed,column}$ (MPa)	$E_{oed,soil}$ (MPa)	$E_{oed,column}/E_{soil,oed}$
Present study	coarse-grained	50 kPa	$E_{oed,column} = 80 - 22200$ MPa	500	6,5	40
	bonded			5000	15	500
Kirsch (2004)	coarse-grained	75 - 200 kPa	$E_{oed,soil} = 0.5 - 20$ MPa	100	2	50
Han & Gabr (2002)	bonded	70 kPa	$E_{Young,column} = 30 - 30000$ MPa	1000	approx. 1	1000
Gangakhedkar (2004)	bonded	60 kPa	$E_{Young,column} = 10 - 30000$ MPa	1000	approx. 5	200
EBGEO (2010)	coarse-grained (geotextile coated)	/	/	/	/	subgrade reaction ratio: 50-75
	bonded			/	/	subgrade reaction ratio: 75

These results can be interpreted in terms of material imperfection. For example, if the column modulus is smaller than planned, the total settlement will be larger than expected, but on the other side the differential settlements will be smaller, reducing thus the forces in the slab. This would lead to a reduction of the column load share as well, compensating thus the possible related decrease of the compressive strength in the bonded column case (see Fig. 6.2). These results would be qualitatively similar for combined systems without LTP.

For the single column case with bonded material, a similar conclusion is expected with a minimum modulus ratio of 500 for typical pile behaviour. Coarse-grained columns are in general not loaded as single columns, but highly loaded stone columns would show a pronounced bulging in the upper part of the column as shown earlier in Fig. 2.45 (Kirsch 2004, Bohn 2012).

For the bonded column case which is the focus of the present work, variations of the column material are not particularly critical as long as the modulus ratio remains above approximately 500. These recommendations are valid for single columns as well as for columns in combined systems. A local defect or the absence or failure of the column material may be much more critical. This question can be treated as geometrical imperfections.

6.3.2 Column geometrical imperfections

Apart from a diameter reduction over the whole length, none of the considered geometrical imperfection has a negative effect on the geotechnical bearing capacity of the single column. There are no increased settlements under service loads either. Bulging, local necking, inclination and curvature lead even to a small increase of bearing capacity thanks to an increased soil support effect due to the imperfection.

Geometrical imperfections concern essentially the structural failure. The most damaging geometrical imperfection types for non-reinforced concrete single columns are a necking in the upper part of the column and a load eccentricity larger than 1/8 of the column diameter. An inclination up to 3 % can be tolerated. Second order analytical calculations and 3D FEM calculations reflected a relatively small sensitivity of single columns to curvature; an initial curvature larger than 100 m poses no problem for all column diameters under consideration.

The effects of all imperfection types considered on structural column failure get more significant with smaller column diameters. A particular sensitivity is observed for column diameters smaller than 40 cm, corresponding to the order of usual diameter for rigid inclusions.

The results can be interpreted and partially extended to combined cases with or without LTP, under single footings or under large loading areas:

- a column diameter reduction would lead to a lower load attracted in the column (load redistribution in the column group or in the grid) and thus to a reduced risk of column breaking, due to the reduced column reaction in comparison with the case without imperfections. However, this may lead to increased settlements if several columns are affected, which is decisive since combined systems are often designed based on settlement requirements (see section 2.7). Furthermore, the design of systems like rigid inclusions requires a consideration of all interactions in the system (e.g. positive and negative skin friction). This implies that reliable geometry parameters are required. Thus neither a column necking nor a column bulging are desirable in combined systems;
- an inclination or a curvature would not be more problematic in combined systems than in a single column. The bearing capacity would remain unchanged. The soil support effect would be even increased compared to the single column case, thanks to the loading of the soil at the top of the system, limiting the risks of structural failure;
- the load eccentricity is not really relevant in combined systems since the load redistributes in the system and remains thus approximately centred on the column. The tolerance should depend on this redistribution ability of the system which is directly dependent on the total foundation area. Nevertheless, a position offset may lead to a local increase of settlements or to a differential settlement between the column and the surrounding soil. The extreme case in this matter would be a footing of small dimensions resting on few columns with the loss of one column.

The recommendations from the present work are given in Table 6.6 together with the tolerances from EN 1536 (2010), EN 12699 (2015), EN 14699 (2005), from ASIRI (IREX 2012) and from the CSV-Guideline (DGGT 2002).

Table 6.6 Existing tolerances and recommendations for geometrical imperfections

	Tolerances	Recommendations from the present work (unreinforced columns)
Single column		
Diameter change over length Necking Bulging	No tolerance given	Necking to be avoided (in particular in upper part)
Inclination	2%·D for bored piles (EN 1536) 4%·D for displacement piles (EN 12699) 2%·D for micropiles (EN 14199)	3%·D (50-100%·B at column toe)
Curvature	No tolerance given	100 m radius (2.5%·D at half column length)
Eccentricity	10-15 cm for bored piles (EN 1536), 12.5%·B for B = 1 m 10 cm for displacement piles (EN 12699), 12.5%·B for B = 1 m 10 cm for micropiles (EN 14199), 33%·B for B = 0.15 m	$1/8 \cdot B = 0.125 \cdot B$
Combined system		
Diameter change over length Necking Bulging	No tolerance given for reduction 30% increase for cases with LTP (ASIRI)	Necking and bulging to be avoided
Inclination	CPRF: a priori same tolerances as single column 2%·D for stabilizing columns (CSV-guideline) 2%·D for rigid inclusions (ASIRI)	less strict than single column
Curvature	No tolerance given	less strict than single column
Eccentricity	CPRF: a priori same tolerances as single column 5 cm for stabilizing columns (CSV-guideline) 5-10 cm for rigid inclusions under footings (ASIRI) 20 cm for rigid inclusions under large loading areas (ASIRI)	less strict than single column

The difference in sensitivity between the single column case and the column in a combined system is reflected in the safety concepts as well (see section 2.7 and Fig. 2.50): as long as the column diameter remains above 25 cm (lower limit in ASIRI), the necessity of a check of the geotechnical bearing capacity of the single column does not depend on the column itself or on its diameter, but on the stability of the global system. The problem is rather on the side of the structural capacity, which has to be checked in all cases and which may be more critical for small column diameters.

7 Summary and outlook

Combined foundation systems like rigid inclusions (RI) are a relatively recent foundation concept. They represent a further development of combined pile-raft systems (CPRF), comprising a load transfer platform (LTP) between the columns and the structure and often using small-diameter unreinforced concrete columns for vertical loads. Calculation methods and design concepts are available for such systems in particular in France, based on measured pressuremeter (PMT) modulus values. The conventional pile design consisting only of a bearing capacity check for the individual column cannot be applied to such combined systems. The expected settlements may be larger due to a significant load proportion supported by the soil, requiring a detailed analysis of the load-settlement behaviour and of the load distribution. Furthermore, in systems using rigid inclusions, the comparably small column diameter, often without reinforcement, results in a potential particular sensitivity of such systems in particular with respect to execution imperfections.

The present work contributes to the development of displacement-based calculation and design methods for combined systems under vertical loads, in particular on an international level where in general no in situ soil modulus values are measured. Possible particularities of such systems, like the sensitivity of unreinforced small-diameter columns, also had to be investigated.

A reasonable safety concept for rigid inclusions is given in the French ASIRI recommendations (IREX 2012). It has been developed using the concepts of the European geotechnical design standard Eurocode 7 (EN 1997-1 2004-2009-2013) for conventional foundations, where applicable. In ASIRI, a distinction is made between two domains of application: domain 1 where the system is used for an increase of the bearing capacity and domain 2 where it is used only for settlement reduction. In domain 1, the safety checks for the columns are identical to those for conventional pile foundations. In addition, the bearing capacity of the footing is checked, with a reduced load due to the presence of the columns. Thus in domain 1, the system is considered on the safe side from all possible foundation point of views. In domain 2, only serviceability checks have to be performed, including a verification of the internal bearing capacity of the columns. The use of such column systems in domain 2 corresponds in a sense to the design philosophy of the CPRF-guideline (Hanisch et al. 2002, Katzenbach and Choudhury 2013), where no verification of the bearing capacity of single piles is required, and where only the overall stability of the system and of course the structural bearing capacity of the piles have to be checked. A prerequisite for the application of the safety concept after ASIRI is a calculation model reproducing accurately enough the interactions inside the system. In particular, the model shall

depict the load transfer in the load transfer platform (LTP) and shall include the load transfer mechanisms between columns and soil.

In the present work, the load transfer method (LTM) is identified as an appropriate method for the calculation of combined systems with relatively simple geometries. It is a straightforward engineering tool with a simple presentation of the most important results for a soil-column system. The soil-column interaction in terms of skin friction and tip resistance is described by deformation-dependent load transfer curves (or “t-z” and “q-z” curves or mobilisation curves). Empirical non-linear load transfer curves are recommended for an accurate representation of the real behaviour. The continuum calculations carried out using the finite element method (FEM) with the commercially available software Plaxis (2014) proves that the column load-settlement behaviour cannot be accurately described using the usual correlations for soil moduli. Continuum methods therefore require preliminary time-consuming calibration studies for the single column case.

In order to obtain a reliable load transfer method (LTM) modelling, first the different elements of a combined system are investigated separately, and then a combination of the results is proposed.

For large rafts, the well-established oedometer method is recommended. For single footings, the linear method based on the analogy between soil loading in the pressuremeter test and under single footings seems to be the most reliable one for working load levels. However, the internationally more common linear oedometer method for footings can be used as well. The non-linear load-settlement behaviour of single footings up to failure is analysed based on measurements given in the literature. This yields the proposal of a hyperbolic load-settlement curve for footings, calibrated on a reference linear method used in practice. This mobilisation curve for the footing is defined in a way to match the linear reference method selected for one third of the ultimate load.

The behaviour of single piles is investigated thoroughly based on numerous available instrumented and non-instrumented pile load tests with different pile and soil types. Since generally in the international practice no pressuremeter tests are carried out, a reliable alternative to the well-proven load transfer curves after Frank and Zhao (1982), which are based on the pressuremeter modulus, is sought. For this purpose, the reliability with respect to the stiffness of existing load transfer curves from the literature is analysed. This analysis shows that defining the stiffness of the curves via any measured soil property different from the pressuremeter modulus is not efficient. Cubic root and hyperbolic axial load transfer curves are proposed. If the stiffness parameters of these curves cannot be directly fitted on an instrumented pile load test on the site, the

use of fixed values of these parameters for all pile and ground types proves to be appropriate as a simplified approach. For single pile settlement calculations, conservative values of these parameters may be used. For applications in combined systems where skin friction in opposite directions may occur, average values of the parameters should be used. The stiffness accuracy of the proposed curves depends strongly on an accurate estimation of the ultimate skin friction and tip resistance values. On the contrary, the initial stiffness of the Frank and Zhao curves is fully described by the pressuremeter modulus, avoiding thus stiffness errors due to a wrong estimation of the ultimate values. This approach should therefore be preferred if pressuremeter test results are available.

The proposed mobilisation curves for the shallow and pile foundation behaviours are combined and extended in order to provide a calculation tool for all combined systems, with and without load transfer platform (LTP), using the pressuremeter modulus or not. As a part of the present work, the proposed method is implemented as the LTM option into the software KID (Keller Company 2015). The prediction with the developed model matches very well the measurements made for 3 different cases from the literature: a field test with a load transfer platform (LTP) conducted as part of the ASIRI project (IREX 2012), a combined pile-raft test foundation (Borel 2001) and the combined pile-raft foundation of the high-rise building Westend 1 (Reul 2000). Furthermore, the parametric study for the transition between the combined pile-raft foundation case (CPRF) and the rigid inclusion case (RI) is based on these cases. It shows a smooth transition between both systems and a potential for optimisation with a significant reduction of the internal forces in the columns and in the rigid slab if a load transfer platform (LTP) is used. In addition, a comparison with 3D finite element calculations for a theoretical footing case with columns confirms that the developed load transfer method is very reliable for simple geometries.

In order to assess possible specific features of small-diameter unreinforced columns in combined systems, sensitivity investigations using the axisymmetric and 3D finite element method (FEM) with the software Plaxis (2013, 2014) are performed. They indicate that all systems including rigid columns can be calculated basically in a similar manner as long as the modulus ratio between the column and the soil is larger than 500. For such ratios, the concept of skin friction and tip resistance is applicable similarly to piles. By nature stone columns behave differently and their design has to be made with the already established methods for this system. Geometrical imperfections impact mainly the structural integrity of small-diameter unreinforced columns. However, these effects are reduced in combined systems compared to the single column case due to the possibility of redistribution of the loads within the system. Diameter reductions or increases in general as well as eccentricities in the case of concentrated loads can lead to

a failure of the column. A column inclination up to 3 % and a curvature radius down to 100 m can be tolerated.

In short, the following aspects have been identified in the present work as decisive for a unified and safe design on an international level of combined systems like combined pile-raft foundations (CPRF) and rigid inclusions (RI) under vertical loads:

- determining the appropriate calculation parameters from in situ ground investigation tests for the behaviour of the soil under the shallow foundation, in particular with respect to the size of the foundation, to the loading type and to the load level (general usual correlations in Appendix C);
- using the safety concept according to the ASIRI recommendations (IREX 2012) which are compatible with the Eurocode 7 (EN 1997-1 2004-2009-2013);
- for relatively simple geometries, using the straightforward load transfer method (LTM) as a practical and accurate engineering tool. The Frank and Zhao (1982) load transfer curves should be preferred due to the direct use of the measured in situ soil modulus. Otherwise, the proposed cubic root or hyperbolic load transfer curves are recommended;
- for complex geometries, using the finite element method (FEM), preferably with soil constitutive models similar to the Hardening Soil Model (Plaxis 2013, Plaxis 2014). General rules for the choice of the soil modulus to represent the column behaviour cannot be given;
- ensuring a high execution quality especially for small-diameter columns without steel reinforcement. A diameter reduction or diameter increase should be avoided in particular. For concentrated loads (for example a footing with small dimensions), a column offset has to be avoided.

It is appropriate to apply the proposed calculation methods for usual shallow and pile foundation systems as well. A design based on an accurate displacement analysis is indeed encouraged by the Eurocode 7 (EN 1997-1 2004-2009-2013) for all geotechnical structures.

Further research is necessary in the field of displacement-based design of foundations for non-vertical loads and bending moments, as well as for all geotechnical structures which do not fall into the category of combined foundation systems like retaining structures. The target there is as well a representation of both the domain of service loads and the domain of failure in one and the same calculation model. This is in many

cases already possible with the use of complex continuum methods. However, a compromise between the time necessary (for the calculation itself and for the output analyses) and the accuracy always needs to be found in order to promote the use of displacement-based designs. For this purpose, empirical methods based on experience representing the governing interactions in the system are of importance. An increased safety can be achieved by a good execution and preliminary sensitivity analyses, if possible using more advanced soil models than in the present work, including for example second order effects.

8 Zusammenfassung und Ausblick

Kombinierte Gründungssysteme mit Stabilisierungssäulen (“rigid inclusions”, RI) sind ein relativ neues Gründungskonzept. Sie sind eine Weiterentwicklung von kombinierten Pfahl-Plattengründungen (“combined pile-raft foundations”, CPRF), mit einer Lastverteilungsschicht (“load transfer platform”, LTP) zwischen den Säulen und dem Bauwerk und häufig mit unbewehrten Betonsäulen mit kleinem Durchmesser. Berechnungsmethoden und Bemessungskonzepte für solche Systeme liegen vor, insbesondere in Frankreich, beruhend auf der Benutzung von im Pressiometerversuch (PMT) gemessenen Moduln. Die klassische Pfahlbemessung, die im Wesentlichen darin besteht, einen Nachweis der äußeren Tragfähigkeit zu führen, kann für solche kombinierte Systeme nicht angewendet werden. Wegen des signifikanten Lastanteils im oberflächennahen Boden sind größere Setzungen zu erwarten, entsprechend ist eine detaillierte Analyse des Lastsetzungsverhaltens und der Lastverteilung erforderlich. Außerdem können der häufig kleine Durchmesser und der oft unbewehrte Querschnitt von Stabilisierungssäulen zu einer besonderen Empfindlichkeit von solchen Systemen führen.

Die vorliegende Arbeit ist ein Beitrag zur Entwicklung von verformungsbasierten Berechnungen und Bemessungsmethoden für kombinierte Systeme unter Vertikallasten, besonders auf internationaler Ebene, wo im Allgemeinen kein Modul des Bodens in situ gemessen wird. Mögliche Besonderheiten von solchen Systemen, wie die Empfindlichkeit von unbewehrten Säulen mit kleinem Durchmesser, wurden ebenfalls untersucht.

Ein stimmiges Nachweiskonzept für Stabilisierungssäulen ist in den französischen Empfehlungen ASIRI (IREX 2012) enthalten. Es wurde aus den Konzepten der europäischen Bemessungsnorm für die Geotechnik Eurocode 7 (EN 1997-1 2004-2009-2013) für konventionelle Gründungen entwickelt, soweit diese darauf anwendbar sind. In ASIRI wird zwischen zwei Anwendungsdomänen unterschieden: Domäne 1, wenn das System zur Erhöhung der Tragfähigkeit benutzt wird, und Domäne 2, wenn es nur zur Setzungsreduktion verwendet wird. In der Domäne 1 sind Sicherheitsnachweise für die Säulen genauso wie bei einer konventionellen Pfahlgründung zu führen. Zusätzlich wird die Sicherheit der Flachgründung gegen Grundbruch nachgewiesen, mit einer reduzierten Last zur Berücksichtigung der günstigen Wirkung der Säulen. In der Domäne 1 wird das System somit aus allen denkbaren Perspektiven betrachtet. In der Domäne 2 müssen nur Nachweise der Gebrauchstauglichkeit geführt werden sowie zusätzlich ein Nachweis der inneren Tragfähigkeit des Säulenmaterials. Die Domäne 2 entspricht in gewisser Hinsicht der Philosophie der KPP-Richtlinie (Hanisch et al. 2002, Katzenbach und Choudhury 2013), in der kein Nachweis der äußeren Tragfähigkeit der Pfähle gefordert wird, und nur die Gesamtstandsicherheit und die innere Tragfähigkeit

der Pfähle nachgewiesen werden müssen. Voraussetzung für die Anwendung des Sicherheitskonzeptes nach ASIRI ist ein Berechnungsmodell, das die Interaktionen im System wirklichkeitsnah darstellt. Das Modell muss insbesondere die Lastverteilung in der Lastverteilungsschicht (LTP) und die Lastübertragung zwischen Säulen und Boden abbilden.

In der vorliegenden Arbeit wird die Lasttransfermethode (“load transfer method”, LTM) als eine besonders geeignete Methode für die Berechnung von kombinierten Systemen mit relativ einfachen Geometrien identifiziert. Es ist ein ingenieurmäßiges Werkzeug mit einfachen Diagrammen zur Darstellung der wichtigsten Ergebnisse für das Säulen-Boden-System. Die Boden-Säule-Interaktion für Mantelreibung und Spitzendruck wird durch Lasttransferkurven (auch “t-z” und “q-z” Kurven oder Mobilisierungskurven) beschrieben. Empirische nichtlineare Lasttransferkurven werden empfohlen, um das reale Verhalten optimal abzubilden. Kontinuumsberechnungen mit der Finite Elemente Methode (FEM) mit dem Programm Plaxis (2013, 2014) zeigen, dass das Lastsetzungsverhalten der Säule mit den üblichen Korrelationen für Bodenmoduln nicht wirklichkeitsgetreu dargestellt werden kann. Kontinuumsmethoden machen daher zeitaufwändige Kalibrierungsuntersuchungen im Vorfeld für den Fall der Einzelsäule erforderlich.

Um eine zuverlässige Modellierung mit der Lasttransfermethode zu erreichen, werden die verschiedenen Elemente eines kombinierten Systems zunächst getrennt untersucht. Danach wird eine Kombination der Ergebnisse vorgeschlagen.

Für großflächige Flächengründungen wird die bewährte Oedometermethode mit Steifemoduln empfohlen. Für Einzelfundamente mit Lasten im Gebrauchsbereich scheint die Pressiometermethode am besten geeignet zu sein. Sie basiert auf der Analogie zwischen der Bodenbeanspruchung im Pressiometerversuch und der unter dem Einzelfundament. Jedoch kann die international verbreitete Oedometermethode mit Steifemoduln ebenfalls verwendet werden. Das nichtlineare Setzungsverhalten von Einzelfundamenten bis zum Bruchzustand wird mit Hilfe von in der Literatur zitierten Messungen untersucht. Dies führt zu einem Vorschlag mit einer hyperbolischen Lastsetzungskurve für Einzelfundamente, kalibriert im Einzelfall anhand einer in der Praxis verwendeten linearen Referenzmethode. Diese Mobilisierungskurve für das Einzelfundament wird so definiert, dass die Verformung für eine Last entsprechend einem Drittel des Grundbruchwiderstands mit der aus der linearen Referenzmethode übereinstimmt.

Das Verhalten von Einzelpfählen wird mit Nachrechnungen zahlreicher verfügbarer instrumentierter und nicht-instrumentierter Pfahlprobelastungen mit unterschiedlichen Pfahl- und Bodenarten untersucht. Da in der Regel auf internationaler Ebene keine

Pressiometerversuche durchgeführt werden, werden zuverlässige Alternative zu den bewährten auf dem Pressiometermodul beruhenden Lasttransferkurven von Frank und Zhao (1982) untersucht. Dafür wird die Zuverlässigkeit von bestehenden Lasttransferkurven aus einer Literaturaswertung hinsichtlich ihrer Steifigkeit geprüft. Diese Analyse zeigt, dass eine Beschreibung der Last-Setzungs-Kurven mit Hilfe von Ergebnissen aus in situ Versuchen außer denen des Pressiometerversuchs nicht zielführend ist. Lasttransferkurven mit der Form von Kubikwurzel- und Hyperbel-Funktion werden vorgeschlagen. Wenn die Parameter für diese Kurven nicht anhand einer instrumentierten Probelastung in situ kalibriert werden können, erweist sich eine vereinfachte Benutzung von festen Parametern für alle Pfahl- und Bodenarten als hinreichend zutreffend. Zur Beschreibung der Setzung von Einzelpfählen können konservative Werte dieser Parameter verwendet werden. Bei Anwendungen für kombinierte Systeme, in denen bereichsweise positive und negative Mantelreibung auftreten kann, müssen zweckmäßigerweise Durchschnittswerte der Parameter verwendet werden. Der zutreffende Verlauf der vorgeschlagenen Kurven für das Last-Verformungsverhalten hängt stark von einer korrekten Abschätzung der Grenzwerte für Mantelreibung und Spitzendruck ab. Im Gegensatz dazu wird der Anfangsverlauf der Kurven nach Frank und Zhao vollständig durch den Pressiometermodul definiert. Daher werden dort Fehler bei der Steifigkeitsbeschreibung klein gehalten. Dieser Ansatz sollte deswegen bevorzugt werden, wenn Ergebnisse aus Pressiometerversuchen vorliegen.

Die vorgeschlagenen Mobilisierungskurven für die Fälle der Flach- und der Pfahlgründung werden kombiniert und erweitert, um ein Berechnungswerkzeug für alle kombinierte Systeme mit oder ohne Lastverteilungsschicht (LTP) zu entwickeln, mit oder ohne Benutzung des Pressiometermoduls. Als Bestandteil der vorliegenden Arbeit wird die vorgeschlagene Methode als LTM Option in das Programm KID (Keller Company 2015) implementiert. Die Abschätzung mit dem entwickelten Modell stimmt sehr gut mit Messungen an drei verschiedenen kombinierten Gründungen, die in der Literatur beschrieben sind, überein: ein Feldversuch mit einer Lastverteilungsschicht (LTP) im Rahmen des ASIRI Projektes (IREX 2012), ein Versuch mit einer Kombinierten Pfahl-Plattengründung (Borel 2001) und die Kombinierte Pfahl-Plattengründung für das Hochhaus Westend 1 (Reul 2000). Außerdem wird eine parametrische Studie für den Übergang zwischen dem Fall einer kombinierten Pfahl-Plattengründung (CPRF) und eines Systems mit Stabilisierungssäulen (RI) auf Basis dieser Messungen entwickelt. Sie zeigt einen stetigen Übergang zwischen beiden Systemen und bei Inkaufnahme zusätzlicher Verformungen die Möglichkeit einer wirtschaftlichen Optimierung infolge erheblicher Abnahme der Schnittkräfte in den Säulen und in der Platte, wenn eine Lastverteilungsschicht (LTP) vorgesehen wird. Des Weiteren bestätigen 3D Finite Elemente Berechnungen an einem theoretischen Beispiel mit einem Einzelfundament mit Säulen, dass die entwickelte Lasttransfermethode für einfache Geometrien sehr zuverlässig ist.

Um die Auswirkungen der Besonderheiten von unbewehrten Säulen mit kleinem Durchmesser in kombinierten Systemen herauszustellen, werden Sensitivitätsanalysen mit rotationssymmetrischen und 3D Finite Elemente Modellen mit dem Programm Plaxis (2013, 2014) durchgeführt. Diese lassen erkennen, dass alle Systeme mit starren Säulen gleich betrachtet werden können, solange das Modulverhältnis zwischen Säule und Boden größer als 500 bleibt. Für solche Verhältnisse gilt das Konzept von Mantelreibung und Spitzendruck wie bei Pfählen. Schottersäulen verhalten sich von Natur aus davon abweichend und die Bemessung soll mit den etablierten Methoden für dieses System gemacht werden. Geometrische Imperfektionen haben hauptsächlich Auswirkungen auf die Integrität von unbewehrten Säulen mit kleinem Durchmesser. Diese Effekte sind jedoch weniger bedeutsam bei kombinierten Systemen im Vergleich zur Einzelsäule, weil die Lasten sich im System umlagern können. Verkleinerungen und Vergrößerungen des Durchmessers, sowie Lastausmitten bei konzentrierten Lasten, können zu einem Bruch der Säule führen. Eine Schiefstellung der Säule bis zu 3 % und ein Krümmungsradius größer als 100 m können toleriert werden.

Zusammengefasst wurden folgende Aspekte in der vorliegenden Arbeit als entscheidend für eine vereinheitlichte und sichere internationale Bemessung von kombinierten Systemen wie kombinierten Pfahl-Plattengründungen (CPRF) und Stabilisierungssäulen (RI) unter Vertikallasten identifiziert:

- Zutreffende Bestimmung der Berechnungsparameter für das Verhalten des Bodens unter Flachgründungen aus in situ Versuchen, in Abhängigkeit insbesondere von den Gründungsabmessungen, von der Belastungsart und dem Belastungsniveau (allgemein übliche Korrelationen in Appendix C);
- Verwendung des Sicherheitskonzeptes nach den mit dem Eurocode 7 (EN 1997-1 2004-2009-2013) kompatiblen ASIRI Empfehlungen (IREX 2012);
- Benutzung der Lasttransfermethode (LTM) als praxisorientiertes und realistisches ingenieurmäßiges Werkzeug für relativ einfache Geometrien. Die Verwendung der Lasttransferkurven nach Frank und Zhao (1982) werden bevorzugt, wenn der in situ gemessene Pressiometer-Modul vorliegt. Ansonsten werden die vorgeschlagenen Lasttransferkurven mit der Form einer Kubikwurzel- oder Hyperbel-Funktion empfohlen;
- Verwendung der Finite Elemente Methode (FEM) für komplexe Geometrien, vorzugsweise mit Stoffmodellen ähnlich dem "Hardening Soil Model" (Plaxis 2013, Plaxis 2014). Allgemeine Grundsätze für die Wahl des Bodenmoduls für das Verhalten der Säule können hier nicht angegeben werden;

- Qualität bei der Ausführung sicherstellen, insbesondere bei Säulen mit kleinem Durchmesser ohne Bewehrung. Vor allem Variationen beim Säulendurchmesser sollen vermieden werden. Bei konzentrierten Lasten (zum Beispiel Einzelfundament mit kleinen Abmessungen) soll eine Lastexzentrizität vermieden werden.

Die vorgeschlagenen Berechnungsmethoden sind ebenfalls für klassische Flach- und Pfahlgründungen geeignet, denn es ist zu beachten, dass eine Bemessung basierend auf einer realistischen Verformungsberechnung vom Eurocode 7 (EN 1997-1 2004-2009-2013) für alle geotechnischen Bauwerke empfohlen wird.

Weiterer Forschungsbedarf besteht im Bereich der verformungsbasierten Bemessung von Gründungen für nichtvertikale und außermittige Lasten, sowie für alle geotechnischen Bauwerke, die nicht zur Kategorie der kombinierten Gründungen gehören, wie zum Beispiel Stützwände. Das Ziel ist auch hier eine stetige Abbildung sowohl für den Bereich der Gebrauchslasten als auch darüber hinaus bis zum Grenzzustand im gleichen Berechnungsmodell. Das ist in vielen Fällen schon möglich mit der Verwendung von komplexen Kontinuumsmethoden. Allerdings muss immer ein Kompromiss zwischen der benötigten Zeit (für die Berechnung selbst und für die Analyse der Ergebnisse) und der Zuverlässigkeit gefunden werden, wenn verformungsbasierte Bemessungen vorgenommen werden. Dafür sind empirische Methoden, die die entscheidenden Interaktionen im System abbilden, von großer Hilfe. Eine erhöhte Sicherheit kann durch eine gute Ausführungsqualität erreicht werden sowie durch eine vorausgehende Sensitivitätsanalyse, wenn möglich mit hochwertigen Stoffmodellen und zum Beispiel mit Berücksichtigung von Effekten nach der Theorie zweiter Ordnung.

9 Résumé et perspectives

Les systèmes de fondations combinés comme les inclusions rigides (“rigid inclusions”, RI) sont des méthodes relativement récentes. Ils consistent en un développement supplémentaire des fondations mixtes (“combined pile-raft foundations”, CPRF) avec l’utilisation d’un matelas de transfert de charges (“load transfer platform”, LTP) placé entre les colonnes et la structure, le diamètre des colonnes étant généralement faible et le béton des colonnes étant souvent non-armé pour des charges verticales. Des méthodes de calculs et des concepts de sécurité existent pour ces systèmes, notamment en France où le module mesuré lors de l’essai pressiométrique (PMT) est utilisé. Le dimensionnement classique des pieux basé sur une simple vérification de la portance des colonnes isolées ne peut pas être appliqué à ces systèmes combinés. Les tassements peuvent être plus importants du fait de la part significative de charge reprise par le sol, ce qui impose une analyse détaillée du comportement charge-tassement et de la distribution de charge. De plus, les systèmes avec inclusions rigides de diamètre faible, souvent sans armatures de renforcement, peuvent présenter une sensibilité particulière aux imperfections d’exécution.

Le présent travail est une contribution au développement des méthodes de calcul et de dimensionnement en déplacement pour les systèmes combinés sous charge verticale, en particulier à un niveau international où des mesures in situ de module de sol ne sont généralement pas disponibles. Les éventuelles particularités de ces systèmes, notamment la sensibilité de colonnes non renforcées de petit diamètre, devaient également être examinées.

Les recommandations françaises ASIRI (IREX 2012) proposent un concept de sécurité adapté pour les inclusions rigides. Il a été développé sur la base des concepts de la norme européenne pour le dimensionnement des fondations usuelles, l’Eurocode 7 (EN 1997-1 2004-2009-2013), lorsque cela est approprié. Dans ASIRI, la distinction est faite entre 2 domaines d’utilisation : le domaine 1 lorsque le système est utilisé pour une augmentation de la portance et le domaine 2 quand il est utilisé uniquement pour une réduction des tassements. Dans le domaine 1, les justifications pour les colonnes sont similaires à celles pour les fondations sur pieux conventionnelles. De plus, la portance des semelles est également vérifiée, avec réduction de la charge de par l’action favorable des colonnes. Dans le domaine 1, le système est ainsi considéré sous tous les points de vue de fondation possibles. Dans le domaine 2, seules des vérifications d’état de service sont à effectuer, avec une justification de la résistance intrinsèque du matériau des colonnes. L’utilisation des inclusions dans le domaine 2 correspond dans une certaine mesure à la philosophie de dimensionnement des recommandations pour les fondations mixtes (Hanisch et al. 2002, Katzenbach et Choudhury 2013), dans lesquelles seulement la stabilité globale du système ainsi que la résistance intrinsèque

sont à vérifier, et non la portance des pieux isolés. L'application du concept de sécurité selon ASIRI impose un calcul avec un modèle représentant de manière fiable les interactions ayant lieu dans le système. Plus particulièrement, le modèle doit inclure le transfert de charge dans le matelas (LTP) ainsi que les mécanismes de transfert entre colonnes et sol.

La méthode de transfert de charge ("load transfer method", LTM) est identifiée ici comme étant particulièrement adaptée au calcul des systèmes combinés présentant une géométrie relativement simple. Il s'agit d'un outil d'ingénieur pratique avec une représentation simple des résultats principaux pour les systèmes sol-colonnes. L'interaction sol-colonne en termes de frottement et de résistance de pointe est définie par des courbes de transfert de charge (ou courbes "t-z" et "q-z" ou courbes de mobilisation). Des courbes empiriques non-linéaires sont recommandées pour représenter au mieux le comportement réel. Les analyses en milieu continu effectuées avec la méthode des éléments finis ("finite element method", FEM) avec le programme Plaxis (2014) montrent que le comportement charge-tassement de la colonne ne peut pas être correctement représenté avec les corrélations usuelles. Pour les calculs en milieu continu, une étape préliminaire de calibration parfois fastidieuse dans le cas de la colonne isolée est nécessaire.

Dans le but d'obtenir à une modélisation fiable avec la méthode de transfert de charge, les différents éléments d'un système combiné sont tout d'abord examinés séparément, puis une combinaison de ces éléments est proposée.

Pour les fondations superficielles de grandes dimensions (radier, dallage), la méthode oedométrique usuelle est la plus adaptée. Pour les semelles, la méthode linéaire se basant sur l'analogie entre le chargement du sol autour d'une cellule pressiométrique et le chargement de la semelle semble être la plus pertinente pour les charges de service. Cependant, la méthode oedométrique plus courante au niveau international peut également être appliquée. Le comportement non-linéaire des semelles est examiné sur la base de mesures obtenues dans la littérature. Cette étude aboutit à la proposition d'une courbe charge-tassement hyperbolique pour les semelles, calibrée sur l'une des méthodes linéaires de référence utilisée en pratique. Cette courbe de mobilisation pour la semelle est définie de sorte qu'il y ait concordance avec la méthode linéaire de référence choisie pour un tiers de la charge ultime.

Le comportement de pieux isolés est étudié en détail avec un grand nombre d'essais de chargement instrumentés et non-instrumentés pour différents types de pieux et de sol. Du fait que des essais pressiométriques ne sont que très rarement effectués dans la pratique internationale, une alternative aux courbes de transfert de charge éprouvées selon Frank et Zhao (1982), basées sur le module pressiométrique, est recherchée. La

validité de différentes courbes existantes dans la littérature est examinée en termes de raideur. Cette étude mène à la conclusion que l'utilisation d'une propriété de sol mesurée différente du module pressiométrique n'est pas pertinente. Des courbes de transfert de charge de type racine cubique et hyperbolique sont proposées. Si les paramètres de raideur de ces courbes ne peuvent être calibrés sur un essai instrumenté sur le site étudié, ces courbes peuvent être définies de manière simplifiée par des paramètres uniques, valables pour tous types de pieux et de sol. Pour des cas de pieux isolés, des valeurs conservatives de ces paramètres peuvent être utilisées. Pour des applications à des systèmes combinés où le frottement peut apparaître dans des directions contraires, les valeurs moyennes de ces paramètres doivent être utilisées. La raideur des courbes proposées dépend de manière importante d'une bonne estimation des valeurs ultimes de frottement et de résistance de pointe. Au contraire, la raideur initiale des courbes de Frank et Zhao est entièrement définie par le module pressiométrique, ce qui permet d'éviter des erreurs en termes de raideur dans le cas d'une estimation erronée des valeurs ultimes. Cette approche doit ainsi être favorisée si des résultats d'essais pressiométriques sont disponibles.

Les courbes de mobilisation proposées pour les fondations superficielles et pour les pieux sont combinées et étendues au cas des systèmes combinés, avec ou sans matelas (LTP), en utilisant le module pressiométrique ou non. L'implémentation de cette méthode comme option LTM dans le programme KID (Keller Company 2015) fait partie intégrante du présent travail. Les prévisions avec le modèle proposé sont en très bonne adéquation avec les mesures effectuées sur 3 sites documentés dans la littérature : un essai de grande échelle avec matelas (LTP) dans le cadre du projet ASIRI (IREX 2012), un essai sur fondation mixte (Borel 2001) et la fondation mixte de la tour Westend 1 (Reul 2000). L'étude paramétrique illustrant la transition entre le cas de fondation mixte (CPRF) et le cas d'inclusions rigides (RI) s'appuie sur ces cas de référence. Cette analyse montre une transition continue entre les deux systèmes et une possibilité d'optimisation avec une diminution significative des efforts dans les colonnes et dans la fondation superficielle si un matelas (LTP) est utilisé. En complément, une comparaison avec des calculs en éléments finis en 3D dans un cas théorique de semelle sur colonnes confirme que la méthode de transfert de charge développée est très performante pour des géométries simples.

Dans le but de repérer d'éventuelles particularités des colonnes non-renforcées de faible diamètre, une analyse de sensibilité est effectuée avec des modèles éléments finis (FEM) axisymétriques et 3D avec le programme Plaxis (2013, 2014). Elle révèle que tous les systèmes avec colonnes rigides peuvent être calculés d'une manière fondamentalement similaire, tant que le rapport des modules de la colonne et du sol reste supérieur à 500. Pour ces valeurs, le concept de frottement et de résistance de pointe est applicable comme pour les pieux. De par leur nature, les colonnes ballastées

se comportement différemment et leur dimensionnement doit être fait pas les méthodes établies pour ces systèmes. Les imperfections géométriques ont principalement une incidence sur l'intégrité structurelle des colonnes non-armées de petit diamètre. Cependant, ces effets sont atténués dans les systèmes combinés en comparaison avec la colonne isolée du fait des possibilités de redistribution des charges à l'intérieur du système. Une augmentation ou une réduction du diamètre en général, ainsi qu'une excentricité dans le cas de charges concentrées peuvent aboutir à la rupture de la colonne. Une inclinaison de colonne jusqu'à 3 % et un rayon de courbure supérieur à 100 m peuvent être tolérés.

En résumé, les aspects suivants ont été identifiés dans le présent travail comme déterminants pour un dimensionnement unifié et sécuritaire des systèmes combinés comme les fondations mixtes (CPRF) et les inclusions rigides (RI) sous charges verticales :

- déterminer les paramètres de calcul appropriés à partir d'essais de sol in situ pour le comportement du sol sous la fondation superficielle, en particulier en fonction de la taille de la fondation, du type de chargement et du niveau de charge (corrélations usuelles en annexe C) ;
- utiliser le concept de sécurité selon les recommandations ASIRI (IREX 2012) qui sont compatibles avec l'Eurocode 7 (EN 1997-1 2004-2009-2013) ;
- pour les géométries relativement simples, utiliser la méthode de transfert de charge (LTM) en tant qu'outil pratique et fiable de l'ingénieur. Les courbes de transfert de charge selon Frank et Zhao (1982) doivent être préférées du fait de l'utilisation directe du module de sol mesuré in situ. Sinon, les courbes en racine cubique et hyperbolique proposées sont recommandées ;
- pour les géométries complexes, utiliser la méthode des éléments finis (FEM), de préférence avec des lois de comportement de sol similaires au "Hardening Soil Model" (Plaxis 2013, Plaxis 2014). Des règles générales pour le choix du module de sol pour représenter le comportement de la colonne ne peuvent être données ;
- garantir une bonne qualité d'exécution pour les colonnes de petit diamètre en béton non-armé. Une diminution ou une augmentation du diamètre est à éviter en particulier. Pour les charges concentrées (par exemple une semelle de faibles dimensions), un décalage d'implantation doit être évité.

Il est judicieux d'appliquer les méthodes proposées également pour les fondations usuelles superficielles et profondes. Un dimensionnement basé sur un calcul fiable des déplacements est en effet préconisé par l'Eurocode 7 (EN 1997-1 2004-2009-2013) pour toutes les structures géotechniques.

Une recherche plus approfondie est nécessaire dans le domaine du dimensionnement en déplacement pour les charges non verticales et pour les moments, ainsi que pour toutes structures géotechniques qui ne rentrent pas dans la catégorie des fondations combinées comme les parois de soutènement. L'objectif est ici aussi une représentation à la fois du domaine des charges de service et du domaine de la rupture dans un même modèle de calcul. Ceci est dans la plupart des cas déjà possible avec les méthodes complexes pour les milieux continus. Cependant, un compromis doit être trouvé entre le temps nécessaire (pour le calcul lui-même et pour l'analyse des résultats) et la pertinence des résultats afin de promouvoir l'utilisation des méthodes en déplacement. Dans ce but, des méthodes empiriques représentant les interactions déterminantes dans le système sont d'importance notable. Une augmentation du niveau de sécurité est rendue possible par une bonne exécution ainsi que des études de sensibilité préliminaires, si possible en utilisant des modèles plus développés que dans le présent travail, incluant par exemple des effets du second degré.

References

Ackermann, T. (2013)

Ermittlung des Einflusses von geometrischen Ausführungsimperfectionen auf das Verformungsverhalten und Tragverhalten von steifen Baugrundverbesserungselementen (schlanken, unbewehrten Betonsäulen) mit FEM-Berechnungen. Bachelor thesis, Fachhochschule Nordwestschweiz, supervisors: Trunk, U., Bohn, C. and Wehr, J.

Ackermann, T. (2014a)

Ermittlung des Einflusses von geometrischen Ausführungsimperfectionen auf das Verformungsverhalten und Tragverhalten von steifen Baugrundverbesserungselementen (schlanken, unbewehrten Betonsäulen) mit FEM-Berechnungen. Project thesis 1, Fachhochschule Nordwestschweiz, supervisors: Trunk, U., Bohn, C. and Wehr, J.

Ackermann, T. (2014b)

Ermittlung des Einflusses von geometrischen Ausführungsimperfectionen auf das Verformungsverhalten und Tragverhalten von steifen Baugrundverbesserungselementen (schlanken, unbewehrten Betonsäulen) mit FEM-Berechnungen, Modellbildung mit Plaxis 3D. Project thesis 2, Fachhochschule Nordwestschweiz, supervisors: Trunk, U., Bohn, C. and Wehr, J.

Ackermann, T. (2015a)

Ermittlung des Einflusses von geometrischen Ausführungsimperfectionen auf das Verformungsverhalten und Tragverhalten von steifen Baugrundverbesserungselementen (schlanken, unbewehrten Betonsäulen) mit FEM-Berechnungen. Master thesis, Fachhochschule Nordwestschweiz, supervisors: Trunk, U., Bohn, C. and Wehr, J.

Ackermann, T. (2015b)

Plaxis 3D calculations for footing with soil reinforcement columns. Research work, Fachhochschule Nordwestschweiz, supervisors: Bohn, C. and Trunk, U. (private communication)

Alber, D. (2007a)

Das Knicken elastisch gebetteter Balken. Bauingenieur 82, 95-102

Alber, D. (2007b)

Ungewollte Schiefstellung vertikaler Pfähle und Pfahlgruppen. Geotechnik 30, No. 2, 115-122

- Alber, D. (2013)
Der Nachweis der inneren Sicherheit von pfahlartigen Tragelementen im Boden. Bautechnik 90, No. 2, 803-815
- API (1993)
Recommended practice for planning, designing and constructing fixed offshore platforms – Working stress design. 20th Edition, American Petroleum Institute, Washington, D.C.
- Armaleh, S., Desai, C.S. (1987)
Load-deformation response of axially loaded piles. Journal of Geotechnical Engineering 113, No. 12
- Baguelin, F. (2005)
Le calcul des semelles au pressiomètre et l’Eurocode 7. ISP5 – PRESSIO 2005, International Symposium 50 years of pressuremeters, LCPC/Presses de l’école nationale des ponts et chaussées
- Baguelin, F., Bustamante, M., Frank, R. (2005)
The pressuremeter for foundations: French experience. Proceedings of In Situ’86, GT Div., ASCE, Blacksburg, VA, USA
- Baguelin, F., Jézéquel, J.F., Shields, D.H. (1978)
The pressuremeter and foundation engineering. Series on Rock and Soil Mechanics 2, No. 4, Trans Tech Publications
- Baguelin, F., Lay, L., Ung, S.Y. (2009)
Pressiomètre, surconsolidation et tassements dans les sols fins. Proceedings of the XVIIth International Congress on Soil Mechanics and Geotechnical Engineering, Alexandria, Egypt
- Balaam, N.P., Booker, J.R. (1981)
Analysis of rigid rafts supported by granular piles. International Journal for Numerical and Analytical Methods in Geomechanics 5, No. 4, 379-403
- Benz, T. (2007)
Small-strain stiffness of soils and its numerical consequences. PhD thesis, University Stuttgart No. 55

- Besançon, G., Iorio, J.P., Soyez, B. (1984)
Analyse des paramètres de calcul intervenant dans le dimensionnement des colonnes ballastées. International Conference on in situ soil and rock reinforcement, Paris, France, 119-126
- Black, J.A., Sivakumar, V., Bell, A. (2011)
The settlement performance of stone column foundations. *Géotechnique* 61, No. 11, 909-922
- Bohn, C. (2012)
Influence of the column/soil stiffness on the settlement of soil reinforcement columns. Baugrundtagung 2012, Forum for young geotechnical engineers, Mainz, Germany, 175-181
- Bohn, C. (2013a)
Influence of geometrical imperfections of rigid soil reinforcement columns. 5th International Young Geotechnical Engineering Conference, Forum for young geotechnical engineers of 18th International Conference on Soil Mechanics and Geotechnical Engineering, Paris, France
- Bohn, C. (2013b)
Influence of geometrical and material imperfections of rigid soil reinforcement columns. 3^{ème} Conférence Maghrébine en Ingénierie Géotechnique, November 18-19 2013, Algiers, Algeria
- Bohn, C., Frank, R., Lambert, S. (2013)
Foundation settlement calculations with pressuremeter method compared to other methods and resulting correlations. 18th International Conference on Soil Mechanics and Geotechnical Engineering, Parallel session on pressuremeter testing ISP 6, Paris, France
- Bohn, C., Santos, A.L., Frank, R. (submitted in January 2015)
Development of axial pile load transfer curves based on instrumented load tests. Draft submitted to *Journal of Geotechnical and Geoenvironmental Engineering*
- Borel, S. (2001)
Comportement et dimensionnement des fondations mixtes. PhD thesis, Laboratoire Central des Ponts et Chaussées

- Briançon, L., Simon, B. (2010)
Full-scale experiments of pile-supported earth platform under a concrete floor slab and an embankment. Symposium on New Techniques for Design and Construction in Soft Clays, Guarujá, Brazil
- Briançon, L. (2007)
Tranche 1 – Thème 1 – Rapport final. ASIRI national project, internal report 1.07.1.02
- Briaud, J.-L. (2000)
Introduction to soil moduli. Research report, Texas A&M University
- Briaud, J.-L. (2003a)
Y a-t-il un effet de taille et d'encastrement pour les fondations superficielles dans les sables ?. *Revue Française de Géotechnique* 105, 15-27
- Briaud, J.-L. (2003b)
Méthode de détermination de la courbe charge-tassement pour les fondations superficielles dans les sables. *Revue Française de Géotechnique* 105, 29-39
- Briaud, J.-L. (2007)
Spread footings in sand: load settlement curve approach. *Journal of Geotechnical and Geoenvironmental Engineering* 133, No. 8, 905-920
- Briaud, J.-L., Noubani, A., Kilgore, J., Tucker, L.M. (1985)
Correlation between pressuremeter data and other parameters. Research Report, Texas A&M University
- Brinch Hansen, J. (1970)
A revised and extended formula for bearing capacity. Danish Geotechnical Institute No. 28, 5-11
- Burland, J.B. (1989)
"Small is beautiful" – the stiffness of soils at small strains. *Canadian Geotechnical Journal* 26, 499-516
- Burlon, S. (2013)
Database of pile load tests from Ifsttar research institute. (private communication)
- Burlon, S., Frank, R., Baguelin, F., Habert, J., Legrand, S. (2014)
Model factor for the bearing capacity of piles from pressuremeter test results – Eurocode 7 approach. *Geotechnique* 64, No.7, 513-525

Bustamante, M., Gambin, M., Gianceselli, L. (2009)

Pile design at failure using the Ménard pressuremeter: an update. IFCEE 2009, Proc. Int. Foundation Congress Equipment Expo, Orlando, Florida, ASCE Geotechnical Publication No. 186, 127-134

Bustamante, M., Gianceselli, L. (1983)

Calcul de la capacité portante des pieux à partir des essais au pénétromètre statique. Bulletin de Liaison des Laboratoires des Ponts et Chaussées No. 127, 45-62

Bustamante, M., Gianceselli, L. (2006)

Règles de calcul de la portance des pieux aux ELU. Méthode pressiométrique. ELU-ELS 2006, Paris, 23-25 August, 109-118

Bustamante, M. and Jézéquel, J.-F. (1975)

Mesure des élongations dans les pieux et tirants à l'aide d'extensomètres amovibles. Travaux 489

Cambefort, H. (1964)

Essai sur le comportement en terrain homogène des pieux isolés et des groupes de pieux. Annales de l'Institut Technique du Bâtiment et des Travaux Publics No. 204, SSF/44, Paris, France, 1479-1518

Canépa, Y., Garnier, J. (2003)

Le comportement des fondations superficielles - études expérimentales – Etat de l'art. International Symposium on shallow foundations FONDSUP 2003, Laboratoire Central des Ponts et Chaussées

Cassan, M. (1988)

Les essais in situ en mécanique des sols – 1. Réalisation et interprétation. Eyrolles

CFMS (Comité Français de Mécanique des Sols), Union Syndicale Géotechnique (2011)

Recommandations sur la conception, le calcul, l'exécution et le contrôle des colonnes ballastées sous bâtiments et sous ouvrages sensibles au tassement. French recommendations for stone columns, Version No. 2

Christoulas, S., Frank, R. (1991)

Deformation parameters for pile settlement. Xth European Conference of Soil Mechanics, Florence, Italy

- Combarieu, O. (1988a)
Calcul d'une fondation mixte semelle-pieux sous charge verticale centrée.
Publication of Laboratoire Central des Ponts et Chaussées
- Combarieu, O. (1988b)
Amélioration des sols par inclusions rigides verticales – Application à
l'édification de remblais sur sols médiocres. *Revue Française de Géotechnique*
44, 57-79
- Combarieu, O. (1990)
Fondations superficielles sur sol amélioré par inclusions rigides verticales. *Revue
Française de Géotechnique* 53, 33-44
- Combarieu, O. (1999)
Historique des fondations mixtes en France. Comité Français de Mécanique des
Sols, Meeting of 1999.10.06
- Combarieu, O. (2006)
L'usage des modules de déformation en géotechnique. *Revue Française de
Géotechnique* 114, 3-32
- Combarieu, O. (2007)
Remblais sur sol médiocre et inclusions rigides – Nouvelle approche du
dimensionnement. Publication of the French National Project ASIRI
- Combarieu, O. (2008)
Remblais sur sol médiocre et inclusions rigides – Amélioration de l'approche du
dimensionnement. *Revue Française de Géotechnique* 122, 45-54
- Combarieu, O. (2008)
Formules pour le calcul du tassement des sols compressibles par la méthode
œdométrique. *Revue Française de Géotechnique* 124, 31-44
- Combarieu, O., Canépa, Y. (2001)
L'essai cyclique au pressiomètre. *Bulletin de Liaison des Laboratoires des Ponts
et Chaussées* No. 233, 37-65
- Coyle, H.M., Reese, L.C. (1966)
Load transfer for axially loaded piles in clay. *Journal of the Soil Mechanics and
Foundations Division, ASCE*, 92, SM2, 1−26

Cudmani, R.O. (2001)

Statische, alternierende und dynamische Penetration in nichtbindigen Böden. Publication of Institut für Bodenmechanik und Felsmechanik der Universität Fridericiana in Karlsruhe No. 152

Cudmani, R.O., Osinov, V. (2001)

The cavity expansion problem for the interpretation of cone penetration and pressuremeter tests. Canadian Geotechnical Journal 38, 622-638

Cuira, F., Simon, B. (2009)

Deux outils simples pour traiter des interactions complexes d'un massif renforcé par inclusions rigides. XVIIth International Congress on Soil Mechanics and Geotechnical Engineering, Alexandria, Egypt

Dauvisis, J.-P., Ménard, L. (1964)

Etude expérimentale du tassement et de la force portante des fondations superficielles. Sols-Soils 10, 11-30

Degny, E., Romagny, J.-C. (1989)

Calcul des efforts et déplacements dans les groupes de pieux: le programme Goupil. Bulletin de Liaison des Laboratoires des Ponts et Chaussées No. 162, 3-12

DGGT (Deutsche Gesellschaft für Geotechnik) (2002)

Merkblatt für die Herstellung, Bemessung und Qualitätssicherung von Stabilisierungssäulen zur Untergrundverbesserung, German recommendations for stabilizing columns (CSV-guideline)

DGGT (Deutsche Gesellschaft für Geotechnik) (2010)

Empfehlungen für den Entwurf und die Berechnung von Erdkörpern mit Bewehrungen aus Geokunststoffen (EBGEO), 2nd version. English version "Recommendations for design and analysis of earth structures using geosynthetic reinforcements" (2011)

DGGT (Deutsche Gesellschaft für Geotechnik) (2012)

Empfehlungen des Arbeitskreises "Pfähle" (EA-Pfähle), 2nd version. English version "Recommendations on piling" (2014)

Dhouib, A., Blondeau, F. (2005)

Colonnes ballastées – Techniques de mise en oeuvre, domaines d'application, comportement, justification, contrôle, axes de recherche et développement. Presses de l'Ecole Nationale des Ponts et Chaussées

- Dhouib, A., Wehr, J., Soyez, B., Priebe, H.J. (2004)
Méthode de Priebe: origine, développements et applications. ASEP-GI, International Symposium on Ground Improvement, Laboratoire Central des Ponts et Chaussées
- Duncan, J.M., Chang, C.Y. (1970)
Nonlinear analysis of stress and strain in soils. Journal of the Soil Mechanics and Foundations Division SM5, ASC, 1629-1653
- El-Mossallamy, Y. (1996)
Ein Berechnungsmodell zum Tragverhalten der Kombinierten Pfahl-Plattengründung. Technische Universität Darmstadt No. 48
- El-Mossallamy, Y., Franke, E. (1997)
Pfahl-Plattengründungen, Theorie und Anwendung. Bautechnik 74, No. 11, 755-764
- Estephan, R., Frank, R., Degny, E., Perlo, S. (2006)
GOUPEG: Application de la méthode "hybride" pour le calcul du comportement des groupes et des réseaux élémentaires de micropieux. Bulletin de Liaison des Laboratoires des Ponts et Chaussées No. 260, 55-68
- Everett, J.P. (1991)
Load transfer functions and pile performance modelling. Geotechnics in the African environment, Blight et al., Balkema, Rotterdam, 229-234
- Fernandez Polido, U., Ferreira França, H., José Rocha de Albuquerque, P., Felix, M., and Koehler, T. (2014)
Prova de carga à compressão instrumentada, em estaca cravada coldada in loco. COBRAMSEG 2014, Goiânia, Brazil
- Fleming, W.G.K. (1992)
A new method for single pile settlement prediction and analysis. Geotechnique 42, No. 3, 411-425
- Fleming, K., Weltman, A., Randolph, M., Elson, K. (1985)
Piling Engineering. 1st edition, Wiley, USA
- Fleming, K., Weltman, A., Randolph, M., Elson, K. (1985)
Piling Engineering. 3rd edition, Taylor & Francis, USA

- Frank, R. (1974)
Etude théorique du comportement des pieux sous charge verticale. PhD thesis, Paris IV, Paris, France
- Frank, R. (1985)
Recent developments in the prediction of pile behaviour from pressuremeter tests. From theory to practice on deep foundations, Porto Alegre, Brazil
- Frank, R. (1991)
Some recent developments on the behaviour of shallow foundations. Proceedings of the Xth European Conference on soil mechanics, Florence, Italy
- Frank, R. (1999)
Calcul des fondations superficielles et profondes. Presses des Ponts. Complements with lecture notes including update according to Eurocode 7 (2013, 2014)
- Frank, R. (2009)
Design of foundations in France with the use of Menard pressuremeter tests. Soil Mechanics and Foundation Engineering 46, No. 6, 219-231
- Frank, R. (2010)
Some aspects of research and practice for foundations design in France. 11th Šuklje day, Sept 17th 2010
- Frank, R., Kalteziotis, N., Bustamante, M., Christoulas, S. (1991)
Evaluation of performance of two piles using pressuremeter method. Journal of Geotechnical Engineering 117, No. 5, 695–713
- Frank, R., Kovarik, J.-B. (2005)
Comparaison des niveaux de sécurité, calage d'un coefficient de modèle pour la résistance ultime des pieux sous charges axiales. Revue française de géotechnique 110, 51 – 67
- Frank, R., Zhao, S.R. (1982)
Estimation à partir des paramètres pressiométriques de l'enfoncement sous charge axiale de pieux forés dans les sols fins. Bulletin de Liaison des Laboratoires des Ponts et Chaussées No. 119, 17-24
- Franke, E. (1979)
Setzungen von Pfählen und Pfahlgruppen. No reference information

- Franke, E., Lutz, B., El-Mossallamy, Y. (1994)
Pfahlgründungen und die Interaktion Bauwerk-Baugrund. *Geotechnik* 17, 157-172
- Gambin, M. (1963)
Calcul du tassement d'une fondation profonde en fonction des résultats pressiométriques. *Sols-Soils* 7, 11-28
- Gambin, M. (1979)
Utilisation du module pressiométrique et de la pression limite pour le calcul des fondations. *Sols-Soils* 28, 14-23
- Gambin, M. (2003)
Etude élémentaire d'un mythe. International Symposium on shallow foundations FONDSUP 2003, Laboratoire Central des Ponts et Chaussées
- Gambin, M. (2005)
Essais pressiométriques, Chapitre 4. In "Reconnaissance des terrains in situ", *Traité MIM (Mécanique et Ingénierie des Matériaux), Série Géomécanique*, Hermès Sciences Lavoisier Ed., I. Sharour and R. Gourves, 104-146
- Gambin, M. (2009)
Eoliennes et module d'Young. Technical note to the president of CFMS
- Gambin, M., Flavigny, E., Boulon, M. (1996)
Le module pressiométrique : historique et modélisation. XI^e colloque franco-polonais en mécanique des sols et des roches appliquée, Gdańsk, Poland
- Gambin, M., Frank, R. (2009)
Direct design rules for piles using Ménard Pressuremeter Tests. IFCEE 2009, Proc. Int. Foundation Congress Equipment Expo, Orlando, Florida, ASCE Geotechnical Publication No. 186, 111-118
- Gambin, M., Gomes Correia, A., Antao, A. (2002)
Validité de la mesure du module dans le domaine des petites aux moyennes déformations par essais de chargement in situ. International Symposium on the identification and determination of soil and rock parameters for geotechnical design PARAM 2002, Laboratoire Central des Ponts et Chaussées
- Gangakhedkar, R. (2004)
Geosynthetic reinforced pile-supported embankments. Master thesis, University of Florida

Glandy, M., Frossard, A. (2002)

Justification d'une fondation superficielle sur un sol renforcé d'inclusions. Annales du Bâtiment et des Travaux Publics No. 1, pp. 45-53

Gomes Correia, A., Nunez Antao, A., Gambin, M. (2005)

Comparaison des modules de déformation obtenus par essais de chargement à la plaque et essais pressiométriques. ISP5 – PRESSIO 2005, International Symposium 50 years of pressuremeters, LCPC/Presses de l'école nationale des ponts et chaussées

Goulet, G., Hulo, Y., Jézéquel, J. (1964)

Comparaison entre les résultats de chargement statique d'un pieu et les prévisions déduites des essais géotechniques. Sols-Soils 11, 21-31

Greenwood, D.A. (1970)

Mechanical improvement of soils below ground surface. Conference on Ground Engineering, Institution of civil engineers, London, United Kingdom, 11-22

Gwizdała, K. (1996)

The analysis of piles settlements employing load-transfer functions (in Polish). Technical University Gdańsk, Zesz. Nauk. PG No. 532, Budownictwo Wodne No. 41

Hamidi, B., Nikraz, H., Varaksin, S. (2010)

Correlations between CPT and PMT at a dynamic compaction project. Proceedings of 2nd International Symposium on Cone Penetration Testing, Huntington Beach, California

Han, J., Gabr, M.A. (2002)

Numerical analysis of geosynthetic-reinforced and pile-supported earth platforms over soft soil. Journal of geotechnical and geoenvironmental engineering 128, No. 1, 44-53

Hanisch, J., Katzenbach, R., König, G. (2002)

Kombinierte Pfahl-Plattengründungen, Richtlinie für den Entwurf, die Bemessung und den Bau von Kombinierten Pfahl-Plattengründungen („KPP-Richtlinie“ or CPRF-guideline)

- Hirayama, H. (1990)
Load-settlement analysis for bored piles using hyperbolic transfer functions. *Soils and Foundations* 30, No. 51, Japanese Society of Soil Mechanics and Foundation Engineering, 55-64
- Holzlohner, U. (1999)
Der nichtlineare heterogene Halbraum. *Geotechnik* 22, No. 2, 96-113
- Höppner, R. (2011)
Feldversuche mit Vollverdränger-Betonsäulen. Diploma thesis, Universität Kassel
- IREX (Institut pour la Recherche et l'Expérimentation en Génie civil) (2004)
Recommendations of the French national project on micropiles FOREVER. Operation of the civil and urban engineering network, France
- IREX (Institut pour la Recherche et l'Expérimentation en Génie civil) (2012)
Recommendations of the French national project on rigid inclusions ASIRI. Operation of the civil and urban engineering network, France
- Katzenbach, R. (2015)
Lecture notes "Studienunterlagen Geotechnik". Technische Universität Darmstadt
- Katzenbach, R., Bohn, C., Wehr, J. (2011)
Vergleich der Sicherheitskonzepte bei Baugrundverbesserungsmethoden mit Betonsäulen. 19th Darmstadt Geotechnical Conference, Darmstadt, Germany
- Katzenbach, R., Choudhury, D. (2013)
ISSMGE Combined Pile-Raft Foundation Guideline. Technische Universität Darmstadt
- Keller Company (2013)
CSC, Rigid Inclusions. Brochure 35-02E
- Keller Company (2015)
User manual, KID (Keller Improvement Designer), internal Keller software
- Kempfert, H.-G., Göbel, C., Alexiew, D., Heitz, C. (2004)
German recommendations for reinforced embankments on pile-similar embankments. 3rd Geosynthetics Conference EUROGeo3, Munich, Germany, 279-283

- Kirsch, F. (2004)
Experimentelle und numerische Untersuchungen zum Tragverhalten von Rüttelstopfsäulengruppen. PhD thesis, Technische Universität Braunschweig
- Klobe, B. (2007)
Die erdstatische Berechnung geotechnischer Flächentragwerke. Bautechnik 84, No. 2, 94-102
- Kraft, L.M., Ray, R.P., and Kagawa, T. (1981)
Theoretical t-z curves. Journal of Geotechnical Engineering 107, No. 11, 1543-1561
- Krasiński, A. (2010)
Model tests of screwed piles. From Research to Design in European practice, Bratislava, Slovak Republic, June 2-4
- Krasiński, A. (2011)
Advanced field investigations of screw piles and columns. Archives of civil engineering 57, No. 1, 45-57
- Krasiński, A. (2012a)
Proposal for calculating the bearing capacity of screw displacement piles. Studia Geotechnica et Mechanica 34, No. 4, 41-51
- Krasiński, A. (2012b)
Pale przemieszczeniowe wkręcane. Nośność i praca w gruntach niespoistych, Habilitation, Gdańsk University of Technology, 259 p.
- Kudella, P., Reul, O. (2002)
Hypoplastic analyses of piled rafts. 5th European conference – Numerical methods in geotechnical engineering, Laboratoire Central des Ponts et Chaussées
- Le Roy, R., Parant, E., Boulay, C. (2005)
Taking into account the inclusions' size in lightweight concrete compressive strength prediction. Cement and concrete research 35, 770-775
- Liu, J., Xiao, H.B., Tang, J., and Li, Q.S. (2004)
Analysis of load-transfer of single pile in layered soil. Computers and Geotechnics 31, 127-135

- Lunne, T., Robertson, P.K. and Powell, J.J.M. (1997)
Cone penetration testing in geotechnical practice. Blackie Academic/Chapman & Hall, E&FN Spon, 312 p.
- Lutenegger, A.J., Adams, M.T. (2003)
Characteristic load-settlement behaviour of shallow foundations. FONDSUP 2003, International Symposium on shallow foundations, Laboratoire Central des Ponts et Chaussées, Paris, France, Vol. 2, 381-392
- Lutz, B. (2002)
Beitrag zur Modellierung des Tragverhaltens kombinierter Pfahl-Plattengründungen (KPP) unter Verwendung geotechnischer Messungen. Technische Universität Darmstadt No. 63
- Lutz, B., El-Mossallamy, Y., Richter, T. (2006)
Ein einfaches, für die Handrechnung geeignetes Berechnungsverfahren zur Abschätzung des globalen Last-Setzungsverhaltens von Kombinierten Pfahl-Plattengründungen. Bauingenieur 81
- Mader, H. (1989)
Untersuchungen über den Primärspannungszustand in bindigen überkonsolidierten Böden am Beispiel des Frankfurter Untergrundes. Technische Universität Darmstadt No. 29
- Magnan, J.-P. (2006-2007)
Lecture notes “Mécanique des sols et des roches”. Ecole Nationale des Ponts et Chaussées
- Mair, R.J., Wood, D.M. (1987)
Pressuremeter testing – Methods and interpretation. Construction Industry Research and Information Association (London)
- Marchal, J. (1971)
Calcul du tassement des pieux à partir des méthodes pressiométriques. Bulletin de Liaison des Laboratoires des Ponts et Chaussées No. 52, 22 -25
- McVay, M. C., Townsend, F. C., Bloomquist, D. G., O’Brien, M. O., Caliendo, J. A. (1989)
Numerical analysis of vertically loaded pile groups. Foundation Engineering Congress: Current Principles and Practices, Evanston, IL, 675-690

- Meek, J.W. (1996)
Das Knicken von Verpresspfählen mit kleinem Durchmesser in weichem, bindigem Boden. Bautechnik 73, No. 3, 162-168
- Meier, C.P., Schanz, T. (1998)
Verformungsabschätzungen für Gründungen mittels Rüttelstopfverdichtung. 5th Darmstadt Geotechnical Conference, Darmstadt, Germany
- Ménard, L. (1957)
An apparatus for measuring the strength of soils in place. Master thesis, University of Illinois
- Ménard, L. (1961)
Influence de l'amplitude et de l'histoire d'un champ de contraintes sur le tassement d'un sol de fondation. Vth International Conference on Soil Mechanics and Foundation Engineering
- Ménard, L. (1963a)
Calcul de la force portante des fondations sur la base des résultats des essais pressiométriques. Sols-Soils 5, 9-29
- Ménard, L. (1963b)
Calcul de la force portante des fondations sur la base des résultats des essais pressiométriques – Seconde Partie : Essais expérimentaux et conclusion. Sols-Soils 6, 9-30
- Ménard, L., Rousseau, J. (1962)
L'évaluation des tassements – Tendances nouvelles. Sols-Soils 1, 13-30
- Moseley, M.P., Kirsch, K. (2004)
Ground Improvement. 2nd edition, Spon Press, New York
- Nogneng, D. (2013)
Theoretical basis of algorithm for single pile, rigid slab, embankment and footing calculation options of Keller internal KID-LTM software, part of internship, supervisors: C. Bohn and S. Lambert (Keller Fondations Spéciales), and complements as student work (private communication)
- Nunez, M., Dias, D., Alves dos Santos, B., Simon, B. (2010)
Modélisation continue : chargement d'inclusions isolées. ASIRI national project, internal report 4.10.4.1 "Tranche 4"

Nutt, N.R.F. (1993)

Development of the cone pressuremeter. PhD thesis, University of Oxford

O'Neill, M.W., Ghazzaly, O.I. (1977)

Analysis of three-dimensional pile groups with non-linear soil response and pile-soil-pile interaction. Offshore Technology Conference, Houston, Texas, USA, 245-256

Okyay, U.S. (2010)

Etude expérimentale et numérique des transferts de charge dans un massif renforcé par inclusions rigides - Application à des cas de chargements statiques et dynamiques. PhD thesis in the scope of ASIRI, INSA Lyon and Université Claude Bernard – Lyon 1

Perlo, S. (2003)

Etude numérique par l'approche hybride des groupes de pieux. PhD thesis, Ecole Nationale des Ponts et Chaussées - CERMES

Philipponnat, G., Hubert, B. (2000)

Fondations et ouvrages en terre. Eyrolles, 576 p.

Pichler, P. (2014)

Rechnerische Untersuchungen zum Tragverhalten von Mikropfählen. Master thesis, Technische Universität Graz

Plaxis (2013)

Plaxis 3D 2013 manual, Editors: Brinkgreve, R.B.J., Engin, E. and Swolfs, W.M., Netherlands

Plaxis (2014)

Plaxis 2D Anniversary Edition manual, Editors: Brinkgreve, R.B.J., Engin, E. and Swolfs, W.M., Netherlands

Plaxis (2015)

Plaxis 3D Anniversary Edition manual, Editors: Brinkgreve, R.B.J., Kumarswamy, S. and Swolfs, W.M., Netherlands

Poulos, H.G. (1981)

Pile foundations subjected to vertical loading. Symposium on Geotechnical Aspects of Coastal and Offshore Structures, Bangkok, Thailand

- Poulos, H.G., Davis, E.H. (1968)
The settlement behaviour of single axially loaded incompressible piles and piers. *Geotechnique* 18, 351-371
- Powell, J.J.M., Shields, C.H., Frank, R., Dupla, J.-C., Mokkelbost, K.H. (2005)
A cone pressuremeter method for design of axially loaded piles in clay soils. *ISP5 – PRESSIO 2005, International Symposium 50 years of pressuremeters*, LCPC/Presses de l'école nationale des ponts et chaussées
- Priebe, H. (1976)
Abschätzung des Setzungsverhaltens eines durch Stopfverdichtung verbesserten Baugrundes. *Bautechnik* 53, No. 5, 160-162
- Priebe, H. (1978)
Abschätzung des Scherwiderstandes eines durch Stopfverdichtung verbesserten Baugrundes. *Bautechnik* 55, No. 8, 281-284
- Priebe, H. (1988)
Zur Abschätzung des Setzungsverhaltens eines durch Stopfverdichtung verbesserten Baugrundes. *Bautechnik* 65, No. 1, 23-26
- Priebe, H. (1995)
Die Bemessung von Rüttelstopfverdichtungen. *Bautechnik* 72, No. 3, 183-191
- Priebe, H. (2003)
Zur Bemessung von Rüttelstopfverdichtungen - Anwendung des Verfahrens bei extrem weichen Böden, bei schwimmenden Gründungen und beim Nachweis der Sicherheit gegen Gelände- oder Böschungsbruch. *Bautechnik* 80, No. 6, 380-384
- Priebe, H. (2004)
Le dimensionnement des colonnes ballastées. *ASEP-GI, International Symposium on Ground Improvement, Laboratoire Central des Ponts et Chaussées*
- Randolph, M.F. (1983)
Design of piled raft foundations. *Proc. Int. Symp. on Recent Developments in Laboratory and Field Tests and Analysis of Geotechnical Problems, Bangkok*, 525-537
- Randolph, M.F. (1994)
Design methods for pile groups and piled rafts. *13th International Conference for Soils Mechanics and Foundation Engineering, New Delhi, India*, 61-82

- Randolph, M.F., Wroth, C.P. (1978)
Analysis of deformation of vertically loaded piles. Journal of the geotechnical engineering division 104, No. 2, 1465-1488
- Randolph, M.F., Wroth, C.P. (1979)
An analysis of the vertical deformation of pile groups. Geotechnique 29, No. 4, 423-439
- Reul, O. (2000)
In-situ-Messungen und numerische Studien zum Tragverhalten der Kombinierten Pfahl-Plattengründung. Technische Universität Darmstadt No. 53
- Reul, O. (2002)
Untersuchungen zur effizienten Setzungsreduktion von Kombinierten Pfahl-Plattengründungen. Bautechnik 79, No. 3, 160-166
- Richter, T., Lutz, B. (2010)
Berechnung einer Kombinierten Pfahl-Plattengründung am Beispiel des Hochhauses "Skyper" in Frankfurt/Main. Bautechnik 87, No. 4, 204-211
- Rudolph, M. (2005)
Beanspruchung und Verformung von Gründungskonstruktionen auf Pfahlrosten und Pfahlgruppen unter Berücksichtigung des Teilsicherheitskonzeptes. Universität Kassel No. 17
- Rostami, A. (2013)
Modelling of the load-settlement behaviour of piles with the finite element method. Report of internship at Keller Holding GmbH (private communication)
- Sabatini, P.J., Summers, P., Villet, W., Clukey, E.C., Richardson, K. (2012)
Observational and numerical evaluation of defects in deep mixing method columns used for LNG process train structural foundation support. 37th Annual Conference on Deep Foundations, Houston, Texas, USA, 181-190
- Sanglerat, G. (1972)
The penetrometer and soil exploration. Elsevier, Amsterdam
- Santos, A. L. (2013a)
Development of mobilization functions for skin friction and tip resistance without pressuremeter parameters. Project thesis, MSROE Master, Ecole Nationale des Ponts et Chaussées, supervisors: Bohn, C. and Frank, R

Santos, A. L. (2013b)

Calibration and numerical implementation of mobilization curves for pile skin friction and tip resistance based on pile load tests. Master thesis, MSROE Master, Ecole Nationale des Ponts et Chaussées, supervisors: Bohn, C. and Lambert, S. (Keller Fondations Spéciales)

Schweiger, H.F., Sedighi, P., Henke, S., Borchert, K.-M. (2014)

Numerical modelling of ground improvement techniques considering tension softening. Geotechnical Aspects of Underground Constructions in Soft Ground, Korean Geotechnical Society, Seoul, Korea, 209-214

Seed, H. B., and Reese, L. C. (1957)

The action of soft clay along friction piles. American Society of Civil Engineers Transactions

Shen, W.Y., Chow, Y.K., Yong, K.Y. (2000)

Practical method for settlement analysis of pile groups. Journal of Geotechnical and Geoenvironmental Engineering 126, No. 10, 890-897

Smolczyk, U., (2001)

Grundbau-Taschenbuch. 6th edition, Ernst & Sohn, Berlin

Sovinc, I. (1981)

Buckling of piles with initial curvature. 10th ICSMFE, Stockholm, Sweden, Vol. 2.

Soyez, B. (1985)

Méthodes de dimensionnement des colonnes ballastées. Bulletin de Liaison des Laboratoires des Ponts et Chaussées No. 1, 35-51

Techniques Louis Ménard (1975)

Interpretation and Application of Pressuremeter Test Results. General Notice (notice D60 an.), Sols-Soils 26, 5-45

Techniques Louis Ménard (1976)

Règles relatives à l'exécution des essais pressiométriques sur le terrain. Notice de base dite "Notice Exécution" (D10) No. 27, 5-24, and translation "Principles of Pressuremeter Testing" (notice D10 an.)

Techniques Louis Ménard (1978a)

Calcul rapide de la force portante ou de la fiche d'un pieu. Notice (notice D32)

Techniques Louis Ménard (1978b)

Estimation rapide des tassements des fondations superficielles rigides sous charges statiques. Notice (notice D37)

Tomlinson, M., and Woodward, J. (2008)

Pile design and construction practice. Taylor & Francis, USA & Canada

Trunk, U., Sondermann, W., Bohn, C., Ackermann, T. (2014)

Ermittlung des Einflusses von geometrischen Ausführungsunperfektionen auf das Verformungs- und Tragverhalten von steifen Baugrundverbesserungselementen mit FEM-Berechnungen. 21st Darmstadt Geotechnical Conference, Darmstadt, Germany, 67-78

Van Eekelen, S.J.M., Bezuijen, A., Lodder, H.J., Van Tol, A.F. (2012)

Model experiments on piled embankments – Part II. Geotextiles and Geomembranes 32, 82-94

Van Impe, W.F. (2001)

Récents mises au point en amélioration et renforcement des sols – Réflexions sur l'efficacité des colonnes ballastées. XVth International Congress on Soil Mechanics and Geotechnical Engineering, Istanbul, Turkey, 309-312

Van Impe, W.F., De Beer, E. (1983)

Improvement of settlement behaviour of soft layers by means of stone columns. VIIIth European Congress on Soil Mechanics and Geotechnical Engineering, Helsinki, Finland, 309-312

Van Impe, W.F., De Clercq, Y. (1994)

A piled raft interaction model. General report, Stuttgart

Van Wambeke, A. (1962)

Méthodes d'investigation des sols en place – Etude d'une campagne d'essais comparatifs. Sols-Soils 2, 9-18

Van Weele, A.F. (1999)

Pile foundation failure, expensive but instructive. Stuttgarter Symposium 1999, Stuttgart, Germany

Vautrain, J. (1980)

Comportement et dimensionnement des colonnes ballastées. Revue française de géotechnique 11, 59-73

- Verbrugge, J.-C. (1981)
Evaluation du tassement des pieux à partir de l'essai de pénétration statique.
Revue Française de Géotechnique 15, 75-82
- Viggiani, C., Mandolini, A., Russo, G. (2012)
Piles and pile foundations. Spon Press, New York
- Vijayvergiya, V.N. (1977)
Load-movement characteristics of piles. Ports'77: 4th Annual Symposium of the
Waterway, Port, Coastal, and Ocean Division, Long Beach, California, USA, 269-
284
- Vogt, N. (2015)
Lecture notes "Vorlesungsskript Grundbau". Technische Universität München
- Vogt, N., Vogt, S., Kellner, C. (2009)
Buckling of slender piles in soft soil. Bautechnik Special issue 2009, 98-112
- Wang, Z., Xie, X., and Wang, J. (2012)
A new nonlinear method for vertical settlement prediction of a single pile and pile
groups in layered soils. Computers and Geotechnics 45, 118-126
- Wehr, J., Sondermann, W. (2011)
Risiken bei der Bemessung von Baugrundverbesserungsmethoden und
pfahlähnlichen Traggliedern. Bauingenieur 86, 459-463
- Wimmer, H., Ofner, R. (2006)
Traglastberechnungen von Mikropfählen in weichen Böden. Bauingenieur 81, 53-
60
- Wind, H. (1992a)
Baugrunderkundungsbohrungen Hessische Landeszentralbank, Frankfurt am Main
– Bohrlochaufweitungsversuche. Report of pressuremeter tests in Frankfurt clay,
report Nr. 9/92-PR, Versuchsanstalt für Bodenmechanik und Grundbau,
Technische Hochschule Darmstadt
- Wind, H. (1992b)
Baugrunderkundungsbohrungen Japan-Center, Frankfurt am Main –
Bohrlochaufweitungsversuche. Report of pressuremeter tests in Frankfurt clay,
report Nr. 13/92, Versuchsanstalt für Bodenmechanik und Grundbau, Technische
Hochschule Darmstadt

Youssef, E. (1994)

Etude théorique et expérimentale du flambement des pieux. PhD thesis, Ecole Nationale des Ponts et Chaussées - CERMES

Zaeske, D., Kempfert, H.-G. (2002)

Berechnung und Wirkungsweise von unbewehrten und bewehrten mineralischen Tragschichten über punkt- und Linienförmigen Traggliedern. Bauingenieur 77, 80-86

Zhang, Q.-Q., Zhang, Z.-M., and He, J.-Yu (2010)

A simplified approach for settlement analysis of single pile and pile groups considering interaction between identical piles in multilayered soils. Computers and Geotechnics 37, 969-976

List of standards

DIN EN 1992-1-1 (2011)

Eurocode 2: Bemessung und Konstruktion von Stahlbeton- und Spannbetontragwerken – Teil 1-1: Allgemeine Bemessungsregeln und Regeln für den Hochbau. Deutsches Institut für Normung e.V. (DIN)

DIN EN 1992-1-1/NA (2013)

Nationaler Anhang – National festgelegte Parameter – Eurocode 2: Bemessung und Konstruktion von Stahlbeton- und Spannbetontragwerken – Teil 1-1: Allgemeine Bemessungsregeln und Regeln für den Hochbau. Deutsches Institut für Normung e.V. (DIN)

DIN EN 1997-1 (2014)

Eurocode 7: Entwurf, Berechnung und Bemessung in der Geotechnik – Teil 1: Allgemeine Regeln. Deutsches Institut für Normung e.V. (DIN)

DIN EN 1997-1/NA (2010)

Nationaler Anhang – National festgelegte Parameter – Eurocode 7: Entwurf, Berechnung und Bemessung in der Geotechnik – Teil 1: Allgemeine Regeln. Deutsches Institut für Normung e.V. (DIN)

DIN EN 1997-2 (2010)

Eurocode 7: Entwurf, Berechnung und Bemessung in der Geotechnik – Teil 2: Erkundung und Untersuchung des Baugrunds. Deutsches Institut für Normung e.V. (DIN)

DIN 1054 (2010)

Baugrund – Sicherheitsnachweise im Erd- und Grundbau – Ergänzende Regelungen zu DIN EN 1997-1. Deutsches Institut für Normung e.V. (DIN)

DIN 18134 (2012)

Baugrund – Versuche und Versuchsgeräte – Plattendruckversuch. Deutsches Institut für Normung e.V. (DIN)

DIN 4017 (2006)

Baugrund – Berechnung des Grundbruchwiderstands von Flachgründungen. Deutsches Institut für Normung e.V. (DIN)

DIN 4019 (2015)

Baugrund – Setzungsberechnungen. Deutsches Institut für Normung e.V. (DIN)

EN 12699 (2015)

Execution of special geotechnical works – Displacement piles. European Committee for Standardization (CEN)

EN 14199 (2015)

Execution of special geotechnical works – Micropiles. European Committee for Standardization (CEN)

EN 1536 (2010)

Execution of special geotechnical works – Bored piles. European Committee for Standardization (CEN)

EN 1992-1-1 (2004) + AC (2010)

Eurocode 2: Design of concrete structures – Part 1-1: General rules and rules for buildings. European Committee for Standardization (CEN)

EN 1997-1 (2004) + AC (2009) + A1 (2013)

Eurocode 7: Geotechnical design – Part 1: General rules. European Committee for Standardization (CEN)

EN 1997-2 (2007) + AC (2010)

Eurocode 7: Geotechnical design – Part 2: Ground investigation and testing. European Committee for Standardization (CEN)

EN ISO 22476-1 (2012)

Geotechnical investigation and testing – Field testing – Part 1: electrical cone and piezocone penetration test. European Committee for Standardization (CEN)

EN ISO 22476-4 (2012)

Geotechnical investigation and testing – Field testing – Part 4: Ménard pressuremeter test. European Committee for Standardization (CEN)

NF EN 1992-1-1 (2005)

Eurocode 2 : Calcul des structures en béton – Partie 1-1 : règles générales et règles pour les bâtiments. Association Française de Normalisation (AFNOR)

NF EN 1992-1-1/NA (2007)

Eurocode 2 : calcul des structures en béton – Partie 1-1 : règles générales et règles pour les bâtiments - Annexe Nationale à la NF EN 1992-1-1:2005 - Règles générales et règles pour les bâtiments. Association Française de Normalisation (AFNOR)

NF EN 1997-1 (2014)

Eurocode 7 : Calcul géotechnique – Partie 1 : règles générales. Association Française de Normalisation (AFNOR)

NF EN 1997-1/NA (2006)

Eurocode 7 : Calcul géotechnique – Partie 1 : règles générales – Annexe Nationale à la NF EN 1997-1. Association Française de Normalisation (AFNOR)

NF EN 1997-2 (2007)

Eurocode 7 : Calcul géotechnique – Partie 2 : Reconnaissance des terrains et essais, 2nd print 2010. Association Française de Normalisation (AFNOR)

NF P94-110-1 (2000)

Sols : reconnaissance et essais, Essai pressiométrique Ménard, Partie 1 : Essai sans cycle. Association Française de Normalisation (AFNOR)

NF P94-110-2 (1999)

Sols : reconnaissance et essais, Essai pressiométrique Ménard, Partie 2 : Essai avec cycle. Association Française de Normalisation (AFNOR)

NF P94-113 (1996)

Sols : reconnaissance et essais, Essai de pénétration statique. Association Française de Normalisation (AFNOR)

NF P94-117-1 (2000)

Sols : reconnaissance et essais, Portance des plates-formes – Partie 1 : module sous chargement statique à la plaque (EV2). Association Française de Normalisation (AFNOR)

NF P94-117-3 (2008)

Sols : reconnaissance et essais, Portance des plates-formes – Sols : reconnaissance et essais - Portance des plates-formes - Partie 3 : coefficient de réaction de Westergaard sous chargement statique d'une plaque. Association Française de Normalisation (AFNOR)

NF P94-261 (2013)

Justification des ouvrages géotechniques – Normes d'application nationale de l'Eurocode 7 – Fondations superficielles. Association Française de Normalisation (AFNOR)

NF P94-262 (2012)

Justification des ouvrages géotechniques – Normes d'application nationale de l'Eurocode 7 – Fondations profondes. Association Française de Normalisation (AFNOR), 2nd print 2013

Appendix A. Soil deformation parameters and settlement of usual foundations

A.1 General aspects

Different “soil moduli” or soil deformation parameters, meaning a relation between stress and strain in soils, can be defined for soils, given that the behaviour of soils is highly dependent on the boundary conditions and on the loading type. The idea of a modulus of the soil is always related to Hooke’s elasticity theory implying a complete reversibility of strains, and based on analogies with tests executed on ideal elastic materials.

The Young’s modulus for elastic materials E has been defined for the uni-axial compression or tension test on a rigid material (Fig. A.1), which requires no lateral confinement for its stability, on the contrary to many soils. The horizontal expansion of the elastic material is defined using the Poisson’s ratio ν between 0 and 0.5, $\nu = 0.5$ meaning an incompressible material with no volume change ($\Delta V = 0$).

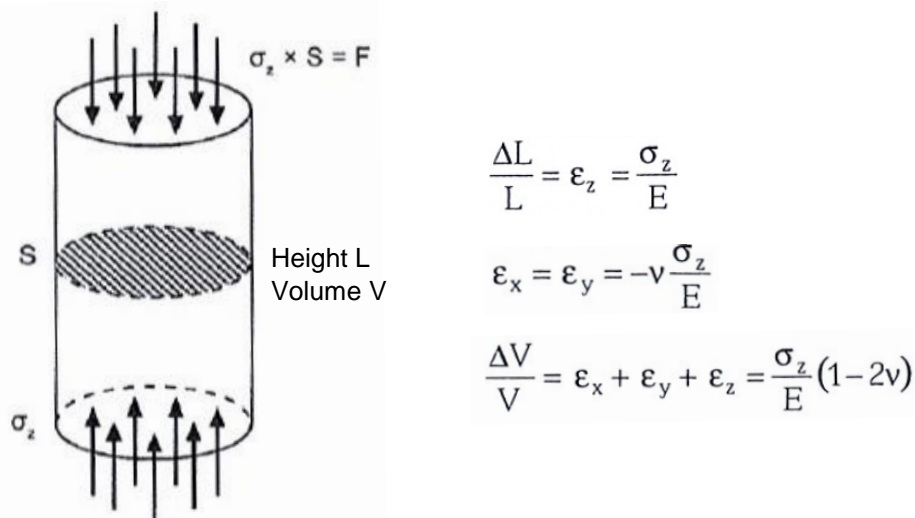


Fig. A.1 Compression uni-axial test on elastic material (Combarieu 2006)

Ideal isotropic linear elastic materials (further simply named “elastic”) show a linear stress-strain curve, so that only one modulus can describe the whole behaviour. For all real materials and for soil in particular, different values have to be defined depending on the absolute value of stress and strain. A greater strain leads in this case to a smaller modulus. Fig. A.2 shows the stress-strain curve for an ideal elastic material and for a soil under so-called “tri-axial” conditions (here horizontal isotropic constraint $\sigma_2 = \sigma_3$).

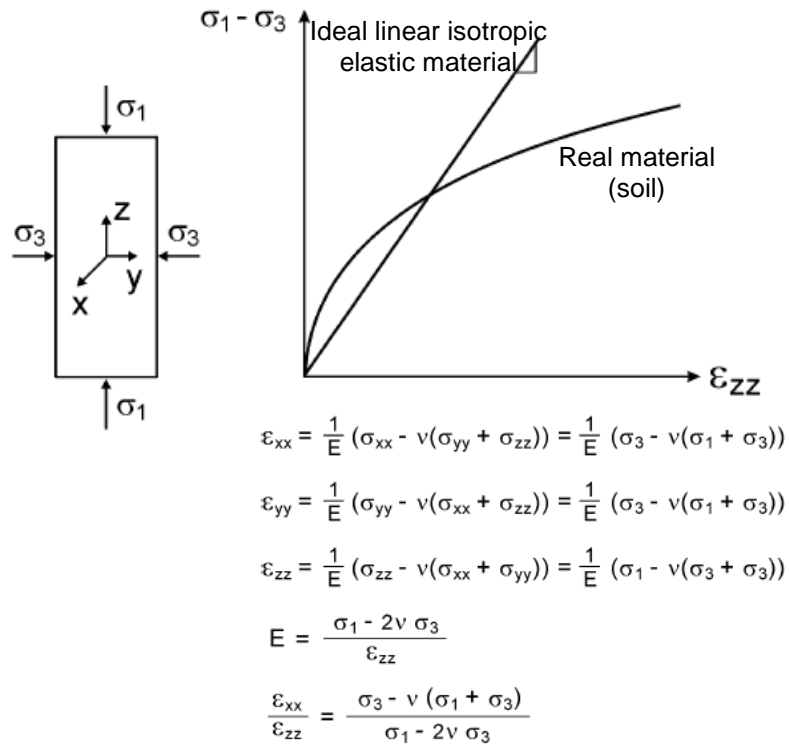


Fig. A.2 Compression tri-axial test on elastic material and on soil (Briaud 2000)

A soil modulus E is in kN/m^2 (kPa) and should not be confused with a soil stiffness K in kN/m , K being defined as an applied force divided by the displacement experienced by the loaded area, or with a coefficient of subgrade reaction k in kN/m^3 defined as a load pressure divided by a displacement. The stiffness and the coefficient of subgrade reaction are not soil properties and depend on the size of the loading area (Briaud 2000).

Different moduli for soils can be defined, in analogy to the curve for an elastic material (Fig. A.3).

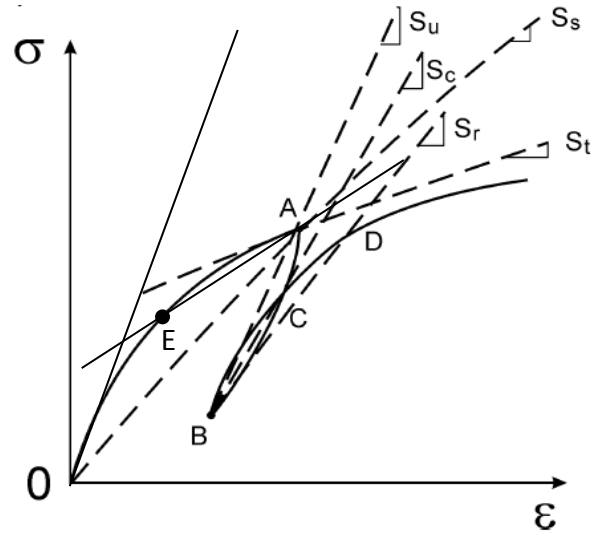


Fig. A.3 Different slopes in stress-strain curve, adapted from (Briaud 2000)

In Fig. A.3, a “secant modulus from the origin” would be linked to the slope between the points O and A, and would define the first loading of a spread footing (plate load test) for example. It is important to note that the modulus decreases if the strain increases. A “secant modulus” can be defined between any points of the curve, for example A and E, between two different load levels. The “tangent modulus” defined from the slope of the tangent line to point A would correspond to an incremental loading, and decreases if the strain increases. The slope between point A and B (mean slope of the curve between these points) corresponds to an “unloading modulus”. A modulus between point B and D would be a “reloading modulus”. The slope between C and D corresponds to a repeated (cyclic) loading case.

An additional modulus could be defined as the tangent at the origin of the curve. This “initial modulus” is much greater than the secant or tangent modulus in the usual relative deformation range for foundations of 10^{-3} to 10^{-2} . The initial modulus can be considered as an elasticity modulus for soil states with reversible deformations, but only up to relative deformations of an order of 10^{-5} (Combarieu 2006). This high rigidity of the soil at small strains has been examined by Burland (1989) in practical cases. Ménard (1961) indicates as well a ratio of 3 for most soils and up to 20 for very soft soils between the modulus for micro-deformations E_e (10^{-6} to 10^{-5}) and the modulus under strains of 10^{-3} to 10^{-2} . In Fig. A.4, the modulus is represented for the case of a cylindrical expansion in terms of absolute deformations, which after division by the diameter of a pressuremeter probe (approximately 10 cm) give a strain range of 10^{-6} to 10^{-1} .

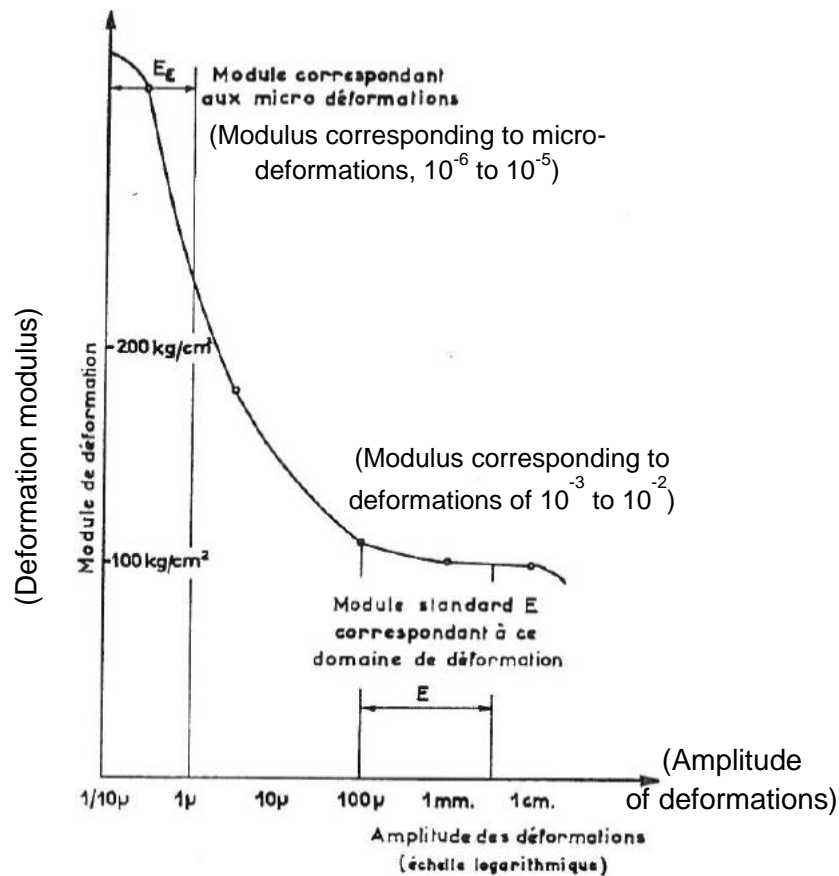


Fig. A.4 Modulus vs. amplitude of deformations (Ménard 1961)

The cyclic moduli for the deformation range of foundations can come close to this initial modulus (small deformations) but remains smaller (Combarieu 2006).

The tri-axial testing is in general not directly used for settlement calculations and no common method has been developed for this, since several time-expensive tests, for each stress condition at each depth, would be necessary for such an application. Tri-axial tests are commonly used to determine the parameters of shear resistance (cohesion and friction angle). Consequently, several tests with different constraint stresses σ_3 or σ_c have to be carried out. This is the opportunity to show that the modulus increases with the confinement and thus with the depth (Fig. A.5), even if in general no modulus is directly defined from this test for practical foundation design. Indeed, a direct application of “tri-axial moduli” would be too time-consuming, because a new test would have to be carried out at each considered depth, unlike in the simplified oedometric method (laterally confined conditions, see next section), where only one test can approximate the behaviour of the soil for different depth and stress levels as long as the layer is homogeneous.

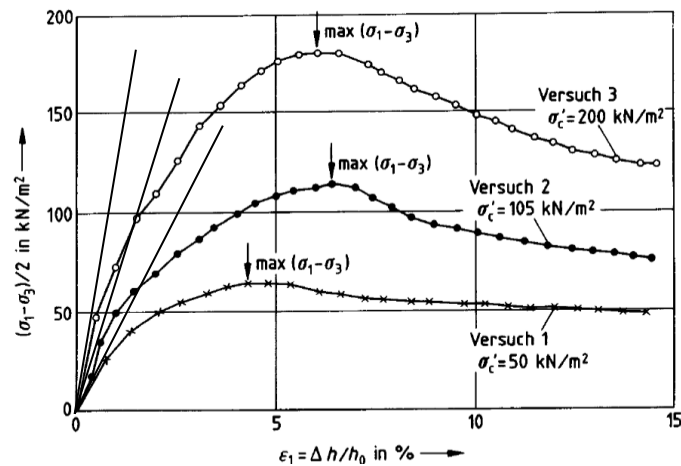


Fig. A.5 Different initial slopes for different confinement level in tri-axial tests (Katzenbach, lecture notes 2015)

It is then clear that a Young's modulus makes no sense for soils (Gambin 2009). One could only define an "equivalent Young's modulus" associated to a given loading type condition with a back analysis using the theoretical elastic solution for this loading type (Gambin et al. 1996, Gambin et al. 2002). A Young's modulus is however sometimes required for elastic or for the elastic domain in elastic-plastic (for example with Mohr-Coulomb plasticity criterion) numerical modelling. It is for such simple models compulsory to choose the modulus to be computed in adjusting a modulus known from laboratory tests or in situ tests with consideration of the deformation range expected and of the loading type.

Soil moduli depend on the direction of loading due to anisotropic properties of soils, on the direction of loading, either static (unidirectional), cyclic (bidirectional) or cyclic with change of direction of loading (see hypoplastic modelling in Fig. A.6), and on the loading rate as well.

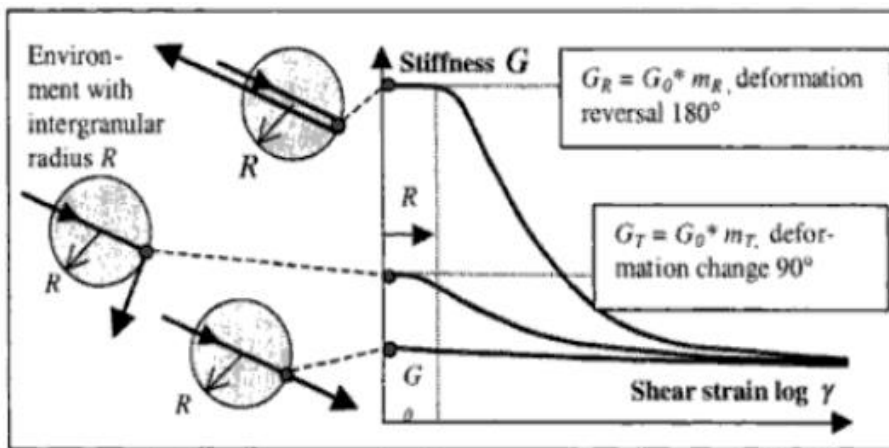


Fig. A.6 Shear modulus depending on shear strain and loading direction in hypoplastic model (Kudella and Reul 2002)

A.2 Oedometer test

The most used laboratory test to derive deformation parameters and moduli of fine saturated soils for practical applications is the compression test on a laterally confined sample (oedometer test). On a mechanical point of view, this test corresponds to the above presented uni-axial test with full lateral confinement (Fig. A.7), that is with no lateral deformation. This test was developed to measure the time-settlement behaviour of soils, which is relevant only for cohesive soils. However, this test and the moduli which can be defined from it are in practice sometimes extended to coarse-grained soils.

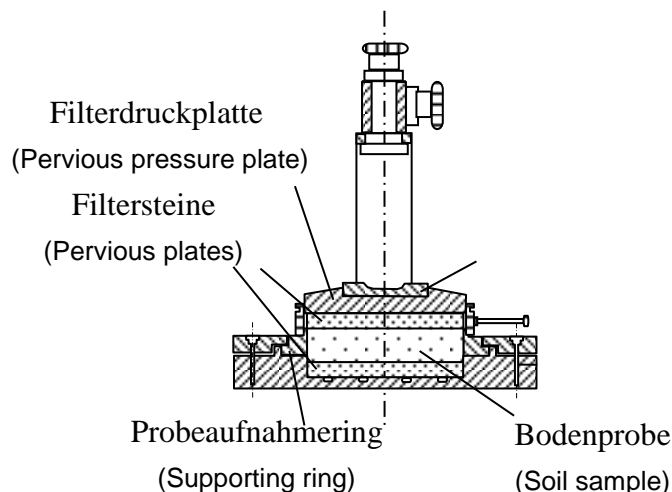


Fig. A.7 Oedometer test (Katzenbach, lecture notes 2015)

In oedometric conditions, the axial deformation is much reduced compared to the uni-axial or tri-axial compression under the same load. Using the analogy with the theory of elasticity again, an “oedometer modulus” E_{oed} can be defined from the Young’s modulus as in (Eq. A.1) and (Eq. A.2).

$$E_{oed} = E \cdot \frac{1-\nu}{(1+\nu) \cdot (1-2\nu)} \quad (\text{Eq. A.1})$$

$$\varepsilon_z = \frac{\sigma_z}{E} \cdot \frac{(1+\nu) \cdot (1-2\nu)}{1-\nu} = \frac{\sigma_z}{E_{oed}} \quad (\text{Eq. A.2})$$

A Poisson’s ratio of $\nu = 0.5$ corresponds in theory to an incompressibility of the material; in that case E_{oed} is infinite.

The load case under a fill or under very large load areas, where the lateral deformation of a soil element is prevented because of the similar loading of the adjacent soil element, is similar to this ideal oedometer case with no lateral deformation. Thus settlement calculations are often done using this mechanical analogy (Fig. A.8). This model is sometimes extrapolated to shallow foundations of limited dimensions as a simplified method. This approach is however controversial, due to the existing shearing lateral deformations in this load configuration.

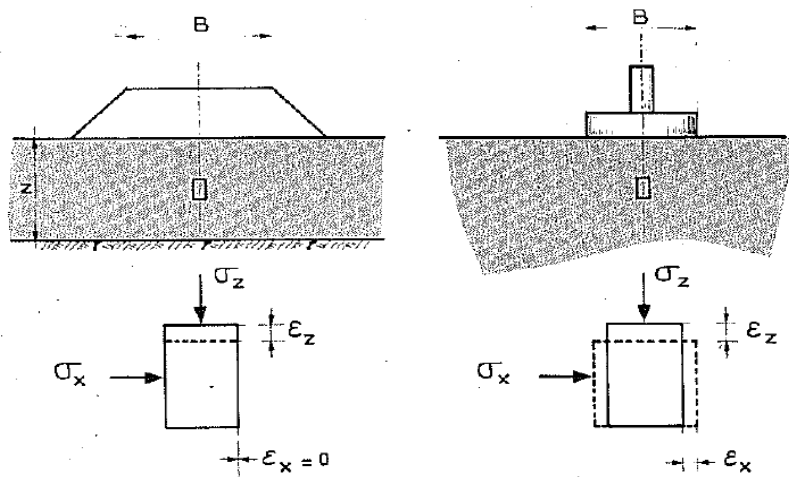


Fig. A.8 Deformation of soil element under large and limited loading area (Baguelin et al. 1978)

In the reality of soil mechanics, the relation between stress and strain for a soil element in an oedometer test is absolutely not linear. As already seen, the tangent or the secant modulus of the soil (in a given stress range) increases with the constraint and thus with

the mean load applied. It is here important to notice that the curvature of the line in the oedometer test is oriented in the opposite direction than for the usual stress-strain curve for soils (Fig. A.9), due to the rigid wall around the probe (Fig. A.7). This corresponds to a spherical or pure compression stress field in an elastic-plastic material, where deviatoric or shear stresses are not considered (Ménard 1961) (Fig. A.10).

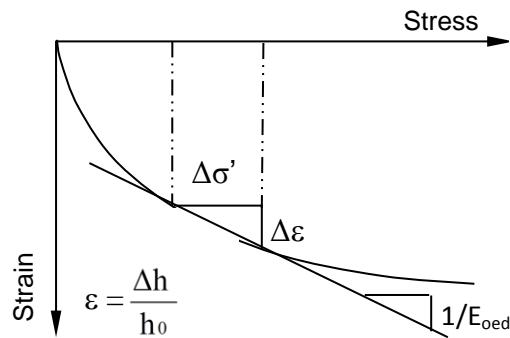


Fig. A.9 Stress-strain curve in oedometer test (non-linearity)

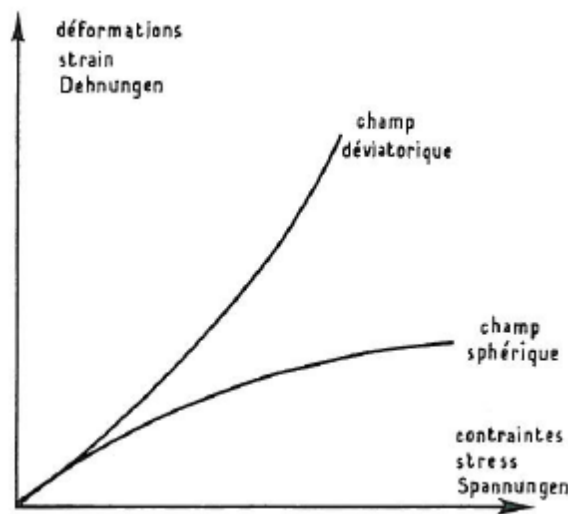


Fig. A.10 Influence of the nature of stress field on stress-strain relationship (Ménard 1961)

The compression index C_C can be used alternatively to E_{oed} as the ratio in a semi-logarithmic scale between the void ratio e (reflecting the strain level) and the stress, and if necessary the swelling index C_S for repeated load or for stresses smaller than the preconsolidation pressure (Fig. A.11). The settlement calculation is given in (Eq. A.3) (H_i : layer thickness).

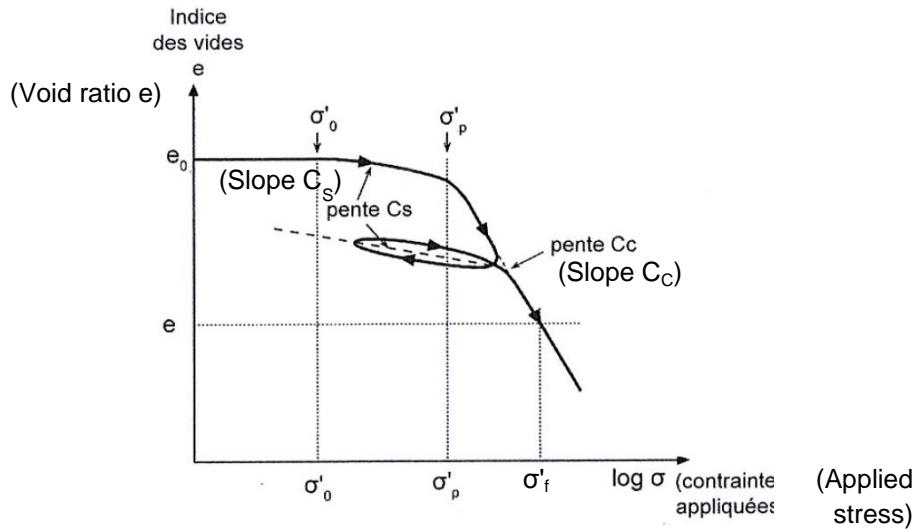


Fig. A.11 Void ratio vs. applied stress in logarithmic scale curve in oedometer test (adapted from Combarieu 2006)

$$s = \sum_i \frac{H_i}{1 + e_{0,i}} \left[C_{s,i} \cdot \log \frac{\sigma'_{p,i}}{\sigma'_{0,i}} + C_{c,i} \cdot \log \frac{\sigma'_{f,i}}{\sigma'_{p,i}} \right] \quad (\text{Eq. A.3})$$

A conversion of the parameter C_C for normally consolidated soils in terms of secant oedometric modulus between two given points 1 and 2 is possible (e_1 : initial pore ratio for point 1), and reflects again the stress-dependency of the oedometric modulus (Eq. A.4).

$$E_{oed} = \frac{(\sigma'_2 - \sigma'_1) \cdot (1 + e_1)}{C_C \cdot \log \frac{\sigma'_2}{\sigma'_1}} \quad (\text{Eq. A.4})$$

The use of the oedometer parameters (E_{oed} or C_C/C_S) for settlement calculation under assumed infinitely widespread loads, or for layers with a small thickness in comparison to the width of the loading area, implies a very careful determination of the modulus in each segment of a relatively fine subdivision of the soil strata, taking into account the increase of modulus with the total stress level in each segment (due to the applied and overburden load).

The application of this theory to shallow foundations limited in space (segmentation oedometric method, with for example an E_{oed} determined for each stress level) is based in general on the linear elastic vertical stress distribution based on Boussinesq (1885), cited for example by Vogt (2015) shown as “applied load” curve in Fig. A.12. The settlement calculation is made using integration in depth under the plate. It is namely

commonly accepted to approximate the vertical stress in the soil with this linear elastic distribution (Frank 1991), even if some dissipation effects occur in soils unlike a perfect elastic material. This integration is made in general down to the critical depth defined as the depth where the stress from the applied load reaches 20 % of the overburden stress. The result of this calculation is supposed to give the primary (consolidation) settlement.

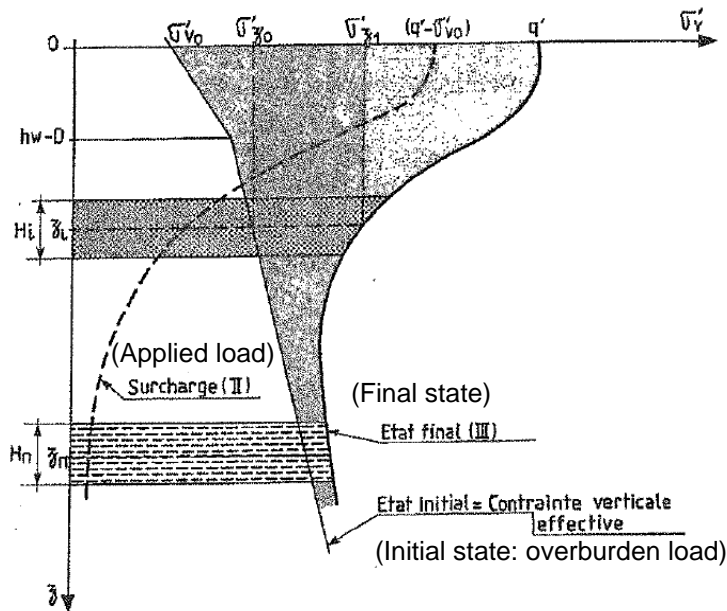


Fig. A.12 Load distribution and segmentation for oedometric settlement method under shallow foundations (Philipponnat and Hubert 2000)

This method requires special corrective measures to take into account the real stress-strain relationship (here closer to a tri-axial evolution), the increase of the modulus for the smaller deformations in depth compared to the deformations directly under the plate (increase of strain with smaller deformations not represented in the oedometric test), and if necessary the instantaneous deviatoric settlement of the soil, corresponding to an undrained deformation (Frank 1991). The oedometric method for shallow foundations without correction overestimates in general the consolidation settlement (Frank 1991). Indeed, the decrease of the modulus due to the possibility of lateral deformations is more than compensated by the tridimensional dissipation of load in soils (residual stress in depth smaller than in the elastic case).

For example Skempton and Bjerrum (1957), cited by Frank (1999), propose a corrective factor smaller than 1, depending on the consolidation level and on the ratio of the thickness of the soil layer to the width of the plate, in order to take into account tridimensional effects in the consolidation settlement (Fig. A.13).

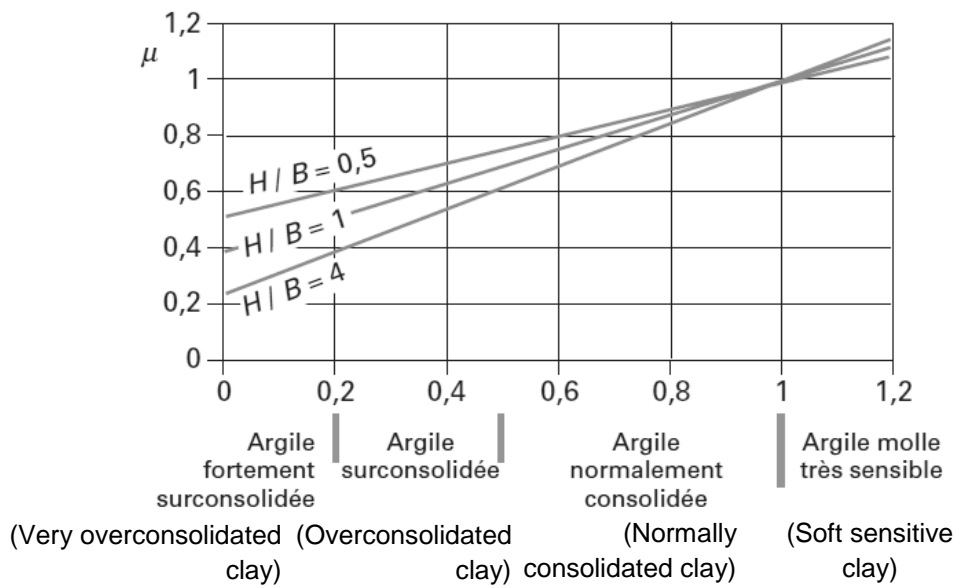


Fig. A.13 Corrective factor μ to take into account the tridimensional effects after Skempton and Bjerrum (1957), cited by Frank (1999)

In a similar way, Burland et al. (1977), cited by Frank (1999), propose for clays a reduction of the calculated consolidation settlement s_{oed} under single footings to get a more realistic value s_c , and a correspondence for the instantaneous one s_i :

(Eq. A.5) and (Eq. A.6) apply for overconsolidated clays.

$$s_i = 0,5 \text{ to } 0,6 \cdot s_{oed} \quad (\text{Eq. A.5})$$

$$s_c = 0,4 \text{ to } 0,5 \cdot s_{oed} \quad (\text{Eq. A.6})$$

(Eq. A.7) and (Eq. A.8) apply for normally consolidated clays.

$$s_i = 0,1 \cdot s_{oed} \quad (\text{Eq. A.7})$$

$$s_c = s_{oed} \quad (\text{Eq. A.8})$$

For both cases, the total settlement is approximately equal to s_{oed} after Burland et al. (1977), cited by Frank (1999).

The approximately linear increase of the modulus in the stress-strain curve due to the increase of confining (overburden and additional) stress is already represented in the oedometer test as well as in the tri-axial test (see Fig. A.5). On the contrary, the increase of the modulus due to the smaller deformations in depth is not represented in the oedometer test (unlike in the tri-axial test). Holzlöhner (1999) recommends as well an increase of the modulus with the depth, in the case of single footings, to take into account the smaller deformations in depth. It seems relevant to correct the calculated modulus from a oedometer test for the deepest layers with a realistic factor corresponding to the ratio between an elastic modulus at small strains and a modulus for usual strains directly under small foundations (see Fig. A.4), or for usual strains over the whole depth under very large foundations (where the oedometer-method has proven to be very realistic).

Since both alternative methods with E_{oed} or C_C/C_S are equivalent, the same corrective factors and the same correction of the modulus for small strains should be considered if the C_C/C_S -method is used for single footings.

A.3 Plate load test

This in situ test consists in loading a rigid normalized circular plate on the surface of the soil. The plate load test is standardized in the French standard NF P94-117-1 (2000) with a plate diameter of 60 cm, and in the German standard DIN 18134 (2012) with a plate diameter of 30 cm. It was originally developed for the calculation of stresses and deformations under shallow foundations, but is nowadays rather employed for the structural design of pavements. This is the case in particular for the Westergaard test (NF P94-117-3 2008), with a plate diameter of 60, 75 or 76.2 cm (Fig. A.14). It is used to determine the modulus or coefficient of subgrade reaction of the load transfer platform in road construction as well.



Fig. A.14 Plate load test – Westergaard type (Cassan 1988)

The plate load test is particularly interesting, insofar as it is the only way to define an “equivalent Young’s modulus” E for the soil by means of analogy to the elasticity theory, corresponding to the loading type of a shallow foundation with dimensions comparable to those of the normalized plate. This modulus is a secant modulus obtained from a load equal to 0.

The settlement s of a circular plate (radius R) under a pressure q on a half-space (Young’s modulus E , Poisson’s ratio ν) in the theory of linear isotropic elasticity is presented in (Eq. A.9), (Eq. A.10) and (Eq. A.11). It is based on the Boussinesq theory (1885), citey for example by Vogt (2015).

$$s = 2 \cdot \frac{1-\nu^2}{E} \cdot q \cdot R \text{ at the centre of a flexible plate} \quad (\text{Eq. A.9})$$

$$s = \frac{4}{\pi} \cdot \frac{1-\nu^2}{E} \cdot q \cdot R \text{ at the edge of a flexible plate} \quad (\text{Eq. A.10})$$

$$s = \frac{\pi}{2} \cdot \frac{1-\nu^2}{E} \cdot q \cdot R \text{ for a rigid plate or at the} \quad (\text{Eq. A.11})$$

characteristic point of a fully flexible plate

The test is in general made with rigid plates. A more representative mechanical modulus for this test can be defined as in (Eq. A.12), leading to the relationship between the load and the settlement in (Eq. A.13).

$$E_v = \frac{E}{1-\nu^2} \quad (\text{Eq. A.12})$$

$$s = \frac{\pi}{2} \cdot \frac{q \cdot R}{E_v} \quad (\text{Eq. A.13})$$

A.4 Pressuremeter test (PMT)

The pressuremeter test was patented by Louis Ménard in January 1955, and developed in the scope of his master thesis at the University of Illinois in 1957 (Ménard 1957). The reason to develop such a test device was the lack of accuracy of the usual elastic methods for the calculation of settlements of shallow foundations at that time. The idea of a cavity expansion came to make an observation of deviatoric deformations in soils possible, which have to be taken into account under shallow foundations, on the contrary of large pavement or fill loading cases, where the stress field is basically spherical (simple compression). The evolution of this method has been described in Soil-Soils Journal in the 1960's and 1970's. It has been shown that analogies between the borehole expansion and the deformation around the base of the pile can be easily found as well.

The Ménard PMT test is standardized in the European standard EN ISO 22476-4 (2012) and in the French standards NF P94-110-1 (2000) and NF P94-110-2 (1999).

The PMT (Fig. A.15) is typically performed by inserting a cylindrical probe (44.6 to 76 mm outside diameter, length-diameter ratio 7 to 10 to ensure an perfect radial deformation at the level of the central measuring cell) into an open borehole, bringing it at the test depth, and then inflating a flexible membrane in the lateral direction with a given pressure applied stepwise (Fig. A.16 and Fig. A.17), each load increment being maintained for 60 seconds. The resulting volume changes in the cell are then measured at each pressure step. The results have then to be corrected by subtracting the resistance of the membrane itself and the expansion of the tubing. This test is performed at different depth in the borehole to provide a profile of the PMT parameters of the soil.

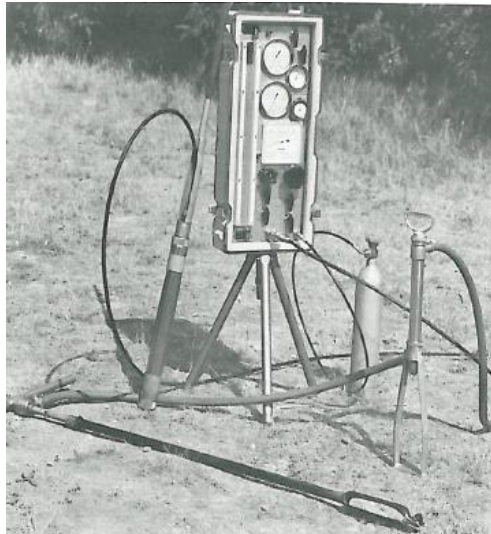


Fig. A.15 Basic pressuremeter unit (Baguelin et al. 1978)

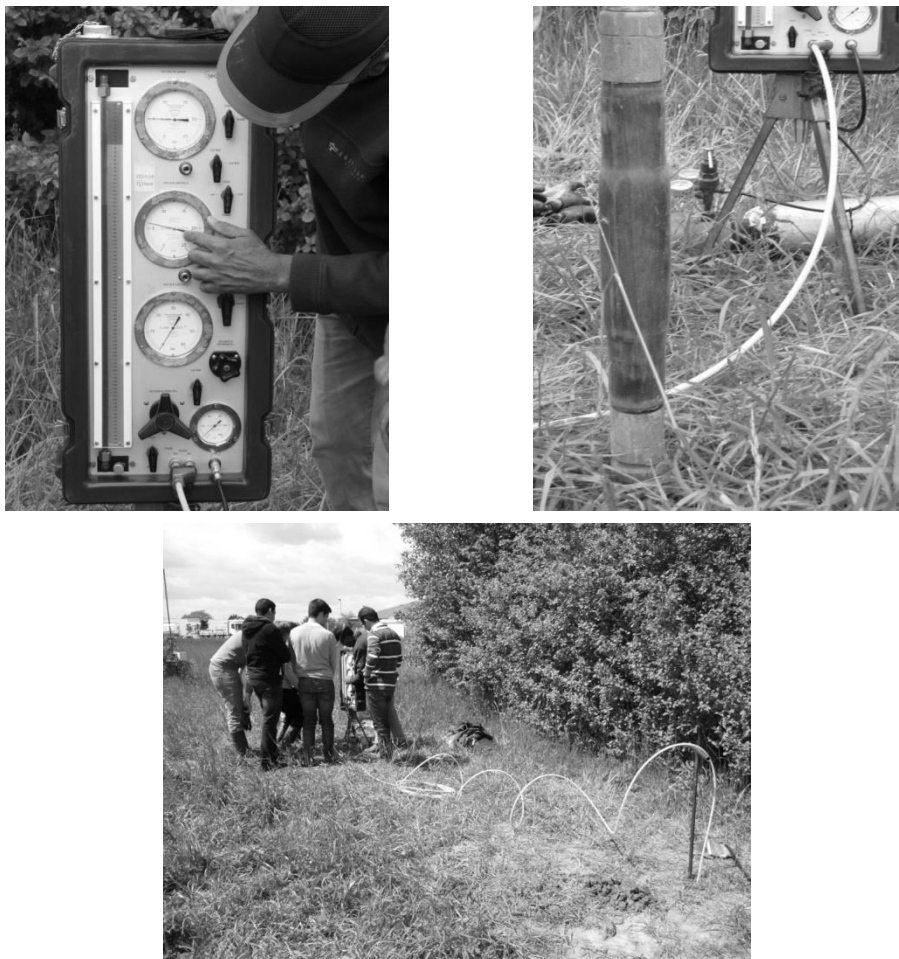


Fig. A.16 Pressuremeter testing on test field of Navier-Géotechnique (Cermes) in Lognes, France

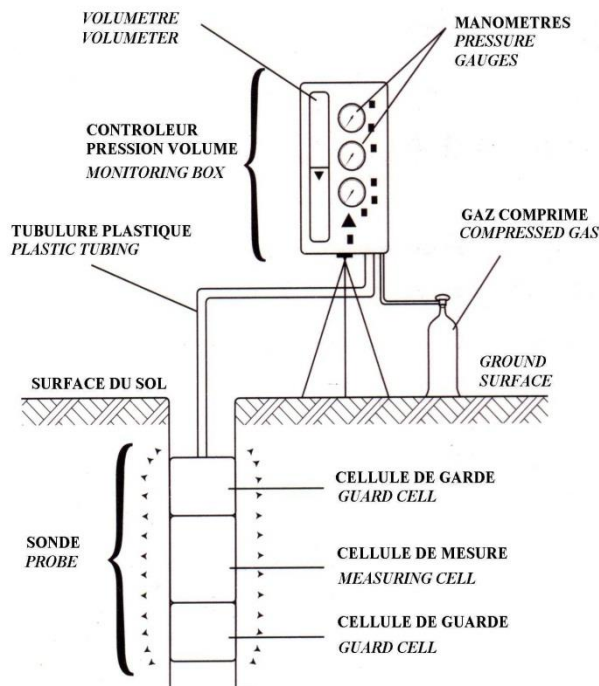


Fig. A.17 Main components of a pressuremeter unit (Gambin 2005)

In the standardized Ménard PMT test, the diameter of the borehole is slightly larger than the diameter of the probe. The state of stress in the soil is then definitely disturbed, and the first non-linear stress-strain phase in the test consists in bringing the probe and the soil in contact. An approximately linear phase follows. In the last phase, the volume expansion becomes much larger, until a limit pressure is reached (Fig. A.18).

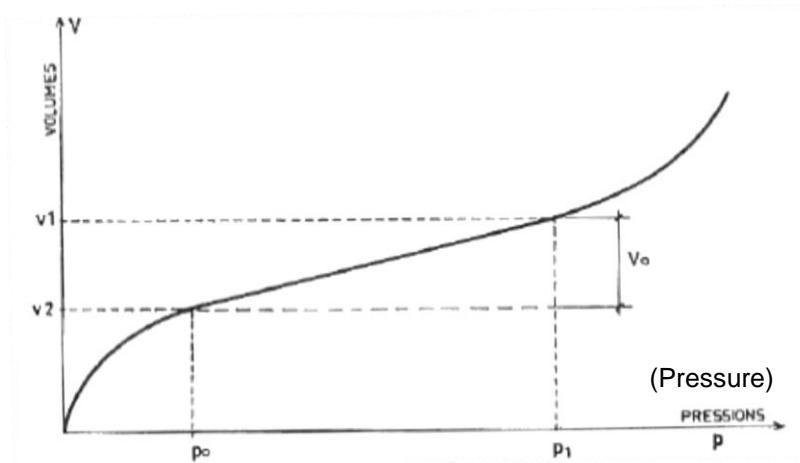


Fig. A.18 Shape of a pressuremeter curve (Cassan 1988)

The whole pressuremeter theory and the foundation design methods, which have been developed and which are still in use today correspond to this real pressuremeter curve including the first re-contacting phase. The use of the pressuremeter design methods requires a very careful execution, as presented for example by Techniques Louis Ménard (1976). Some attempts have been made however to examine the reaction of the soil without disturbance, using a so called self-boring pressuremeter (SPB) or “pressiomètre autoforeur” (PAF) in France. Such devices have been developed to make possible a measurement of the earth pressure at rest K_0 , like the Camkometer developed by Wroth in the 1970's.

Ménard examined a corrected curve eliminating the non-representative first part, in order to present the real variation of the modulus during a pressuremeter test, in particular at small strains (not visible in a standardized test). He defined 3 different phases in the curve: the true elastic phase with a real elastic modulus E_e for very small strains in the order of 10^{-6} (corresponding to the strains produced by wave propagation in the soil), the pseudo-elastic phase where a tangent pressuremeter modulus E_M for strains of 10^{-3} to 10^{-2} is defined, and the plastic phase, where no modulus can be defined anymore. A cyclic modulus E_a for unloading and reloading (in the same strain range as E_M) can additionally be defined (Fig. A.19). The value of this modulus is similar to the one of the elastic modulus at small strains, and this cyclic phase can be assumed to be elastic too. According to Combarieu (2006), the ratio between the elastic modulus at small strains and the modulus in the pseudo-elastic phase ranges from 3 for clay up to 6-7 for sand and gravel. Different indicative values, higher for clay than for coarse-grained soils, are given by Smolczyk in 2001 (Fig. A.20), here with reference to a oedometer modulus (most likely for usual strain levels under foundations), and for usual small strains for the dynamic modulus.

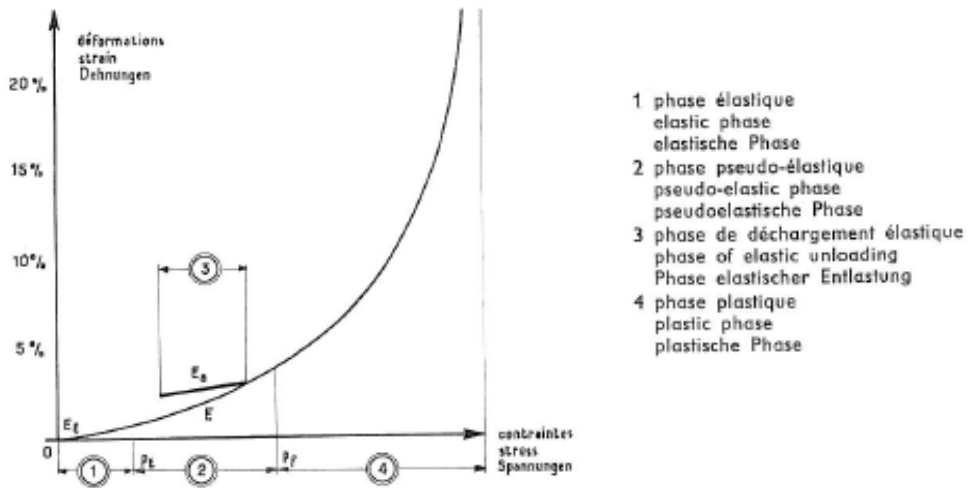


Fig. A.19 Corrected pressuremeter curves with different phases (Ménard and Rousseau 1962)

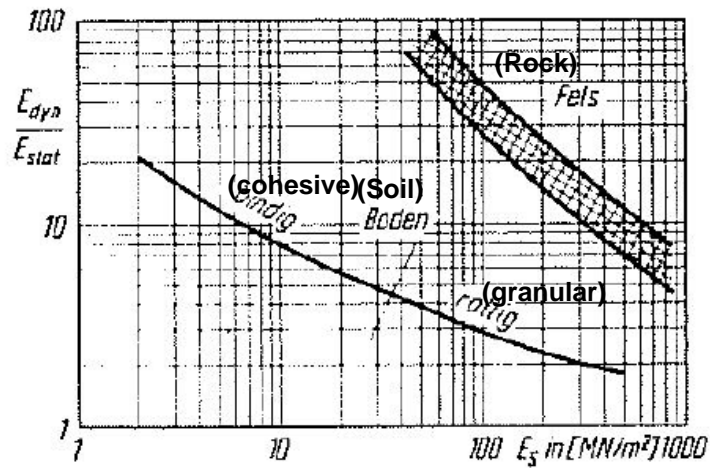


Fig. A.20 Ratio between oedometer modulus and dynamic modulus (Smolczyk 2001)

The cavity expansion loading case corresponds to a shearing of the soil rings around the cell (Fig. A.20), so that strictly speaking only an apparent shear modulus G of the soil can be measured.

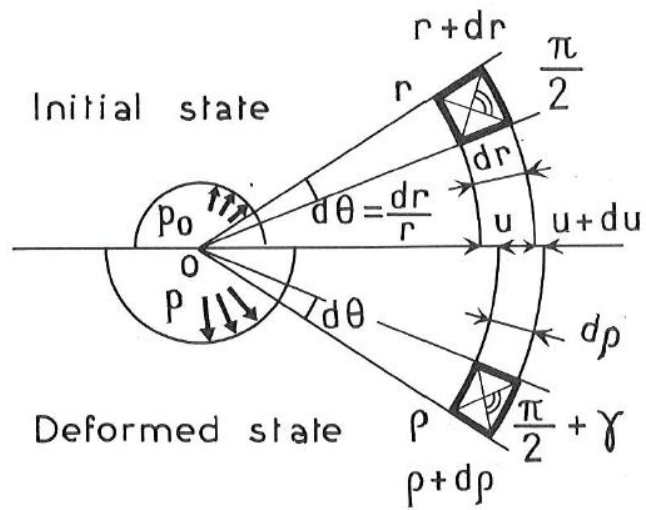


Fig. A.21 Deformation of an initial square ring element for the cylindrical cavity expansion (Baguelin et al. 1978)

Shear moduli are in general defined from simple shear tests after (Eq. A.14) and Fig. A.22 (S: application surface of the force F).

$$G = \frac{\tau}{\gamma} = \frac{F/S}{\gamma} \tag{Eq. A.14}$$

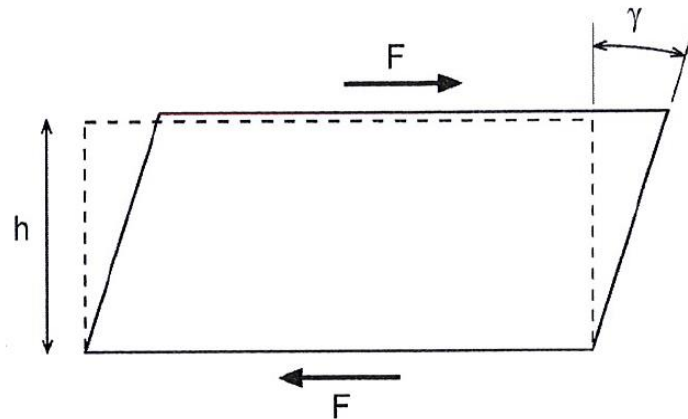


Fig. A.22 Distortion in simple-shear test (Combarieu 2006)

Just like compression moduli, the shear modulus is decreasing with the distortion (Fig. A.23).

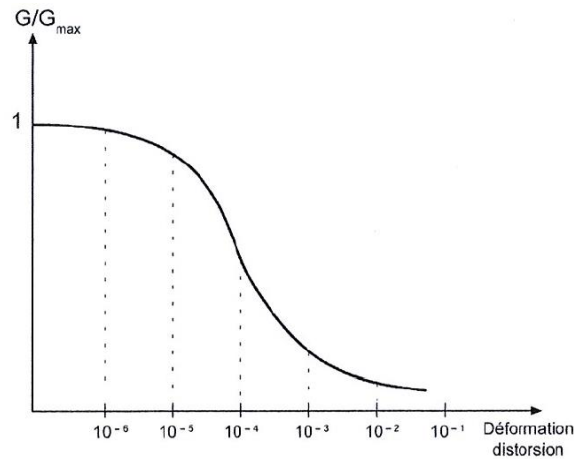


Fig. A.23 Evolution of shear modulus with distortion (Combarieu 2006)

The shear modulus G of the soil undergoing a pressuremeter test is defined by analogy with the theoretical elastic response of a medium under a radial cavity expansion loading after (Eq. A.15) (R : radius of the cylindrical cavity; ΔR : variation of the radius under the load increment Δp in the cavity).

$$\frac{\Delta R}{R} = \frac{1}{2G} \cdot \Delta p \quad (\text{Eq. A.15})$$

Given that compression moduli are more common in the usual practice, this measured shear modulus G in the pseudo-linear part of the curves is converted into a so called pressuremeter modulus E_M corresponding to the strain range of the pseudo-elastic phase. Therefore the common relationship between shear and compression moduli for an elastic soil is applied (Eq. A.16). A value of 0.33 for the Poisson's ratio of soils is here used as convention for the definition of E_M from G . So this means that E_M would be the Young's modulus if the medium was elastic with a Poisson's ratio of 0.33.

$$E_M = 2 \cdot (1 + \nu) \cdot G \quad (\text{Eq. A.16})$$

In the standardized pressuremeter test, the volume change is in general measured instead of the radius change. The volume change is expressed in (Eq. A.17), (Eq. A.18) and (Eq. A.19) (L : length of the probe).

$$\Delta V \cong L \cdot [\pi \cdot (R + \Delta R)^2 - \pi \cdot R^2] \cong 2 \cdot \pi \cdot R \cdot \Delta R \cdot L \quad (\text{Eq. A.17})$$

$$V = \pi \cdot R^2 \cdot L \quad (\text{Eq. A.18})$$

$$\Delta V \cong 2 \cdot V \cdot \frac{\Delta R}{R} \quad (\text{Eq. A.19})$$

(Eq. A.20) and (Eq. A.21) result from (Eq. A.16) to (Eq. A.19).

$$\frac{\Delta V}{V} = 2 \cdot \frac{1+\nu}{E_M} \cdot \Delta p \quad (\text{Eq. A.20})$$

$$\frac{\Delta V}{\Delta p} = 2 \cdot \frac{1+\nu}{E_M} \cdot V \quad (\text{Eq. A.21})$$

The pressuremeter modulus E_M is thus proportional to the inverse of the slope of the pressuremeter curve in the usual diagram with the volume on the vertical axis. Mean values of E_M for different types of soils are given in Table A.1.

Table A.1 Usual values of E_M for different types of soils (Techniques Louis Ménéard 1975)

<u>Soil</u>	<u>E in bars</u>
mud, peat	2 to 15
soft clay	5 to 30
medium clay	30 to 80
stiff clay	80 to 400
marl	50 to 600
loose silty sand	5 to 20
silt	20 to 100
sand and gravel	80 to 400
sedimentary sands	75 to 400
limestone	800 to 200.000
recent fill	5 to 50
old fill	40 to 150

This pressuremeter modulus E_M is thus absolutely not to be assimilated to an elastic modulus of the soil. It does not reflect any reversibility in this strain range of 10^{-3} to 10^{-2} , and is only valid for a first loading case in that strain range. The main use and the only standardized way to use the pressuremeter results to estimate the deformations in soils is the semi-empirical method developed by Ménéard. All other applications using the pressuremeter modulus and correlations for other methods (in particular numerical methods) not taking into account the strain range are a misunderstanding and a misemployment of this parameter.

To make his theory closer to the settlement observations, Ménard had to define an additional factor α depending on secondary influence factors. This factor is approximately the square root of the ratio between the pressuremeter modulus E_M and the cyclic modulus E_a (Ménard and Rousseau 1962) as in (Eq. A.22). This coefficient represents the non-linearity of the soil behaviour. The factor α would be equal to 1 in a perfectly elastic material.

$$\alpha = \sqrt{\frac{E_M}{E_a}} \quad (\text{Eq. A.22})$$

Another definition of this coefficient α associates a so called compression modulus and a tension modulus of the soil in the same strain range as E_M . According to Ménard, equivalent moduli or specific Young's moduli E_e corresponding to a given loading type can be defined for each test type as a combination of the internal compression modulus E^+ and of the smaller internal tension modulus E^- in the ground (Ménard 1961). In (Eq. A.23), a and b depend on the test or on the foundation type.

$$E_e = \sqrt[a+b]{(E^+)^a \cdot (E^-)^b} \quad (\text{Eq. A.23})$$

The modulus E_M is the specific Young's modulus E_e associated with the pressuremeter test. For a cylindrical stress field, $a = b = 1$, leading to (Eq. A.24).

$$E_M = \sqrt{E^+ \cdot E^-} \quad (\text{Eq. A.24})$$

In the case of a uniform stress distribution like for example under a very widespread pavement loading compared with the thickness of the compressible soil layer, $a = 1$ and $b = 0$. The associated modulus for that loading type is the oedometer modulus E_{oed} , corresponding to (Eq. A.25) for the same strain range.

$$E_e = E_{oed} = E^+ \quad (\text{Eq. A.25})$$

This explains why the compression modulus E^+ in the ground is often considered as the oedometer modulus in the same strain range (Combarieu 2006, Ménard 1961, Ménard and Rousseau 1962). The ratio between E^- and E^+ can be close to 1 for very cohesive soils and smaller than 1/3 for weakly structured soils. The coefficient α is subsequently defined as the square root of this ratio and as the ratio between E_M and E^+ (Eq. A.26).

$$\alpha = \sqrt{\frac{E^-}{E^+}} = \sqrt{\frac{E^- \cdot E^+}{E^+ \cdot E^+}} = \frac{E_M}{E^+} \quad (\text{Eq. A.26})$$

The value of α is approximately 1 for artificially compacted soils, 1/2 to 2/3 for unsaturated clays, 1/2 for saturated clays and silts, and 1/3 to 1/2 for sand and gravel (Ménard and Rousseau 1962). Detailed values of α are given by Ménard (1975) and Baguelin et al. (1978) for different types of soils and different consolidation degrees, depending on E_M and on the limit pressure p_l (Table A.2).

Table A.2 Rheological factor α for various soils (Baguelin et al. 1978)

Soil Type	Peat		Clay		Silt		Sand		Sand and gravel	
	E_M/p_l^*	α	E_M/p_l^*	α	E_M/p_l^*	α	E_M/p_l^*	α	E_M/p_l^*	α
Over-consolidated			>16	1	>14	2/3	>12	1/2	>10	1/3
Normally consolidated		1	9-16	2/3	8-14	1/2	7-12	1/3	6-10	1/4
Weathered and/or remoulded			7-9	1/2		1/2		1/3		1/4
Rock			Extremely fractured		Other		Slightly fractured or extremely weathered			
			$\alpha = 1/3$		$\alpha = 1/2$		$\alpha = 2/3$			

(Eq. A.26) implies (Eq. A.27) and (Eq. A.28) if E_{oed} in the same strain range as E_M .

$$\sqrt{\frac{E_M}{E_a}} = \frac{E_M}{E_{oed}} \quad (\text{Eq. A.27})$$

$$E_M = \frac{E_{oed}^2}{E_a} \quad (\text{Eq. A.28})$$

Knowing the value of E_M and of E_{oed} in the same strain range, it is theoretically possible to make a calculation of the cyclic modulus in the strain range of E_M (close to the elastic modulus for very small strains). Example values of $E_M = 5$ MPa, $E_a = 50$ MPa, $E^+ = E_{oed} = 15$ MPa are given for a usual soil in (Ménard and Rousseau 1962), which is consistent with this formula.

The calculation method for settlements under shallow foundations with limited dimensions of Ménard is a semi-empirical method, based on the elasticity theory and corrected with rheological factors in order to take into account the real soil behaviour, and with factors depending on the dimensions and on the shape of the foundation. All

results have been developed and confirmed to agree with experimental results (Baguelin 2005, Dauvisis and Ménard 1964, Ménard 1963a, Ménard 1963b, Ménard 1964). Ménard investigated an embedded shallow foundation and pointed out that the total settlement is a combination of a spherical settlement (true compression with consolidation) and of an instantaneous deviatoric settlement. This method provides the direct use of primary in situ parameters, in particular of the pressuremeter modulus, which corresponds to the same domain of deformations as for the usual shallow and deep foundations as 10^{-3} to 10^{-2} (Combarieu 2006, Gambin et al. 1996). The behaviour of the soil around an embedded foundation corresponds very well to the cavity expansion case. The real behaviour of the soil including the stiffening at small strains at some distance from the load application zone is then taken into account through the use of the pressuremeter modulus, which already includes the real global reaction of the soil for the different deformation levels in the corresponding volume of soil. On the contrary, the pressuremeter modulus has no practical meaning in the case of widespread loads. In that case, the oedometer modulus and the oedometric settlement calculation method are more appropriate (Combarieu 2008). According to Baguelin (2005), the correlation $\alpha = \frac{E_M}{E_{oed}}$ may be used for simple cases to determine E_{oed} for the calculation of settlement under large loading areas if no oedometric tests have been done. This relationship has no meaning according to Combarieu (2006), since the oedometer modulus is essentially stress-dependent, unlikely to E_M .

The calculated settlement by Ménard for shallow foundations is the settlement under a rigid foundation (Techniques Louis Ménard 1978b), which corresponds to the settlement under the characteristic point of a flexible foundation.

The compression settlement is concentrated in a hemispherical zone in the immediate vicinity of the foundation (zone A in Fig. A.24). The deviatoric settlement takes place below the volume corresponding to this hemispherical zone (zone B in Fig. A.24). The settlement of a hemispherical foundation would only consist of this second settlement part.

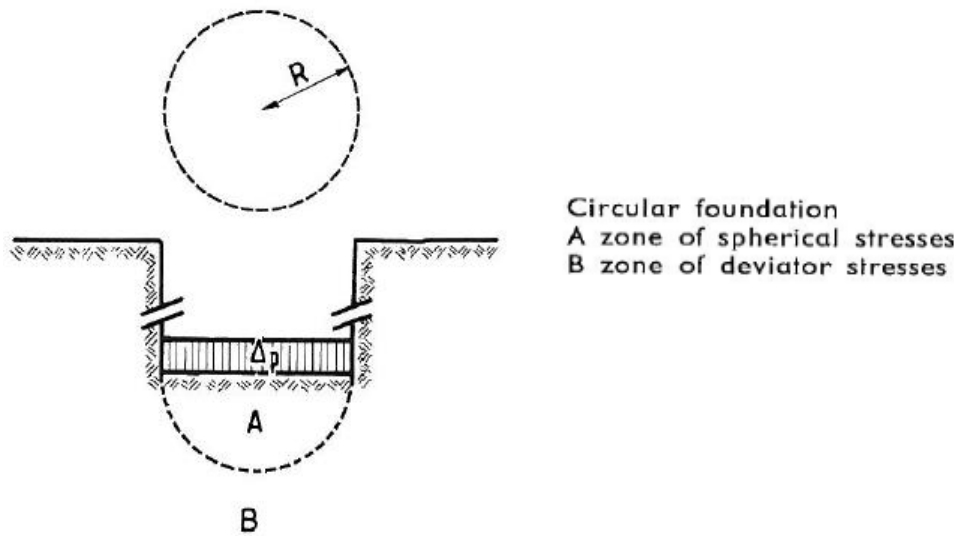


Fig. A.24 Circular foundation with zone of spherical and deviatoric stresses (Ménard and Rousseau 1962)

The settlement due to this deviatoric field under a hemispherical foundation is given in (Eq. A.29) after the theory of elasticity (Ménard and Rousseau 1962):

$$s_{el} = \frac{1+\nu}{3 \cdot E_c(t)} \cdot \Delta p \cdot R \quad (\text{Eq. A.29})$$

This formula has to be adapted for the general case with the pseudo-elastic phase represented through the structural factor α for a circular foundation (Eq. A.30). R_0 is a reference value equal to 0.3 m, function of the diameter of the PMT probes in use. The modulus depends on the time and becomes smaller for long term load application times. The measured pressuremeter modulus E_M corresponds to the loading time of 1 to 2 minutes in the pressuremeter test. The presented definition of α corresponds to a calculated settlement taking into account 10 years of moderate creep (shallow foundations being however in general not used for significantly creeping soils), if the measured pressuremeter modulus E_M is inserted in the formula.

$$s_d(10\text{years}) = \frac{1+\nu}{3 \cdot E_M} \cdot \Delta p \cdot R_0 \cdot \left(\frac{R}{R_0} \right)^\alpha \quad (\text{Eq. A.30})$$

The compression fraction s_c of the hemispherical volume is calculated using the segmentation oedometric method (E^+ corresponding to the strain domain of E_M) and takes into account instantaneous, consolidation and moderate creep deformations after 10 years (Eq. A.31).

$$s_c(10\text{years}) = \frac{1}{4.5} \cdot \frac{1}{E^+} \cdot \Delta p \cdot R \quad (\text{Eq. A.31})$$

The total settlement 10 years after the load application time is then equal to the sum of s_c and s_d .

Shape coefficients λ can be introduced for non-circular foundations. These factors, close to the Steinbrenner's ones, depend on the width and length of the foundation. They have been originally defined only for the deviatoric term (Ménard and Rousseau 1962) (Eq. A.32), but have been later extended to the spherical term as in (Eq. A.33) or (Eq. A.34).

$$s_c(10\text{years}) = \frac{1}{4.5} \cdot \frac{1}{E^+} \cdot \Delta p \cdot \lambda_c \cdot R = \frac{1}{4.5} \cdot \frac{\alpha}{E_M} \cdot \Delta p \cdot \lambda_c \cdot R \quad (\text{Eq. A.32})$$

$$s_d(10\text{years}) = \frac{1+\nu}{3 \cdot E_M} \cdot \Delta p \cdot R_0 \cdot \left(\lambda_d \cdot \frac{R}{R_0} \right)^\alpha \quad (\text{Eq. A.33})$$

$$s_d(10\text{years}) = \frac{1+\nu}{3} \cdot \Delta p \cdot R \cdot \lambda_d^\alpha \cdot \frac{1}{E_M \cdot \left(\frac{R}{R_0} \right)^{1-\alpha}} \quad (\text{Eq. A.34})$$

The term $E_M \cdot \left(\frac{R}{R_0} \right)^{1-\alpha}$ can be seen as a modulus increasing with the dimension R of the foundation, because deviatoric deformations become negligible under very large load application areas.

These results are valid for embedded shallow foundations with a minimum embedment of at least one diameter 2R or one width B (correspondence with cavity expansion embedded in the soil). For smaller values of embedment, it has been shown empirically that the settlement has to be increased of up to 20 % (Fig. A.25) (Baguelin 1978, Techniques Louis Ménard 1978b).

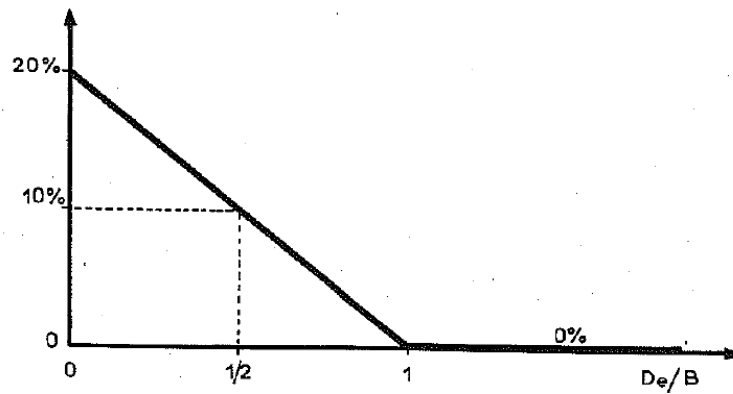


Fig. A.25 Increase of the settlement in case of small embedment (Baguelin et al. 1978)

In general the calculation shows that the deviatoric settlement is approximately 2 to 3 times larger than the consolidation settlement, depending on the value of α . For the case of a circular foundation at the surface, both terms could be compared to the elastic calculation corresponding to the plate load test. The deviatoric term corresponds here to the case $\nu = 0.5$ (no volume change, instantaneous) in (Eq. A.11) and the total settlement is in general calculated with $\nu = 0.33$.

For non-homogeneous soils, a weighting of the pressuremeter moduli of the different layers has to be done. For the spherical settlement term, only the modulus of the first layer under the foundation has to be computed. For the deviatoric term, the weighting is approximately done according to the relative distribution of the deviatoric stress τ from a linear elastic calculation. The definition of the different moduli in depth is given in Fig. A.26.

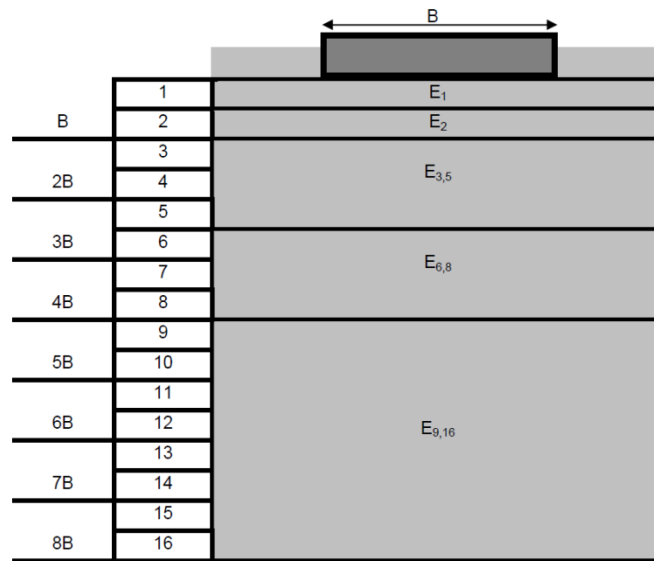


Fig. A.26 Subdivision in layers of thickness $B/2$ for equivalent modulus

In (Eq. A.35), $E_{M,3,5}$, $E_{M,6,8}$ and $E_{M,9,16}$ are the harmonic mean values of the corresponding layers.

$$\frac{4}{E_M} = \frac{1}{E_{M,1}} + \frac{1}{0,85 \cdot E_{M,2}} + \frac{1}{E_{M,3,5}} + \frac{1}{2,5 \cdot E_{M,6,8}} + \frac{1}{2,5 \cdot E_{M,9,16}} \quad (\text{Eq. A.35})$$

The harmonic mean of all layers would be as in (Eq. A.36).

$$\frac{4}{E_{M,m}} = \frac{1}{4 \cdot E_{M,1}} + \frac{1}{4 \cdot E_{M,2}} + \dots + \frac{1}{4 \cdot E_{M,16}} \quad (\text{Eq. A.36})$$

And the formula of Ménard corresponds to (Eq. A.37).

$$\begin{aligned} \frac{4}{E_{M,m}} = & \frac{1}{E_{M,1}} + \frac{1}{0,85 \cdot E_{M,2}} + \frac{1}{3 \cdot E_{M,3}} + \dots + \frac{1}{3 \cdot E_{M,5}} + \frac{1}{7,5 \cdot E_{M,6}} + \dots \\ & \dots + \frac{1}{7,5 \cdot E_{M,8}} + \frac{1}{20 \cdot E_{M,9}} + \dots + \frac{1}{20 \cdot E_{M,16}} \end{aligned} \quad (\text{Eq. A.37})$$

This means that the moduli are differently weighted according to the distance to the base of the foundation and according to the evolution of stress and strains in the soil with the depth (considered to be approximately the one from the theory of elasticity, Fig. A.27).

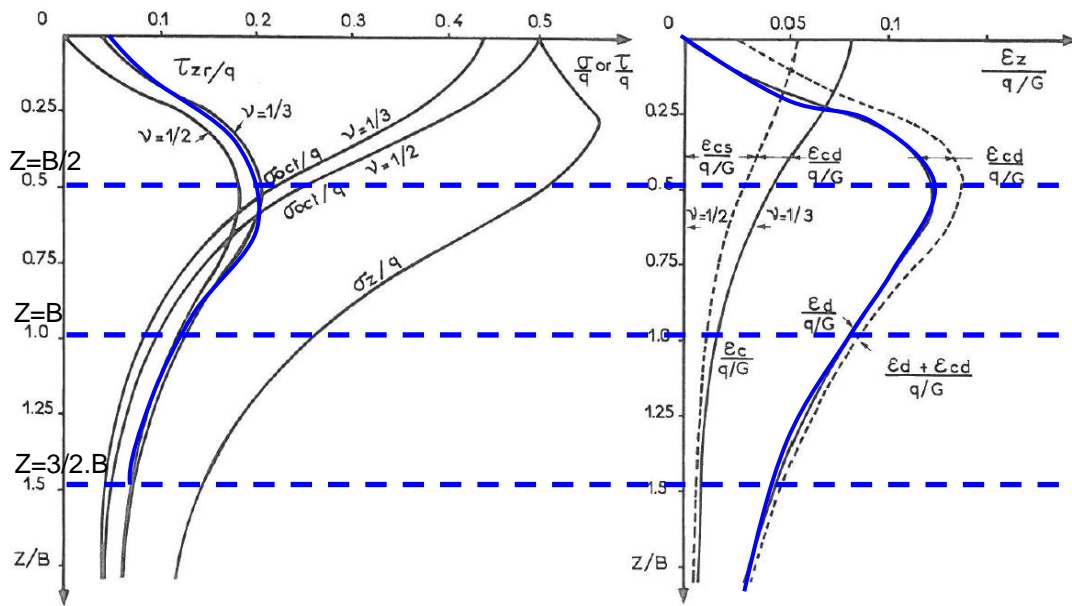


Fig. A.27 Stress and strains along a vertical axis under a rigid circular foundation (elastic) (Baguelin et al. 1978)

A smaller modulus is taken into account down to a depth of B ($E_{M,1}$ and $E_{M,2}$), where the deviatoric stress τ_{zr} and thus the deviatoric deformations ϵ_d are quite high and where local failure zones appear making the modulus smaller.

From a depth of B to $5/2 \cdot B$, the modulus is approximately unchanged. From $5/2 \cdot B$ ($E_{M,6}$ and $E_{M,8}$), a larger modulus is considered with a maximal factor of $20/4 = 5$, corresponding to the stiffness of the soil at very small strains in depth. This means that the deepest layers are almost not concerned and almost do not contribute to the final settlement. In the case of a homogeneous soil, the weighting gives back the pressuremeter modulus of the unique soil layer, which means that after weighting, the pressuremeter strain range is considered as appropriate to model the global behaviour.

It may be possible to reduce the presently considered depth of $8 \cdot B$ to $2.5 \cdot B$, since the usual influence zone in a real soil is rather $2.5 \cdot B$ (Briaud 2003b, 2007), or even smaller down to $1.5 \cdot B$. A real soil dissipates the deviatoric stresses more quickly than an ideal elastic medium, so that the deepest layers may have no influence at all anymore.

The formulas according to Ménard are linear with the load Δp , but this method is actually only valid in the domain of serviceability defined in France by a limitation of the load to a third of the failure load. It has been proven empirically that the results are close to reality in that case (Frank 1991). This implied condition is illustrated by Ménard defining an increasing factor β (Eq. A.38) for the settlement if the safety factor F is smaller than 3 (Techniques Louis Ménard 1975).

$$\beta(F) = \max\left(1; \frac{2}{3} \cdot \frac{F}{F-1}\right) \quad (\text{Eq. A.38})$$

A logarithmic extension of the settlement formula after the pressuremeter theory (approximately linear up to a third of the failure load) has been made by Combarieu (1988a) in the scope of a computational modelling of combined pile-raft foundations for the whole loading range from 0 up to the failure load.

The settlement behaviour of piles can be modelled with the use of pressuremeter parameters as well. The usual method today is based on the so-called “t-z” method, presented first by Gambin (1963) and Marchal (1971), and developed from experimental results by Frank and Zhao in 1982, in the first instance only for fine-grained soils, and later for all soil types (Frank 1985). The load-settlement behaviour of the pile is modelled here in the form of transfer functions, separated for the tip resistance and for the skin friction with a slope proportional to the pressuremeter modulus E_M for the first part of the curve, which is assumed to be linear (Fig. A.28). The ultimate (failure) values (called τ_1 and q_1 in Fig. A.28) can be determined with the help of pressuremeter parameters too (see Appendix B.3).

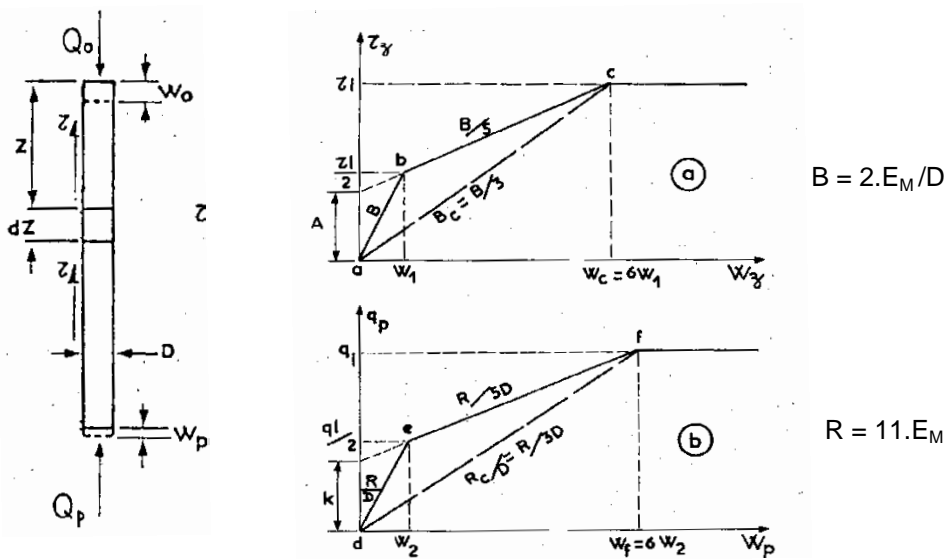


Fig. A.28 Original transfer functions by Frank and Zhao for skin friction (top) and tip resistance (bottom) for fine-grained soils (Frank and Zhao 1982) and (Frank 1985)

Later, these mobilisation functions have been extended to coarse-grained soils (Baguelin et al. 1986). The functions used nowadays are shown in section 2.2.2 (Fig. 2.5), and are valid for bored and displacement piles.

Similar curves have been developed for the lateral displacement of piles, the so-called “p-y” transfer functions (not detailed here) (Baguelin et al. 1986, Gambin and Frank 2009).

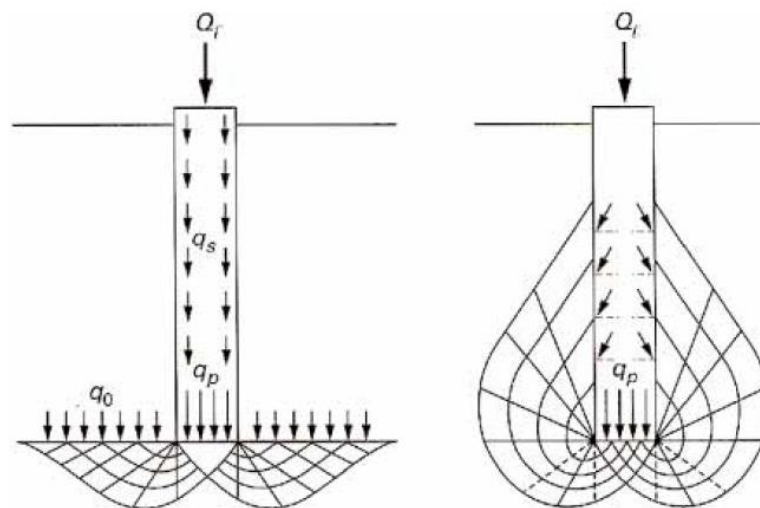


Fig. B.2 Possible failure mechanism under a pile foundation for the methods based on soil shear parameters (Frank 1999)

B.2 Cone penetration test (CPT)

The test equipment consists of a 60° cone with 10 cm^2 base area and 150 cm^2 friction sleeve surface above the cone (Fig. B.3). The cone resistance q_c whilst penetrating the different soil layers is defined as the total required force divided by the projected area of the tip cone, that is the surface of the cylindrical trunk of the device. The axial skin friction f_s at the sleeve of the device can be measured as well, which corresponds to a steel-soil friction index.

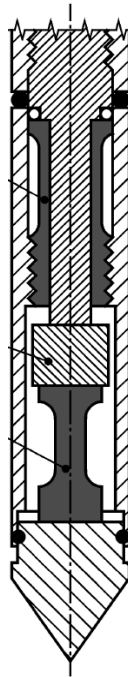


Fig. B.3 Example of a tip of a CPT testing probe after EN ISO 22476-1 (2012)

The CPT is standardized in the European standard EN ISO 22476-1 (2012) and in the French standard NF P94-113 (1996).

Cone penetration is inherently a measure of soil strength. The CPT gives directly a failure parameter of the soil (the cone resistance q_c), but provides no deformation parameter of the soil. Nevertheless, many correlations have been proposed to evaluate the oedometer modulus E_{oad} or an equivalent Young's modulus from q_c for example (see Appendix C about correlations). Cudmani (2001) compared the cone penetration with a spherical expansion and proposed some correlations between the resistance parameters q_c and a spherical limit pressure (see Appendix C as well). Due to inherent differences (in particular different stress/strain paths) between the cavity expansion and the cone penetration, no correlation for deformation parameters has been proposed by Cudmani.

The cone penetration test is a relatively fast and cheap tool for soil investigation, that is why it is extensively used worldwide, for profiling of soils, for determinations of bearing capacity and, as an extension and by means of correlations, for calculations of deformations.

The first application of CPT testing is a very effective soil classification and profiling by using the ratio between q_c and f_s (Nutt 1993).

The strength parameters c and ϕ can be evaluated with the help of correlations but these methods are not really reliable and are not recommended for fine-grained soils in particular (Lunne et al. 1997). The internal friction angle cannot be easily determined using the sleeve friction steel-soil f_s either (Cassan 1988).

The third application is the use of correlations for determining the bearing capacity of shallow or deep foundations. A proposal for the bearing capacity of a shallow foundation or of the tip of a deep foundation q_u for all soil types has been made by Bustamante and Giasenelli (1983), the form of the equation being the same as the one for the pressuremeter method. In (Eq. B.1), q_{ce} is the equivalent cone resistance taking into account several values around the base of the foundation. The factor k_c depends on the type of the soil, on the dimensions and on the embedment of the shallow foundation or on the type of pile for deep foundations.

$$q_u = k_c \cdot q_{ce} \quad (\text{Eq. B.1})$$

Correlations based on this model are proposed for shallow foundations in the NF P94-261 (2013) and for deep foundations NF P94-262 (2012).

A similar proportional relation has been proposed for the skin friction of the pile (Eq. B.2). β depends on the soil type and on the pile type.

$$q_s = \min\left(\frac{q_c}{\beta}; q_{s \max}\right) \quad (\text{Eq. B.2})$$

Empirical values associating the cone resistance q_c and the tip resistance q_b and ultimate skin friction q_s for piles are proposed in the German recommendations EA-Pfähle (DGGT 2012), but only for coarse-grained soils.

Proposals have been made by Meyerhof and Schmertmann for direct calculations of the settlement of shallow foundations, even without using any modulus for the method of Meyerhof, but they are quite limited and only applicable in sands (Frank 1991, Vogt 2011).

B.3 Pressuremeter test (PMT)

One substantial advantage of the pressuremeter test is that it provides both a deformation parameter (E_M) and a failure parameter, the limit pressure p_l , completed with the so-called creep pressure p_f .

In a pressuremeter test, the creep deformations between 30 seconds and 60 seconds load application time are measured, and represented as the creep curve (Fig. B.4 and Fig. B.5). The creep pressure p_f is the pressure separating the quasi-horizontal part of the creep curve and the following strongly increasing part of the curve. The horizontal part of the creep curve corresponds to the quasi-linear part of the pressuremeter curve, where the pressuremeter modulus E_M is measured. The creep pressure is in general used to check the validity of the test, but has no real practical relevance for the design of foundations. The ratio between p_i and p_f is in general around 1.8 (Van Wambeke 1962).

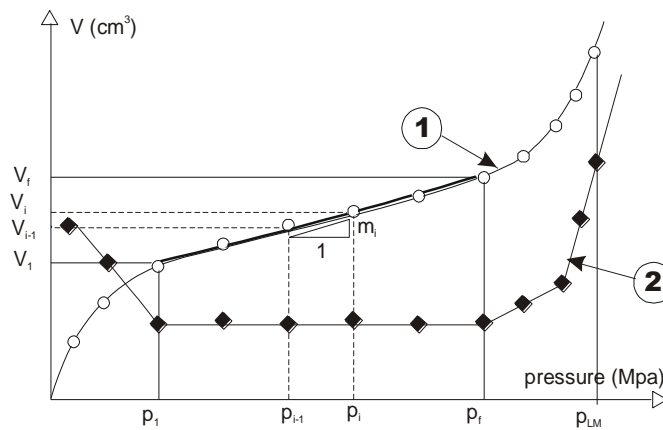


Fig. B.4 1) Pressuremeter curve, 2) Creep pressuremeter curve (Gambin 2005)

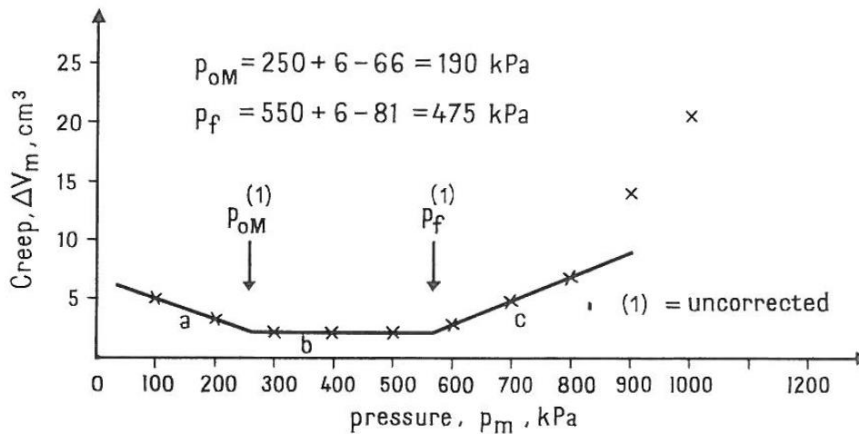


Fig. B.5 Example of creep pressuremeter curve (Baguelin et al. 1978)

The limit pressure p_l is conventionally defined as the pressure corresponding to a doubling of the volume of the cylindrical cell. Mean values of p_l for different types of soils are given in Table B.1.

Table B.1 Usual values of p_l for different types of soils (Ménard 1975)

<u>Soil</u>	<u>p_l in bars</u>
mud, peat	0.2 to 1.5
soft clay	0.5 to 3
medium clay	3 to 8
stiff clay	6 to 20
marl	6 to 40
loose silty sand	1 to 5
silt	2 to 15
sand and gravel	12 to 50
sedimentary sands	10 to 50
limestone	30 to over 100
recent fill	0.5 to 3
old fill	4 to 10

The net limit pressure p_l^* is defined as the limit pressure minus the horizontal pressure at rest p_0 , defined using estimated values of the coefficient of earth pressure at rest K_0 (Eq. B.3). The value of p_0 is usually much smaller than p_l .

$$p_l^* = p_l - p_0 \quad (\text{Eq. B.3})$$

More precise values of the structural or rheological coefficient α are given depending on the ratio E_M/p_l^* (see Table A.2).

Ménard investigated the bearing capacity using the pressuremeter results in the same way for shallow and deep foundations with consideration of a simplified elastic-plastic behaviour of the soil (model 4 in Fig. B.6).

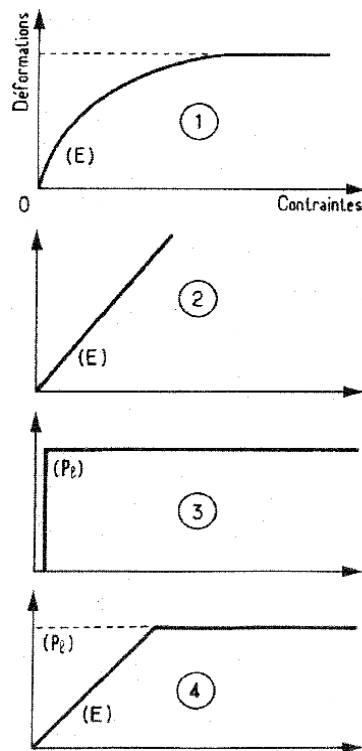


Fig. B.6 Constitutive models for soils -1) real elastic-plastic response, 2) elastic response without failure, 3) plastic rigid response, 4) simplified elastic-plastic model (Gambin 1979)

The previous theories of bearing capacity were in general based on rigid plastic methods, which could not model the mobilisation in the different zones around the foundation base. The state of plastic stress appears only in the immediate vicinity of the base of the foundation (Fig. B.7).

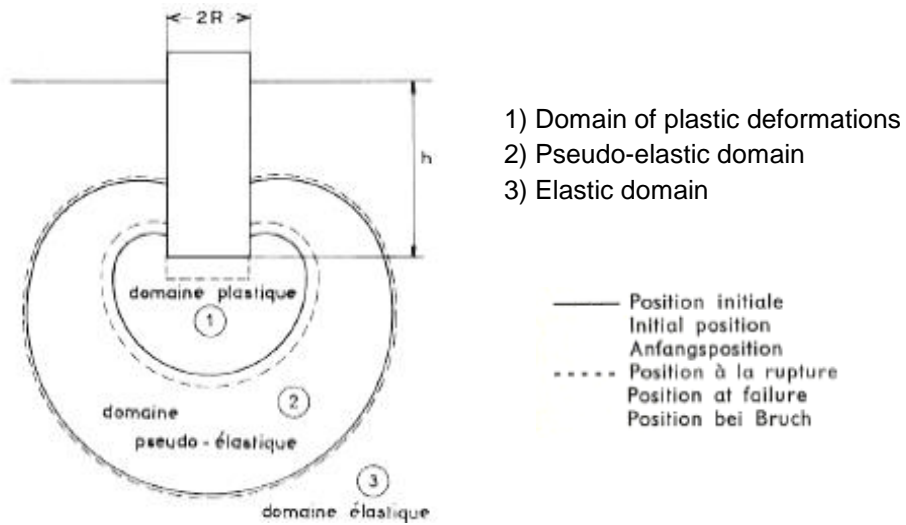


Fig. B.7 Different mobilisation levels of soil strength around foundation base (Ménard 1963a)

The starting point for developing a formula for the bearing capacity is the similarity between the behaviour of the soil around a foundation base in depth and the case of a spherical cavity expansion, with some corrections considering the shape of the pile tip and the fact that spherical conditions are only reached at a given distance from the flat tip surface (Fig. B.8).

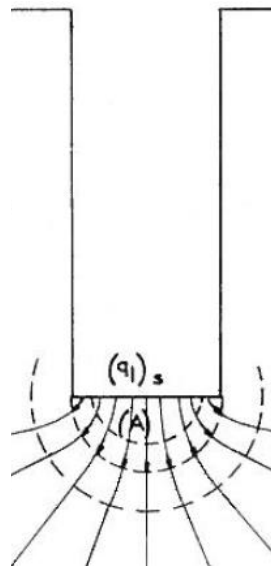


Fig. B.8 Distribution of stress isostatic lines around foundation base (Ménard 1963)

Ménard (1963a) has shown that there is a proportionality between the limit pressure from the pressuremeter test (cylindrical cavity expansion) and the limit pressure from a spherical cavity expansion for a given soil type. The base bearing can thus be related to the limit pressure in the cylindrical case. More details about the comparison between the spherical and cylindrical (pressuremeter-type) expansion, and by extension correlations between the resistance parameters of the PMT with the CPT, can be found in Appendix C about correlations.

Below a given depth, the bearing capacity of the tip of the foundation remains approximately constant in a homogeneous soil. For smaller embedment values the bearing capacity is significantly reduced (Fig. B.9).

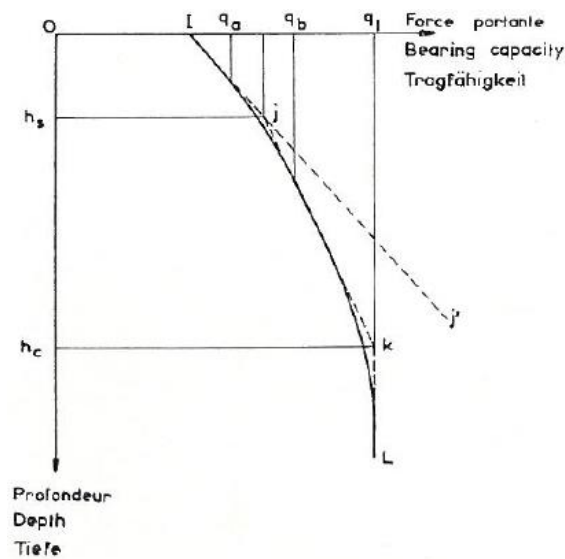


Fig. B.9 Bearing capacity versus depth of embedment (Ménard 1963a)

This can be explained by the fact that plastic phenomena can reach the soil surface for small embedment depths (Fig. B.10). This observation led Ménard to define a critical depth h_c separating the shallow and the deep foundations.

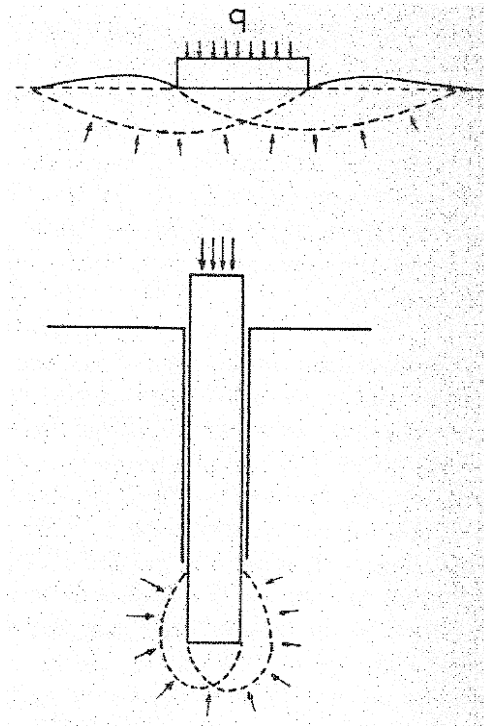


Fig. B.10 Plastic failure zones under shallow and deep foundation (Gambin 1979)

The general equation corresponds to a proportionality with a factor k between the net bearing capacity $q_l^* = q_l - q_0$ (q_0 being the vertical pressure at rest) and the net limit pressure p_l^* (Eq. B.4).

$$q_l^* = k \cdot p_l^* \quad (\text{Eq. B.4})$$

Different values of k have then been determined depending on the depth, on the dimension of the foundation in case of a shallow foundation and on the type of soil. These values have been here again developed and verified by experimental means (Ménard 1963a and 1963b, Goulet et al. 1964, Bustamante et al. 2009).

The skin friction for deep foundation can be derived from pressuremeter tests as well (Techniques Louis Ménard 1978a). This relationship can be explained by the fact that the skin friction is limited by the shear resistance of the soil, and that the limit pressure in the pressuremeter test corresponds to a failure of the soil rings around the probe. Curves have been proposed by Bustamante and Giasenelli for different pile and soil types based on experimentation (Baguelin et al. 1986).

These rules for homogeneous soils have been extended for heterogeneous soils, defining an equivalent limit pressure p_{le}^* which considers the strength of the soil directly above and below the foundation base.

Appendix C. Correlations between soil parameters

C.1 CPT and PMT and other tests parameters

Many investigations have been performed to compare the parameters from the PMT and from the CPT, in particular the resistance parameters from these tests, p_1 and q_c . Some attempts have been made to compare the pressuremeter modulus to the cone resistance q_c , even if failure and deformation parameters are a priori difficult to correlate. The comparison between both devices has led to the idea of a so-called “cone pressuremeter” device, which is not of common use in practice and are be detailed here (Nutt 1993, Powell et al. 2005).

The first experimental investigations have been made by Van Wambeke in 1962 on sands and silts. His study leads to a mean value of 2.4 for E_M/q_c and a mean value of 6 for q_c/p_1 in silts. For sands, E_M/q_c is approximately 1.1 and q_c/p_1 approximately 7.9.

Ménard gave in 1975 ratio intervals for clay, silt and sand (Table C.1).

Table C.1 Ratio spans q_c/p_1 for clay, silt and sand (Techniques Louis Ménard 1975)

Type of soil	R_p/p_1 ($R_p = q_c$)
clay	2.5 to 4
silt	5 to 6
sand	7 to 9

Baguelin presented some results from Nazaret in 1962 for dense sands. The ratio q_c/p_1 over the depth is here about $6000 \text{ kPa} / 600 \text{ kPa} = 10$, and E_M/q_c is about 1 (Fig. C.1), which is consistent with the previous results.

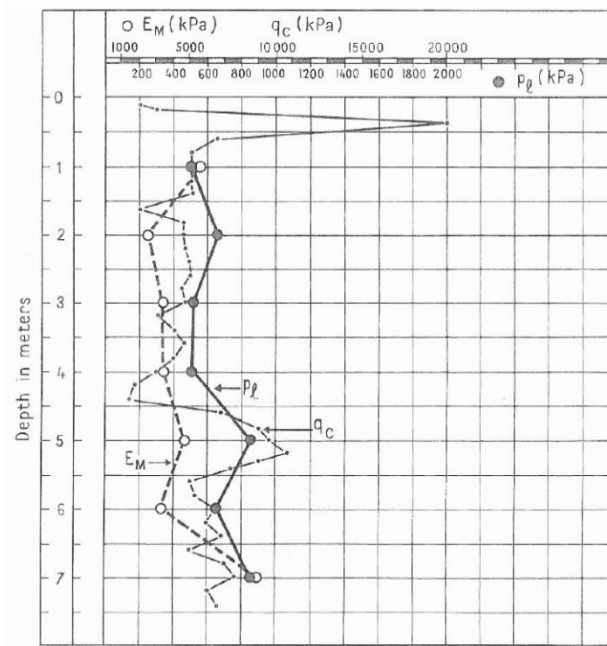


Fig. C.1 Measurements of E_M , p_l and q_c for sand by Nazaret (Baguelin et al. 1978)

Cassan proposed correlations as well, based on own experimental results and considering the results by other authors, in particular for different sand densities (Table C.2).

Table C.2 Correlations between PMT and CPT parameters (Cassan 1988)

Argiles (Clay)	$\frac{q_c}{p_l - p_0} = 3 \text{ à } 3,5$ (to)
	$\frac{E}{q_c} = 3 \text{ à } 4,5$ (normalement consolidées) (normally consolidated)
ou	$\frac{E}{q_c} = 5 \text{ à } 7$ (surconsolidées) (overconsolidated)
Limons (Silt)	$\frac{q_c}{p_l - p_0} = 6$
	$\frac{E}{q_c} = 1,5 \text{ à } 3$
Sables (Sand)	$\frac{q_c}{p_l - p_0} = 8 \text{ à } 10$
	$\frac{E}{q_c} = 1 \text{ à } 1,5$

Cudmani (2001) and Cudmani and Osinov (2001) studied the CPT and the PMT for sands only, from a theoretical mechanical point of view and with experimental results. The CPT cannot be directly modelled as a cylindrical or spherical cavity expansion since the stress paths for both loading cases do not coincide, but Cudmani shows that a relation between the cone resistance and the limit pressure from a spherical cavity expansion can be established through a shape factor k_q , depending on the state of the sand. Using experimental results of q_c for given soil state properties of different sources and the theoretical calculation of the limit pressure for the spherical expansion p_{LS} for the same soil properties, a proportional relation between them has been proposed by Cudmani and Osinov (Fig. C.2). The proportionality factor is essentially variable with the density of the sand, with approximately 2 for loose sands and 6 for dense sands.

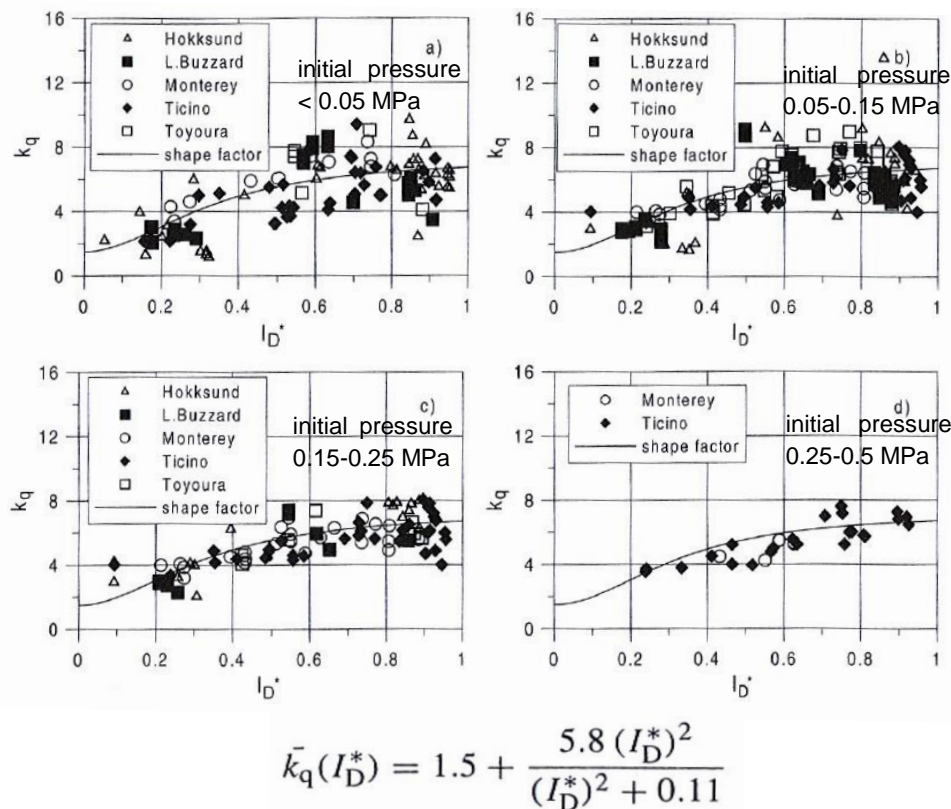


Fig. C.2 Ratio k_q between q_c and p_{LS} for sands of different densities ID^* (Cudmani and Osinov 2001)

However, direct correlations between CPT and PMT have not been investigated by Cudmani. To get a correlation between q_c (CPT) and p_1 (PMT), a relationship between p_1 (cylindrical) and p_{LS} is still necessary. From the different experimental results assembled in Fig. C.3, one can deduce a ratio p_{LS}/p_1 of 1.6 for loose sands and of 2 for dense sands. A theoretical study of Ménard (1963a) leads to comparable results, with 1.8 for loose sands and 2.1 for dense sands (and 1.45 for cohesive soils).

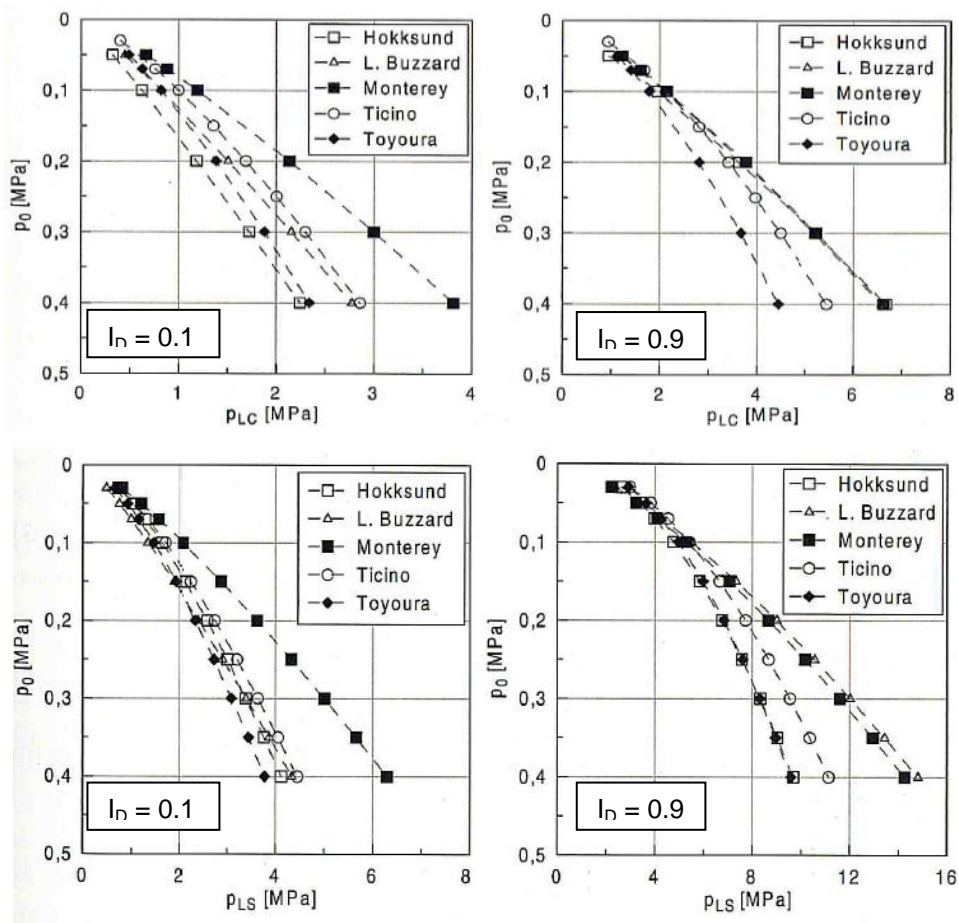


Fig. C.3 p_{LC} ($= p_l$) and p_{LS} for different sands, different p_0 and different ID (Cudmani 2001)

Altogether, the results of Cudmani give a ratio q_c/p_l of 3 for loose sands and 12 for dense sands.

Hamidi et al. reported works on this subject by Baguelin et al. (1978) and by Briaud et al. (1985, reported by Hamidi et al. in 2011). The values presented by Briaud et al. (1985) (Table C.4) are very different from those by Baguelin et al. (Table C.3), Van Wambeke or Ménard, so that one can think that the values for clays and sands may have been exchanged.

Table C.3 q_c^*/p_1^* for different soil types according to Baguelin et al. (1978) in (Hamidi et al. 2011)

Very soft to soft clays	close to 1 or 2.5 to 3.5
Firm to very stiff clay	2.5 to 3.5
Very stiff to hard clay	3 to 4
Very loose to loose sand and compressible silt	1 to 1.5 and 3 to 4
Compact silt	3 to 5
Sand and gravel	5 to 12

Table C.4 Correlations between PMT and CPT according to Briaud et al. (1985) in (Hamidi et al. 2011)

Soil type	PMT parameter	Correlation to CPT
Sand	P_1	$0.2q_c$
	E_p	$2.5 q_c$
Clay	P_1	$0.11 q_c$
	E_p	$1.15 q_c$

Some correlations between the resistance parameters from PMTs, CPTs and SPTs have been proposed by Bustamante and Gianceselli from the LCPC (Laboratoire Central des Ponts et Chaussées, today Ifsttar), shown in Fig. C.4.

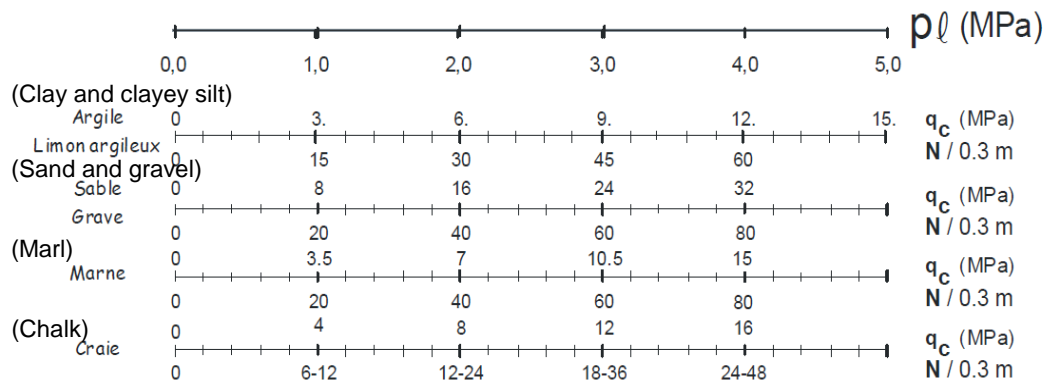


Fig. C.4 Correlation between q_c (CPT), p_1 (PMT) and N (SPT) (Bustamante and Gianceselli 2006)

A summary table of all common in situ parameters from PMTs (including pressuremeter modulus), standard penetration tests, CPTs and dynamic penetration tests is proposed in Table C.5.

Table C.5 Correlations between usual in situ parameters (internal document Keller France)

Argiles et Limons (Clay and Silt)

	Très molle (very soft)	Molle (soft)	Plastique (plastic)	Ferme (stiff)	Très ferme (very stiff)	Dure (rigid)
p_t (MPa)	0.1	0.2	0.4	1	3	
E_M (MPa)	1	2	4	10	30	
N_{SPT} (-)	2	4	8	15	50	
q_c (MPa)	0.4	0.8	1.6	3	10	
q_d (MPa) (above ground water level)	0.4	0.8	1.6	3	10	
q_d (MPa) (below ground water level)	0.4	0.6	1	2	6	
c_u (kPa)	12.5	25	50	100	200	

Sables et graviers (Sand and Gravel)

	Très lâche (very loose)	Lâche (loose)	Moyennement compact (medium)	Compact (dense)	Très compact (very dense)
p_t (MPa)	0.25	0.5	2	4	
E_M (MPa)	2.5	5	20	40	
N_{SPT} (-)	5	10	40	75	
q_c (MPa)	2	4	16	30	
q_d (MPa) (above ground water level)	2	4	15	25	
q_d (MPa) (below ground water level)	2	2.5	10	20	

C.2 CPT parameters and soil moduli

Some indicative values of oedometric moduli can be proposed on the basis of results from CPT for preliminary designs, but only for usual load levels since the oedometric modulus is inherently stress-dependent, and based only on the shallow foundation case since the settlement calculation of deep foundations is still not very common on an international scale.

Oedometric moduli are defined for coarse-grained soils as well as for fine soils in practice, using correlations and thus often without carrying out any oedometric test (which are in general only relevant for fine-grained soils). A factor α (not to be confused with the rheological factor of Ménard) is defined in the Eurocode 7 EN 1997-2 (2007-2010) as the ratio of the oedometric modulus and the cone resistance ((Eq. C.1) and Table C.6). Magnan (2006) indicates that the oedometric modulus calculated after this method corresponds to the secant modulus for an increment of 100 kPa from the preconsolidation stress.

$$E_{oed} = \alpha \cdot q_c \quad (\text{Eq. C.1})$$

Table C.6 Indicative ratio α to determine the oedometric modulus E_{oed} from the cone resistance q_c after EN 1997-2 (2007-2010) (based on Sanglerat 1972)

Soil	q_c	α
Low-plasticity clay	$q_c \leq 0,7$ MPa	$3 < \alpha < 8$
	$0,7 < q_c < 2$ MPa	$2 < \alpha < 5$
	$q_c \geq 2$ MPa	$1 < \alpha < 2,5$
Low-plasticity silt	$q_c < 2$ MPa	$3 < \alpha < 6$
	$q_c \geq 2$ MPa	$1 < \alpha < 2$
Very plastic clay	$q_c < 2$ MPa	$2 < \alpha < 6$
Very plastic silt	$q_c > 2$ MPa	$1 < \alpha < 2$
Very organic silt	$q_c < 1,2$ MPa	$2 < \alpha < 8$
Peat and very organic clay	$q_c < 0,7$ MPa	
	$50 < w \leq 100$ (%)	$1,5 < \alpha < 4$
	$100 < w \leq 200$ (%)	$1 < \alpha < 1,5$
	$w > 200$ (%)	$0,4 < \alpha < 1,0$
Chalks	$2 < q_c \leq 3$ MPa	$2 < \alpha < 4$
	$q_c > 3$ MPa	$1,5 < \alpha < 3$
Sands	$q_c < 5$ MPa	$\alpha = 2$
	$q_c > 10$ MPa	$\alpha = 1,5$

A stress-dependent correlation for a modulus of oedometer type is proposed in EN 1997-2 (2007-2010), recommended for the settlement calculation of spread foundations (Eq. C.2).

$$E_{oed} = w_1 \cdot p_a \cdot \left(\frac{\sigma'_{v0} + 0.5 \cdot \Delta\sigma'_v}{p_a} \right)^{w_2} \quad (\text{Eq. C.2})$$

With: σ'_v : effective vertical stress due to overburden of the soil

$\Delta\sigma'_v$: effective vertical stress due to the load applied

p_a : atmospheric pressure

Stiffness exponent w_2 :

0.5 for sands with a uniformity coefficient ($C_U \leq 3$)

0.6 for clays with low plasticity ($I_p \leq 10$; $w_L \leq 35$)

I_p : plasticity index

w_L : liquid limit

Stiffness coefficient w_1 from CPT results:

For poorly-graded sands ($C_U \leq 3$) above groundwater:

$$167 \cdot \log(q_c) + 113 \quad (\text{range of validity: } 5 \leq q_c \leq 30)$$

For well-graded sands ($C_U > 6$) above groundwater:

$$463 \cdot \log(q_c) - 13 \quad (\text{range of validity: } 5 \leq q_c \leq 30)$$

For low plasticity clays of at least stiff consistency ($0.72 \leq I_c \leq 1.30$) and above groundwater:

$$15.2 \cdot \log(q_c) + 50 \quad (\text{range of validity: } 5 \leq q_c \leq 30)$$

I_c : consistency index

Other correlations to determine a Young's-type modulus for small deformations in the usual SLS domain (defined in general in the order of 10^{-3}) from the cone resistance and sleeve friction are reported in the French standard for shallow foundations NF P94-261 (2013), based on the work of Robertson (Eq. C.3). I_R is determined from (Eq. C.4) to (Eq. C.6) or from Fig. C.5; the value of α_E is given in (Eq. C.7) to (Eq. C.9).

$$E = \alpha_E \cdot (q_c - \sigma_{v0}) \quad (\text{Eq. C.3})$$

$$I_R = \sqrt{(3.47 - \log Q_T)^2 + (1.22 - \log F_R)^2} \quad (\text{Eq. C.4})$$

$$Q_T = \frac{q_c - \sigma_{v0}}{\sigma'_{v0}} \quad (\text{Eq. C.5})$$

$$F_R = 100 \cdot \frac{f_s}{q_c - \sigma_{v0}} \quad (\text{Eq. C.6})$$

For $I_R < 2.2$:

$$\alpha_E = 0.015 \cdot 10^{0.55 I_R + 1.68} \quad (\text{Eq. C.7})$$

For $I_R \geq 2.2$ and $Q_T < 14$:

$$\alpha_E = \frac{Q_T}{1.2} \quad (\text{Eq. C.8})$$

For $I_R \geq 2.2$ and $Q_T \geq 14$:

$$\alpha_E = 11.7 \quad (\text{Eq. C.9})$$

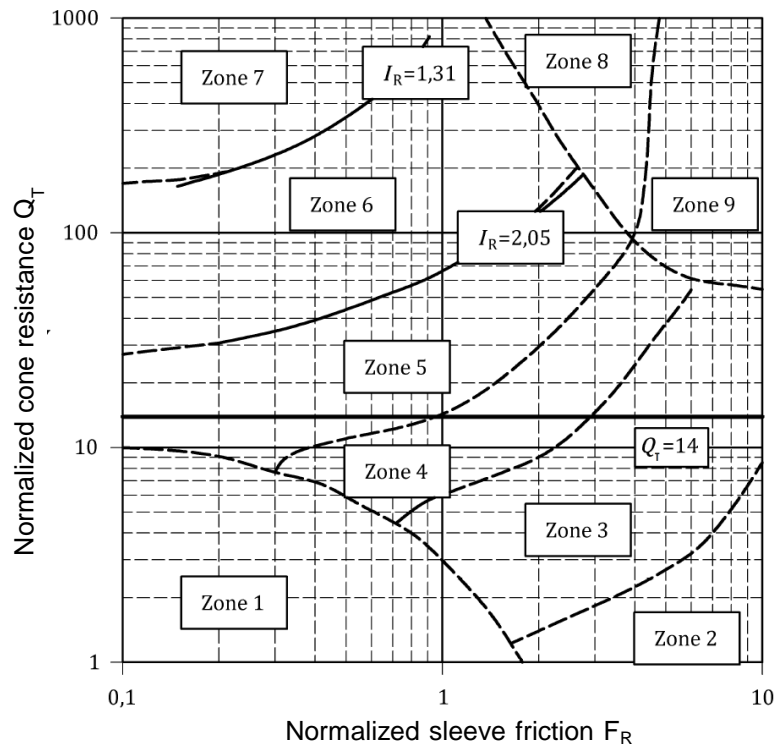


Fig. C.5 Roberston's diagrams after NF P94-261 (2013)

Lunne et al. (1997) suggested considering the load dependency in the determination of the proportionality factor between E and q_c for sands. Fig. C.6 shows the very strong variation of the modulus between very small strains of 0.001 % (10^{-5}) and strains of 1 % (10^{-2}) corresponding to a loading of approximately 30 % of the ultimate limit load in the case of a single footing.

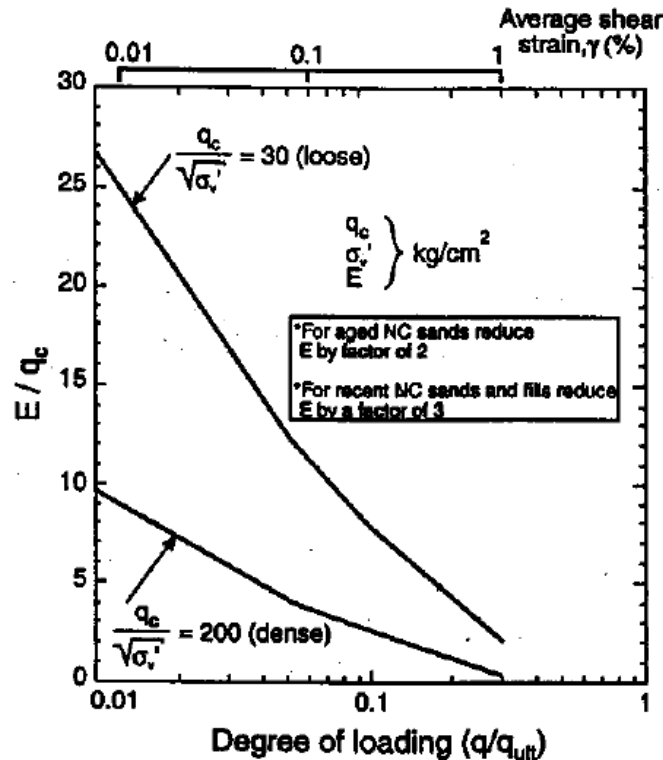


Fig. C.6 Estimation of equivalent Young's modulus for sand based on degree of loading (Lunne et al. 1997)

C.3 Different soil moduli

Speaking of correlations between soil moduli, the main question remains in general a correlation between the pressuremeter modulus, which corresponds to a given measured strain range, with other soil moduli. It can be correlated with oedometric moduli, which depend on the strain range, or with equivalent Young-type moduli, depending on the strain range and on the loading type as well and used in general for numerical applications.

The case of the shallow foundation (large raft or single footing) is in general used for the calibration of moduli before investigating the more complex foundation or soil reinforcement cases. The settlement of the single pile foundation case has not been extensively investigated on an international level yet, considered at the moment only based on the pressuremeter test in France (see Appendix A) or using empirical methods without correlating a soil modulus for this purpose like in EA-Pfähle (DGGT 2012). The French standard for shallow foundations (NF P94-261 2013) recommends calibrating the moduli in each particular case depending on the load level, but gives

some indicative ratio values (here denoted α_{footing}) for serviceability loads under footings and homogeneous soils (Table C.7).

Table C.7 Indicative correlations values $\alpha_{\text{footing}} = E/E_M$ for a single footing loading case under serviceability loads from NF P94-261 (2013)

		(normally consolidated)	E/E_M
(Clay)	Argiles	Normalement consolidées	4,5
		Surconsolidées (overconsolidated)	3
(Silt)	Limons	Normalement consolidés	4,5
		Surconsolidés	3
(Sand)	Sables	Lâches (loose)	4,5
		Denses (dense)	3
(Gravel)	Graves	Lâches	6
		Serrées	4,5

According to the same standard, in the case of large raft foundations, a secant oedometric modulus M may be defined using following correlation using the α -factor from the Ménard-theory (Table A.2), but it remains strongly recommended to use values from laboratory oedometer tests (Eq. C.10).

$$M = \frac{E_M}{\alpha} \quad (\text{Eq. C.10})$$

The definition of an equivalent Young's modulus can be done using a comparison with the same foundation on an elastic medium as well (Gomes Correia et al., Combarieu 2006), if a linear elastic modelling is foreseen for a given project. Combarieu calculated the required Young's modulus E to find the same settlement as the pressuremeter method for an equivalent circular foundation on an elastic medium (Eq. A.11. The results are presented in Table C.8, independently from the value of the load (proportionality in both formulas) but depending on the width of the foundation $2.R$ (R_0 being equal to 0.3 m), on its length L and on the rheological coefficient α .

Table C.8 Comparison of moduli for equality of Ménard settlement method and elastic method (Combarieu 2006)

$\frac{E_M}{E}$ values versus $\frac{R}{R_0}$ and α for $L/2R = 1$.							
$\alpha \backslash R/R_0$	1	2	5	10	15	20	
1	2,08	2,08	2,08	2,08	2,08	2,08	L/2R = 1
2/3	2,33	2,78	3,45	3,85	4,17	4,55	
1/2	2,5	3,23	4,55	5,56	6,25	6,67	
1/3	2,70	4	6,25	8,33	9,09	10	
1/4	2,78	4,35	7,14	10	12,5	14,3	

$\frac{E_M}{E}$ values versus $\frac{R}{R_0}$ and α , for $L/2R = 20$.							
$\alpha \backslash R/R_0$	1	2	5	10	15	20	
1	2,94	2,94	2,94	2,94	2,94	2,94	L/2R = 20
2/3	4,17	5	6,25	7,14	7,70	8,33	
1/2	5	6,67	9,1	11,1	12,5	14,3	
1/3	6,25	9,1	14,3	20	20	25	
1/4	6,67	11,1	16,7	25	25	33	

So the smaller the plate and the larger the rheological factor, the smaller the ratio E_M/E required between the moduli, so the larger the required elastic modulus required for equivalent results. This is consistent with the assumption that the modulus is larger for smaller deformations, which is the case under small foundations.

In the same way, correlations can be defined between a given analytical calculation method (using a certain modulus) and an elastic-plastic numerical calculation (modulus and plasticity parameters), where local plastic points can be considered unlike in fully elastic methods.

Generally, the comparison between soil moduli depends on the studied methods and the use which is aimed at for this modulus. In any case, the theoretical relationship between E and E_{oed} for an elastic medium (Eq. A.1) should be avoided for soils.

Appendix D. Main properties of pile load tests in database

D.1 Instrumented non-displacement pile load tests

Pile type	Ground type at tip	Source and number	Execution technique	Diameter B (m)	Length D (m)	Soil over length	Ground test
Non-displacement	Fine-grained	Ifsttar 35 A	bored (recovered casing)	0.68	20.2	fine-grained	PMT/CPT
		Ifsttar 35 B	bored (recovered casing)	0.88	27	fine-grained	PMT/CPT
		Ifsttar 37	bored (with slurry and recovered casing)	0.8	25.3	fine-grained	PMT/CPT
		Ifsttar 62 FTC	continuous flight auger	0.5	12	fine-grained	PMT/CPT
		Ifsttar 66.1	continuous flight auger	0.55	11.3	fine-grained	PMT
		Ifsttar 91	continuous flight auger	0.62	16	fine-grained	PMT
		Keller Poland PP2	continuous flight auger	1	10.5	coarse-grained fine-grained	/
		Keller Poland PP3	continuous flight auger	1	16.5	coarse-grained fine-grained	/
		Keller Poland CFA P1	continuous flight auger	0.63	12.54	fine-grained	CPT
	Keller Poland CFA P2	continuous flight auger	0.63	12.69	fine-grained	CPT	
	Coarse-grained	Keller Poland CFA 8	continuous flight auger	0.43	5.53	coarse-grained fine-grained	PMT/CPT
		Soft rock	Ifsttar 23	bored (with slurry and recovered casing)	0.63	19.25	coarse-grained soft rock
	Ifsttar 29		bored (with slurry and recovered casing)	0.63	13	fine-grained coarse-grained soft rock	CPT
	Ifsttar 32		bored (with and without recovered casing)	0.6	9.8	fine-grained coarse-grained soft rock	PMT/CPT
	Ifsttar 79		bored (with slurry and recovered casing)	0.8	12.5	fine-grained soft rock	PMT
	Ifsttar 173		bored (recovered casing)	0.62	23.4	fine-grained soft rock	PMT

D.2 Instrumented displacement pile load tests

Pile type	Ground type at tip	Source and number	Execution technique	Diameter B (m)	Length D (m)	Soil over length	Ground test
Displacement	Fine-grained	Ifsttar 40	screw cast in place	0.55	17	fine-grained	PMT
		Ifsttar 60 MP1	driven steel, H profile	0.43	14	fine-grained	PMT/CPT
		Ifsttar 62.4 PPII 7.5 m	sheet pile wall	1.92	7.5	fine-grained	PMT/CPT
		Ifsttar 62.4 PPII 12 m	sheet pile wall	1.92	12	fine-grained	PMT/CPT
		Ifsttar 62 BMO	driven cast in place	0.545	12	fine-grained	PMT/CPT
		Ifsttar 62 CF I	driven steel, closed-ended	0.533	7.5	fine-grained	PMT/CPT
		Ifsttar 62 CF II	driven steel, closed-ended	0.533	12	fine-grained	PMT/CPT
		Keller France ASIRI flot	screw cast in place	0.36	6	fine-grained	PMT
	Coarse-grained	Keller Brazil Ecopile	driven cast in place	0.46	17.55	fine-grained	CPT
		Ifsttar 39 B	driven steel, closed-ended	0.608	44.8	fine-grained coarse-grained	PMT/CPT
		Ifsttar 166	screw cast in place	0.58	15.5	coarse-grained fine-grained	PMT
		Krasiński b1 p3	screw cast in place	0.36	14.4	fine-grained coarse-grained	CPT
		Krasiński b1	screw cast in place	0.36	7.5	fine-grained coarse-grained	CPT
		Krasiński b2 p1	screw cast in place	0.4	10.4	fine-grained coarse-grained	CPT
		Krasiński b2	screw cast in place	0.36	7.1	fine-grained coarse-grained	CPT
		Krasiński b3 p1	screw cast in place	0.4	10.1	fine-grained coarse-grained	CPT
		Krasiński b3 p2	screw cast in place	0.36	9.6	fine-grained coarse-grained	CPT
		Krasiński b3	screw cast in place	0.36	8.9	fine-grained coarse-grained	CPT
		Krasiński b4 p3	screw cast in place	0.36	10.5	fine-grained coarse-grained	CPT
		Krasiński b4	screw cast in place	0.36	8.7	fine-grained coarse-grained	CPT
		Krasiński b6 p3	screw cast in place	0.36	10.5	fine-grained coarse-grained	CPT
		Krasiński b1 p1	screw cast in place	0.4	10.1	fine-grained coarse-grained	CPT
		Keller France ASIRI anc	screw cast in place	0.36	7.4	fine-grained	PMT
		Keller Poland INSER 4	screw cast in place	0.42	6.1	fine-grained coarse-grained	PMT/CPT
		Keller Poland INSER 5	screw cast in place	0.42	5.55	fine-grained coarse-grained	PMT/CPT
		Keller Poland FDP 7	screw cast in place	0.43	5.55	fine-grained coarse-grained	PMT/CPT
		Keller Poland SDP 1	screw cast in place	0.45	6	fine-grained coarse-grained	PMT/CPT
		Keller Poland SDP 3	screw cast in place	0.45	4.74	fine-grained coarse-grained	PMT/CPT
	Soft rock	Ifsttar 28 P2	driven steel, closed-ended	0.445	10.2	coarse-grained soft rock	PMT/CPT
		Ifsttar 113	driven steel, coated	0.37	18.8	fine-grained soft rock	PMT
		Ifsttar 119	screw cast in place	0.67	8.4	fine-grained soft rock	PMT
		Ifsttar 141 A	driven cast in place	0.508	19	fine-grained soft rock	PMT/CPT
Keller France St Quentin		screw cast in place	0.3	6.6	fine-grained soft rock	PMT/CPT	
Keller France Manom		screw cast in place	0.3	7	fine-grained coarse-grained soft rock	PMT/CPT	

D.3 Non-instrumented non-displacement pile load tests (or considered as such)

Pile type	Ground type at tip	Source and number	Execution technique	Diameter B (m)	Length D (m)	Soil over length	Ground test	
Non-displacement	Fine-grained	Keller Poland 170	continuous flight auger	0.63	7.7	fine-grained	CPT	
		Keller Poland 171	continuous flight auger	0.63	7.7	fine-grained coarse-grained	CPT	
		Keller Poland 177	continuous flight auger	0.63	8.6	fine-grained coarse-grained	CPT	
		Keller Poland 178	continuous flight auger	0.63	12.1	fine-grained	CPT	
		Keller Poland 179	continuous flight auger	0.63	14.1	fine-grained	CPT	
	Coarse-grained	Keller Poland 124	continuous flight auger	0.63	15.9	coarse-grained	CPT	
		Keller Poland 125	continuous flight auger	0.63	16.1	coarse-grained	CPT	
		Keller Poland 126	continuous flight auger	0.63	18.3	coarse-grained	CPT	
		Keller Poland 127	continuous flight auger	0.63	19	coarse-grained	CPT	
		Keller Poland 128	continuous flight auger	0.63	20.2	fine-grained coarse-grained	CPT	
		Keller Poland 129	continuous flight auger	0.63	20.2	fine-grained coarse-grained	CPT	
		Keller Poland 130	continuous flight auger	0.43	21.6	fine-grained coarse-grained	CPT	
		Keller Poland 131	continuous flight auger	0.43	21.6	fine-grained coarse-grained	CPT	
		Keller Poland 132	continuous flight auger	0.63	16.8	fine-grained coarse-grained	CPT	
		Keller Poland 134	continuous flight auger	0.63	25.6	fine-grained coarse-grained	CPT	
		Keller Poland 153	continuous flight auger	0.63	25.8	fine-grained coarse-grained	CPT	
		Keller Poland 159	continuous flight auger	0.8	13.2	coarse-grained	CPT	
		Keller Poland 160	continuous flight auger	0.8	19.2	coarse-grained	CPT	
		Keller Poland 161	continuous flight auger	0.8	15.2	coarse-grained	CPT	
		Keller Poland 162	continuous flight auger	0.8	17.2	coarse-grained	CPT	
		Keller Poland 268	continuous flight auger	0.43	7.5	coarse-grained	CPT	
		Soft rock	IFSTTAR 18 A	bored (recovered casing)	0.42	6	fine-grained soft rock	PMT
			IFSTTAR 22 A	bored (recovered casing)	0.56	13	fine-grained coarse-grained soft rock	PMT
	IFSTTAR 22 B		bored (recovered casing)	0.52	16	fine-grained coarse-grained soft rock	PMT	
	IFSTTAR 29		bored (with slurry and recovered casing)	0.63	13	fine-grained coarse-grained soft rock	PMT/CPT	
	IFSTTAR 149		bored (recovered casing)	0.9	16.6	fine-grained coarse-grained soft rock	PMT	

D.4 Non-instrumented displacement pile load tests (or considered as such)

Pile type	Ground type at tip	Source and number	Execution technique	Diameter B (m)	Length D (m)	Soil over length	Ground test
Displacement	Fine-grained	Keller France Boue	screw cast in place	0.27	6.3	fine-grained coarse-grained	PMT
		Keller Poland 18	screw cast in place	0.4	9.1	fine-grained coarse-grained	CPT
		Keller Poland 25	screw cast in place	0.4	10	coarse-grained	CPT
		Keller Poland 26	screw cast in place	0.4	11.2	fine-grained coarse-grained	CPT
		Keller Poland 27	screw cast in place	0.4	14.7	fine-grained coarse-grained	CPT
		Keller Poland 28	screw cast in place	0.4	14.9	fine-grained	CPT
		Keller Poland 83	screw cast in place	0.4	11	fine-grained coarse-grained	CPT
		Keller Poland 84	screw cast in place	0.4	11	fine-grained coarse-grained	CPT
		Keller Poland 115	screw cast in place	0.36	11.6	fine-grained coarse-grained	CPT
		Keller Poland 168	pre-cast concrete driven	0.4	12	fine-grained	CPT
		Keller Poland 176	screw cast in place	0.4	10.1	fine-grained coarse-grained	CPT
		Keller Poland 191	pre-cast concrete driven	0.4	9.4	fine-grained	CPT
		Keller Poland 192	pre-cast concrete driven	0.4	10	fine-grained coarse-grained	CPT
		Keller Poland 194	pre-cast concrete driven	0.4	10.4	fine-grained coarse-grained	CPT
		Keller Poland 195	pre-cast concrete driven	0.4	10.4	fine-grained coarse-grained	CPT
		Keller Poland 196	pre-cast concrete driven	0.4	10.4	fine-grained coarse-grained	CPT
		Keller Poland 203	pre-cast concrete driven	0.4	9.4	fine-grained	CPT
		Keller Poland 205	pre-cast concrete driven	0.4	9.4	fine-grained coarse-grained	CPT
		Keller Poland 206	pre-cast concrete driven	0.4	9.4	fine-grained coarse-grained	CPT
		Keller Poland 207	pre-cast concrete driven	0.4	9.4	fine-grained	CPT
	Keller Poland 212	pre-cast concrete driven	0.4	13.4	coarse-grained fine-grained	CPT	
	Keller Poland 219	pre-cast concrete driven	0.4	9.4	fine-grained	CPT	
	Coarse-grained	Keller France Liverdun	screw cast in place	0.27	8	fine-grained coarse-grained	PMT
		Keller Poland 3	screw cast in place	0.4	9	coarse-grained	CPT
		Keller Poland 5	screw cast in place	0.4	13.4	coarse-grained	CPT
		Keller Poland 9	screw cast in place	0.4	11	coarse-grained	CPT
		Keller Poland 10	screw cast in place	0.4	16	coarse-grained	CPT
		Keller Poland 12	screw cast in place	0.4	8.5	coarse-grained	CPT
		Keller Poland 15	screw cast in place	0.4	8.2	coarse-grained	CPT
		Keller Poland 19	screw cast in place	0.4	11.5	coarse-grained fine-grained	CPT
		Keller Poland 102	driven cast in place	0.4	13	coarse-grained	CPT
		Keller Poland 163	driven cast in place	0.508	13.4	fine-grained coarse-grained	CPT
		Keller Poland 164	driven cast in place	0.508	16.3	fine-grained coarse-grained	CPT
		Keller Poland 197	pre-cast concrete driven	0.4	7.4	fine-grained	CPT
		Keller Poland 198	pre-cast concrete driven	0.4	7.4	fine-grained coarse-grained	CPT
		Keller Poland 199	pre-cast concrete driven	0.4	7.4	fine-grained coarse-grained	CPT
		Soft rock	IFSTTAR 1 A1	concrete driven precast	0.45	24	fine-grained coarse-grained
	IFSTTAR 1 B1		driven steel, closed-ended	0.35	17.4	fine-grained coarse-grained soft rock	PMT
	IFSTTAR 1 B2		driven steel, closed-ended	0.35	22.5	fine-grained coarse-grained soft rock	PMT
	IFSTTAR 1 B3		driven steel, closed-ended	0.35	16.7	fine-grained coarse-grained soft rock	PMT
	IFSTTAR 49		driven steel, open-ended	0.5	21.5	fine-grained coarse-grained soft rock	PMT
	Keller France Gueshart		screw cast in place	0.27	7.5	fine-grained coarse-grained soft rock	PMT
	Keller France Le Havre		screw cast in place	0.27	15.8	fine-grained coarse-grained soft rock	PMT/CPT